CO_2 DYNAMICS IN A RIVER SYSTEM: MASS BALANCE, HYDROLOGICAL, GEOCHEMICAL AND BIOCHEMICAL IMPACTS

Saša Zavadlav

Doctoral Dissertation
Jožef Stefan International Postgraduate School
Ljubljana, Slovenia, May 2013

Evaluation Board:

Assoc. Prof. Dr. Nives Ogrinc, Chairman, Jožef Stefan Institute, Jamova cesta 39, Ljubljana

Prof. Dr. Tadej Dolenec, Member, Faculty of Natural Sciences and Engineering, Aškerčeva 12, Ljubljana

Prof. Dr. Ivan Sondi, Member, Faculty of Mining, Geology and Petroleum Engineering, Pierottijeva 6, Zagreb

MEDNARODNA PODIPLOMSKA ŠOLA JOŽEFA STEFANA
JOŽEF STEFAN INTERNATIONAL POSTGRADUATE SCHOOL

Saša Zavadlav

CO_2 DYNAMICS IN A RIVER SYSTEM: MASS BALANCE, HYDROLOGICAL, GEOCHEMICAL AND BIOCHEMICAL IMPACTS

Doctoral Dissertation

DINAMIKA CO_2 V REČNEM SISTEMU: MASNA BILANCA, HIDROLOŠKI, GEOKEMIJSKI IN BIOKEMIJSKI VPLIVI

Doktorska disertacija

Supervisor: Assoc. Prof. Dr. Sonja Lojen

Ljubljana, Slovenia, May 2013

Index

Abstract

A 3-year systematic investigation (2007–2010) of water chemistry using conventional and stable isotope tracers helped us delineate hydro-biogeochemical processes in the karstic Krka River watershed. By mineralogical and stable isotopic examination of tufa deposits and combining the results with water chemistry, we were able to evaluate the suitability of tufa deposits as recorders of environmental conditions in the time of their precipitation in a complex karstic environment with diffusive groundwater recharge. This is particularly crucial in the palaeoenvironmental studies. The main aims of the study were (1) to quantitatively determine calcite versus dolomite dissolution, carbonate weathering rates and associated CO_2 consumption, (2) to provide a detailed insight into the CO_2 dynamics in the watershed and (3) to evaluate the potential use of tufa precipitates as natural recorders of environmental conditions.

The Krka water geochemistry is influenced by enhanced carbonate weathering caused by dissolution of calcite and dolomite via carbonic acid within the watershed. The Mg^{2+}/Ca^{2+} molar ratio in the waters is a useful tool for reconstructing sources of water dissolving different lithological types. A downstream decreasing trend of Mg^{2+}/Ca^{2+} molar ratios revealed that the headwaters of the Krka are recharged by groundwaters dissolving predominantly dolomite bedrock, whereas the tributaries and groundwater discharging into the main channel in the lower reaches dissolve predominantly calcite/limestone lithology. Dolomite dissolution contributes over 70 % of the total carbonate dissolved load in the headwaters while in downstream sections, dissolution of dolomite contributes only ~ 50 % of the total dissolved carbonate load. Due to high solubility of carbonate bedrock that covers over 80 % of the Krka watershed area and intensive water-rock interaction in the aquifer(s), the carbonate weathering rates (CWR), ranging from 186 t/km^2/yr to 293 t/km^2/yr and associated CO_2 consumption of 16×10^5 mol of C/km^2/yr are amongst the highest on a global scale.

As found in numerous studies (named throughout the *Discussion* section) stable isotopes of oxygen and carbon were found useful for tracing water and dissolved carbon fluxes in the watershed. Mean residence times (MRT) of Krka waters were estimated to range from 1.3 to 4.7 years; the highest MRT were in the upper reaches (average ~ 3.0 years) showing that waters reflect isotopic composition of groundwaters that were in longer contact with the aquifer bedrock compared to those recharging the lower reaches (average MRT 1.6 years). The dissolved inorganic carbon (DIC) in Krka is a mixture of carbon derived from soil CO_2 and from carbonate dissolution, which reflects in high DIC (3.61–5.94 mM) and pCO_2 content (up to $10^{-1.2}$ bars). Based on the $\delta^{13}C_{DIC}$ values of the headwaters (average -13.6 ‰) we found that carbonate mineral dissolution primarily occurs under open system conditions. In comparison with the $\delta^{13}C_{DIC}$ values in the headwaters, the DIC in the main stream and the tributaries exhibited higher δ (average -12.6 ‰). The enrichment of DIC with ^{13}C downstream ranged from 0.1 ‰ to 2.6 ‰ resulting from CO_2 outgassing caused by equilibration between dissolved and atmospheric CO_2 rather than photosynthesis or in-stream calcium carbonate precipitation.

The mass balance calculations showed that carbonate dissolution prevails in spring and summer, whereas degradation of organic matter in the soil horizon was found to be more

expressed in autumn and winter. The lowest DIC fluxes were calculated for summer (average 2.0×10^8 mol/month), while the highest were usually observed in spring and autumn due to increased discharge (average 5.4×10^8 mol/month and 5.5×10^8 mol/month, respectively). The estimated total diffusive loss of CO_2 ranged from 2.0×10^8 to 3.0×10^8 mol of C/yr; the CO_2 fluxes were in general the highest in autumn and the lowest in summer. Based on the diffusion boundary layer model, we estimated that ~ 1.3×10^8 mol of C/yr is deposited as calcite in the main stream of Krka.

Tufa in Krka is dominantly low Mg-calcite with significant amount (up to 19 %) of detrital component (calcite, dolomite and quartz). The most prominent macroscopic feature of Krka tufa is its porous structure with cavities of 5 mm to over 1.5 cm in size, whereas the internal structure of presently forming tufa deposits in Krka is strongly related to organic particles recognized as vacuolar facies (after Manzo et al., 2012). Two main types of calcite precipitates were recognized; first is sparry cement calcite filling intergranular space that is clearly of inorganic origin and the second type is fine-crystalline calcite (micrite, microsparite) with dendrolitic or laminated texture that resembles organic growth. Besides sparitic cements, voids contain detrital material, among which quartz and carbonate grains were recognized.

The precipitation of tufa in the Krka River is conditioned by turbulent conditions and high water temperatures rather than elevated Ca^{2+} and HCO_3^- concentrations. The presence of biota acts as a substrate for calcite precipitation, whereas detrital component fills the pores lowering the porosity of tufa deposits. The precipitation rates of calcite deposition in Krka River were calculated assuming diffusion boundary layer conditions and considering the density of tufa to be 2.2 g/cm^3. The rate of precipitation in Krka River amounts to 0.7 to 2.1 mm/yr, which is consistent with the findings from thin section examination, where we observed that growth rate of tufa in the Krka is from 1 to ~2 mm/yr when assuming a combination of dense and porous layer in the laminated fabric presents a one year cycle of calcite precipitated.

Evaluation of the extent to which tufa deposits reflect environmental conditions using isotope fractionation equations published in the literature highly depends on the temperature constants developed for particular equations. Moreover, $\delta^{18}O$ values and Mg/Ca molar ratios in Krka waters are not related to water temperature changes, thus leading to discrepancies in the interpretation of (palaeo)environmental conditions. We found that none of the published fractionation equations fit our situation, which means that Krka tufas are unsuitable for the interpretation/reconstruction of environmental conditions during calcite precipitation based on theoretically postulated facts. This could be mainly due to complex processes associated with isotopic fractionation during tufa precipitation, diffusive groundwater input in the Krka watershed that constantly changes biogeochemical conditions in the water and/or significant fraction of detrital component in tufa.

Povzetek

S pomočjo konvencionalnih metod ter z analizo stabilnih izotopov smo tekom triletne študije (2007–2010) ovrednotili hidrološke ter biogeokemične procese v kraškem porečju reke Krke. Mineraloška analiza ter analiza stabilnih izotopov lehnjaka v kombinaciji z analizo kemije vode nam je omogočila oceniti primernost lehnjakov kot paleoindikatorjev. Glavni cilji študije so bili (1) kvantitativno določiti raztapljanje kalcita proti dolomitu, oceniti kinetiko raztapljanja karbonata in posledično porabljanje CO_2, (2) podrobno ovrednotiti dinamiko CO_2 sistema v porečju ter (3) oceniti možnost uporabe lehnjakov kot paleoindikatorjev.

Geokemijska sestava reke Krke odraža kemijsko raztapljanje karbonatov (kalcita in dolomita) v porečju, ki poteka zaradi delovanja ogljikove kisline. Molarno razmerje Mg^{2+}/Ca^{2+} v rečni vodi je uporabno orodje za razlikovanje med vodami, ki drenirajo različna litološka območja. Razmerje Mg^{2+}/Ca^{2+} vzdolž toka pada, kar kaže na to, da se reka v zgornjem delu napaja s podzemnimi vodami, ki drenirajo pretežno dolomitno podlago, medtem ko pritoki in podzemne vode v spodnjem delu toka drenirajo predvsem kalcitno (apnenčasto) podlago. Raztapljanje dolomita prispeva v zgornjem toku več kot 70 % k celotnemu deležu ionov, ki so posledica raztapljanja karbonatne kamnine, medtem ko je ta delež v spodnjem toku samo ~ 50 %. Zaradi dobre topnosti karbonatne podlage, katere je v porečju reke Krke več kot 80 % in zaradi razmeroma dolgih zadrževalnih časov vode v vodonosniku, je ocenjena hitrost raztapljanja karbonata (CWR), ki je med 186 t/km^2/leto in 293 t/km^2/leto, vključno s pripadajočo porabo CO_2 (16×10^5 mol of C/km^2/leto), med najvišjimi na globalni ravni.

Povprečni zadrževalni čas (MRT) v reki Krki je bil ocenjen med 1,3 do 4,7 let; najvišji MRT je bil določen v zgornjem toku (povprečno ~ 3,0 leta) kar kaže na to, da voda odraža izotopsko sestavo podzemnih vod, ki so bile dlje časa v kontaktu z matično kamnino, kot pa vode v spodnjem toku s povprečnim MRT 1,6 let. Visoke koncentracije anorganskega ogljika (3,61–5,94 mM) ter pCO_2 (do $10^{-1.2}$ bar) kažejo, da so procesi respiracije in razgradnje organske snovi v tleh ter raztapljanje karbonatnih kamnin glavni izvori DIC-a v porečju reke Krke. Na podlagi vrednosti $\delta^{13}C_{DIC}$ v zgornjem toku (povp. -13,6 ‰) smo pokazali da raztapljanje kamninske podlage poteka v pogojih odprtega sistema. V primerjavi z $\delta^{13}C_{DIC}$ vrednostmi zgornjega toka, odraža DIC v spodnjem toku ter pritokih višje δ vrednosti (povp. -12,6 ‰). Obogatitev DIC s težjim ogljikovim izotopom vzdolž toka je bila med 0,1 ‰ do 2,6 ‰, najverjetneje zaradi izhajanja CO_2 v atmosfero, ki je prej posledica ekvilibracije med raztopljenim in atmosferskim CO_2, kot pa proces fotosinteze ali pa obarjanje kalcijevega karbonata.

Izračuni masne bilance raztopljenega anorganskega ogljika v porečju reke Krke kažejo, da raztapljanje karbonatne kamnine k celotnemu kroženju DIC-a največ doprinese spomladi in poleti, medtem ko je doprinos z razgradnjo organske snovi največji pozimi in jeseni. Najnižji fluksi DIC-a so bili v poletnih mesecih (povp. $2,0 \times 10^8$ mol/mesec), najvišji pa spomladi in jeseni zaradi visokih pretokov (povp. $5,4\times10^8$ mol/mesec in $5,5 \times 10^8$ mol/mesec). Izhajanje CO_2 iz reke je znašalo med $2,0\times10^8$ in $3,0\times10^8$ mol C/leto; izhajanje je bilo najvišje jeseni in najnižje poleti. Na podlagi modela difuzijske mejne plasti smo ocenili, da se v reki ~ $1,3\times10^8$ mol C/leto obori kot $CaCO_3$.

Mineraloško gledano je lehnjak v reki Krki nizko Mg-kalcit z dokaj visoko vsebnostjo (do 19 %) detritične komponente (kalcit, dolomit in kremen). Najočitnejša lastnost lehnjaka v Krki je njegova poroznost; v precipitatu se pojavljajo praznine velikosti od 5 mm do preko 1.5 cm. Notranja struktura je najbolj podobna vakuolarnem faciesu (po Manzo et al., 2012), ki je izredno podobna rasti mahov in alg, ki obraščajo lehnjakove pregrade. Dva tipa kalcitnih kristalov gradita lehnjak: prvi je sparitni kalcit anorganskega nastanka s simetričnimi kristalnimi oblikami in zapolnjuje medzrnske prostore, medtem ko fino-kristalinični mikritni in mikrosparitni kalcit tvorita dendrolitni in laminacijski facies, ki sta po strukturi podobna cianobakterisjkim filamentom. Prazne prostore navadno zapolnjujeta sparitni kalcit in/ali detritični material.

Obarjanje lehnjaka v reki Krki je odvisno predvsem od turbulentnosti vode in visokih temperatur v vodi (> 10 °C) in v le manjši meri od stanja nasičenosti s kalcitom in visokih koncentracij Ca^{2+} in HCO_3 ionov. Hitrosti precipitacije kalcita v reki Krki smo izračunali z modelom, ki predpostavlja difuzijsko mejno plast med precipitatom in vodo (Dreybrodt and Buhmann, 1991). Pri gostoti 2,2 g/cm^3, določeni na vzorcih lehnjaka z reke Krke, smo izračunali, da je hitrost obarjanja lehnjaka od 0,7 do 2,1 mm/leto, kar sovpada z opažanji iz preparatov vzorcev lehnjaka pod svetlobnim mikroskopom. Enoletni cikel laminacijskega faciesa sestoji iz temnih in gostih lamin ter svetlih in poroznih lamin, ki nakazujejo na obarjanje v pomladnih in poletnih mesecih, ko je rast cianobakterij najobilnejša. Ponavljajoči se cikli v debelino merijo od 1 do 2 mm.

V kolikšni meri geokemijska sestava lehnjakovih precipitatov odraža okoljske razmere, v katerih se je lehnjak obarjal, je predvsem odvisno od uporabljene teoretične ravnotežne enačbe oz. njenih temperaturnih konstant. Izračuni paleookoljskih razmer se navadno opirajo na določitev temperature v vodi v času precipitacije lehnjaka, pri čemer sta najpogosteje uporabljena geokemijska parametra $\delta^{18}O$ in molarno razmerje Mg/Ca v precipitatu in vodi. V primeru reke Krke $\delta^{18}O$ in Mg/Ca v vodi nista temperaturno odvisna, zato je njuna uporaba kot temperaturnih indikatorjev vprašljiva in lahko vodi do napačnih interpretacij. Ugotovili smo, da izračunane frakcionacijske obogatitve med kalcitom in vodo odstopajo od vseh ravnotežnih temperaturnih enačb, dostopnih v literaturi. Zato sklepamo, da se lehnjak v reki Krki izloča pod neravnotežnimi pogoji. To je verjetno posledica kompleksnih procesov, povezanih z izotopsko frakcionacijo med izločanjem $CaCO_3$ iz vode, in stalnega napajanja reke s podzemno vodo, kar hitro spreminja kemijsko stanje v reki. Pomembno je tudi omeniti, da δ vrednosti lehnjaka odstopajo od pričakovane vrednosti avtigenega precipitata zaradi prisotnosti detritične komponente v lehnjaku.

Abbreviations

α	=	Isotope fractionation factor
CWR	=	Carbonate weathering rates
DBL	=	Diffusion boundary layer
DIC	=	Dissolved inorganic carbon
DOC	=	Dissolved organic carbon
EC	=	Electrical conductivity
ε	=	Isotope enrichment factor
δ	=	Delta, relative isotopic composition, value given in per mil (‰)
$\delta^{13}C$	=	Isotopic composition of carbon
$\delta^{15}N$	=	Isotopic composition of nitrogen
$\delta^{18}O$	=	Isotopic composition of oxygen
$\delta^{34}S$	=	Isotopic composition of sulphur
Ω	=	Saturation state
ω	=	Thickness of the water layer
φ	=	Thickness of DBL layer
pCO_2	=	Partial pressure of carbon dioxide
POC	=	Particulate organic carbon
PN	=	Particulate nitrogen
R_{CO2}	=	CO_2 consumption rates
ρ	=	Reaction rate constant
SI	=	Saturation index
T	=	Temperature
TA	=	Total alkalinity

1 Introduction

The most essential challenges in the science and technology of a global climate change are effective accounting of the global carbon budget and understanding of how carbon cycle paths and processes affect the atmosphere – hydrosphere – biosphere – lithosphere system (Tans et al., 1990; Esser et al., 2011; Cao et al., 2012). Atmospheric CO_2 concentrations increased from ~280 ppm before the industrial revolution to over 395 ppm in January 2013 (Tans, 2013). The modern increase in atmospheric CO_2 concentration reflects roughly about half of the CO_2 emissions from human activities, and the other half has been sequestered in the oceans and the terrestrial biosphere (Tans et al., 1990).

Riverine systems are importantly involved in the global carbon biogeochemical cycle, not only transporting carbon from terrestrial environment to the ocean and consuming atmospheric CO_2 via rock weathering, but also exchanging CO_2 with the atmosphere and precipitating carbonate minerals in the streams (Richey, 2005). The latter two processes are especially pronounced in areas with predominantly carbonate bedrock, e.g. karst. Current estimates suggest that inland waters transport, mineralize and bury ~ 2.7 Pg of C/yr, similar to the size of the terrestrial carbon sink for anthropogenic emissions of 2.8 Pg C/yr (Battin et al., 2009). Despite covering a proportionally small area (0.004 %), Battin et al. (2009) argue that continental waters have a significant role in the CO_2 sequestration and suggested that quantification of carbon fluxes into and out of inland waters could prove critical for constraining estimates of terrestrial ecosystem carbon fluxes. Their argumentation was supported by theoretical calculations and field monitoring evidence of Liu et al., (2010) who found that dissolved inorganic carbon in river waters (resulting from the combined action of carbonate dissolution, the global water cycle and the photosynthetic uptake of dissolved inorganic carbon by aquatic organisms) accounts for 29.4 % of the terrestrial CO_2 sink and was so far an underestimated sink for atmospheric CO_2.

While silicate weathering is considered to be a principal process of removing CO_2 from the atmosphere on a long-term scale, carbonate weathering plays a more important role on carbon cycling on a short-term scale (Liu et al., 2010). The importance of carbonate dissolution on atmospheric CO_2 sequestration has received relatively little study due to the fact that carbonates cover only ~ 15 % of Earth's land surface. Beginning with the launch of the UNESCO/IUGS IGCP379 program "Karst Processes and the Carbon Cycle (1995–1999)", the study of carbon cycle effects by karstification has received increasing attention from researchers around the world (Cao et al., 2012 and references there in). These studies have shown that due to higher dissolution rate, carbonates are more sensitive to environmental and climatic changes, the rate being closely correlated with precipitation, temperature, soil thickness and vegetation (Cao et al., 2012).

A continuous outcrop of carbonate rocks in the Southeast Europe is a large karst area affected by temperate and Mediterranean climate. It provides a valuable insight into the carbon dynamics in karst environment since carbonate weathering in the watersheds strongly affects the development of karst landforms and epikarst structures. This study addresses the carbonate cycle in a karst $CO_2 – H_2O – CaCO_3$ dynamic system in a small watershed of the Krka River (Slovenia), where the water chemistry is characterized by

groundwater input, CO_2 exchange with the atmosphere and active $CaCO_3$ precipitation. A hydro-geochemical concept was applied in this study to provide a better insight into weathering processes, CO_2 consumption rates, and characterization of water chemistry and in-stream processes that impact the carbonate cycle in a karst watershed of the Krka River. In order to present the essence and the meaning of findings of our research in a clear and concise manner the thesis is structured as follows. First, theoretical basis on the dynamics of riverine systems, carbonate cycle, and the use of stable isotopes as tracers in aquatic and terrestrial carbonate studies are briefly presented based on findings from previous studies. The text in the subsequent chapters elucidate what were the aims and hypothesis of the research, provide a description on geological, geomorphological and hydro-meteorological settings of the study area, and explains which materials and methods were used to achieve the purpose of this study. The results are explained in a separate chapter followed by discussion that is divided into two parts. The first part elaborates the evolution of the hydrogeochemistry in the Krka watershed, while the second focuses on the mineralogy and stable isotope geochemistry of tufa in Krka River. Finally, the main findings are synthesized in the *Conclusions*.

1.1 The dynamics of a riverine system

A riverine system integrates hydrological and biogeochemical cycles of water and of dissolved and particulate inorganic and organic compounds. The hydrological aspect of a riverine system is based on the water balance and dynamics of water through atmosphere-biosphere-hydrosphere system within a watershed. The rivers are fed by precipitation, by direct overland runoff, through springs and seepage, or from melt water at the edges of snowfields and glaciers. The contribution of direct precipitation on the water surface is usually minute, while river water losses result from evapotranspiration, and seepage and percolation into adjacent soils and aquifer (Rozanski et al. 2001). The balance of water input and loss sustains surface discharge, which mobilizes dissolved solutes and particulate materials from the landscape. The biogeochemistry of rivers is established as the interplay of terrestrial, biological, and geochemical weathering reactions that produce a suite of dissolved and particulate inorganic and organic compounds, via a series of pathways. The fundamental processes controlling the distribution of solute species in river waters are (1) rock weathering within the watershed, (2) physical transport via runoff, and (3) production and mineralization by terrestrial and aquatic biota (Richey, 2005).

Therefore, the river water chemistry is to a large extent a product of interplay between lithology, climate and land use (Roy et al., 1999; Gaillardet et al, 1999; Sun et al., 2010; Schulte et al., 2011). These processes are studied widely in order to differentiate and assign importance to the variables, with special emphasis on significance of rock weathering on ocean geochemistry (e.g. Meybeck, 1987; Szramek et al., 2011) and on the global carbon cycle (e.g. Amiotte-Suchet et al., 2003). Important sources of riverine carbon are geological processes (weathering), aquatic photosynthesis and CO_2 exchange with the atmosphere. To constrain the sources and cycling of water and solutes in river systems, hydrological and geochemical analyses serve as a good tool to evaluate riverine water hydro-bio-geochemical state. Initially, studies of river waters were focused on concentrations of particulate and dissolved constituents, enabling calculation of fluxes and mass balances for entire watersheds (Schulte et al., 2011 and references therein). Over the last few decades, the data on inorganic and organic constituents was complemented by isotope tracers, including stable water and carbon isotopes (Barth et al., 1998; Amiotte-Suchet et al., 1999; Aucour et al., 1999; Telmer and Veizer, 1999; Kendall and Coplen, 2001; Hélie et al., 2002; Darling et al., 2004; Kanduč et al., 2007a; Doctor et

al., 2008; Brunet et al., 2009; Ferguson et al., 2011; Schulte et al., 2011; Zavadlav et al., 2013).

1.1.1 Water chemistry, weathering and CO_2 consumption in carbonate watersheds

The water chemistry of continental freshwater varies widely and is governed by (1) the varying composition of rainfall and atmospheric dry deposition, (2) the modification of atmospheric inputs by evapotranspiration, (3) the varying inputs from weathering reactions and organic matter decomposition, (4) differential uptake by biological processes in soils, and (5) anthropogenic pollution (Gibbs, 1970; Andrews et al., 1996; Gaillardet et al., 1999). Which variable dominates depends on the lithology type, climate conditions and land use in the area.

Many studies on river water chemistry have found that weathering processes, particularly chemical, have a significant control on the geochemical composition of inland waters. Physical weathering or erosion is a mechanical process which fragments rocks, minerals and organic matter into smaller particles (Mackenzie and Lerman, 2006), thus enhancing the surface of bedrock for chemical dissolution. For example, rivers draining intensely weathered soils and sediments in tropical areas (e.g. Rio Negro in the Amazonian basin) have low total cation concentrations (< 0.2 mM) but are enriched with sodium, silica, iron, aluminium and hydrogen ions. In contrast, rivers draining easily erodible carbonate rocks (e.g. Xijiang in China) are characterized by high total cation concentrations (> 3 mM) and are rich with calcium, magnesium and bicarbonate ions (Andrews et al., 1996).

Chemical weathering is a process involving interactions between hydrological and biogeochemical factors that ultimately control the atmospheric CO_2 sequestration in the terrestrial environment (Schulte et al., 2011) and has a prominent effect on the geochemical composition of inland waters. A large number of studies worldwide have demonstrated that chemical weathering is affected by several co-dependant natural factors, e.g. lithology, climate, runoff, relief, elevation and vegetation. However, their relative importance remains debatable and the majority of studies suggest that particularly lithological variations are dominant controls of water chemistry (Gaillardet et al., 1999; Roy et al., 1999; Amiotte-Suchet et al., 2003). Some studies proposed that the effect of runoff controls the weathering (Millot et al., 2002; Tipper et al., 2006), while others consider that temperature variations are more important (Galy and France-Lanord, 1999; Dalai et al., 2002). There are also studies considering factors such as water-rock contact time and physical erosion to be more important (Oliva et al., 2003; Hagedorn and Cartwright, 2009; Sun et al., 2010).

Fluvial chemistry of world rivers in both tectonically stable and active regimes show that the geochemical composition of waters is dominated by the rapid weathering of carbonates and slower dissolution of aluminosilicate rock, with relatively minor contributions from primary basement formations (Andrews et al., 1996 and references therein). Thermodynamic data for carbonate mineral dissolution indicate that dolomite has a greater solubility relative to calcite at temperatures below 25 °C (Drever, 1997). Calcite and dolomite dissolution occurs via carbonic acid (H_2CO_3) as follows:

$$CaCO_3 + CO_2 + H_2O \leftrightarrow Ca^{2+} + 2HCO_3^- \quad (1)$$

$$MgCa(CO_3)_2 + CO_2 + H_2O \leftrightarrow Mg^{2+} + Ca^{2+} + 2HCO_3^- \quad (2)$$

Chemical weathering intensity/rates in the terrestrial environment is often quantified by using dissolved elemental riverine fluxes (Gaillardet et al., 1999; Szramek et al., 2007;

Sun et al., 2010). HCO_3^- content in the river is a convenient tracer of weathering intensity in the watershed. The continental HCO_3^- fluxes are influenced by both lithology and runoff; bicarbonate values of < 0.5 meq/L are generally observed in pure silicate watersheds while higher values reflect the increasing contribution of carbonate weathering (Figure 1; Szramek et al., 2007).

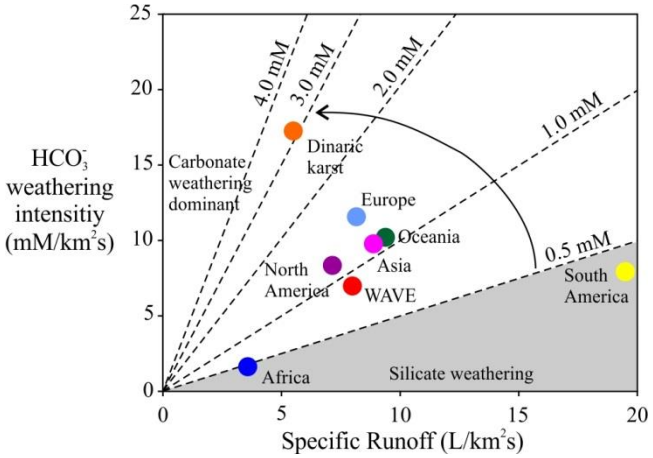

Figure 1: *Weathering intensity (expressed as HCO_3^- mM/km^{2}s versus runoff (L/km^{2}s) for the continental land masses worldwide (adopted from Szramek et al., 2007).* The world average value (WAVE) is calculated from the average world alkalinity concentration and land surface area. Dashed lines indicate the corresponding bicarbonate alkalinity concentration (meq/L). Silicate weathering has HCO_3^- values < 0.5 meq/L, while increasing values indicate increasing proportions of carbonate mineral weathering. The value of weathering intensity for Dinaric karst is obtained from Szramek et al. (2011).

1.2 Environmental isotopes as tracers

Stable isotopes are atoms with the same number of protons and electrons but a different number of neutrons. It is convenient to denote isotopes in the form ${}^m_n\mathrm{E}$, where the *m* denotes the mass number (i.e. sum of the number of protons and neutrons in the nucleus) and the *n* denotes the atomic number of an element *E*. The stable isotopes used in ecological studies are dominated by the lighter elements (H, C, O, N, and S) because (1) they dominate biological compounds, (2) they have low atomic mass, and (3) the percent increase in mass caused by the addition of a single neutron is greatest for these elements (Hoefs, 2009).

Due to differences in mass and consequently in the physicochemical properties, the behaviour of stable isotopes is controlled by kinetic and vibrational energy. This leads to isotope fractionations, which is put simply, the partitioning of isotopes between two substances or two phases of the same substance with different isotope ratios. The greatest differences between isotopes occur among the lightest elements.

Several mechanisms lead to isotopic fractionation, most important being equilibrium and kinetic fractionations. **Equilibrium fractionations** (or isotope exchanges) are those in which the distribution of isotopes differs between chemical substances (reactant vs. product) or phases (vapour vs. liquid) when a reaction is in equilibrium. In these reactions, the reactants and products remain in close contact in a closed, well-mixed system in which back reaction can occur and chemical equilibrium can be attained. The extent of the difference in final and initial masses in equilibrium reactions is temperature dependant, with the greatest differences occurring at the lowest temperatures. Heavier isotopes tend to accumulate in denser phases.

Kinetic isotope effects arise in unidirectional and often incomplete reactions and are

associated with processes such as evaporation, diffusion, dissociation reactions, and biologically mediated effects. In general, the light isotope of an element will diffuse more rapidly than the heavy isotope, which results in accumulation of lighter isotope in the product. Biological processes are excellent examples of kinetic isotope reactions. Organisms preferentially use the lighter isotopic species because of the lower energy "costs" associated with breaking the bonds in these molecules, resulting in significant fractionation between the substrate (heavier) and the biologically mediated product (lighter). Kinetic isotopic fractionations of biologically-mediated processes vary in magnitude, depending on reaction rates, concentrations of products and reactants, environmental conditions and, in the case of metabolic transformations, species of the organism. In general, slower reaction steps show greater isotopic fractionation than faster steps because the organism has time to be more selective (Kendall and McDonnell, 1988).

Isotopic fractionation is quantified with fractionation factor (α) and separation/enrichment factor (ε). In a chemical reaction, where reactants transform into products, the fractionation factor (α) is defined as the ratio of two isotope ratios:

$$\alpha_{\text{product-reactant}} = R_{\text{product}}/R_{\text{reactant}} \quad (3)$$

where *R* is the ratio of heavier to light isotopes in instantaneous reactant and product. Fractionation factors and the isotopic composition (δ values) of two substances are related according to:

$$\alpha_{A\text{-}B} = (1000+\delta_A)/(1000+\delta_B) \quad (4)$$

where *A* and *B* represent different substances. The magnitude of α is dependent on many factors, of which temperature is generally the most important (Hoefs, 2009). Most equilibrium fractionation factors have their value around 1 (e.g. α = 1.030 means that a substance *A* is by 30‰ enriched in heavy isotope than substance *B*). Since isotope fractionations are generally small, it has become common practice in recent years to replace the α by the ε value, because $\varepsilon \times 1000$ approximates the fractionation in parts per thousand, similar to the δ value. The enrichment factor is defined as:

$$\varepsilon_{A\text{-}B} = \alpha_{A\text{-}B}\text{-}1 \quad (5)$$

where ε value denotes what is the enrichment or depletion of the product with heavy isotope compared to the reactant (e.g. +10 ‰ or -10 ‰).

Because the differences between various materials are exceedingly small, it is a common practice in isotope geochemistry to express isotopic composition in terms of delta (δ) values. δ values are reported relative to an internationally accepted standard and expressed in parts per thousand deviation from that standard:

$$\delta\ (‰) = \left(\frac{R_{\text{sample}}}{R_{\text{standard}}}\text{-}1\right) \times 1000 \quad (6)$$

where *R* is the ratio of heavy-to-light (rare-to-abundant) isotope, R_{sample} is that ratio in the sample, and $R_{standard}$ is that in the standard. A positive δ value indicates that the sample has more of the heavy isotope than does the standard, whereas a negative δ value indicates that the sample has less of the heavy isotope than the standard. There are several common means to compare the isotopic composition of two materials, including heavy vs. light, high vs. low values, more vs. less positive, and enriched vs. depleted. The latter is used only with additional clarification as to which isotope the sample is enriched or depleted in.

Naturally occurring isotopes of light elements (hydrogen, oxygen, carbon, nitrogen and sulphur) are widely applied in environmental studies (e.g. Clark and Fritz, 1997; Kendall

and McDonnell, 1988; Hoefs, 2009). These elements are the most principal components of various compounds in the hydro-, geo- and biosphere. The large relative mass differences between heavy and light isotope of elements lead to isotope partitioning of the same element in the course of physicochemical processes (Hoefs, 2009).

Briefly, the typical uses of stable isotopes in hydrogeochemical studies include (1) identification of sources and sinks of the water and solutes, (2) identification of transport mechanisms, (3) identification of transformation processes, (4) characterization of flowpaths, and (5) assessment of biological and geochemical cycle of elements within an ecosystem. Stable isotope techniques are often used along with measurements of major and minor trace elements and judicious amounts of hydrologic data to test hypothesis about hydrologic and geochemical mechanisms and also provide input for mass-balance calculations and quantitative constraints on reaction progress (Kendall and McDonnell, 1988). Isotope biogeochemistry addresses the application of isotopes of constituents that are dissolved in the water or are carried in the gas phase. Isotopes commonly used in solute isotope biochemistry research include the isotopes of carbon, nitrogen and sulphur. Unlike the isotopes in the water molecules, the ratios of solute isotopes can be significantly altered by reaction with biological and/or geological materials as the water moves through the catchment. As such, the isotopes of solutes can provide us with information on flowpaths and relative contributions of solute sources to surface- and groundwater (Kendall and McDonnell, 1988).

1.2.1 Residence times of surface waters

Spatial and temporal distribution of water within the watershed is characterized by its hydrological, geological and meteorological conditions. The most important factors of a water balance are precipitation, evaporation and runoff, which are a function of climate (air temperature, duration of sunlight, wind speed), relief, rocks and soils, vegetation, and anthropogenic factors (Frantar, 2008). The water balance in a watershed can be simply described as:

$$Q = P - ET \tag{7}$$

where, Q is discharge, P is the amount of precipitation and ET is evapotranspiration. Water in rivers has two main sources: (1) recent precipitation that has reached the river either by surface runoff or by rapid flow through the shallow subsurface flowpaths and (2) groundwater.

Due to their conservative behaviour, the stable oxygen isotopes of water ($\delta^{18}O$) are ideal tracers of water sources and movement, and provide relatively unambiguous information about residence times and relative contributions from different water sources (Kendall and McDonnell, 1988). Variations in the stable-isotope composition in a watershed water balance are mainly caused by phase changes (evaporation, condensation, melting) and simple mixing of waters with different origin (e.g. mixing of surface- and groundwater). As this water infiltrates and travels through the basin, it retains most of its initial isotopic signature. Changes due to CO_2 uptake, degassing and exchange with carbonate rock in the aquifer have little effect because their total molar contribution to the water is only a tiny fraction (Kendall and McDonnell, 1988).

Isotopic signatures of rivers often preserve that of precipitation (Kendall and Coplen, 2001), however, isotopic composition of river waters is influenced by land-use and the interaction between aquifer and groundwater, which might mask the original isotopic composition of precipitation. The use of isotopic tracers in a hydrological cycle within riverine systems in conjunction with modelling techniques has proved a valuable aid in field research oriented towards understanding hydrological flowpaths that provide a

means of estimating watershed residence times (DeWalle et al., 1997; Soulsby et al., 2005; Rodgers et al., 2005; Ogrinc et al., 2008a).

1.3 The carbon cycle

Carbon is a fundamental component of the terrestrial and oceanic biosphere, hydrosphere and atmosphere. It is an essential constituent of organic and inorganic matter, important part of metabolism in organisms, and critical to chemical weathering of rocks. A conceptual biogeochemical model that reflects geological, biological, chemical and physical processes of carbon transfer between different reservoirs is a convenient tool to describe the storage, flows and transformations of carbon (in the form of carbon dioxide; Figure 2).

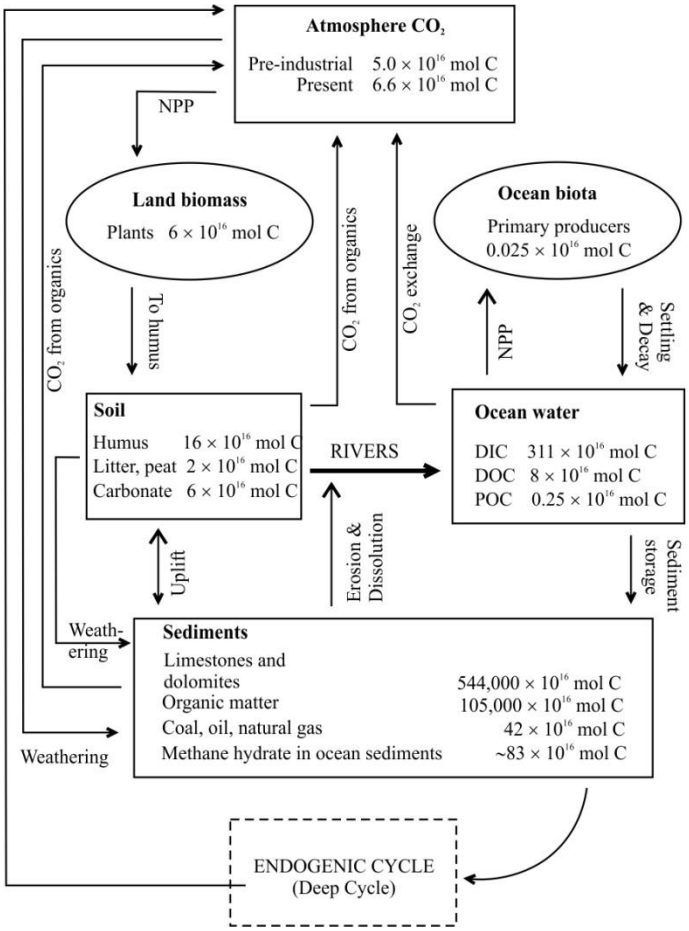

Figure 2: *Global biogeochemical cycle of carbon (from Mackenzie and Lerman, 2006).* Major carbon reservoirs are carbonate sediments, oceans, land biomass (soils and biota) and atmosphere.

An important regulator of global atmospheric CO_2 concentrations is chemical weathering of crystalline and sedimentary rocks at the Earth's surface. In short, rock weathering consumes CO_2, mainly of atmospheric/soil origin, and produces aqueous bicarbonate and carbonate ions, which are then transported into the oceans by rivers (Sun et al., 2010). On a geological time scale, chemical weathering of silicate rocks and the formation of carbonate rocks ultimately plays a key role in the consumption and release of atmospheric CO_2 (Gaillardet et al., 1999; Oliva et al., 2003); the CO_2 consumed by carbonate dissolution is balanced by the CO_2 released to the atmosphere by carbonate precipitation and sedimentation in the oceans, while chemical weathering of silicate rocks acts as a net sink for atmospheric CO_2. These processes removed CO_2 from the air and

sequestered that carbon in carbonate rocks, and reduced concentration of CO_2 from about 25 % in the primitive atmosphere to 0.03–0.04 % in the modern atmosphere (Cao et al., 2012). Moreover, consumption of atmospheric CO_2 directly affects the long-term global air temperature (Gaillardet et al., 1999; Amiotte-Suchet et al., 2003), which in turn determines the chemical weathering rates and the associated CO_2 consumption (Sun et al., 2010).

Recent calculations estimated that by far the largest reservoir of carbon is in marine sediments and sedimentary materials on land (~ 78×10^6 Gt of C). Most of this material is not in contact with the atmosphere and cycles through the solid Earth and plays only a minor role in the short-term cycle of carbon (Andrews et al., 1996). Next in size is the carbon reservoir of the oceans; the total mass of carbon in the global oceans, consisting mostly of dissolved inorganic carbon, is about 38×10^6 Gt. Terrestrial ecosystems (land biosphere and hydrosphere) contain carbon in the form of living organisms (plants, animals, microorganisms etc.), soils and dissolved carbon in waters. At present the atmosphere contains approximately 800 Gt of carbon in the form of CO_2 (Mackenzie and Lerman, 2006).

1.3.1 Carbon in natural waters

An important aspect of the carbon cycle is its dominant control on acid-base reactions in natural waters. Most importantly, it determines the pH and therefore speciation of elements and mineral saturation, and regulates alkalinity which determines the degree to which waters are buffered against changes in the pH. Carbon species in aqueous environment compose a carbonate system and a primary source is atmospheric $CO_{2(g)}$. When CO_2 dissolves in the water, it reacts with water and dissociates to form three different carbon species (Figure 3): dissolved CO_2 ($CO_{2(aq)}$), bicarbonate ($HCO_{3(aq)}^-$) and carbonate ($CO_{3(aq)}^{2-}$). Strictly, there is also the form of carbonic acid (H_2CO_3) but its amount is much lower than the other species, thus it is ignored for simplicity here. The carbonate system is governed by several equilibrium reactions listed below with dissociation constants at 25 °C (Stumm and Morgan, 1981; Appelo and Postma, 2009):

$$K_H = [CO_2]/pCO_2 = 10^{-1.5} \quad (8)$$

$$K_1 = [H^+][HCO_3^-]/[CO_2] = 10^{-6.3} \quad (9)$$

$$K_2 = [H^+][CO_3^{2-}]/[HCO_3^-] = 10^{-10.3} \quad (10)$$

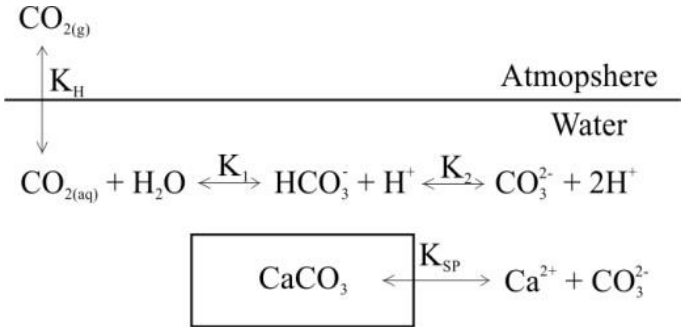

Figure 3: *Schematic illustration of the carbonate system (from Shiraishi, 2008).* The carbonate system in natural waters is comprised of dissolved carbon species: carbonic acid, bicarbonate ions and carbonate ions.

The solubility product (K_{SP}) of calcium carbonate is expressed as:

$$K_{SP} = \left[Ca^{2+}\right]\left[CO_3^{2-}\right] \quad (11)$$

Despite the fact that the riverine carbon cycle begins with the formation of carbonic acid in the atmosphere, the direct impact commences in the soil zone. Rainwater in equilibrium with atmospheric CO_2 has a low CO_2 partial pressure (pCO_2) of $10^{-3.5}$ and a pH of 5.6 (Stumm and Morgan, 1981). As the rainwater percolates into the ground, it equilibrates with soil CO_2. The soil CO2 derives from decomposition of organic matter and respiration, consequently leading to increased pCO_2 levels of the percolating water of 10^{-1} to 10^{-3} (Appelo and Postma, 2009). The concentration of DIC in the subsurface water may be further increased by carbonate dissolution in the aquifer, which raises the pH and moves the equilibrium towards a higher content of CO_3^{2-}.

The sum of $CO_{2(aq)}$, $HCO_3^-{}_{(aq)}$ and $CO_3^{2-}{}_{(aq)}$ represents the dissolved inorganic carbon, which is denoted as DIC. In natural waters, another important parameter is the alkalinity of the water. In the freshwater settings, carbonate alkalinity (CA) is almost the same as total alkalinity (TA):

$$DIC = [CO_2] + \left[HCO_3^-\right] + \left[CO_3^{2-}\right] \quad (12)$$

$$CA = \left[HCO_3^-\right] + 2\left[CO_3^{2-}\right] \quad (13)$$

The relative proportions of carbon species are controlled by pH and can be calculated using the above equations (8–10). Carbonic acid dominates at low pH, HCO_3^- at moderate and CO_3^{2-} at highly alkaline conditions (Figure 4). In the solution, dissolved CO_2 hydrates and dissociates into HCO_3^- and CO_3^{2-}, which is accompanied with isotopic fractionation (Table 1). The largest fractionation occurs during CO_2 hydration.

Table 1: *Fractionation factors for carbonate species at varying temperatures*.

Author		
Vogel et al. (1970)	$10^3 \ln {}^{13}\alpha_{CO_{2(aq)}\text{-}CO_{2(g)}} = -0.373 \cdot 10^3 / T(K) + 0.19$	(14)
Mook et al. (2000)	$10^3 \ln {}^{13}\alpha_{HCO_3\text{-}CO_{2(g)}} = 9.552 \cdot 10^3 / T(K) - 24.10$	(15)
Deines et al. (1974)	$10^3 \ln {}^{13}\alpha_{CO_3\text{-}CO_{2(g)}} = 0.87 \cdot 10^6 / T(K)^2 - 3.34$	(16)
Bottinga et al. (1968)	$10^3 \ln {}^{13}\alpha_{CO_{2(g)}\text{-}CaCO_3} = -2.9880 \cdot 10^6 / T(K)^2 + 7.6663 \cdot 10^3 / T(K) - 2.4612$	(17)

The reactions of calcite and dolomite dissolution (equations 1–2) are fundamental chemical reactions for understanding the water chemistry of rivers draining carbonate bedrock and the behaviour of $CaCO_3$ dissolution and precipitation in nature (Stumm and Morgan, 1981). Dissolution of carbonate rocks is sensitive to the partial pressure of CO_2, hence, the higher the CO_2 concentration, the greater will be the amount of calcite/dolomite dissolved (Clark and Fritz, 1997).

In addition, the DIC concentration in water depends on the "openness" of the groundwater - soil CO_2 system; under open system conditions, calcite dissolution proceeds with a constant supply of soil CO_2, which is typical of the unsaturated zone where gas and aqueous phases coexist. Under closed system conditions, in saturated zones, where the soil CO_2 used for carbonate dissolution is not replenished by new amounts of CO_2. Thus, the amount of dissolution and the final DIC concentrations will be

lower (Clark and Fritz, 1997).

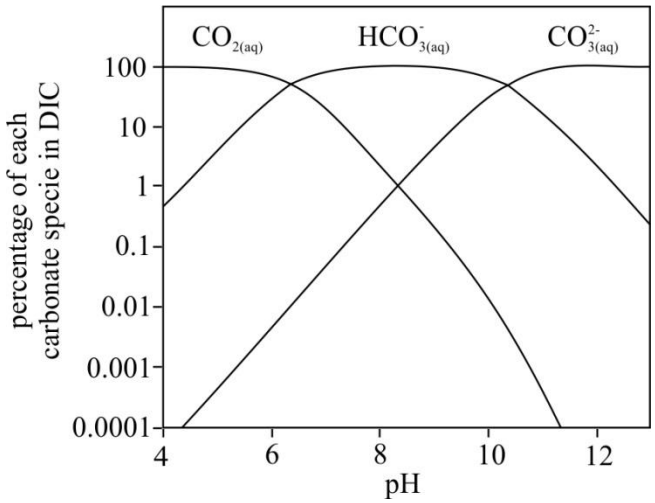

Figure 4: *Distribution of carbon species in water at different pH.* Relative percentage of carbonate species as a function of pH at 25 °C (Appelo and Postma, 2009).

1.3.2 The riverine carbon cycle

The riverine carbon pool consists of particulate and dissolved inorganic and organic carbon. Generally, the dissolved inorganic carbon (DIC) is the primary component in the rivers (Figure 5). The dominant species of DIC in rivers with pH between 7.5 and 8.5 is HCO_3^-. A prominent feature of most rivers, especially in the karst areas, is their significantly higher partial pressure of CO_2 (pCO_2) compared to the atmosphere ($10^{-3.5}$, Telmer and Veizer, 1999). The dominant source of CO_2 in rivers is groundwater with usually high CO_2 concentrations (up to $10^{-1.5}$, Clark and Fritz, 1997) due to its link to weathering and the soil zone. The behaviour of CO_2 in the main channel will depend on the input from the tributaries, which are usually poorly degassed, respiratory turnover to CO_2 or decline due to photosynthesis, lithological changes downstream (Telmer and Veizer, 1999), and equilibration with or evasion to the atmosphere (Schulte et al., 2011).

In terrestrial high-latitude regions, the $\delta^{13}C$ value of C_3 plant ecosystem that dominates globally is -27 ‰ (Deines, 1980). Diffusive loss of CO_2 from degradation of organic matter and transport through the soil horizon will fractionate the carbon, thus yielding $\delta^{13}C$ values of soil CO_2 of -23 ‰ (Cerling et al., 1991). Groundwaters record nearly the same $\delta^{13}C$ as that in soil (Aravena et al., 1992), however, additional carbon source to the DIC pool comes from carbonate dissolution in the aquifer with $\delta^{13}C$ values of 0 ± 3 ‰ (Schidlowski et al., 1983). The resulting $\delta^{13}C$ values of groundwater will then reflect mixing proportions of carbon of soil and carbonate origin. Further on, the DIC is subjected to several in-stream processes which alter its carbon isotopic composition. Photosynthesis in the water column preferentially selects the lighter carbon, thus enriching the remaining DIC with ^{13}C, while during respiration lighter carbon is added to the pool, resulting in lower $\delta^{13}C_{DIC}$ values. The third process, exchange with the atmosphere, involves equilibration between gaseous CO_2 and DIC. Although temperature-dependant, the isotopic fractionation between atmospheric CO_2 with $\delta^{13}C$ value of -7.7 ‰ (Schulte et al., 2011) and aqueous CO_2 is about +8 ‰ (Mook et al., 1974; Zhang et al., 1995). Thus, atmospherically equilibrated DIC would yield $\delta^{13}C$ value of ~ 0 ‰.

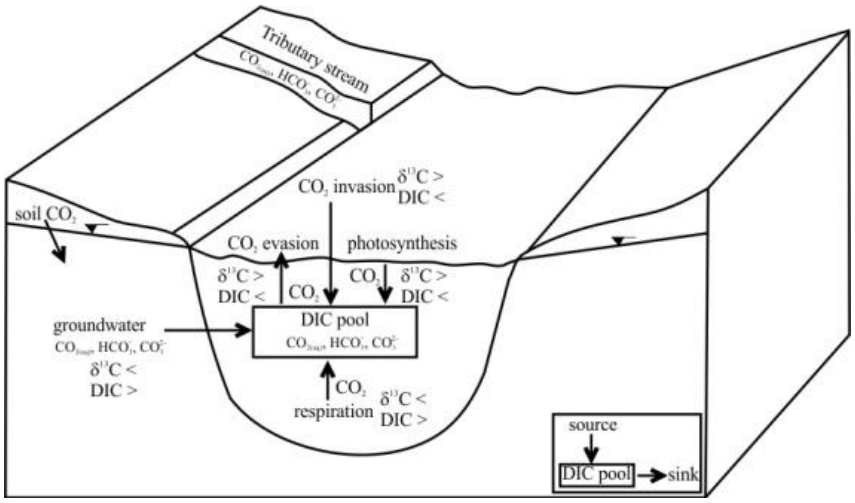

Figure 5: *Schematic diagram of carbon sources and processes in a riverine system.* Changes in $\delta^{13}C_{DIC}$ and DIC concentrations are related to different sources and processes that control riverine DIC (adopted from Atekwana and Krishnamurthy, 1998).

1.4 Tufa

Tufa is a freshwater deposit precipitated from karst water of meteoric origin (Ford and Pedley, 1996). It is found in many karst regions of the world, where it forms spectacular terraces, cascades and dams (Pentecost, 2005). The mechanisms of tufa formation have been investigated in many studies since the 1980s. First, meteoric water passes through the soil, equilibrates with soil atmosphere that has high pCO_2, and dissolves underlying carbonate rock. Precipitation of calcite in natural waters can be simply shown by the following reaction:

$$Ca^{2+} + 2HCO_3^- \leftrightarrow CaCO_3 + CO_2 + H_2O \quad (18)$$

When water recharges from subsurface, CO_2 degasses due to large differences between atmospheric and water pCO_2, shifting the carbonate equilibrium towards an increase of saturation with respect to calcite (Figure 6). Thus, tufa precipitation has important influence on both the hydrochemical evolution of river systems and the global carbon cycle because a large amount of CO_2 is released from the water to the atmosphere during the precipitation (Chen et al., 2004).

Several mechanisms have been proposed to explain tufa formation, varying from abiotic to biotic explanations. Numerous studies have established that CO_2 loss and $CaCO_3$ dissolution/precipitation are the two principal processes determining changes in water chemistry in fast flowing freshwater streams (e.g. Kempe and Emeis, 1985; Herman and Lorah, 1988; Merz-Preiß and Riding, 1999) in contrast to lakes or slow-flowing streams, where CO_2 levels are lower and photosynthetic uptake of HCO_3^- is more significant (Kempe and Emeis, 1985). Microscopic and in-vitro experiment studies of tufa precipitation showed that the presence of biofilms (freshwater algae and mosses) influences the morphology (e.g. Janssen et al. 1999, Manzo et al., 2011) and promotes the precipitation of calcite in water (Rogerson et al., 2008).

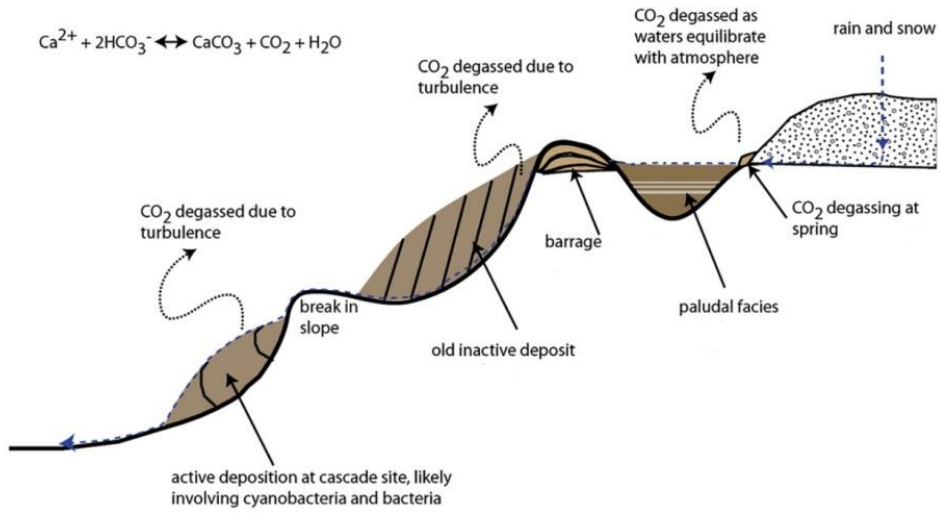

Figure 6: *Carbonate deposition in fluvial settings based on the perched springline model of Pedley et al. (2003; from Brasier, 2011).* As a result of contact with organic-rich soils, groundwaters have high pCO_2 levels, CO_2 degasses when waters are in contact with the atmosphere. CO_2 degassing, promoted by water turbulence and biological activity downstream, leads to calcite saturation and consequently to calcite precipitation.

1.4.1 Tufa proxies

In recent years, tufas have become increasingly important as palaeoclimate archives. Similar to speleothems and lake sediments, tufas record environmental and climate conditions and/or changes during their precipitation (Kano et al., 2003; Andrews, 2006; Kawai et al., 2006). Most commonly used tufa proxies for the reconstruction of climate/environmental conditions are stable isotopes of carbon ($\delta^{13}C$) and oxygen ($\delta^{18}O$) and trace elements of Ca, Mg, and Sr (e.g. Andrews, 2006, Matsuoka et al., 2001; Ihlenfeld et al., 2003; Kano et al., 2003; Lojen et al., 2004, 2009; Kawai et al., 2006; Hori et al., 2008; Yan et al., 2012).

1.4.1.1 Stable isotope proxies

The carbon and oxygen isotope composition of the precipitated calcite depends on the (a) isotope value of the parent solution, and (b) on isotope fractionation processes between the different species involved in the process of calcite precipitation. The $\delta^{18}O$ values of the precipitated calcite depend on the $\delta^{18}O$ values of water that comprises the main reservoir of oxygen atoms. In case of $\delta^{13}C$, the bicarbonate comprises the main reservoir of carbon atoms (in the pH range 7.5 to 8.5).

Since the late 1960s, many papers were published dealing with both theoretical and experimental determination of equilibrium isotope fractionation factors between the different species and phases involved in calcite precipitation (Polag et al., 2010). A simple quadratic equation presents the basis of the relation between fractionation factor and temperature:

$$10^3 \ln\alpha_{\text{product - reactant}} = aT^2 + bT + c \qquad (19)$$

where α is the fractionation factor and *a*, *b* and *c* are system specific constants achievable by calibration of measured parameters (for example $\delta^{18}O$ of calcite and water T) with linear fitting. The corresponding fractionation factor in the case of $\delta^{13}C$ in the calcite (cc) – HCO_3^- system is $^{13}\alpha_{\text{cc-HCO3}}$ (designation after Polag et al., 2010), or, as a more

descriptive value, expressed as the isotopic enrichment factor, $^{13}\varepsilon_{cc\text{-}HCO3}$ with $\varepsilon = (\alpha\text{-}1)\cdot 1000‰$. In case of $\delta^{18}O$ in the calcite (cc) – water (w) system, the enrichment factor is expressed as $^{18}\varepsilon_{cc\text{-}w}$.

Isotopic fractionation factors can be measured with laboratory experiments (e.g. Romanek et al., 1992; Kim and O'Neil, 1997; Dietzel et al., 2009), or determined from measurements of natural systems in geochemical equilibrium (e.g. Coplen, 2007). Different techniques for the determination of temperature dependence of fractionation enrichment $^{13}\varepsilon_{cc\text{-}HCO3}$ and $^{18}\varepsilon_{cc\text{-}w}$ were developed over the years and due to differences in the experimental set-ups or empirical data treatment, a large variability of the published temperature dependence of fractionation factors highlights a general problem. Most commonly used equilibrium fractionation factors in the studies of calcite – water relations are listed in Table 2.

Table 2: *The fractionation factors for C in the calcite – HCO_3^- system ($^{13}\alpha_{cc\text{-}HCO3}$) and for O in the calcite – water system ($^{18}\alpha_{cc\text{-}w}$).*

Author	Equilibrium equation	
Deines et al. (1974)	$10\cdot\ln^{13}\alpha_{cc\text{-}HCO3} = 0.095\cdot 10^6/T(K)^2 + 0.90$	(20)
Mook (2000)	$10^3\cdot\ln^{13}\alpha_{cc\text{-}HCO3} = -4.23\cdot 10^3/T(K) + 15.10$	(21)
O'Neil et al. (1969)	$10^3\cdot\ln^{18}\alpha_{cc\text{-}w} = 2.78\cdot 10^6/T(K)^2 - 3.39$	(22)
Friedman and O'Neil (1977)	$10^3\cdot\ln^{18}\alpha_{cc\text{-}w} = 2.78\cdot 10^6/T(K)^2 - 2.89$	(23)
Kim and O'Neil (1997)	$10^3\cdot\ln^{18}\alpha_{cc\text{-}w} = 18.03\cdot 10^3/T(K) - 32.42$	(24)
Mook (2000)	$10^3\cdot\ln^{18}\alpha_{cc\text{-}w} = 19.668\cdot 10^3/T(K) - 37.32$	(25)
Coplen (2007)	$10^3\cdot\ln^{18}\alpha_{cc\text{-}w} = 17.4\cdot 10^3/T(K) - 28.6$	(26)

The equilibrium fractionation factors are frequently used to test if calcite was precipitated under conditions of isotopic equilibrium. The oxygen isotopic fractionation between calcite and water serves as a method to estimate calcite precipitation temperature (McCrea, 1950; Epstein et al., 1953; Kim and O'Neil, 1997). Though it has never been ambiguously proven that calcite spontaneously precipitated from aqueous solution is in oxygen isotopic equilibrium, it is still assumed that calcite slowly precipitated from aqueous solutions at low temperatures forms very close to or at oxygen isotopic equilibrium (Kim and O'Neil, 1997), though carbonates spontaneously precipitate from the solution at relatively high supersaturation ($\Omega >> 1$), which is rare in natural systems. Just recently, Dietzel et al. (2009) reported on kinetic effect from experimental study of oxygen isotopic fractionation during inorganic calcite precipitation by spontaneous precipitation at various pH of solution, precipitation rates, and temperatures using the CO_2 diffusion technique. This study supports Coplen (2007)'s view that laboratory calibration of isotopic fractionation factor is challenging and is subjected to more uncertainty than desired because it is difficult (and perhaps nearly impossible) to precipitate calcite in oxygen isotopic equilibrium in laboratory experiments. In general,

oxygen fractionation factors evaluated in laboratory experiments are lower than those reported by Coplen (2007) for up to two orders. This is due to more similar simulations of nature in laboratory experiment (variable temperature, pH and precipitation rate of calcite). Nevertheless, published $^{18}\varepsilon_{cc\text{-}w}$ relations show similar temperature dependence (Figure 7a).

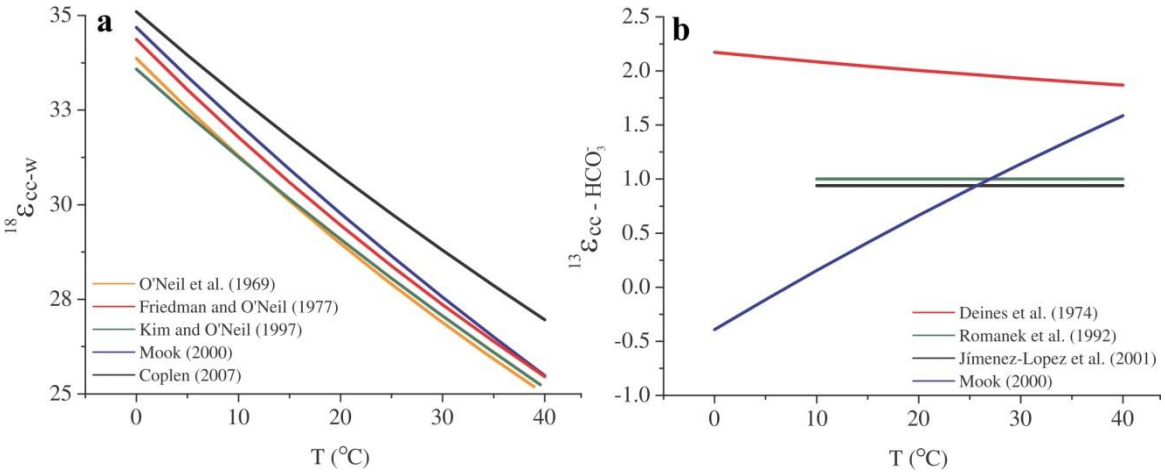

Figure 7: *Temperature dependant fractionation enrichment factors between calcite and water determined in laboratory experiments.* Temperature dependence of fractionation enrichment factor of (**a**) $^{13}\varepsilon_{cc\text{-}HCO3}$ in case of $\delta^{13}C$ given relative to VPDB in the calcite – water system, and (**b**) $^{18}\varepsilon_{cc\text{-}w}$ in case of $\delta^{18}O$ given relative to VSMOW.

Temperature equations, from which water temperature can be calculated based on known $\delta^{18}O$ values of water and calcite, are widely used in palaeoclimatological studies. One of the first palaeotemperature equations was established by Craig (1965) in a set of laboratory experiments and later a number of derivatives of this equations were developed (Table 3). Commonly, either the Anderson and Arthur (1983)'s or Hays and Grossman (1991)'s version proposed specifically for meteoric cements.

Table 3: *Temperature equations for the calcite – water system. $\delta^{18}O$ for calcite (cc) and water (w) are reported relative to VPDB and VSMOW, respectively.*

Author	Temperature equation	
Craig (1965)	$T(°C) = 16.9 - 4.2(\delta^{18}O_{cc} - \delta^{18}O_w) + 0.13(\delta^{18}O_{cc} - \delta^{18}O_w)^2$	(27)
Anderson and Arthur (1983)	$T(°C) = 16.0 - 4.14(\delta^{18}O_{cc} - \delta^{18}O_w) + 0.13(\delta^{18}O_{cc} - \delta^{18}O_w)^2$	(28)
Hays and Grossman (1991)	$T(°C) = 15.7 - 4.36(\delta^{18}O_{cc} - \delta^{18}O_w) + 0.12\left(\delta^{18}O_{cc} - \delta^{18}O_w\right)^2$	(29)

In contrast to oxygen isotopic fractionation, completely different temperature relationships exist for $^{13}\varepsilon_{cc\text{-}HCO3}$ (Figure 7b) determined in laboratory experiments. Mook (2000) predicted increasing $^{13}\varepsilon_{cc\text{-}HCO3}$ with increasing temperature, whereas Deines et al. (1974) obtained an inverse relationship. On the contrary, the equilibrium fractionation factors of Romanek et al. (1992) and Jímenez-Lopez et al. (2001) show no temperature dependence obtaining a constant value of 1.0 ‰ and 0.94 ‰, respectively.

1.4.1.2 Geochemical proxies

Natural calcites contain measurable quantities of trace elements (e.g. Mg, and Sr) providing proxies for reconstruction of (palaeo)climate/environmental conditions in the time of mineral precipitation. The ratio of trace element to calcium in solution is related to the same ratio in a homogenous solid phase by use of partition coefficient (D). For a particular trace element (X = Mg, Sr), the partition coefficient is expressed as:

$$D_X = (X/Ca)_{calcite} / (X/Ca)_{solution} \quad (30)$$

The partitioning of Sr between calcite and the parent solution depend on temperature, crystal growth rate and presence of other ions in the solution (Huang and Fairchild, 2001; Mucci and Morse, 1983). The D_{Sr} was found to increase from 0.06 to 0.08 with increasing calcite precipitation rate in the laboratory experiment of Huang and Fairchild (2001). In addition, the distribution of Sr/Ca relates to temporal changes in water fluxes and selective release during carbonate rock weathering (Ihlenfeld et al., 2003).

In contrast to Sr and Ba, the partitioning of Mg seems to be related only to temperature changes. Huang and Fairchild (2001) observed the behaviour of Mg in laboratory experiment designed to mimic the geometry, hydrodynamics, and low-ionic strength conditions encountered in natural karst caves. They found that (1) D_{Mg} is constant up to Mg/Ca ratio of unity (this range covers the vast majority of karstic and other freshwater environments), and (2) in the range between 15 to 25 °C D_{Mg} increases linearly with temperature, independently of the Mg concentration. Thus, they conclude that the key control on partitioning of Mg between calcite and solutions with low Mg/Ca ratios (≤ 1) is temperature (Huang and Fairchild, 2001), whereas growth rate is unimportant (Mucci, 1987). Over the last two decades, several studies on speleothems and few on tufas have attempted to exploit the temperature dependence of Mg/Ca ratio (e.g. Ihlenfeld et al., 2003; Lojen et al., 2009). These studies demonstrated that Mg/Ca ratio in a solid phase correlates not only with temperature but also depends on hydrological conditions. For example, in arid area, where tufa precipitates only in wet season, Ihlenfeld et al. (2003) found that calculated water temperatures retrieved from Mg/Ca ratios in tufa provided close approximations of average annual water temperature variations, whereas in the study of groundwater-fed karstic system Lojen et al. (2009) found that calculated temperatures yield values with up to 10 °C conservatively estimated uncertainty.

2 Aims and Hypothesis

The study of biogeochemical processes in the forested Krka watershed is the first comprehensive study of this area in the context of riverine CO_2 dynamics, thus contributing to knowledge about weathering intensity, in-stream calcium carbonate precipitation and photosynthesis/respiration cycle in karstic environment. The mobility of carbon in the environment is complex, thus following the carbon cycle is a multi-dimensional project and understanding sources and sinks is critical. Because carbonate weathering has significant control on the geochemical composition of river water, it is important to get better understanding of the relationships between chemical weathering of carbonate rocks and hydrogeochemistry of river water through systematic studies on geochemical compositions of river water draining carbonate-dominated terrain. Additionally, the Krka River exhibits active tufa precipitation which influences the hydrochemistry of the water in the river and alters the carbon cycle on a watershed scale.

The particular challenge of proposed theme is to identify the processes affecting CO_2 dynamics in a complex groundwater-fed river system with dominant diffuse subsurface recharge. Since the accuracy of estimates of the geochemical fluxes and understanding their dynamics within the watershed is related to sampling frequency (Hélie et al., 2002), we carried out a systematic 3-year long investigation on the hydrogeochemistry and carbonate system in the Krka River and its tributaries using different tracers to achieve the following objectives:

1. To determine whether the Krka watershed acts as a net source or sink of CO_2 by studying the chemical weathering processes and associated CO_2 consumption in the Krka River watershed. This will be achieved by (a) determining major ion composition of the Krka River and its tributaries, (b) evaluating natural and/or human factors impacting the water geochemistry, (c) investigating the impact of dolomite versus calcite dissolution on the geochemistry of the waters, (d) identifying seasonal and spatial variations in the geochemistry of the waters in the watershed, and (e) quantifying rock weathering rates and associated CO_2 consumption.
2. To characterize water fluxes and sources by (a) describing spatial and temporal variability in $\delta^{18}O$ of the precipitation and of the surface waters in the Krka watershed, and (b) to determine the mean residence time of water.
3. To provide a detailed insight into the CO_2 dynamics in the Krka waters by (a) constraining the major sources of dissolved inorganic carbon in the Krka watershed via interpretation of carbon isotope data and subsequently characterize how the in-stream processes affect the evolution of the inorganic carbon pool within the river, (b) revealing seasonal and spatial variations of dissolved organic and inorganic carbon, and CO_2 fluxes, and (c) employing thermodynamic and diffusion models and carbon mass balance calculations.
4. To evaluate the potential use of tufa precipitates in the Krka River as environmental/climate archives by (a) determining stable carbon and oxygen

isotopic composition of the precipitates, (b) correlating tufa and water isotopic and geochemical proxies with current environmental and hydrochemical conditions in the area, and (c) understanding contemporary hydrochemical processes affecting tufa precipitation and *vice versa*.

The hypothesis:

1. The CO_2 dynamics within a watershed is conditioned with its sources and processes that significantly influence its pathways in the CO_2 – water system. Due to dissolution of the predominantly carbonate bedrock the CO_2 dynamics in a karstic watershed of the Krka River is expected to be mainly influenced by the intensity of carbonate rock weathering, rather than by respiration/degradation of organic matter or by in-stream processes, such as CO_2 outgassing, *in-situ* photosynthesis and/or $CaCO_3$ precipitation.
2. Terrestrial carbonates are excellent indicators of conditions and/or changes in their precipitating environment. Their particular usefulness has been shown in the climate studies, however, their credibility remains questionable, especially in tufas, precipitated from groundwater-fed rivers, characterized by diffuse recharge. Precipitation of tufa depends on geochemical and biochemical conditions in the river, which affect the isotopic fractionation between water and precipitated minerals. Due to variable hydro-geochemical and biological conditions in the CO_2 – water system of the Krka we hypothesise that geochemical proxies revealed from the tufa precipitates are expected to be unreliable in terms of reflecting "equilibrium" conditions.

3 Study Area of the Krka River Watershed

Krka River watershed covers about 2,350 km^2 and with a length of 96 km Krka River is the largest tributary of Slovenian part of the Sava River, which drains waters into the Danube River. Krka watershed is situated in the Dinaric Alps, a type region of karst topography. Dinaric Alps are situated in the north-west of the Dinaric carbonate platform, a large karst region in south-east Europe that separates the Adriatic Sea in the south-east and the Alps in the north-west (Figure 8). Typical karst topographic features in the Dinaric region are karstic plateaus, planated lowlands and plains. River network in the region is limited to karstic disappearing streams with few exceptions, one of them being the valley of the Krka River. The karst has a role of a short-term surface water retention area, and therefore the characteristics of the discharges of the karstic rivers are distinctly special (Frantar and Hrvatin, 2008).

Krka is the largest and most important ecosystem in the SE Slovenia providing a habitat for many plants and animals. Due to its karstic characteristics, numerous caves occur in the area. All these geomorphological and biological features have put the Krka River on the map of Natura 2000 nature-protection programme.

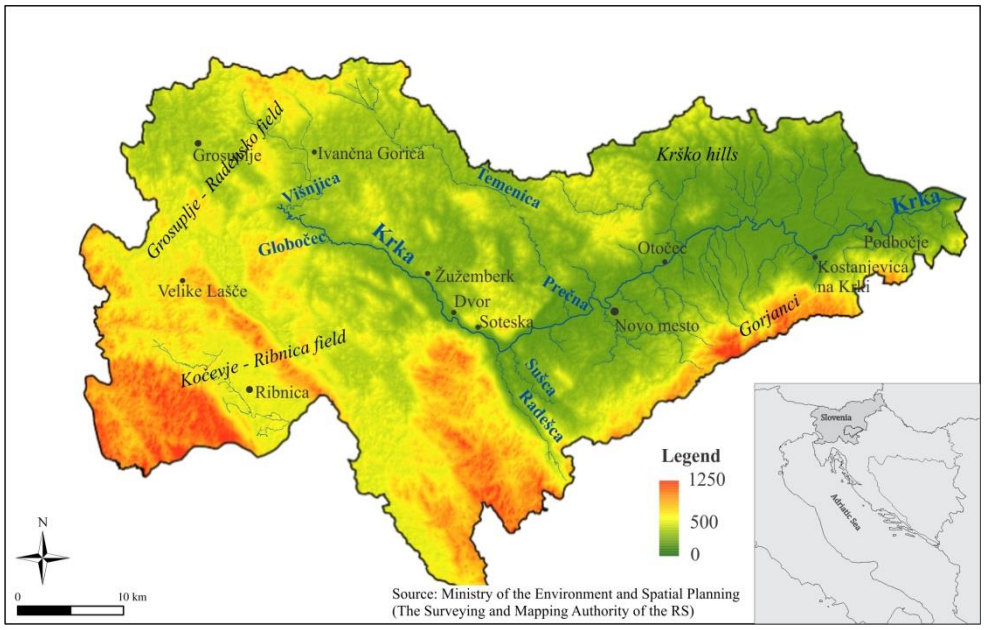

Figure 8: *A topographic map of the Krka watershed.* The river valley is surrounded by high hills in the southern flanks of the watershed, whereas in the north, the average altitude is around 350 m above sea level. At first a narrow valley significantly broadens in the east. The picture in the bottom of the right corner shows the position of the watershed on a regional scale.

3.1 Geological setting

Geology of the Krka River basin covers lithological units ranging in age from Permian quartz sandstones and conglomerates to Quaternary alluvial deposits (Buser, 1974; Buser and Cajhen, 1965; Pleničar and Premru, 1970, 1977). Over 80 % of the watershed

consists of Mesozoic carbonate sedimentary rocks (Triassic dolomites, and limestones of Jurassic and Cretaceous age) and approximately 17 % of Quaternary sediments (red and brown shale, sandstones and siltstones). Permian rocks, e.g. red claystones, quartz sandstones and conglomerates cover less than 2 % of the watershed surface area (Figure 12).

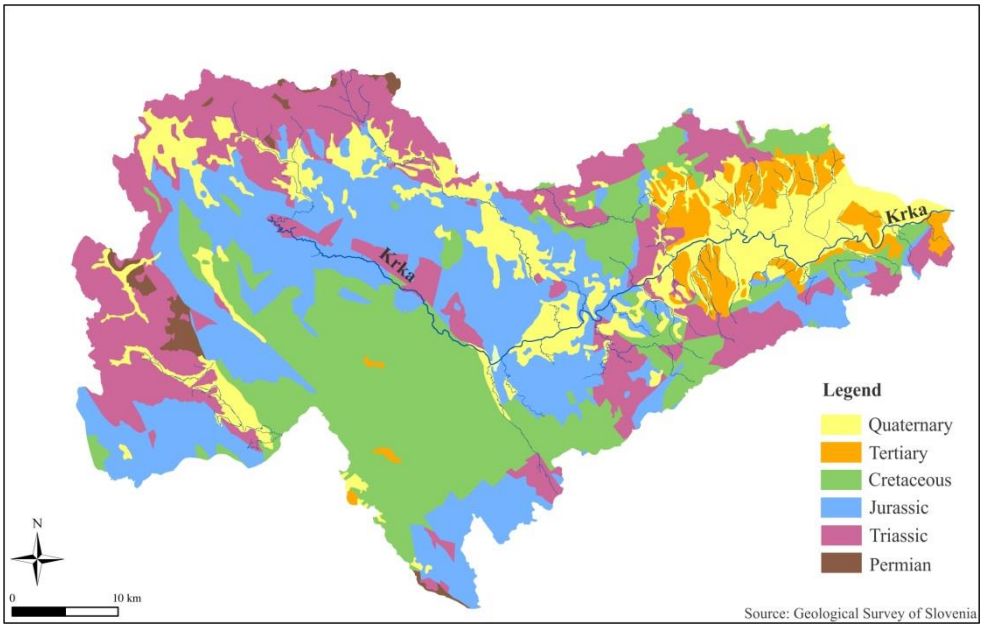

Figure 9: *Geological units in the Krka watershed.* The majority of the watershed consists of Mesozoic carbonate rocks covering the hills and plateaus. Quaternary and Tertiary alluvial sediments are spread in the flat river valley (modified after Buser and Cajhen, 1965; Pleničar and Premru, 1970).

The river is due to past tectonic activities divided into two parts; in the western part, the channel follows the direction of Žužemberk fault (NW-SE) forming a narrow and deep canyon (Figure 10). After Soteska, the river follows the alpine faults E-W direction. There are three types of karstified aquifers present in the watershed: two shallow aquifers with fracture- and/or intergranular-rock type, and a deep thermal aquifer, which is recharged through local tectonic zones. The first two aquifers are important sources of drinking water supply.

The headwaters and the upper reaches of the Krka are fed mainly by groundwater from the broad karst hinterland in north- and south-west areas of the watershed. Groundwater recharging the headwaters originates from a shallow karstified aquifer of Triassic carbonates, claystone, sandstone, and conglomerates. In the area of *Grosuplje-Radensko field*, younger Quaternary and Tertiary sediments can also be found (red and brown clay, and sandstones). Small streams in this area disappear underground on a contact between dolomite and limestone formations and recharge the Krka as groundwater. In the upper reach of the Krka, from the spring to Soteska (Figure 10), the bedrock formation consists of alterations of dolomites and limestones of Mesozoic age. The lower reaches, from Soteska to the outflow, the area is wider and forms a broad and plain river alley. The valley is formed mostly of Triassic dolomites and limestones in the hills of Gorjanci in the south and Krško in the north. In the area of the foot of the hills Cretaceous shales, and Tertiary and Quaternary sediments (sand, sandstones, clay, and conglomerates) are present (Buser and Cajhen, 1965).

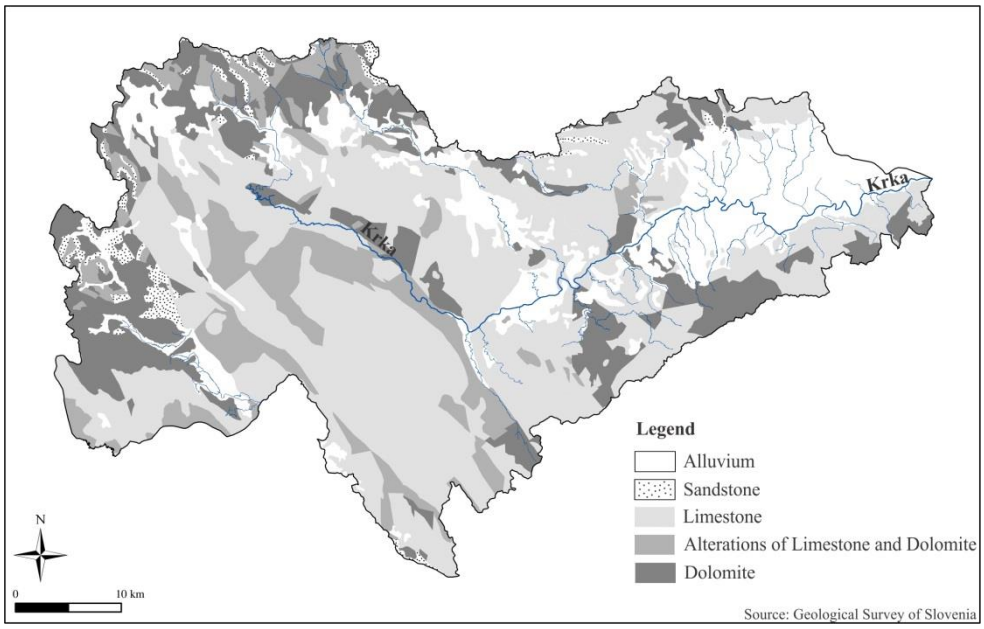

Figure 10: *A simplified geological map with lithological units.* Carbonate rocks are the dominant rock-type in the watershed and due to their solubility and highly fractured nature they turned the area into a typical karst landscape. Alluvial and sand sediments are mainly present in the flat parts of the river valley (modified after Buser and Cajhen, 1965; Pleničar and Premru, 1970).

3.2 Hydro-geomorphology

Waters in the Krka watershed are recharged by groundwater in the headwater catchment area, which accounts for about 260 km^2 of the whole watershed area, by the tributaries that drain approximately 700 km^2 of the watershed and from the diffused groundwater input throughout the course of the river (Kogovšek and Petrič, 2002). The waters rise to the surface at two main springs, at an elevation of 238 m. The major spring emerges from a large cave and ~ 50 m lower the second, minor spring Poltarca (Figure 8).

After almost 30 km of flow through a narrow, up to 100 m deep canyon, the river enters a wide plain area where it discharges into the Sava River at the elevation of 139 m. The groundwater from a broad karst hinterland *Grosuplje-Radensko field* recharges the headwaters (Figure 11), whereas the groundwaters from *Suha krajina* and *Kočevje-Ribnica field* recharge the river in the upper reaches through numerous karstic springs located at the main channel. Many surface streams, with a recharge area from *Gorjanci* and *Krško hills*, discharge into the river in the eastern part of the watershed (Figure 8, Plut, 1990).

The tributaries in the west have karstic characteristics and present large groundwater springs in the area discharging into the river after only few kilometres flow on the surface. The Višnjica and Prečna tributaries drain mostly alluvial deposits and are the only non-karst streams in the upper part of the watershed (Buser and Cajhen 1965). Prečna tributary is actually a continuation of Temenica tributary, which disappears underground twice and finally discharges into Krka named as Prečna tributary. Numerous small surface streams in the eastern part of the watershed are of small size and often dry.

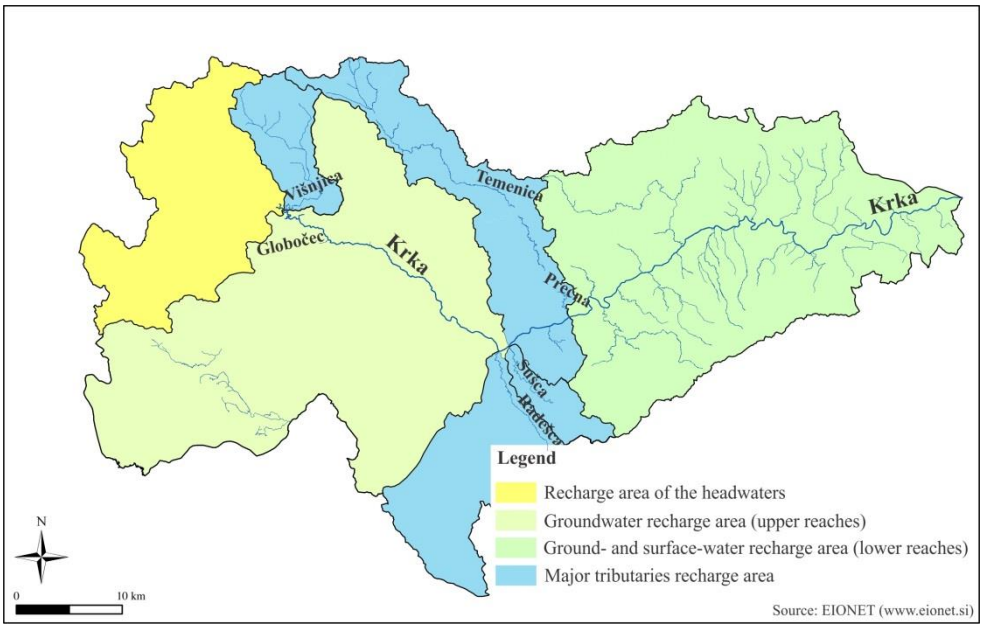

Figure 11: *Major hydrological recharge areas in the Krka River watershed.* The Krka River and its tributaries are mainly recharged by groundwater. Only the Višnjica tributary has some non-karstic characteristics because it drains mostly alluvial deposits. Map source: EIONET.

3.3 Hydro-meteorological characteristics of the Krka watershed

Climate in the Krka watershed is of temperate continental type. Air temperature has the strongest effect on evapotranspiration and, indirectly, on discharges when temperatures below freezing cause the retention of precipitation in solid forms (Frantar, 2008). Discharge regime is an indicator of the average fluctuation of the river discharge during the year. The factors that shape the discharge regime are numerous and diverse, the most important being: the climate, the relief, the geology, soil, vegetation and anthropogenic activities. The most important factor in Slovenia is the climate, as the discharge regimes are primarily dependent on the annual distribution of precipitation and temperature as well as on the duration of the snow cover.

The annual precipitation cycle in the Krka River watershed is conditioned by the continental climate type that exerts the greatest influence in the region (Dolinar, 2008). Precipitation regime in the Krka watershed (and in Slovenia in general) does not experience strong differences between wet and dry periods and is almost evenly distributed throughout all seasons. However, based on data from 1971 to 2000, the highest amounts of precipitation occur during summer downpours and storms, while the driest months are those in the winter (Dolinar, 2008). The amount of precipitation gradually decreases from west to east (Figure 12).

Discharge regime in the Krka River is of Dinaric pluvial-nival type (Frantar and Hrvatin, 2008), which is characterized by fairly equalized spring and autumn peaks and very pronounced differences between the winter and summer lows (Figure 13).

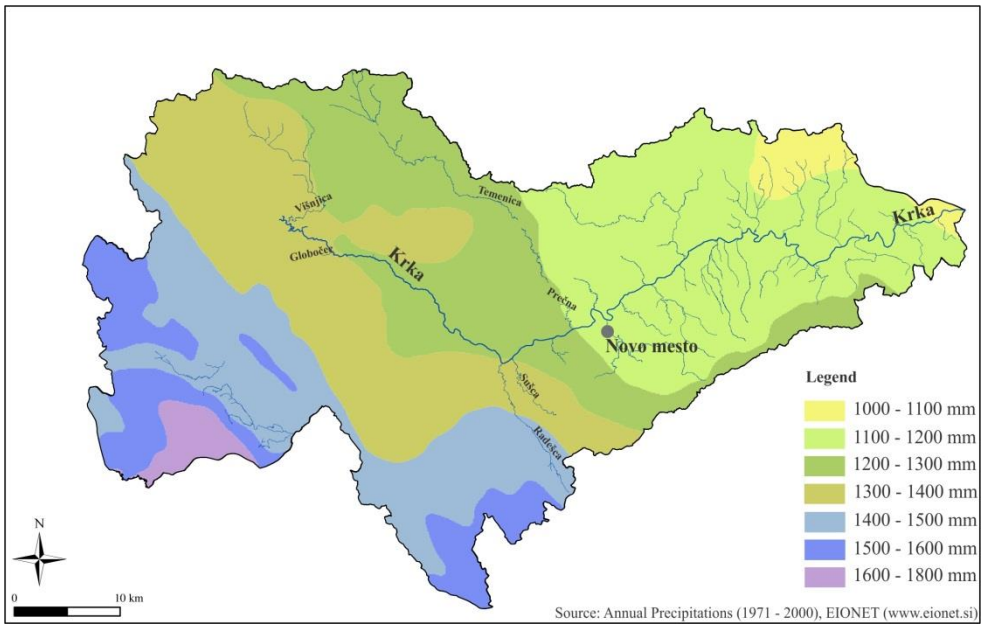

Figure 12: *Distribution of precipitation in the Krka watershed based on annual precipitation amounts in a period of 1971–2000 (EIONET).*

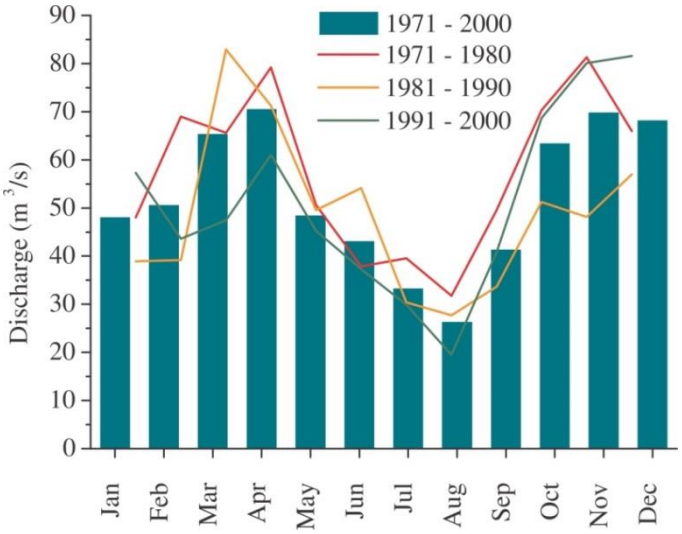

Figure 13: *Discharge regime of the Krka River*. The discharge regime of Krka is of pluvial-nival type (Frantar and Hrvatin, 2008) with peaks in spring and autumn.

3.4 Land use

Krka River drains a sparsely populated area with extensive agricultural activities in the eastern part. Over 65 % of the watershed area is forested with predominantly beech, fir, spruce, chestnut and oak, especially in the west and south-west. About 28 % of the area is used for cultivation (mostly wheat and corn), and only about 2 % of the area is urbanised and used for industrial purposes. Agriculture and population are concentrated in the east of the watershed (Figure 14).

Soils in the Krka River watershed vary in terms of relief and geological background. Rendzinas and brown forest soils are typical for the carbonate areas. On the flat relief of alluvial bedrock (fine silt and clay deposits) in the eastern part of the watershed where floods are frequent, eutric brown, gley and pseudogley soils are found (Repe, 2004). Average soil depth within the watershed is over 70 cm, on steep relief at higher altitudes

up to 30 or 50 cm (Figure 15).

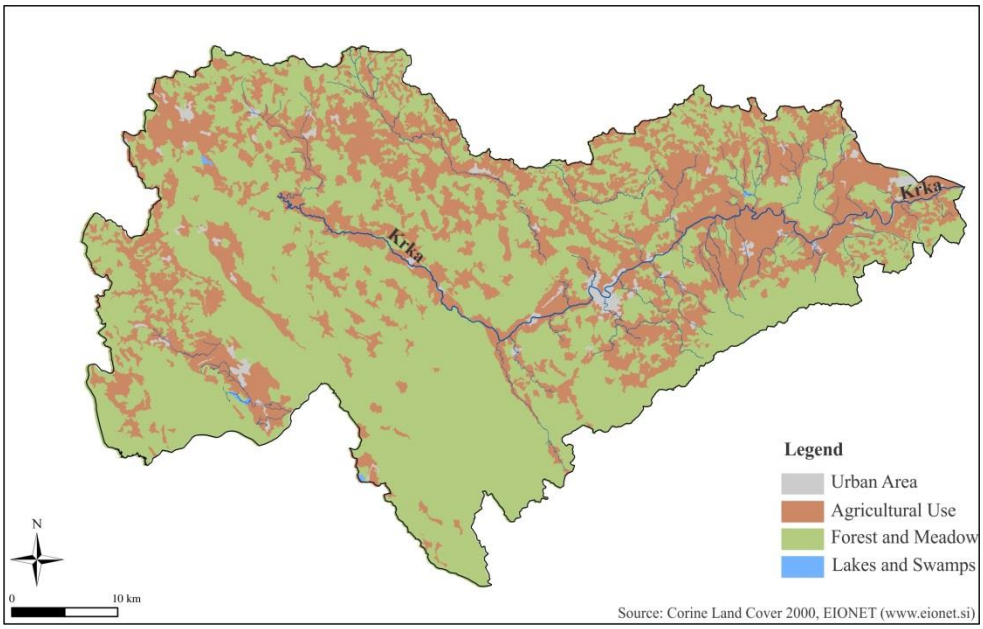

Figure 14: *Land use in the Krka watershed*. The watershed is highly forested at higher altitudes (< 650 m), whereas the land used for agricultural activities is located mainly in the flat areas of the watershed.

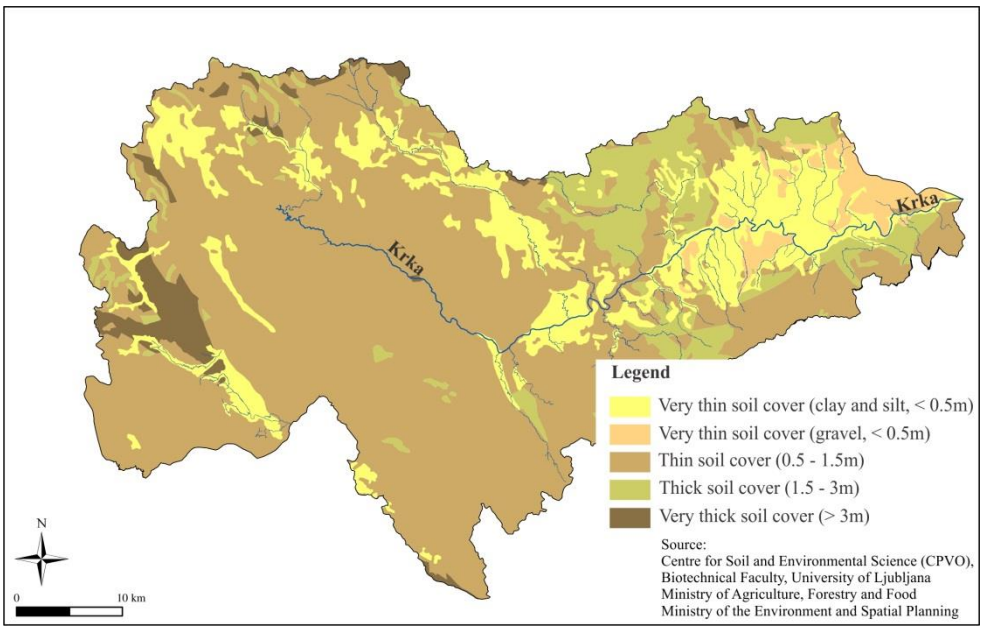

Figure 15: *Soil cover in the Krka watershed.* Due to intensive weathering of carbonate bedrock, the soil cover in the Krka watershed can be up to 3 m thick. The thickness of the soil cover mainly ranges from 0.5 to 1.5 m. The thinnest soil cover is in the river valley, especially in the east.

4 Materials and Methods

For the purposes of this study, river water samples and tufa precipitates were collected. Water samples were analysed for determining the content of major ions (Ca^{2+}, Mg^{2+}, Na^{+}, K^{+}, Sr^{2+}, Ba^{2+}, Cl^{-}, SO_4^{2-}, NO_3^{-}), dissolved inorganic and organic carbon (DIC and DOC), and total alkalinity. To distinguish major processes affecting hydro-bio-geochemistry in the watershed stable isotopic composition of oxygen ($\delta^{18}O$) in water and precipitation, dissolved inorganic carbon ($\delta^{13}C_{DIC}$), particulate organic carbon ($\delta^{13}C_{POC}$) and nitrogen ($\delta^{15}N_{PN}$) and sulphate ($\delta^{34}S_{SO4}$) was determined. Tufa samples were examined with optical microscopy and analysed for mineralogical and elemental composition.

The most important aspect on success of any environmental investigation primarily depends on collection of representative samples, contamination free sample handling and storage, adopting appropriate sample decomposition techniques if needed and finally precise and accurate estimation of parameters of interest by standard or advanced analytical techniques (Das, 2008). In this section, the sampling procedures are described first, followed by a detail overview on petrological, field and chemical analyses used to assess the aims of the study. Finally, principles of thermodynamic modelling and isotope fractionation calculations are described.

4.1 Sampling scheme and procedures

4.1.1 Water and precipitation sampling

To achieve highly resolved seasonal and spatial variability of hydro- and biogeochemical processes in the Krka watershed water samples from the main stream and major tributaries of the river were collected between November 2007 and November 2010 on 23 sampling campaigns. The sampling locations, 13 in the main stream of the Krka River and 6 in its major surface tributaries, are shown in Figure 16. Sampling sites were selected on the basis of the tributary position (before and after the confluence with the main channel), spatial distribution of bedrock, tufa barrier occurrence, and population density. Basic watershed characteristics are presented in Table 4.

Data on the amount of precipitation, and daily and monthly discharge was obtained from the meteorological monitoring stations and discharge gauges (Figure 16) operated by The Environmental Agency of the Republic of Slovenia (ARSO). From 2009 to 2010, the precipitation was collected at the precipitation collection station at Dvor pri Žužemberku operated by the ARSO (http://www.arso.gov.si; Figure 16). The sampling period for monthly precipitation lasted from the beginning to the end of the month. Rainwater and/or snow was collected in a separatory funnel each day and the sub-samples were combined in one bottle at the end of each calendar month according to the IAEA recommendations advised in the frame of the GNIP (Global Network of Isotopes in Precipitation) project. Prior to storage, the snow was melted at room temperature. At the end of each calendar month, the monthly precipitation sample was filtered through 2 µm pore size ashless filters (589/3 Whatman, UK). 30 mL of the bulk sample was stored in tightly closed HDPE bottles and kept in dark at 4 °C until analysis.

In water quality surveys, there are typically two types of water samples taken; grab-

samples and composite-samples (Hem, 1985). Composite samples consist of a mixture of several individual grab-samples collected over a period of time (each sample is taken in proportion to the amount of flow at that time). Composite samples provide an estimate of average water quality over a period of sampling, whereas the grab-samples characterize water quality at a particular time, and can only represent the conditions at a particular time. For this study, as for many water surveys, grab-samples were collected for practical reasons such as cost and field logistics.

Table 4: *Sampling network characterization of the Krka headwaters, stream water and tributaries.* Data sources: [1]EIONET (www.eionet.si), [2](Ministry of the Environment and Spatial Planning, The Surveying and Mapping Authority of the Republic of Slovenia).

	Sampling point	Location	Drainage area (km^2)[1]	Height above sea level (m)[2]	Distance from the spring (km)[2]
Krka River headwaters	W1	Gradiček	321	283	0.0
	W2	Poltarica		282	0.5
Krka River stream water	W4	Krka		272	1.7
	W5	Zagradec		251	8.0
	W7	Vrhovo		200	14.5
	W8	Žužemberk		194	18.1
	W9	Dvor		186	22.2
	W10	Soteska	1,105	173	28.4
	W13	Straža		169	34.4
	W15	Češča vas (NM)	1,701	168	39.1
	W16	Otočec		165	51.5
	W17	za Otočcem		164	53.0
	W18	Kostanjevica na Krki	2,238	150	76.2
	W19	Velike Malence	2,350	143	95.0
Krka River tributaries	W3	Višnjica	76	274	0.9
	W6	Globočec		252	8.5
	W11	Radešca	237	171	30.8
	W12	Sušica	36	174	31.9
	W14	Temenica (Prečna)	228	168	38.9

Where possible, the water samples were collected in the channel centre, mostly from road bridges, and at lateral position where the water was most likely to be well mixed. If access was difficult, the water samples were taken as far as possible from the stream bank. Samples were collected using a high density polyethylene (HDPE) jug attached to a rope rolled up to a wide plastic holder. The sampling jug was rapidly lowered below the water surface, preventing the collection of any surface water and floating materials (litter etc.). Once full, the jug was rinsed three times before samples were stored into flask containers. Water and precipitation samples were always stored into new (pre-cleaned) HDPE or glass containers. The sampling and measuring equipment was handled with great care by keeping it clean and maintained in good working order before use and at the end of sampling.

If required, the water samples were filtered through different size-pore filters prior to collection. Table 6 lists the required containers, treatment and preservation technique, maximum storage times, dates of collection, analytical techniques used, and location of the laboratory where analyses were performed. A brief description of the table content is provided here.

Samples for major ion, total alkalinity, DIC and DOC analysis were filtered through 0.45 μm pore-size filters with SFCA membranes (Millipore, UK) and then poured into 60 mL HDPE bottles (Nalgene, USA). Samples for cation analyses were acidified with

Suprapur HNO_3 acid (Merck, Germany) until the pH was below 2 (the volume of acid added was 1 mL per 100 mL of water sample). 12 mL aliquots of water samples for $\delta^{13}C_{DIC}$ analyses were filtered through 0.20 µm pore-size glass-filters with SFCA membranes (Millipore, UK) to suppress bacterial activity and stored in glass serum vials (Exetainer, UK) filled with no headspace. 3 L water samples were collected in pre-washed HDPE bottles for the analyses of isotopic composition of particulate organic carbon (POC) and nitrogen (PN), and sulphate. All water samples were stored at 4 °C until analysis. Water samples for stable isotope analysis of POC, PN and sulphate were filtered through GF/F glass microfiber filters (0.07 µm pore size, Whatman, UK) immediately upon arrival to the laboratory. Total alkalinity and $\delta^{13}C_{DIC}$ values of water samples were determined within 24 hours of sample collection.

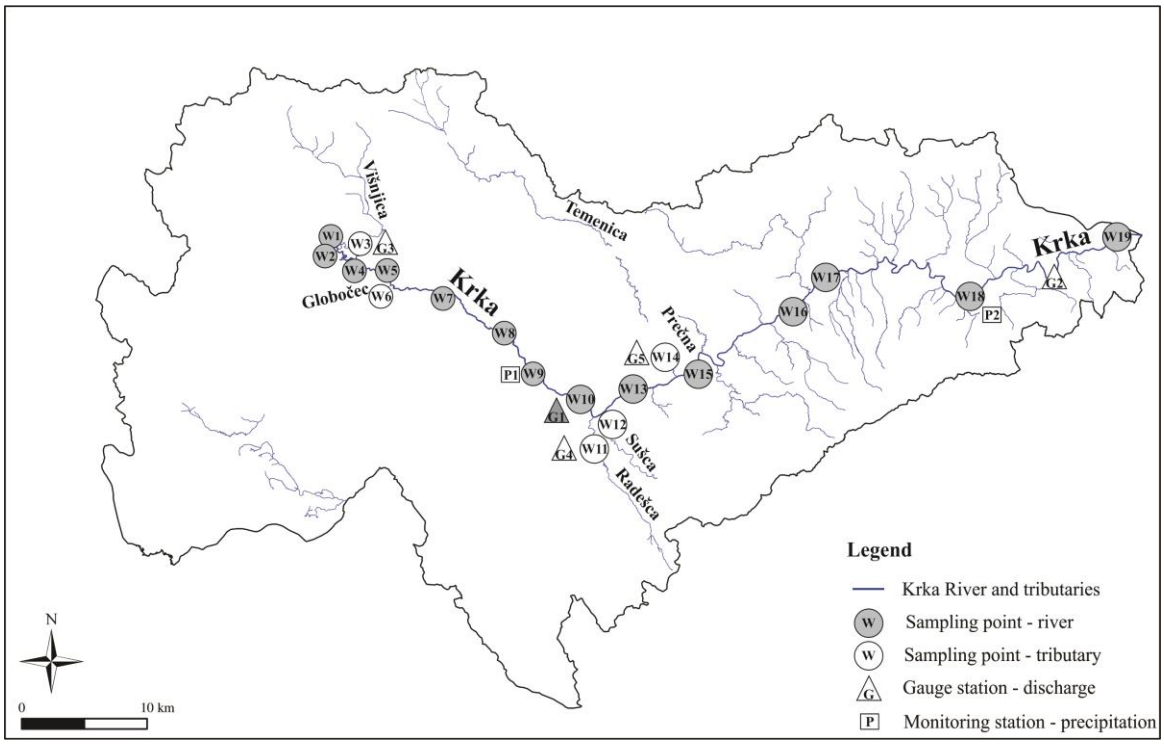

Figure 16: *Water sampling network in the Krka watershed.* The map shows water sampling points (W) in the main channel (coloured circles) and in the tributaries (open circles), discharge gauge stations (G; triangles) and precipitation monitoring stations (P; squares).

4.1.2 Tufa and rock sampling

Tufa samples were collected on 16 largest barriers (Figure 16) that occur in the upper reaches of the Krka River. Characteristics of sampling locations are given in Table 5. Tufa specimens were collected in September 2008 using a geological hammer. After collection they were placed into individual plastic bags and marked properly. After arrival to the laboratory, the samples were dried at room temperature, crushed to powder and stored into new plastic bags. The powder was then analysed for elemental, mineralogical and isotopic composition. In addition, 4 lithologically different bedrock samples, representative for the Krka watershed, were taken.

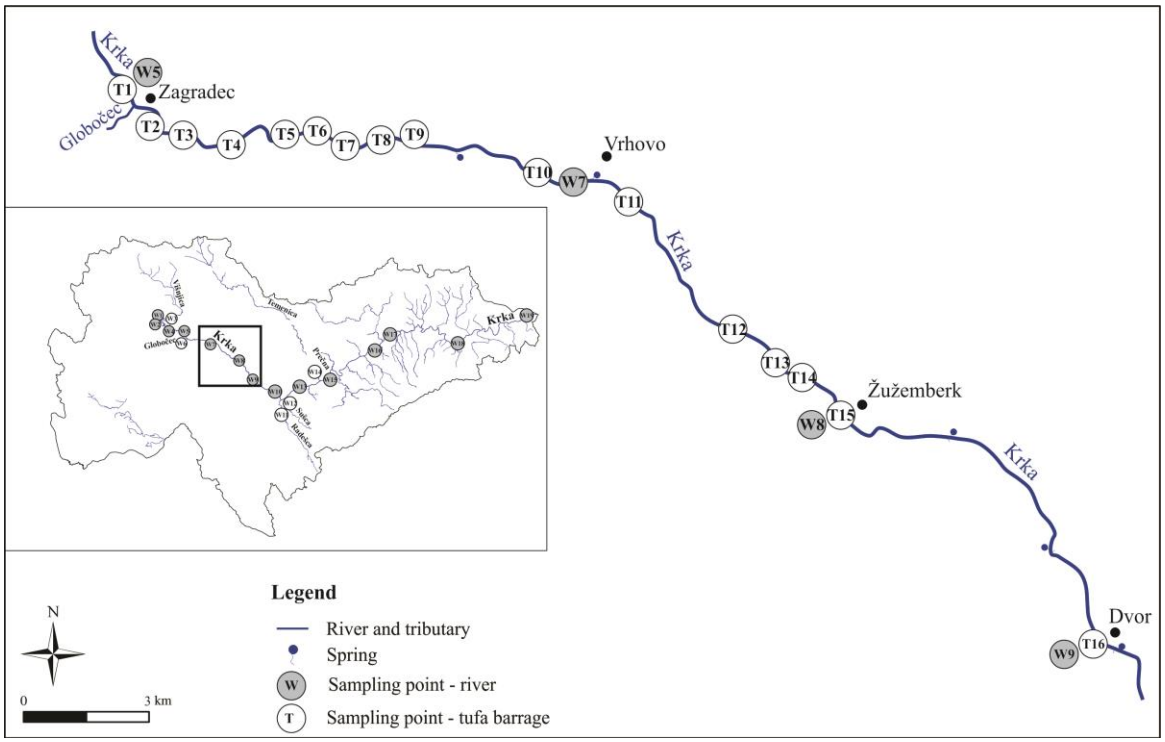

Figure 17: *Locations of sampled tufa barrages in Krka River.* The locations of sampled barrages are indicated on the enlarged section of the river in the left side map and are numbered together with letter "T" indicating a tufa barrage sampling point. Water sampling locations in this river section are indicated with "W" as in Figure 16.

Table 5: *Sampling locations of sampled tufa barriers in the Krka stream.* Data source: [1](Ministry of the Environment and Spatial Planning, The Surveying and Mapping Authority of the Republic of Slovenia).

Sampling point	Location	Height above sea level (m)[1]	Distance from the spring (km)[1]
T1	Zagradec	251	7.40
T2	Bevc	250	7.77
T3	Štupnk	249	8.40
T4	Zagraško smrečje	242	9.04
T5	Okluka	239	9.92
T6	Hinavček	235	10.27
T7	Drašča vas 1	233	10.53
T8	Drašča vas 2	232	10.79
T9	Jožman	232	11.18
T10	Rivc	228	11.42
T11	Poljane	219	12.86
T12	Dimc	204	15.24
T13	Kovačnica	198	16.22
T14	Prapreče	197	16.52
T15	Žužemberk	195	17.14
T16	Dvor	186	21.20

Table 6: *List of sampling and storage procedures and analytical techniques used.*

Type of sample	Parameter	Collection	Type of container	Collection technique, treatment and preservation	Maximum holding time	Analytical technique
Water	Temperature	Nov 2007 - Nov 2010	-	at site	-	Mettler Toledo SevenGo proTM SG8, WTW pH/Cond 340i , Corning 315, WTW pH/Cond 340i
	pH					
	Conductivity					
	Cations (Ca^{2+}, Mg^{2+}, Na^{+}, K^{+}, Sr^{2+}, Ba^{2+})		60 mL HDPE bottle	filter (0.45µm), acidify with HNO_3, cool to 4 °C	6 months	ICP-OES
	Anions (Cl^{-}, SO_4^{2-}, NO_3^{-})	Dec 2009 - Nov 2010	30 mL HDPE bottle	filter (0.45µm), cool to 4 °C		IC
	DIC	Nov 2007 - Dec 2008			few days	IC
	DOC					
	Total Alkalinity	Nov 2007 - Nov 2010	60 mL HDPE bottle		24 hours	Titration with 0.0357M HCl
	$\delta^{13}C_{DIC}$	Nov 2007 - Nov 2010	12 ml glass vial	filter (0.20µm), cool to 4 °C		
	$\delta^{18}O$		30 mL HDPE bottle	filter (0.45µm), cool to 4 °C	indefinite (tightly sealed)	
	$\delta^{13}C_{POC}$	Apr 2010 - Nov 2010	3 L HDPE bottle	collect the filtrate using GF/F filters (0.70µm), filters dried at 60 °C, to remove inorganic carbon acidify with 1M HCl	water < 24 hours, filter (indefinite)	IRMS
	$\delta^{15}N_{PN}$			collect the filtrate using GF/F filters (0.70µm), filters dried at 60 °C		
	$\delta^{34}S_{SO4}$			filter (0.70µm), lower pH to 2 with 3M HCl, precipitate $BaSO_4$ by adding $BaCl_2$ solution, and collect filtrate		

Table 6: *Continued.*

Type of sample	Parameter	Collection	Type of container	Collection technique, treatment and preservation	Maximum holding time	Analytical technique
Precipitation	$\delta^{18}O$	Jan 2009 - Dec 2010	30 mL HDPE bottle	filter (2.0 µm), cool to 4 °C	indefinite (tightly sealed)	IRMS
Tufa	$\delta^{13}C_{tufa}$	Sept 2008	plastic bag	dried and powdered	indefinite	IRMS
	$\delta^{18}O_{tufa}$					
	mineralogy					XRD
	element analyses (major and trace elements)					FUS - ICP
	C and N analyses (C_{tot}, C_{org}, N_{tot})					CHNS-EA
Carbonate rocks	$\delta^{13}C_{carb}$	Sept 2008	plastic bag	dried and powdered	indefinite	IRMS
	element analyses (Ca, Mg, Sr, Ba)					XRF

ICP-OES (Inductively Coupled Plasma/Optical Emission Spectrometry)
ICP-MS (Inductively Coupled Plasma/Mass Spectrometry)
IC (Ion Chromatography)
IRMS (Isotope Ratio Mass Spectrometry)
XRD (X-Ray Diffraction)
XRF (X-Ray Fluorescence)
FUS-ICP (Fusion Inductively Coupled Plasma)
CHNS-EA (Carbon, Hydrogen, Nitrogen and Sulphur Elemental Analyzer)

4.2 Field measurements

Measurements of physicochemical parameters - water temperature, pH and electrical conductivity (EC) - are best accomplished directly in the field by using portable probes. In campaigns from November 2007 to December 2008, we used a portable meter Mettler Toledo *SevenGo pro*^{TM} SG8 for temperature and pH measurements, and Corning meter for electrical conductivity. In 2009 and 2010 sampling campaigns, we used a WTW 340i pH/Cond meter for determining all these parameters.

Prior to use, pH meters were calibrated against commercially available buffer solutions. A Mettler Toledo SevenGo proTM SG8 pH meter was calibrated against three buffer solutions (Mettler Toledo) with pH values of 4.01, 7.00 and 9.21. The WTW 340i pH probe was calibrated against two buffer solutions (WTW) with pH values of 7.00 and 10.00. In both cases, replicate measurements produced an analytical error (1σ) of ±0.1 °C for temperature, ±0.01 unit for pH. The probes for EC measurements were calibrated against KCl solutions (Carlo Erba) of 200 and 500 μS/cm. Replicate measurements of both EC meters used in this study produced an analytical error of ±0.5 %.

4.3 Petrological analyses

Petrological analyses of density measurements, X-ray diffraction and transmitted light microscopy were performed only on tufa samples.

4.3.1 Determination of density of tufa samples

The density of tufa samples was measured on 8 samples. After collection, the samples were weighted (wet weight) immediately upon arrival into the laboratory and dried at room temperature for few days until they were completely dry. The samples were weighted again (dry weight) and the difference between the wet and dry weight was considered as density of the sample.

4.3.2 X-Ray Diffraction analyses

The mineral composition of the samples was determined by X-Ray Powder Diffraction (XRD) using a Philips PW3710 X-ray diffractometer equipped with Cu Kα radiation and a secondary graphite monochromator. The analyses and data treatment were performed at the Faculty of Natural Sciences and Engineering, University of Ljubljana. Data on samples were obtained at 40 kV and a current of 30 mA in a range from 2 to 70° 2θ, with a speed of 3.4 0 2Theta/min. The diffraction patterns were identified with a X'Pert HighScore Plus software with installed PAN-ICSD database. The relative error of the quantification was 5–10 %.

4.3.3 Transmitted light microscopy

After air drying and macroscopic description of collected tufa samples, a more detailed study was carried out on selected samples by conventional transmitted light microscopy of thin sections using Zeiss Axioplan2 microscope. Prior to preparation of thin sections, the samples were first broken into small pieces of approximately 5 × 5 cm and impregnated and confirmed with epoxidal pitch (Araldite). The process was repeated several times. Afterwards, the samples were left to dry for a few days and were then cut into thin sections.

4.4 Chemical analyses

Chemical analyses of water include total alkalinity and major ion concentrations measurements, and stable isotope analyses of oxygen in water, carbon in DIC and POC, nitrogen in PN and sulphur in sulphate. Tufa and carbonate rock samples were anaysed for elemental composition and stable isotope compositions of oxygen and carbon.

4.4.1 Dissolved inorganic carbon (DIC) and dissolved organic carbon (DOC) analyses

The concentrations of DIC and DOC were analysed using a Tekmar Dohrmann DC-190 TOC analyser (Rosemount Analytical Inc., USA) at the Laboratory for Environmental Sciences and Engineering at the National Institute of Chemistry (Slovenia). Primarily, concentrations of total carbon (TC) and dissolved inorganic carbon (DIC) were measured by converting carbon components in the water sample into CO_2 gas. The concentration of DOC was calculated as a difference between TC and DIC concentrations. The analytical precision in case of DIC is ±2 %, while in case for DOC is ±5 %.

4.4.2 Total alkalinity analyses

The alkalinity of a solution is defined as the capacity of solutes it contains to react with and neutralize acid (Hem, 1985). In natural waters, it generally corresponds to measurements of the bicarbonate concentration as the inorganic carbon system is the dominant contributor to alkalinity and, if pH is below 8.3, carbonate concentration is negligible. In theoretic terms, the alkalinity is equivalent to the amount of acid necessary to reach the inflection point of the titration curve between HCO_3^-, H_2CO_3 and CO_2 (Marchetto et al., 1997).

Total alkalinity of a water sample was determined using Gran titration (Gieskes, 1974). The method consists of a stepwise titration, with pH measurements after several additions of titrant acid, in the pH range of 4.5. The proportionality of acid added to the resulting pH was used to determine the equivalence point with a simple mathematical method. The whole procedure on analytical method and mathematical calculation is described below.

The pH meter was standardized using buffer solutions with pH values of 4.01, 7.00, and 9.21 (Mettler Toledo, UK) and as titrant acid we used a certified 0.0357 N HCl (KEFO EEC: 231-714-2). 15 mL of a water sample and a magnetic stir bar was added to a beaker, which was put onto a magnetic stirrer. The sample was first titrated with a particular amount of HCl (0.0357 N) to a pH of 4.50 (4.45–4.55). The amount of acid added was noted down. We continued the titration in 100 µL increments until the pH dropped to approximately 3.2. After each titrant addition we allowed pH reading to stabilize before recording pH.

Mathematically, the volume of titrant added at the equivalence point may be determined from the Gran function (Stumm and Morgan, 1981):

$$F=(V_0+V)\times 10^{-pH} \tag{31}$$

where F is Gran function, V_0 is volume of the acid added when pH drops to 4.5, and V is the total volume of the acid added after pH of 4.5. The alkalinity is reported in equivalents per litre using the following formula:

$$TA = \frac{C_{HCl} \times V_{HCl}}{V_{sample}} \quad (32)$$

where *TA* is total alkalinity, C_{HCl} is titrant concentration (in mol/L), V_{HCl} is volume of acid added, and V_{sample} is volume of the water sample. The overall analytical error of alkalinity measurements was determined on replicate samples and by using standard solution of Na_2CO_3. The analytical error of alkalinity measurements on replicate samples was determined to be ±5 %.

4.4.3 Major ion concentration analyses

Cation concentrations (Ca^{2+}, Mg^{2+}, Na^{+}, K^{+}, Sr^{2+} and Ba^{2+}) were determined by inductively coupled plasma/optical emission spectrometry (ICP/OES). Concentrations were determined using a Jobin Yvon Horiba ICP-OES at the University of Michigan (USA; samples collected in 2007 and 2008) and a Perkin-Elmer Optima 5300 DV ICP-OES instrument at the University of Arizona (USA; samples collected in 2009 and 2010). The accuracy of measurements was controlled by using standard solutions with known element concentrations (SLRS-4, and NIST 1643e). The analytical precision was estimated to be ±2 %.

Concentrations of anions (Cl^{-}, SO_4^{2-} and NO_3^{-}) were determined by a Dionex Ion Cromatograph (IC) DX 600 at the Department of Hydrology and Water Resources, University of Arizona (USA). The standard solutions of known concentration of a particular element were used for accurate measurements of anion concentrations. The analytical error of the method was below ±2 %.

To check the internal analytical consistency charge balance error (C.B.E.), calculations were performed for each sample. The charge balance calculations are based on anion – cation balance, which is defined as a percentage difference between the total positive charge and the total negative charge, defined as follows (Murray and Wade, 1996):

$$\text{C.B.E. (\%)} = \frac{\sum(\text{cations - anions})}{\sum(\text{cations + anions})} \cdot 100 \quad (33)$$

where contributions to charge are in units of meq/L. The majority of the data were within ±5 % and those whose C.B.E was calculated to be over ± 10 % were excluded from further data processing.

4.4.4 Elemental analyses

Tufa samples were analysed for C, N, Ca, Mg, Na, K, Sr and Ba content, while the rock samples were analysed for Ca, Mg, Sr and Ba. Elemental analysis of total carbon (C_{tot}), organic carbon (C_{org}) and total nitrogen (N_{tot}) were performed using a CHN EA1108 – Elemental Analyzer (CarloErba Instruments, UK) at the National Institute of Biology (Slovenia). For each analysed element, approximately 10 mg of sample was weighted into silver capsules (9 × 5 mm). In case for C_{tot} and N_{tot}, the capsules with the sample were tightly closed and analysed in the analyser, whereas for C_{org} analysis, the sample was gradually acidified with 0.1M, 0.5M, 1M, 2M and 6M HCl. The sample was ready to analyse when no dissolution of carbonate occurred after acidification with 6M HCl (Pella and Colombo, 1978). The capsules were dried in the oven at 60 °C overnight and afterwards tightly closed and analysed.

In the analyser, the samples were oxidized at 950 °C in a pure oxygen environment using tungstic oxide/zirconium oxide as catalysts. During this process, gasses were produced (e.g. CO_2 and NO_x) and passed through a column of elemental copper, wherein

NO_x's were reduced to N_2 and halogen compounds removed. After being brought to a constant pressure, temperature, and volume, the resulting gases were homogenized in a mixing chamber, and separated in a stepwise steady-state manner. Concentrations of C and N were detected as a function of their thermal conductivities (Ryba and Burgess, 2002). The sulphanilamide ($H_2NC_6H_4SO_2NH_2$) was used as a standard to achieve the accuracy of the measurements of ±3 %, while the precision of ±3 %, was assured by replicate measurements of the samples and standards.

Major elements (Ca, Mg, Na, K) and selected trace elements (Sr and Ba) in tufa samples were measured by fusion – inductively coupled plasma (FUS-ICP) at the AcmeLab, Canada. Samples were first fused with a lithium borate flux and heated until the sample is completely dissolved to form a perfectly homogenous mass. The molten material is poured into a high purity acid (usually HNO_3) and as such analysed by ICP. To determine the accuracy of the measurements, the following certified reference materials (CRM) were used NIST 694, NIST 696, NIST 1633b, DNC-1, GBW 07113, W-2a, DTS-2b, SY-4 and BIR-1a. The accuracy, based on CRM measurements, was ±5 %.

4.4.4.1 X – Ray fluorescence analysis

Elemental analyses of the carbonate bedrock (limestone and dolomite) were performed using Termo Scientific NITON X-Ray Fluorescence analyser (model XL3t GOLDD 900S-He) at the Faculty of Natural Sciences and Engineering, University of Ljubljana. The samples of solid rocks were cut into pieces to obtain a flat surface of the analysed rock sample. In the process of measurements the "Mining" filter of the original producer was used. The accuracy of measurements was controlled by using certified reference materials NIST 1d and NIST 88b with known element concentrations. The analytical precision was estimated to be ±2 %.

4.4.5 Stable isotope analysis

All stable isotope analyses of river water, particulate organic carbon and nitrogen, and tufa samples were performed in the laboratories of the Group for the Isotope Geochemistry at the Department of Environmental Sciences at the Jožef Stefan Institute (Slovenia).

The isotope ratio mass spectrometers (IRMS) used in this study were Europa Scientific 20–20 with ANCA TG and ANCA SL preparation module, IsoPrime MS with MultiFlow Bio module and Varian MAT 250 IRMS. Analytical precision and accuracy were evaluated using certified reference materials (CRM) and working standards (WS). The latter were prepared in the laboratory. Working standards for $\delta^{13}C_{DIC}$ analyses were calibrated using gaseous CO_2 certified reference materials RM8562, RM8563, and RM8564, while the working standards of tap water, snow and ice for $\delta^{18}O$ analyses were calibrated against VSMOW2, GISP and SLAP2 reference materials. Reference materials were always added into a batch of samples for additional accuracy determinations. The list of all standards used for stable isotope analysis and their δ values are reported in Table 7.

The results of stable isotope analyses in this study are reported using the δ notation as a difference in parts per mil of the isotopic ratios of $^{18}O/^{16}O$, $^{13}C/^{12}C$, $^{15}N/^{14}N$ and $^{34}S/^{32}S$ in the sample from those of the international reference materials VSMOW (Vienna Standard Mean Ocean Water) for hydrogen and oxygen, VPDB (Vienna Pee Dee Belemnite) for carbon, AIR for nitrogen and VCDT (Vienna Canyon Diablo Troilite) for sulphur. The precisions of the measurements were as follows: ±0.1 ‰ for $\delta^{18}O$ in water, ±0.2 ‰ for $\delta^{13}C$ in DIC and POC, ±0.3 ‰ for $\delta^{15}N$ in PN, ±0.3 ‰ for $\delta^{34}S$ in SO_4^{2-}, and

±0.05 ‰ for $\delta^{13}C$ and $\delta^{18}O$ in $CaCO_3$.

Table 7: *List of reference and working materials used for stable isotope analyses.* All δ values are certified or recommended (*) values reported by the IAEA (www.iaea.au). The δ values of Working Standards were determined in the Laboratory of Stable Isotope Geochemistry at the Department of Environmental Sciences (Jožef Stefan Institute).

	Name	Analyte	Material	δ value (‰)
Certified Reference Materials	RM8562	$\delta^{13}C_{DIC}$	$CO_{2\ (g)}$	-3.72 ± 0.04
	RM8563			-41.59 ± 0.06
	RM8564			-10.45 ± 0.04
	VSMOW2	$\delta^{18}O$	Water	0 ± 0.02*
	SLAP2	$\delta^{18}O$		-55.5 ± 0.02*
	GISP	$\delta^{18}O$		-24.76 ± 0.09
	IAEA CH-3	$\delta^{13}C_{POC}$	Cellulose	-24.74 ± 0.041
	IAEA CH-6		Sucrose	-10.45 ± 0.03
	IAEA CH-7		Polyethylene	-32.15 ± 0.05
	IAEA N-1	$\delta^{15}N_{PN}$	Ammonium Sulphate	+0.4 ± 0.2
	IAEA N-2			+20.3 ± 0.2
	IAEA SO-5	$\delta^{34}S_{SO4}$	Barium Sulphate	+0.5 ± 0.2*
	IAEA SO-6			-34.1 ± 0.2*
	NBS 127			+20.3 ± 0.4*
	IAEA CO-1	$\delta^{13}C_{tufa,\ carb}$	Marble	+2.492 ± 0.030
		$\delta^{18}O_{tufa}$		-2.4 ± 0.1*
	IAEA CO-8	$\delta^{13}C_{tufa,\ carb}$	Calcite	-5.764 ± 0.032
		$\delta^{18}O_{tufa}$		-22.7 ± 0.2*
	IAEA CO-9	$\delta^{13}C_{tufa,\ carb}$	Barium Carbonate	-47.321 ± 0.057
		$\delta^{18}O_{tufa}$		-15.6 ± 0.2*
	NBS 18	$\delta^{13}C_{tufa,\ carb}$	Calcite	-5.014 ± 0.035
		$\delta^{18}O_{tufa}$		-23.2 ± 0.1*
	NBS 19	$\delta^{13}C_{tufa,\ carb}$	TS - Limestone	+1.95
		$\delta^{18}O_{tufa}$		-2.20
Working Standards	CO2/1 ISO TOP (Messer)	$\delta^{13}C_{DIC}$	$CO_{2\ (g)}$	-3.62 ± 0.2
	CO2/2 ISO TOP (Messer)			-46.92 ± 0.2
	DIC standard (Carlo Erba)		$Na_2CO_{3\ (aq)}$	-10.8 ± 0.2**
	DIC standard (Fisher Scientific)			-4.5 ± 0.2**
	snow	$\delta^{18}O$	Water	-19.67
	tap water	$\delta^{18}O$		-9.07
	milliQ	$\delta^{18}O$		0.38
	Europa N	$\delta^{15}N_{PN}$	Urea	+2.5 ± 0.2
	KH-2	$\delta^{13}C_{tufa,\ carb}$	Limestone	+1.97
		$\delta^{18}O_{tufa}$		-2.96

4.4.5.1 Stable isotope analyses of water samples and precipitation ($\delta^{18}O$)

The water equilibration method developed by Epstein and Mayeda (1953) was used for determination of oxygen isotopic composition ($\delta^{18}O$) in water samples and precipitation. The analysis is not carried out directly on the sample but on an equilibration CO_2 gas that is introduced into the headspace of the sample vessel in a flow of helium. The isotopic equilibration between CO_2 and water is as follows:

$$^{16}CO_2 + H_2{}^{18}O \leftrightarrow C^{16}O^{18}O + H_2{}^{16}O \quad (34)$$

The $\delta^{18}O$ values of samples collected in 2008 were determined by using a Varian MAT 250 isotope ratio mass spectrometer (IRMS), whereas the IsoPrime IRMS with a MultiFlow Bio module was used for the analysis of water and precipitation samples collected in 2009 and 2010. First, the water sample is introduced into a sample vial and then flushed with an equilibration gas mixture. During the flushing stage, the air that was originally present in the headspace of the vial is replaced with the CO_2 and helium mixture using a double-hole needle which allows the equilibration gas to flow through the headspace. Once the headspace has been flushed, the samples are left to isotopically equilibrate with the mixed gas. The equilibration reaction is faster at higher temperatures and lasts for 4.5 hours at temperature 40 °C. After the equilibration, the gas is sampled with the needle, separated by chromatography and passed to the mass spectrometer.

4.4.5.2 Stable isotope analyses of dissolved inorganic carbon ($\delta^{13}C_{DIC}$)

For carbon isotope analyses in dissolved inorganic carbon, we used a gas evolution technique (Atekwana and Krishnamurthy, 1998). This procedure uses glass vials to collect, react and extract DIC from natural water samples by converting DIC into gaseous CO_2 via acidification of a water sample. The carbon isotope ratios of DIC ($\delta^{13}C_{DIC}$) in water samples collected during 2008 were determined using a Europa Scientific 20–20 IRMS with an ANCA-TG preparation module, while samples collected in 2009 and 2010 were analysed on an IsoPrime mass spectrometer with a MultiFlow Bio module. Both spectrometers are equipped with autosampler bench.

The method employs septum-capped glass vials (Labco exetainer, UK) that can be analysed using an autosampler. Prior to analysis, a few droplets of phosphoric acid were added into the vial and flushed with He 6.0 in the autosampler by penetrating the butyl rubber septa of the exetainer's disposable caps using a double-hole needle. Three aliquots of the water sample were injected into the exetainer using a needle syringe and left for 24 hours at room temperature. A special care was taken to avoid small air bubbles that become trapped in the syringe while the sample is drawn up. The CO_2 in the headspace of the exetainer was analysed for stable carbon isotope composition.

The isotopic composition of DIC in water samples collected in sampling campaigns during 2008 was measured on Europa Scientific 20–20 IRMS with ANCA-TG preparation module. The amount of sample used was 6 mL. Water samples collected in 2009 and 2010 were analysed on IsoPrime IRMS with a MultiFlow Bio module and the amount of sample used was 2 mL. Both instruments were calibrated against NIST reference materials described below. The differences between the results obtained from Europa Scientific 20–20 and IsoPrime IRMS were in the range of analytical error.

Because there are no durable DIC standards available for stable isotope analysis, the precision and accuracy of the measurements was verified by using working standard solutions of Na_2CO_3 (Carlo Erba and Fisher Scientific) with a concentration of 4.8 mM to control the accuracy of measurements and $\delta^{13}C_{DIC}$ values of -10.8 ‰ and -4.5 ‰ values (Kanduč, 2006).

4.4.5.3 Stable isotope analyses of sulphate ($\delta^{34}S_{SO4}$)

Dissolved sulphate was precipitated as $BaSO_4$ by adding a saturated solution of 1M $BaCl_2$ and 3M HCl to lower the pH of water to prevent $CaCO_3$ precipitation. The precipitate was collected on a GF/F glass filter paper (Whatman, UK) and washed with deionized water. The filters were dried at 60 °C. 1 mg of precipitated $BaSO_4$ was scratched of the filter and put into a tin capsule (SerCon, UK). Few granules of SiO_2 – V_2O_5 mixture were added into the capsule. The $\delta^{34}S$ values of sulphate were determined using Europa Scientific 20–20 IRMS with ANCA-SL preparation module.

4.4.5.4 Stable isotope analyses of carbonate rocks ($\delta^{13}C_{carb}$) and tufa ($\delta^{13}C_{tufa}$)

The method for analysing stable carbon and oxygen isotopic composition of carbonates is based on treatment of a carbonate sample with ortophosphoric acid (McCrea, 1950):

$$CaCO_{3(s)}+H_3PO_{4(s)}\rightarrow Ca_3(PO_4)_{2(l)}+3H_2O_{(l)}+3CO_{2(g)} \quad (35)$$

The tufa samples were analysed for stable carbon and oxygen isotopic composition ($\delta^{13}C_{tufa}$ and $\delta^{18}O_{tufa}$), whereas the carbonate rock samples were analysed only for stable carbon isotopic composition ($\delta^{13}C_{carb}$). The phosphoric acid used for the analyses was prepared by heating a mixture of 85 % H_3PO_4 (Acros Organics, UK) and 99.9 % P_2O_5 (Sigma Aldrich, UK) following the procedure described in Sharp (2007). Such solution is known as ortophosphoric acid with a density of ~1.9 g/cm^3 and since it does not contain any water, it is suitable for determination of stable oxygen isotopic composition in carbonates.

Approximately 10 to 20 mg of bulk tufa sample was weighed into a glass vial. Into a special side canal of the vial 2 mL of H_3PO_4 was added. The vial was then attached to a line connected to a vacuum system. When all the air was pumped out of the system, each vial was leaned in a way that the acid in the canal poured onto the tufa sample. The vials were then placed into a water bath at 65 °C for few hours and left over night to let the reactions complete. At room temperature only calcite reacts, while the dolomite completely dissolves at temperatures < 50 °C. The released CO_2 was then introduced into the Varian Mat 250 IRMS inlet system and analysed on the mass spectrometer collector. Because the CO_2 analysed contains only 2/3 of oxygen from the carbonate and 1/3 stays in the water (equation 35), a fractionation factor of 1.03086 (Friedman and O'Neil, 1977) had to be considered in the final reporting of isotopic composition of tufa samples.

The $\delta^{13}C_{carb}$ was analysed on Europa Scientific 20–20 with ANCA-TG preparation module. The procedure of measurements is identical to the one described in the section 4.4.5.2 However, the sample preparation was slightly modified; in case of carbonate rock analyses, approximately 8–10 mg of powdered rock or filter fragments in the case of PIC analyses, were placed into the exetainer. The exetainer was then purged with He (6.0) and afterwards, heated 100 % H_3PO_4 was added. The released headspace CO_2 was then used for measuring the carbon isotopic composition of carbonate rocks ($\delta^{13}C_{carb}$).

4.4.5.5 Stable isotope analyses of particulate organic matter ($\delta^{13}C_{POC}$ and $\delta^{15}N_{PN}$)

For isotope analysis of particulate organic carbon ($\delta^{13}C_{POC}$) and nitrogen ($\delta^{15}N_{PN}$), 3 L of water was filtered immediately upon arrival to the laboratory. The water samples were filtrated through pre-combusted (at 450 °C for 4.5 hours) GF/F glass filters with 0.07 µm pore size (Whatman, UK). For $\delta^{13}C_{POC}$ analysis the suspended matter, collected on the filter, was treated with 1M HCl acid to remove the inorganic carbonate fraction, whereas the filters used for $\delta^{15}N_{PN}$ analysed directly. The samples were scratched from the filters and added into tin capsules (SerCon, UK); approximately 1 mg of the filtrated matter was needed for determining $\delta^{13}C_{POC}$ and 5 mg for determining $\delta^{15}N_{PN}$ values. The tin capsules were compressed and placed into autosampler together with standard and reference materials. Each sample was then combusted at 1000 °C in the oxidation tube flushed with O_2 gas. The resulting gases are first lead to the reduction tube filled with cooper and heated to 600 °C, and then to the gas chromatograph. The gas of interest, CO_2 in the case of $\delta^{13}C$ analyses or N_2 in the case of $\delta^{15}N$ analyses, is then transferred into the mass spectrometer.

4.5 Thermodynamic modelling and isotope fractionation calculations

Geochemical calculations were performed with the computer program PHREEQC (Parkhurst and Appelo, 1999) using a phreeqc database in order to calculate carbon species concentrations, partial pressure of CO_2 (pCO_2), and saturation states/indices with respect to calcite and dolomite in the water samples.

The pCO_2 was obtained from the equation (27):

$$pCO_2 = \frac{[HCO_3^-][H^+]}{K_H K_1} \tag{36}$$

where K_H and K_1 are the temperature-dependant Henry's law and first dissociation constants for CO_2 in water. The saturation states (Ω) and saturation indices (SI) with respect to calcite ($\Omega_{calcite}$ and $SI_{calcite}$, respectively) and dolomite ($\Omega_{dolomite}$ and $SI_{dolomite}$, respectively):

$$\Omega_{calcite} = \frac{[Ca^{2+}][CO_3^{2-}]}{K_{calcite}} \tag{37}$$

$$SI_{calcite} = \log\Omega_{calcite} \tag{38}$$

$$\Omega_{dolomite} = \frac{[Ca^{2+}][Mg^{2+}][CO_3^{2-}]}{K_{dolomite}} \tag{39}$$

$$SI_{dolomite} = \log\Omega_{dolomite} \tag{40}$$

where brackets denote activities of Ca^{2+}, Mg^{2+} and CO_3^{2-} ions and $K_{calcite}$ and $K_{dolomite}$ are solubility products of calcite and dolomite, respectively (Appelo and Postma, 2009).

5 Results

5.1 Hydrochemistry

The multi-year results (2007–2010) of geochemical analyses of water from the main Krka channel and its six major tributaries are shown in Appendix 1. The table presents results on the measurements of physicochemical parameters (water temperature, pH, electrical conductivity), major ion concentrations (Ca^{2+}, Mg^{2+}, Na^{+}, K^{+}, Sr^{2+}, Ba^{2+}, Cl^{-}, SO_4^{2-}, and NO_3^{-}), dissolved inorganic and organic carbon (DIC and DOC), total alkalinity, and stable isotopic composition of carbon in DIC ($\delta^{13}C_{DIC}$), oxygen in water ($\delta^{18}O$), carbon and nitrogen in particulate organic carbon ($\delta^{13}C_{POC}$ and $\delta^{15}N_{PN}$), and sulphur in sulphate ($\delta^{34}S_{SO4}$). The calculated parameters, CO_2 partial pressures (pCO_2) and saturation indices for calcite ($SI_{calcite}$) and ($SI_{dolomite}$) are added to Appendix 1. Stable oxygen isotopic composition ($\delta^{18}O$) of precipitation collected in 2009 and 2010 is reported in Appendix 2.

5.1.1 Hydrological characteristics (water temperature, discharge and precipitation)

The main climatological station for the Krka watershed area is a meteorological station at Novo mesto (Figure 16) where data on climatological measurements (e.g. precipitation amount, air temperatures) are monitored on hourly/daily/monthly basis. The station is operated by ARSO. In the period of 2007 to 2010 the mean annual air temperature at Novo mesto was 10.5 °C. Temperatures in spring and summer were the highest, 20.2 °C and 24.0 °C, respectively, while in autumn and winter the average temperature was 9.1 °C and 6.1 °C, respectively (ARSO).

The average annual amount of precipitation, measured in the period 1971–2000 at Novo mesto meteorological station is 1147 mm (Dolinar, 2008). Based on precipitation amount data from 13 precipitation monitoring stations located in the watershed (Figure 16) the precipitation amounted to 1259, 1143 and 1456 mm in 2008, 2009 and 2010, respectively (Figure 18). The precipitation was almost evenly distributed throughout the year, but was nevertheless higher during the summer (monthly average 350 mm through downpours and storms) than in winter (average 234 mm). Differences in spatial distribution of precipitation in the Krka watershed are clearly pronounced. Due to higher altitude in the west (average 450–600 m above sea level) the average precipitation amount was 1456 mm and 1140 mm in the east (~ 150 m above sea level). Moreover, the snow cover in the west lasted from 5 to 25 days longer than in the east. The longest retention of snow cover lasted for 104 days in 2010 and only 26 and 46 days in 2008 and 2009 (number of days of snow cover observed in the period 1971–2000 was 60–100 days per year, ARSO).

The chemical composition of the precipitation was not determined in this study, however, a knowing major ion content is relevant for further discussion. Here, we report average annual chemical composition of wet deposition (rainwater) in the sampling period of 2008–2010 (Table 8) obtained from the national precipitation monitoring programme of the Environmental Agency of Slovenia.

Table 8: *Mean wet precipitation deposition during 2008 and 2010 at two nearest monitoring stations (Ljubljana and Iskrba) operated by ARSO.* Data was obtained from the ARSO website (http://www.arso.gov.si/zrak/kakovost%20zraka/).

Sampling Year	EC (µS/cm, at 25°C)	pH	Ca^{2+} (µM)	Mg^{2+} (µM)	Na^{+} (µM)	K^{+} (µM)	Cl^{-} (µM)	SO_4^{2-} (µM)	NO_3^{-} (µM)
2008	12.5	5.01	11.48	2.88	14.41	0.90	15.49	13.06	23.06
2009	11.0	5.00	7.98	2.47	10.48	0.90	12.68	12.23	20.80
2010	9.5	5.04	6.36	2.06	7.86	1.28	7.75	8.74	18.22

Continuous river flow data were available for two gauge stations at Soteska and Podbočje (Figure 16). In a sampling period between November 2007 and November 2010 an average monthly discharge at the gauge station Podbočje was 65 m^3/s in winter and autumn, 51 m^3/s in spring, and 32 m^3/s in summer (Figure 18). Above-average quantities usually occurred from December to May. The highest discharges were measured from September to October 2010 due to extremely high amount of precipitation (506 mm), which flooded large areas in the watershed, especially in the east. Precipitation amount and average monthly discharge values measured during 2007 and 2010 are in a weak positive correlation (R = 0.49). On a basis of seasonal groups of the data, the correlation between precipitation and discharge is high in summer (R = 0.89), while during other seasons only a weak positive correlation with a low level of significance (p > 0.05) was observed.

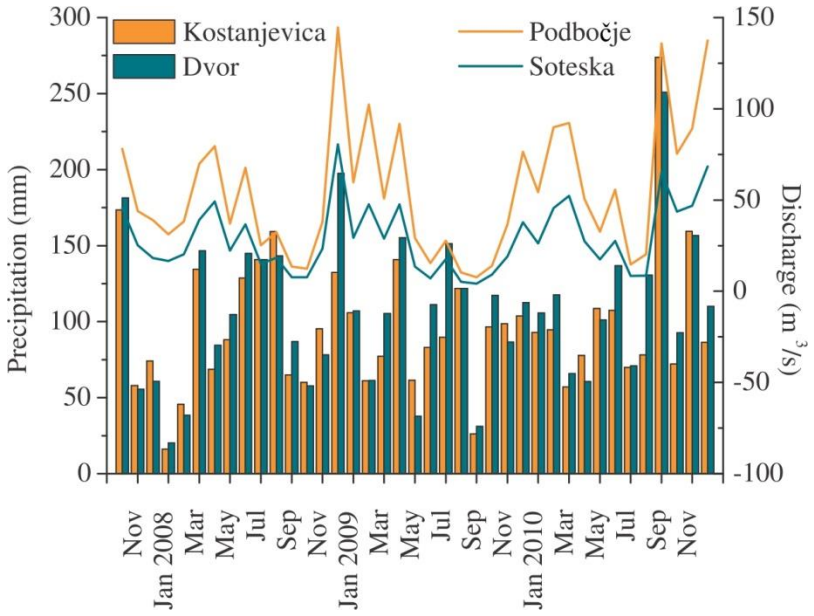

Figure 18*: Precipitation amount and average water discharge in the Krka watershed during 2007 and 2010.* The bars represent precipitation amount at two monitoring stations; the amount at station Dvor is representative for west while that at station Kostanjevica is representative for the east of the Krka watershed. Discharge at gauge stations at Soteska and Podbočje represent the amount of water flow in the upper and lower reaches, respectively. Locations of the monitoring and gauge stations are presented in Figure 16. The data was obtained from the ARSO website.

5.1.2 Physicochemical characteristics

Water Temperature

The water temperatures followed a trend of warm and cold periods. Mean water temperature during the study was 11.7 °C; minimum and maximum values were 4.4 °C (February 2009) and 21.8 °C (August 2010), respectively (Figure 19). The temperatures in the headwaters ranged from 4.4 °C in winter to 14.9 °C in summer (average 10.3 °C). In summer and spring, the water temperatures generally increased downstream, whereas in winter and late autumn an inverse trend was observed. Among the tributaries, the Višnjica and Sušca (sampling points W3 and W12, respectively; Figure 16) exhibited the highest temperatures, up to 21.7 °C and 24.3 °C, respectively. In other tributaries, the water temperatures were lower and ranged from 8.3 to 12.3°C (average 10.8 °C) in tributaries Globočec, Radešca (7.4–13.8 °C) and from 8.3 to 20.0 °C (average 11.8 °C) in Prečna (sampling points W6, W11 and W14, respectively, Figure 16) The differences in water temperatures between the tributaries and the water in the main channel were the largest in summer (Figure 19).

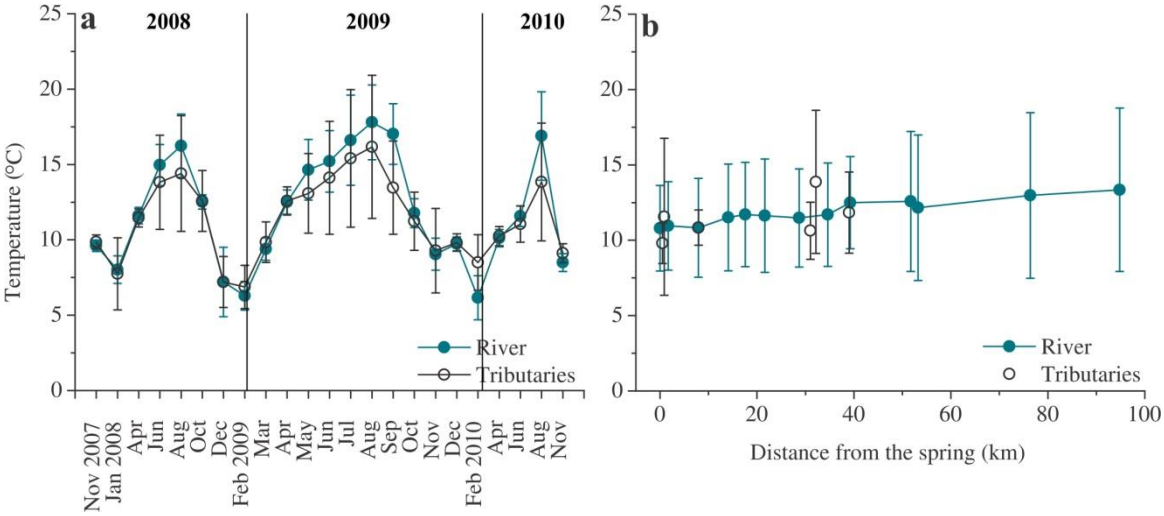

Figure 19: *Seasonal (**a**) and downstream (**b**) variations of temperature in Krka waters.* Points indicate average temperature values and the bars represent standard deviation (1σ) from the average value.

pH

The pH values in the stream water varied from 7.21 to 8.48 (average 7.99 ± 0.27; where ± applies to 1σ). In general, the pH was the lowest in spring and autumn, whereas in summer and winter the pH values were only slightly higher (Figure 20). The pH shows a clear downstream pattern; the lowest pH ranging from 7.10 to 7.73 (average 7.41 ± 0.15) was always measured in the headwaters and gradually increased downstream until sampling point W10 and remained fairly stable thereafter. In all seasons the highest pH was measured in the upper reaches (in the section with tufa barriers), where it ranged from 7.42 to 8.48 (average 8.08). The pH values in the tributaries ranged from 7.38 to 8.52 (average 7.77 ± 0.23). The highest values were observed in the Višnjica tributary (sampling point W3, Figure 20).

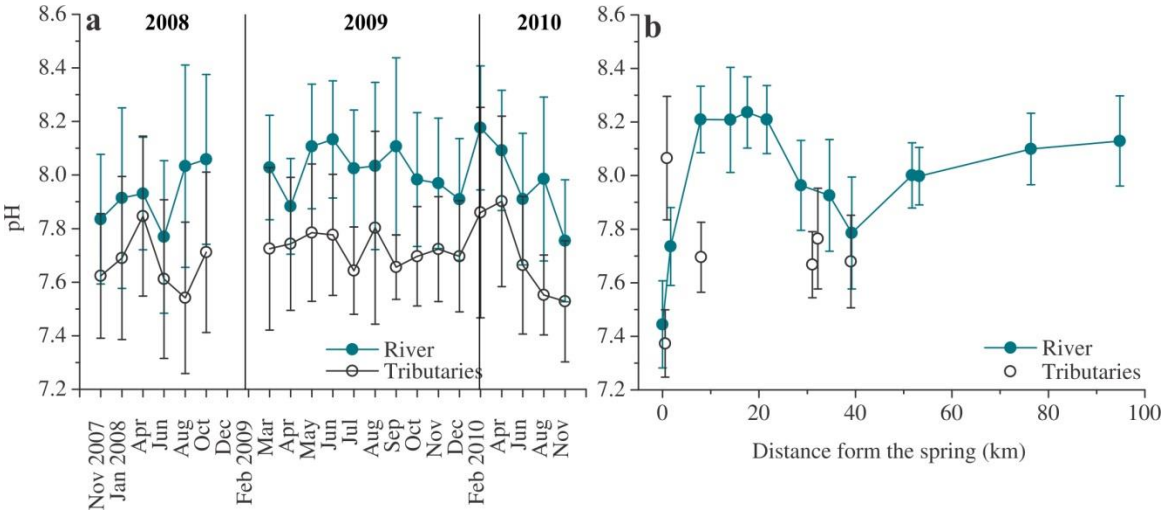

Figure 20: *Seasonal (**a**) and downstream (**b**) variations of pH in Krka waters.* Points indicate average pH values and the bars represent standard deviation (1σ) from the average value.

Electrical Conductivity

Electrical conductivity (EC) in stream water samples ranged from 344 to 534 µS/cm (average 449 µS/cm) and slightly decreased downstream (Figure 21). Similar to pH, no significant seasonal differences were observed for conductivity measurements. The EC values in the tributaries were similar for those draining carbonate bedrock, while in the Višnjica tributary the EC reached up to 656 µS/cm.

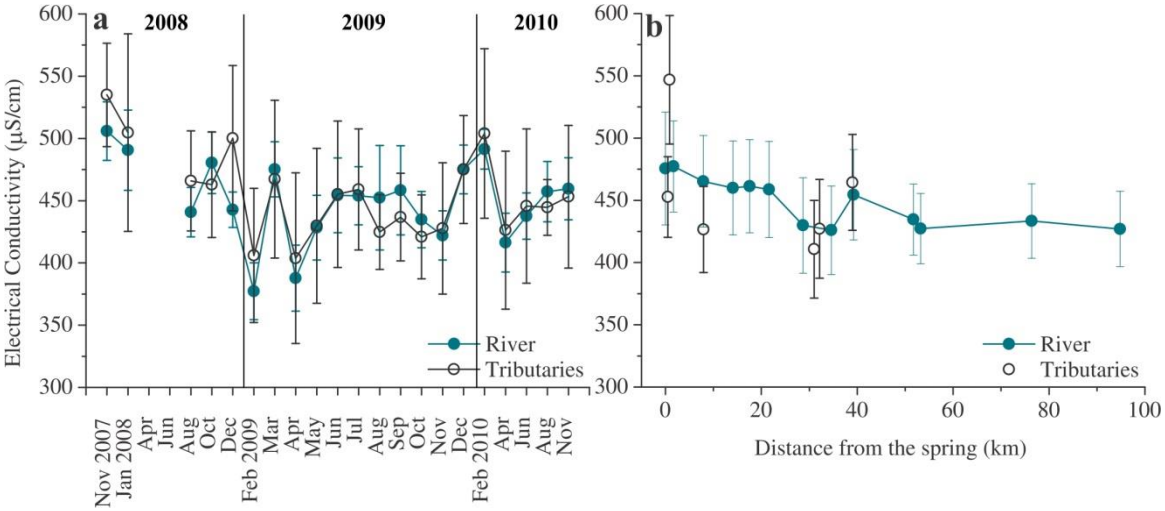

Figure 21: *Seasonal (**a**) and downstream (**b**) variations of electrical conductivity in Krka waters.* Points indicate average EC values and the bars represent standard deviation (1σ) from the average value.

5.1.3 Dissolved solutes

Figure 22 illustrates the relative abundance of major cation and anion components, indicating that the major solute composition of the waters in the Krka watershed is dominated by Ca^{2+}, Mg^{2+} and HCO_3^- ions. All dissolved species showed a weak negative correlation with discharge, demonstrating that the runoff is only a minor factor controlling the behaviour of the species.

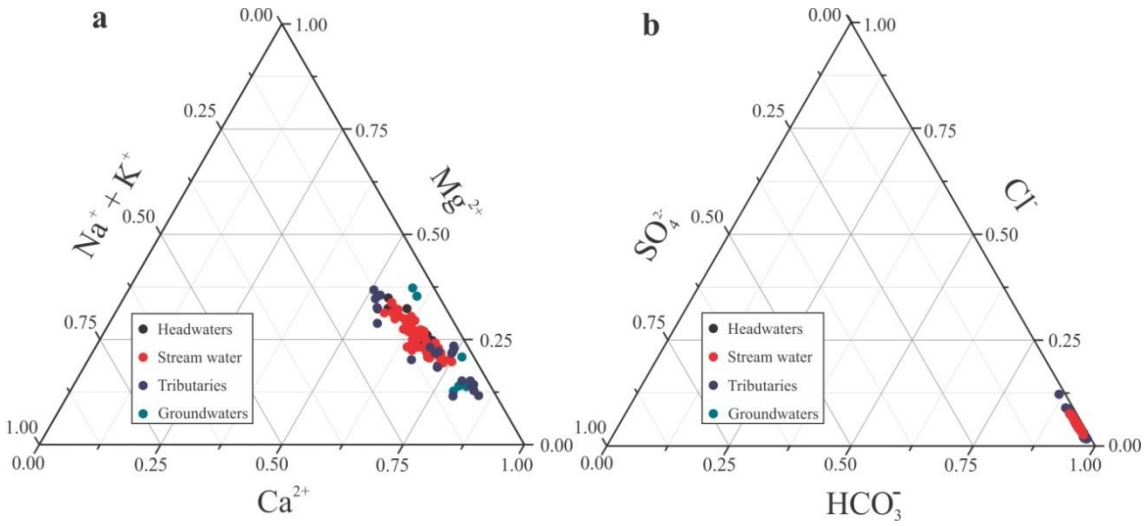

Figure 22: *Ternary diagrams showing major ion chemistry for the headwaters, tributaries, stream water and groundwaters in Krka watershed.* The data shown on the diagram is for the samples collected in 2010 sampling campaigns, in which the samples were analysed for both, cation (**a**) and anion (**b**) concentrations. The data on groundwater ion concentrations was obtained from the ARSO website. The scale presents proportions (× 100 %).

The seasonal and spatial variability of major ion chemistry of the Krka watershed is summarized in Figures 23 to 42. The results of each parameter are based on seasonal and downstream variations; the values shown represent average monthly or annual values and the bars are standard deviation from an average value. A description of results of measured and calculated parameters is provided below.

Cations

Ca^{2+} and Mg^{2+} accounted for 87 to 96 % of the total cations in the stream water and from 88 to 99 % in the tributaries. Na^+ attributed up to 15 % to the total cation budget, K^+ up to 4 %, and Sr^{2+} and Ba^{2+} only up to 0.2 % and 0.01 %, respectively. In the main stream of the Krka, Ca^{2+} concentrations ranged from 1.30 to 1.98 mM (average 1.69 ± 0.13 mM) without any noticeable seasonal or spatial differences (Figure 23a). In general, the lowest average concentrations were measured for summer (1.62 ± 0.11 mM) and spring water samples (1.64 ± 0.09 mM), while in autumn and winter the average Ca^{2+} concentrations were slightly higher, 1.76 ± 0.13 mM and 1.75 ± 0.09 mM, respectively. In comparison with stream water, the Ca^{2+} concentrations in the tributaries followed the same seasonal pattern but were commonly higher and ranged from 1.45 to 2.24 (average 1.84 ± 0.16 mM).

In contrast to Ca^{2+} behaviour (Figure 23b) in the Krka stream water, Mg^{2+} concentrations, ranging from 0.30 to 1.26 mM (average 0.75 ± 0.20 mM), were decreasing downstream (Figure 23d). During all sampling years, the Mg^{2+} concentrations were the lowest in spring (average 0.66 ± 0.19 mM), whereas in other seasons the average concentrations were approximately 0.10 mM higher (Figure 23c). The Mg^{2+} content in the

tributaries was slightly lower than in the main channel, ranging from 0.21 to 0.99 mM (average 0.46 ± 0.18 mM), except in the Višnjica tributary where the Mg^{2+} content was the highest (0.88–1.39 mM).

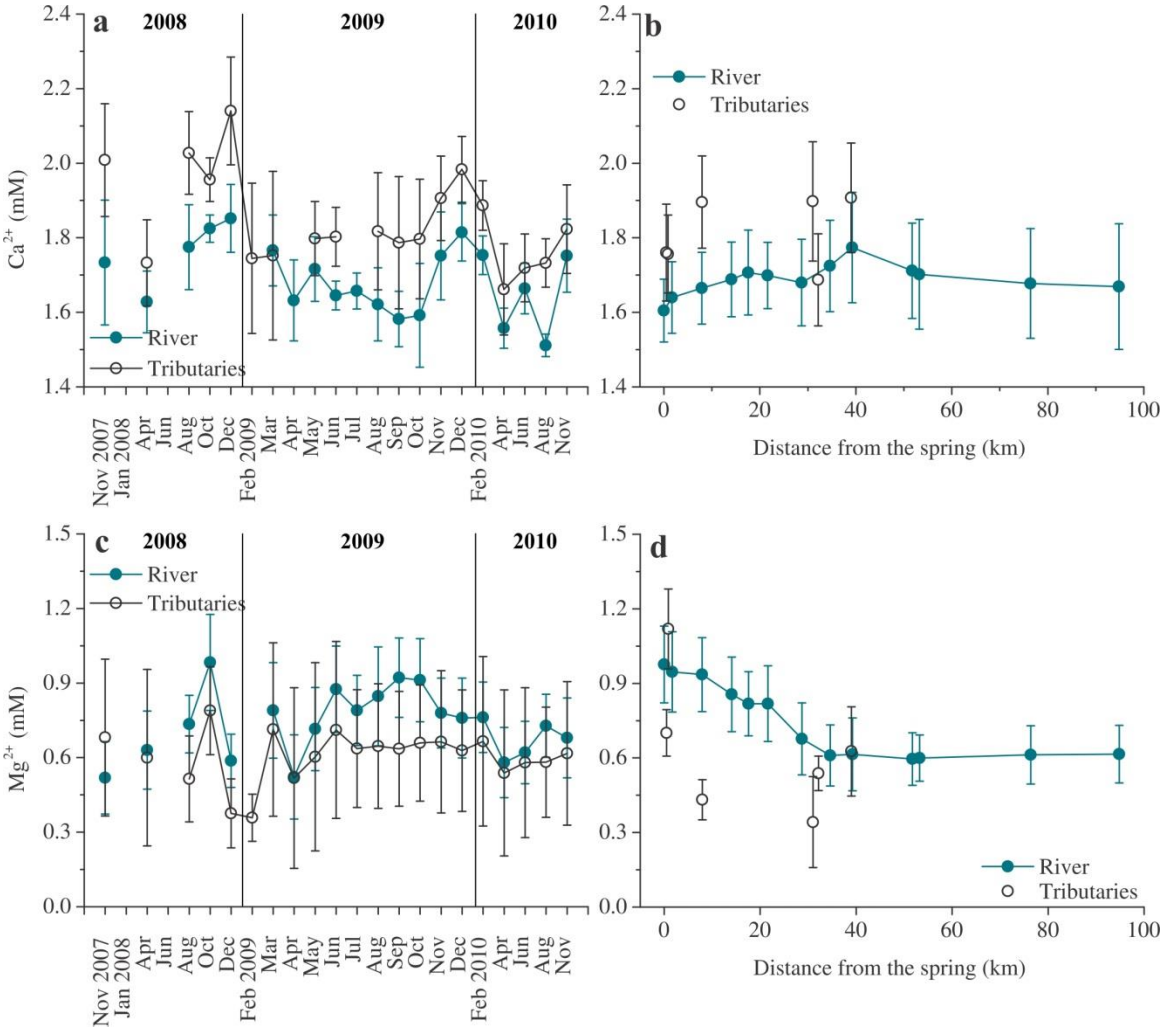

Figure 23: *Seasonal and downstream variations of Ca^{2+} (**a**, **b**) and Mg^{2+} (**c**, **d**) content in Krka waters.* Points indicate average Ca^{2+} and Mg^{2+} concentrations and the bars represent standard deviation (1σ) from the average value.

Na^{+} concentrations attributed up to 15 % of the total cation budget, ranging from 0.08 to 0.37 mM (average 0.17 ± 0.05 mM) in the stream water and showed a slight decreasing pattern downstream (Figure 24b). A similar decreasing pattern was observed for K^{+} content, ranging from 0.002 to 0.09 mM (average 0.03 mM), until sampling point W9 and remained fairly stable afterwards (Figure 26b). The tributaries exhibit slightly lower Na^{+} and K^{+} concentration, ranging from 0.03 to 0.34 mM (average 0.12 mM) and from 0.001 to 0.08 mM (average 0.02 mM), respectively. On the contrary, the Na^{+} and K^{+} content were higher in the Višnjica tributary (average 0.34 mM and 0.04 mM, respectively). Seasonal differences are insignificant, however, the lowest concentrations were observed in spring during all sampling years (Figure 24a,c).

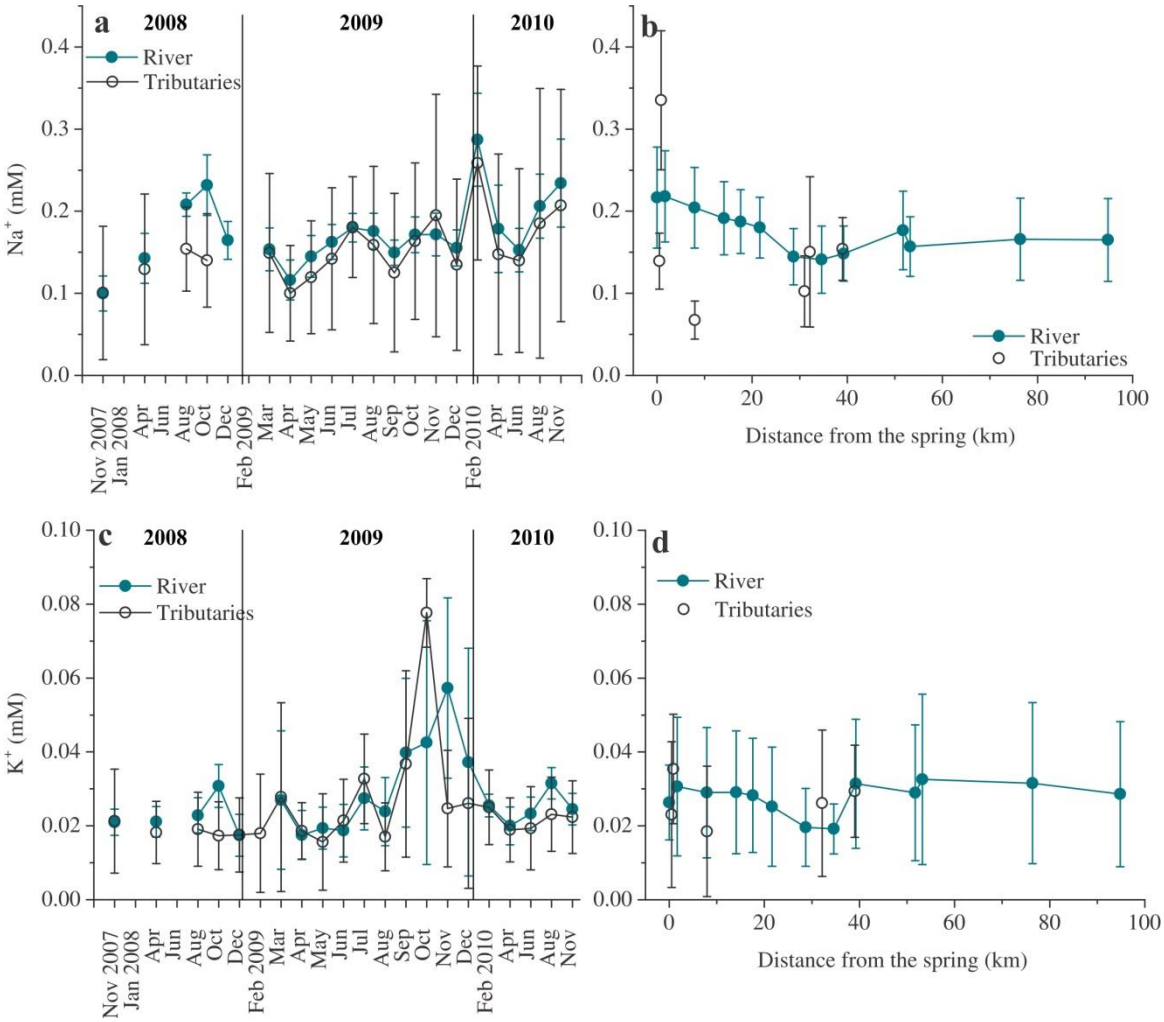

Figure 24: *Seasonal and downstream variations of Na^+ (**a**, **b**) and K^+ (**c**, **d**) content in Krka waters.* Points indicate average Na^+ and K^+ concentrations and the bars represent standard deviation (1σ) from the average value.

The concentrations of Sr^{2+} and Ba^{2+} showed different spatial behaviour; the Sr^{2+} content increased downstream (Figure 25b), whereas the Ba^{2+} concentrations increased in the flow direction (Figure 25d). In comparison with others, the contents of Sr^{2+} and Ba^{2+} were significantly lower, thus it is important to notice that their concentrations are reported in the ranges of μM. The Sr^{2+} content ranged from 0.28 to 1.14 μM (average 0.55 ± 0.15 μM) in the stream water and from 0.27 to 4.64 μM (average 0.81 μM) in the tributaries. Seasonal differences were minor; in general, the highest Sr^{2+} content was in summer and autumn (2008 and 2009) and the lowest in spring and winter Figure 25a). The Ba^{2+} concentrations were similar in the main channel and in the tributaries. They ranged from 0.04 to 0.32 μM (average 0.09 μM) in the stream water and from 0.02 to 0.39 μM (average 0.09 μM) in the tributaries. The lowest content was measured in samples collected in spring months (average 0.07 μM; Figure 25b) while the highest were measured in summer (average 0.13 μM). Exceptionally high Ba^{2+} content was measured in summer 2010 (up to 0.40 μM).

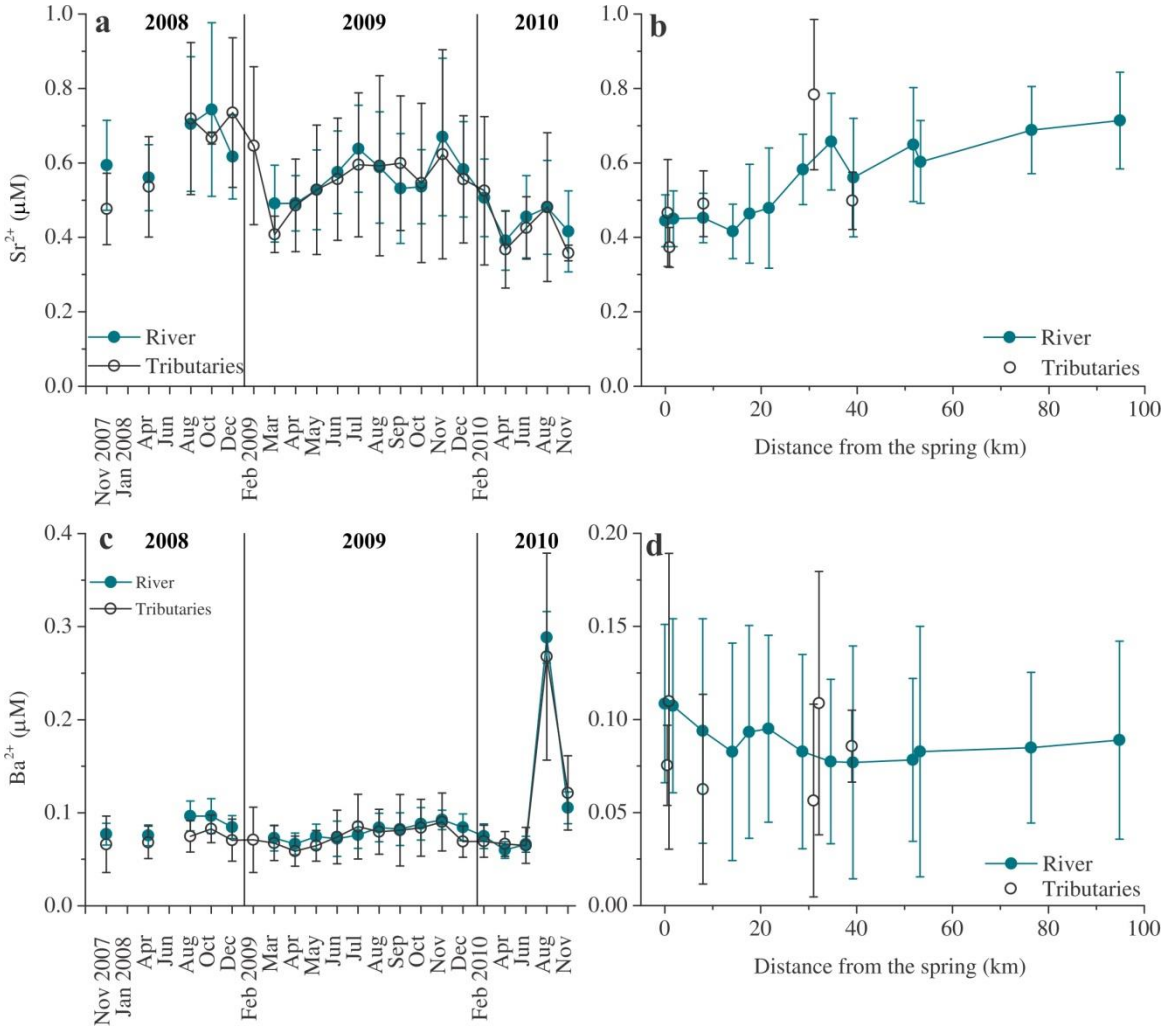

Figure 25: *Seasonal and downstream variations of Sr^{2+} (**a**, **b**) and Ba^{2+} (**c**, **d**) content in Krka waters.* The highest concentrations of Ba^{2+} measured in August 2010 were not considered in the »downstream pattern« plot (**d**). Points indicate average Sr^{2+} and Ba^{2+} concentrations and the bars represent standard deviation (1σ) from the average value.

Anions

The total alkalinity in the Krka River showed a decreasing trend downstream in 2009 and 2010 sampling campaigns. In 2008 such pattern is not clearly observed (Figure 26b). The alkalinity ranged from 3.40 to 5.32 mM (average 4.44 ± 0.41 mM) in the main channel and from 3.44 to 5.99 mM (average 4.46 ± 0.52 mM) in the tributaries. The highest values were always measured in the headwaters, ranging from 3.52 to 5.32 mM (average 4.59 ± 0.42 mM) depending on the season and year of measurement. The highest alkalinity was always observed in summer and autumn seasons, except in 2010, when the highest alkalinity was measured in winter samples (Figure 26a). Nevertheless, samples collected during spring had usually the lowest alkalinity. In comparison to stream water, the tributaries had lower alkalinity (3.44–5.14 mM, average 4.31 ± 0.37 mM), except for the Višnjica (up to 5.99 mM).

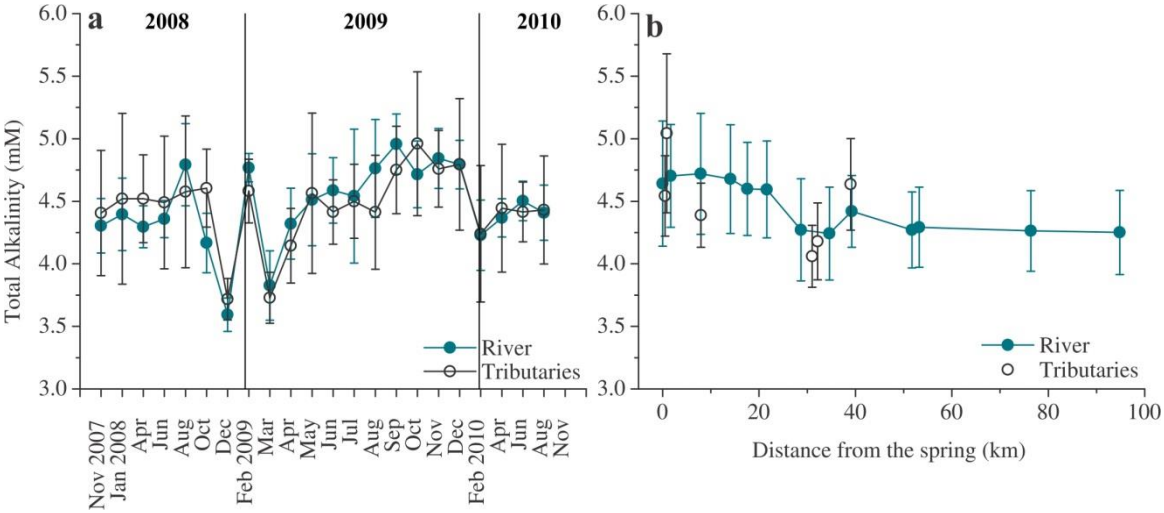

Figure 26: *Seasonal (**a**) and downstream (**b**) variations of total alkalinity in Krka waters.* Points indicate average total alkalinity and the bars represent standard deviation (1σ) from the average value.

The most abundant carbon specie in the Krka waters is the HCO_3^- ion accounting 81 to 94 % in the headwaters, 90 to 98 % in the stream water samples and from 89 to 98 % in the tributaries. Due to lower pH of the headwaters, the presence of dissolved CO_2 comprised up to 19 %, whereas the carbonate ions (CO_3^{2-}) were in the minority accounting for only 0.7 % on average to the total inorganic carbon in all sampled waters.

Moreover, the most abundant among the anions is the bicarbonate ion accounting from 86 to 97 % of the total anion budget. The second most abundant ion is Cl^- contributing up to 12 % to the anion budget and ranging from 0.07 to 0.45 mM (average 0.23 ± 0.07 mM) in stream waters and from 0.05 to 0.79 mM (average 0.22 ± 0.18 mM) in the tributaries (Figure 27a and Figure 27b). SO_4^{2-} and NO_3^- accounted for only up to 2 % and 4 %, respectively. Concentrations of Cl^- and SO_4^{2-} in the main stream showed a decreasing pattern downstream and were the lowest in the spring and the highest in winter (Figure 27b and Figure 27d, respectively). The SO_4^{2-} content varied from 0.04 to 0.07 mM (average 0.06 ± 0.01 mM) in the river and from 0.04 to 0.08 (average 0.05 ± 0.01 mM) in the tributaries (Figure 27c). NO_3^- content in the watershed ranged from 0.02 to 0.19 mM and was the highest in spring and summer (Figure 27e). Average nitrate concentrations were 0.14 mM in the stream water and 0.08 mM in the tributaries.

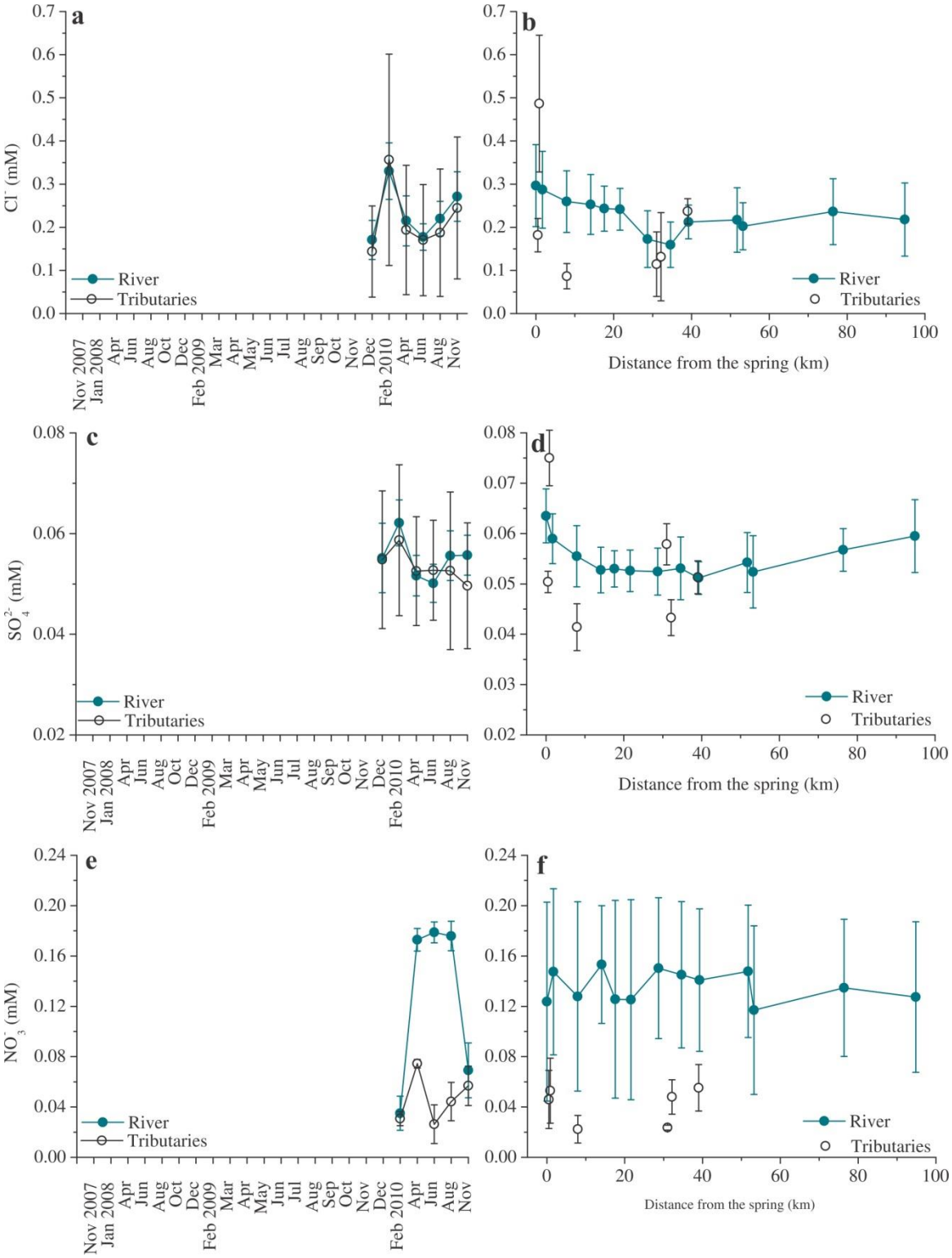

Figure 27: *Seasonal and downstream variations of Cl^- (**a**, **b**), SO_4^{2-} (**c**, **d**) and NO_3^- (**e**, **f**) content in Krka waters.* Points indicate average concentrations of Cl^-, SO_4^{2-}, and NO_3^- and the bars represent standard deviation (1σ) from the average value.

Dissolved inorganic and organic carbon

The concentration of dissolved inorganic carbon (DIC) ranged from 3.61 to 5.94 mM (average 4.63 ± 0.5 mM) and showed similar seasonal and spatial pattern as total alkalinity (Figure 33). A good positive correlation between DIC and total alkalinity (TA) was observed (Figure 28); for the samples collected in the main channel the correlation coefficient R was 0.81 and 0.88 for those collected in the tributaries. Thus, the measured total alkalinity can be described as a carbonate alkalinity (due to good correlations we performed only total alkalinity measurements for the samples collected in 2009 and 2010). In general, measured DIC concentrations were slightly higher than the total alkalinity.

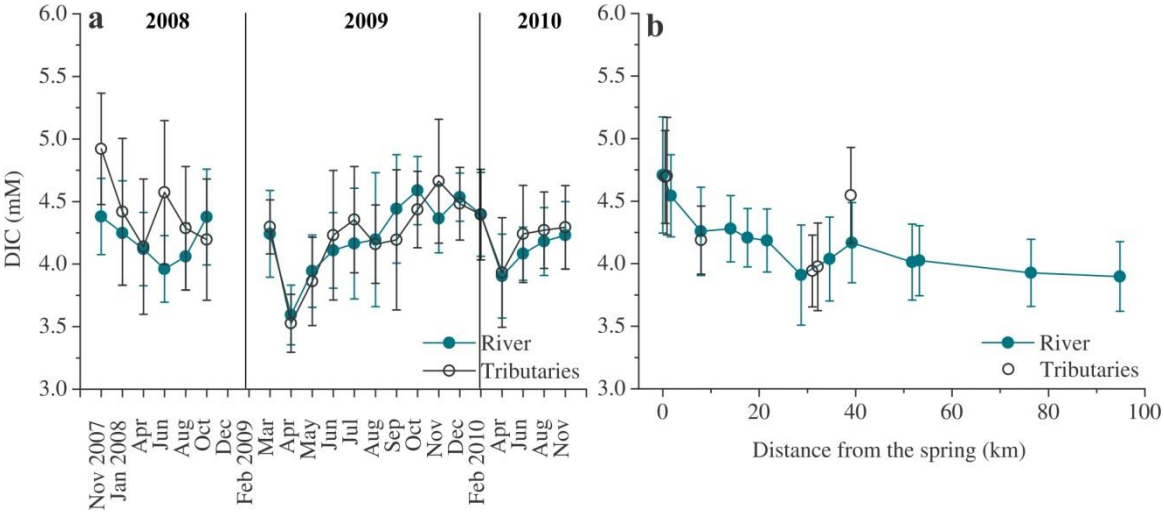

Figure 28: *Seasonal (**a**) and downstream (**b**) variations of calculated DIC content in Krka waters.* Points indicate average DIC values and the bars represent standard deviation (1σ) from the average value.

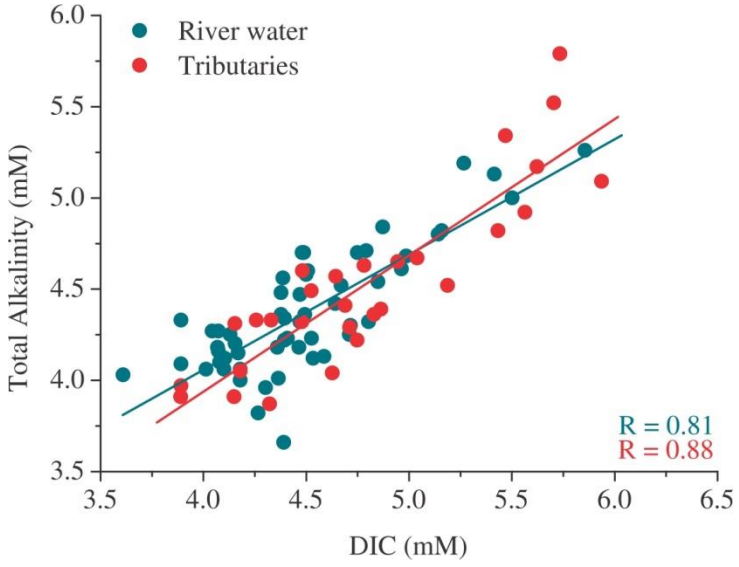

Figure 29: *Total alkalinity versus DIC.* A good correlation between TA and DIC implies that the alkalinity of waters can be attributed to carbonate alkalinity.

The concentrations of dissolved organic carbon (DOC) in the Krka waters ranged from 0.02 to 0.40 mM. The average DOC content in the tributaries was slightly lower (0.16 mM) of that in the main channel (0.18 mM). The lowest concentrations were observed in winter and increased during spring (Figure 30).

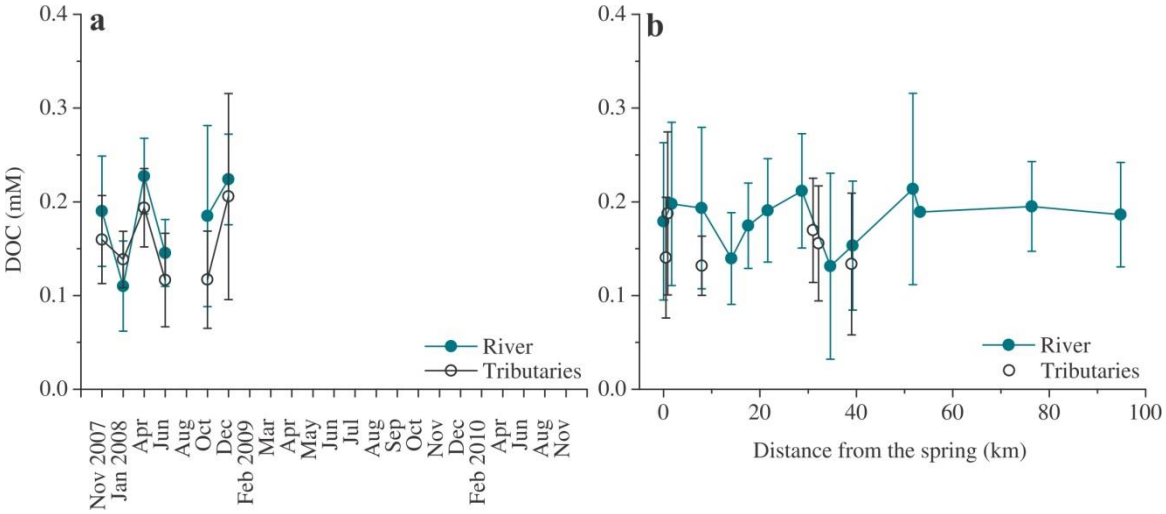

Figure 30: *Seasonal (**a**) and downstream (**b**) variations of DOC content in Krka waters.* Points indicate average DOC content and the bars represent standard deviation (1σ) from the average value.

5.1.4 Stable isotopes

Isotopic composition of precipitation

Marked seasonal variability was observed in the stable isotopic composition of precipitation (Figure 31). The $\delta^{18}O$ values ranged from -17.0 ‰ to -5.4 ‰ (average -10.4 ± 3.2 ‰) and were the lowest in winter (average -14.8 ‰) and autumn (average -11.8 ‰), whereas the isotopic composition in spring and summer was higher (Appendix 2). The average $\delta^{18}O$ values in spring and summer were -8.4 ‰ and -7.3 ‰, respectively (Figure 31).

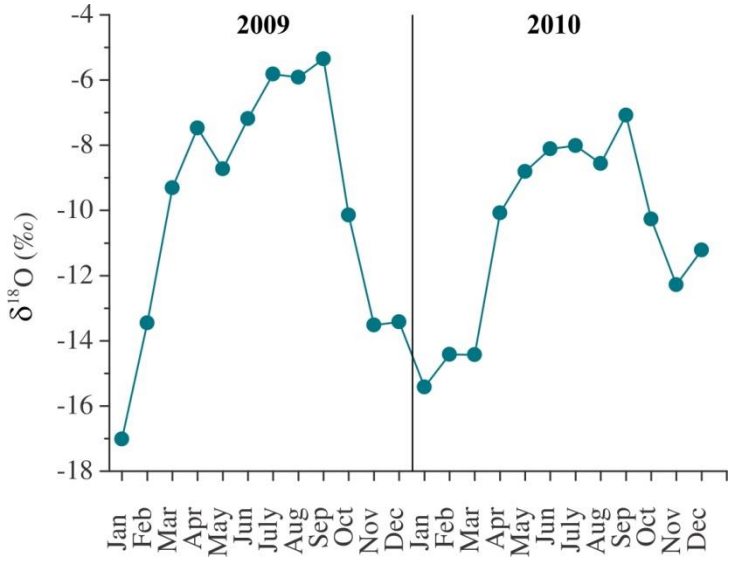

Figure 31: *Seasonal variability of $\delta^{18}O$ in precipitation in the Krka watershed.* Precipitation was collected at precipitation monitoring station Dvor operated by ARSO (Figure 16).

Isotopic composition of river water

The $\delta^{18}O$ values of river water samples ranged from -11.6 ‰ to -8.0 ‰ with average value -9.4 ± 0.6 ‰, respectively. Temporal and spatial variability of $\delta^{18}O$ values of stream water and the tributaries is shown in Figure 32. In general, the highest $\delta^{18}O$ values

were observed in the headwaters and decreased downstream. More pronounced was the seasonal variability. The winter samples had the lowest $\delta^{18}O$ values compared to other seasons, except in 2010 when an opposite pattern was observed. The highest $\delta^{18}O$ values were in summer.

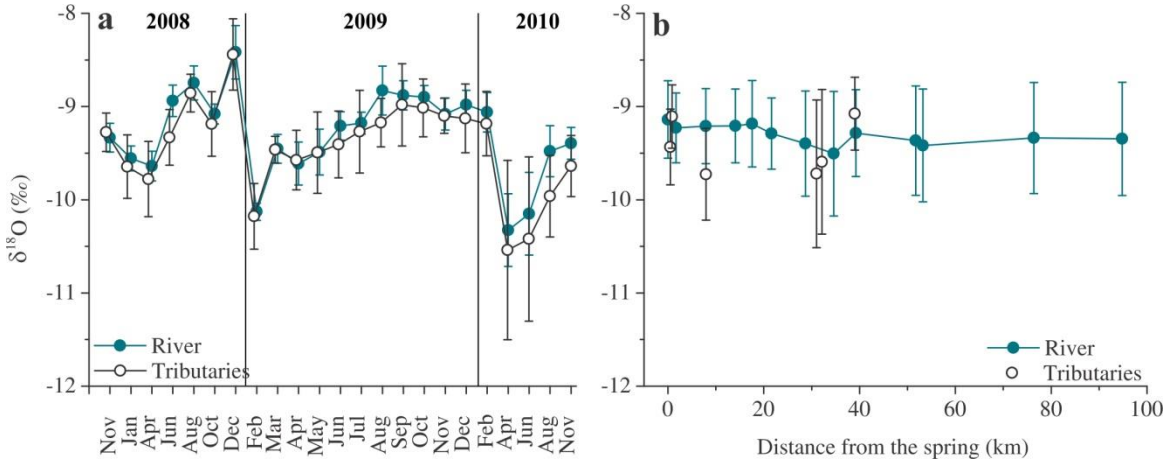

Figure 32: *Seasonal (**a**) and downstream (**b**) variations of $\delta^{18}O$ values in Krka waters.* Points indicate average δ values and the bars represent standard deviation (1σ) from the average value.

Isotopic composition of dissolved inorganic carbon ($\delta^{13}C_{DIC}$)

$\delta^{13}C$ values of DIC ($\delta^{13}C_{DIC}$) in the Krka waters ranged from -16.0 ‰ to -10.5 ‰ (average -12.8 ± 0.1 ‰). Even though no distinctive seasonal or spatial trends were observed during the sampling period, the lowest $\delta^{13}C_{DIC}$ values were always in the headwaters ranging from -16.0 ‰ to -11.3 ‰ (average -13.8 ‰) and increased downstream (Figure 33b); average $\delta^{13}C_{DIC}$ value of stream water was -12.6 ± 0.9 ‰.

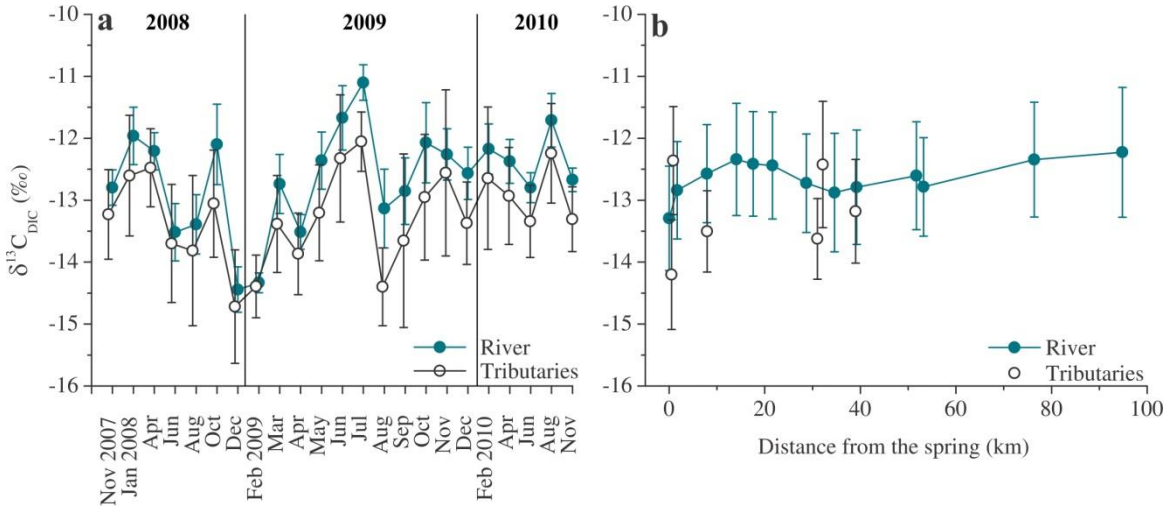

Figure 33: *Seasonal (**a**) and downstream (**b**) variations of $\delta^{13}C_{DIC}$ values in Krka waters.* Points indicate average temperature values and the bars represent standard deviation (1σ) from the average value.

The range of $\delta^{13}C_{DIC}$ values in the tributaries was -15.1‰ to -11.3‰, the highest being in the Višnjica and Sušca tributaries. In 2008, the highest $\delta^{13}C_{DIC}$ values were in winter and significantly decreased during other seasons. An opposite pattern can be observed for samples in 2009; the lowest $\delta^{13}C_{DIC}$ values were in winter and increased during warmer months (Figure 33a). In 2010, the $\delta^{13}C_{DIC}$ values were the lowest during spring and

autumn and increased in summer.

Isotopic composition of suspended components ($\delta^{13}C_{POC}$ and $\delta^{15}N_{PN}$)

Isotopic composition of particulate organic carbon and nitrogen was measured only in 2010 (Appendix 1). The $\delta^{13}C_{POC}$ values ranged from -31.7 ‰ to -25.0 ‰ (average -29.2 ± 1.5 ‰) and were the highest in autumn (average -28.1 ‰), while average $\delta^{13}C_{POC}$ values of -30.3 ‰ were observed in spring and summer. The $\delta^{15}N_{PN}$ values ranged from +2.2 ‰ to +6.8 ‰ (average +5.1 ± 1.1 ‰) and exhibit similar seasonal variation as the isotopic composition of particulate organic carbon. The highest $\delta^{15}N_{PN}$ values were in spring and autumn (average +5.5 ‰), while in summer the average $\delta^{15}N_{PN}$ value was slightly lower (+4.9 ‰).

Stable isotopic composition of sulphur in sulphate ($\delta^{34}S_{SO4}$) was measured in 2010 (Appendix 1). The $\delta^{34}S_{SO4}$ values ranged from +6.1 ‰ to +10.8 ‰ (average +8.4 ± 0.8 ‰). No significant seasonal or downstream changes can be observed in the variations of measured $\delta^{34}S_{SO4}$ values.

5.1.5 Saturation states

The calculated partial pressure of CO_2 (pCO_2) in the Krka waters ranged from $10^{-3.1}$ to $10^{-1.8}$ bars, which corresponds to 710 to 17,780 ppm using the following relationship:

$$pCO_2(\text{ppm}) = 10^{\log\ pCO_2} \times 1{,}000{,}000 \qquad (41)$$

where log pCO_2 is in bar units. The highest pCO_2 values were always in the headwaters (average 8350 ppm) and markedly decreased downstream (Figure 34b). Most pronounced seasonal variations were in 2010, when the highest pCO_2 values were in autumn (average 3690 ppm) and the lowest in winter (average 1470 ppm). No significant seasonal changes could be observed for 2008 and 2009, however, the highest pCO_2 values were in autumn and the lowest seem to be in winter and summer (Figure 34a).

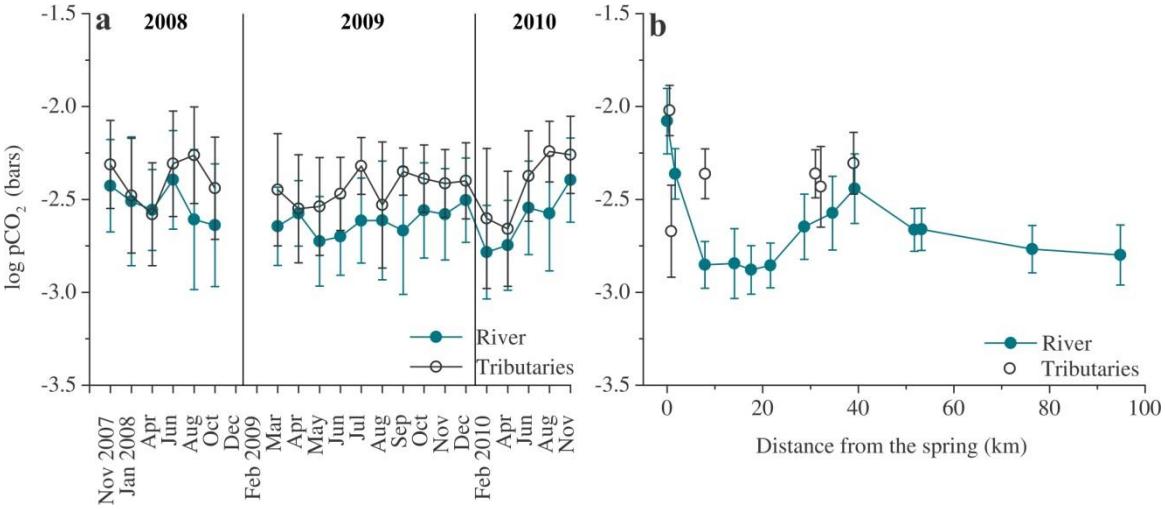

Figure 34: *Seasonal (**a**) and downstream (**b**) variations of calculated log pCO_2 values in Krka waters.* Points indicate average log pCO_2 values and the bars represent standard deviation (1σ) from the average value.

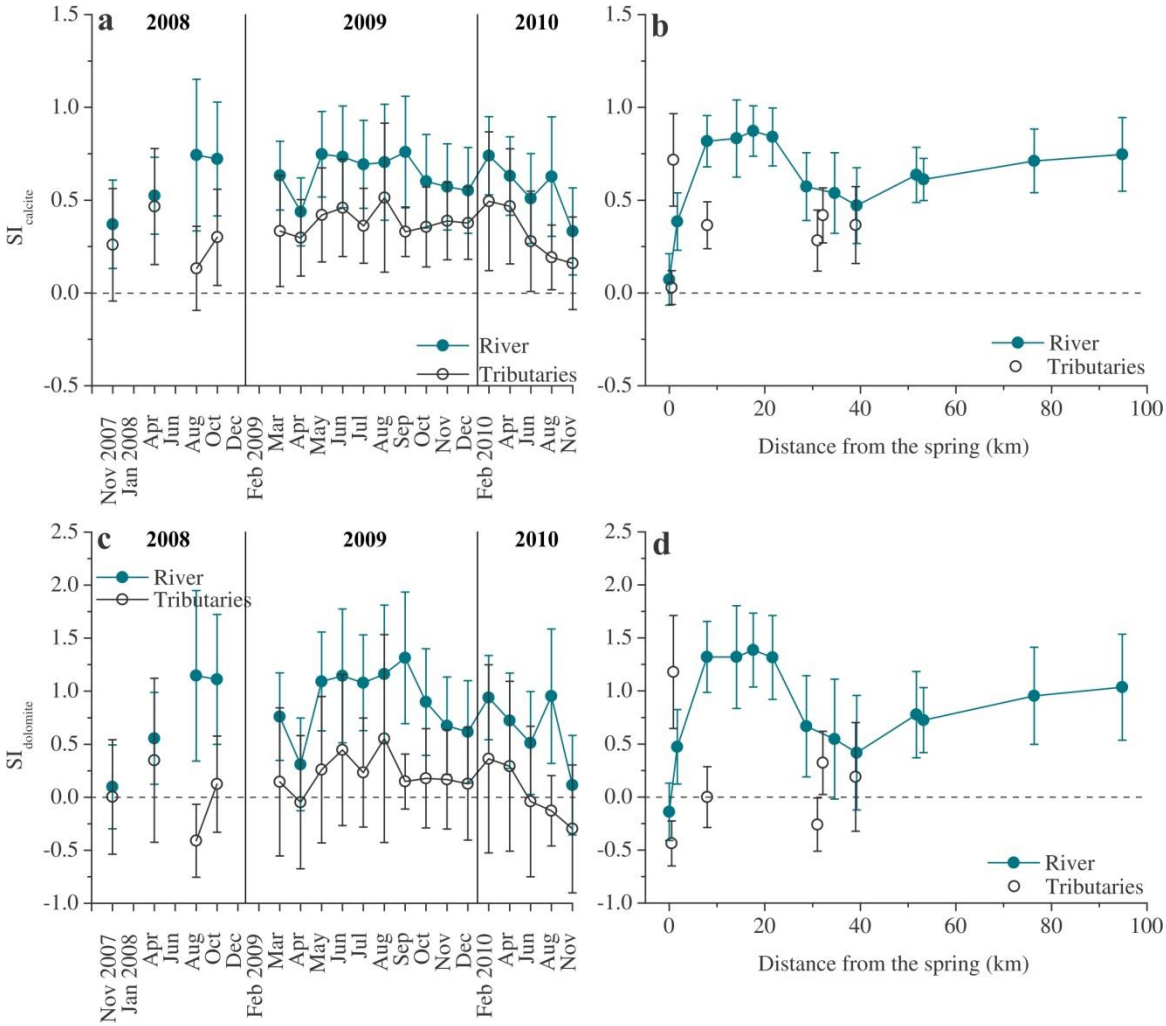

Figure 35: *Seasonal and downstream variations of calculated saturation indices of calcite (**a**, **b**) and dolomite (**c**, **d**) in Krka waters.* Points indicate average $SI_{calcite}$ and $SI_{dolomite}$ values and the bars represent standard deviation (1σ) from the average value. Lines indicate oversaturation (SI > 0) with respect to calcite (a, b) and dolomite (c, d).

Saturation indices (SI) for calcite and dolomite followed the same spatial and seasonal pattern as pH. The SI values for calcite and dolomite ranged from -0.26 to 1.14 (average 0.54; Figure 35a) and from -0.92 to 2.09 (average 0.61; Figure 35c), respectively. Thermodynamically, the saturation conditions indicate dissolution of calcite and dolomite (SI < 0) in the headwaters and precipitaton in the stream waters (Figure 35b,d). The SI values in the tributaries were generally lower than in the main channel (Figure 35).

5.2 Tufa

The results of mineralogical, stable carbon and oxygen isotopic composition and geochemical analyses of tufa samples collected in the stream of Krka River are given in Appendix 3 and Figure 36 to Figure 39.

Tufa in Krka River is a moderately compact precipitate of calcium carbonate. Its most prominent macroscopic feature is a porous structure with cavities of 5 mm to over 1.5 cm in size. Based on weighing wet and dry samples (n = 8) we estimated rough porosity of ranging from 15 to 30 % (average 21 %) and average density of 2.2 g/cm^3.

5.2.1 Tufa mineralogy

The XRD analyses showed that the tufa precipitates were identical in mineralogy, composed of calcite, dolomite and quartz (Appendix 3). The major component is calcite (75 % to 99 %, average 90 %) with quartz and dolomite comprising the rest. The content of dolomite and quartz ranged from 1 % to 19 % (average 6 %) and from 2 % to 8 % (average 5 %), respectively, while the presence of other minerals was too low for quantitative estimations. Mineralogical composition of analysed tufa samples is presented in Figure 36. The highest calcite content was determined in samples T9 and T10 (97 % and 98 %, respectively), while samples T6, T11, T12 and T13 had the lowest calcite content (< 85 %) and the highest dolomite content (> 10 %). Content of quartz was the highest in sample T6 (8 %).

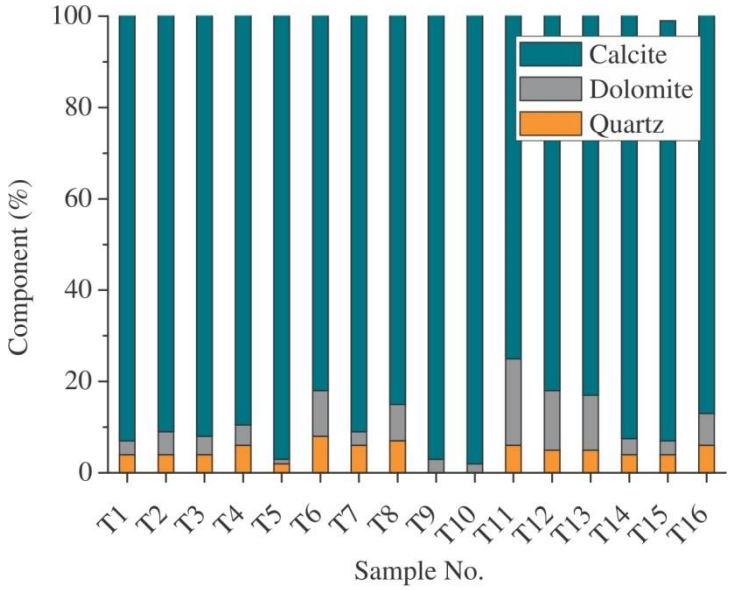

Figure 36: *Mineralogical composition of tufa samples collected in the Krka River stream.*

Figure 36 shows downstream variations in mineralogical composition of tufa samples. Tufa samples collected from the first four dams (Figure 17) have similar quantitative mineralogical composition with ~ 90 % of calcite and almost equal proportions of dolomite and quartz. In the following dams mineralogical composition varies; while sample T5 has 97 % of calcite, samples T6, T7 and T8 have significantly high content of quartz (> 8 %). Mineralogical composition of samples T11, T12 and T13 differentiate the most among all analysed tufa samples; their content of dolomite (12 % to 19 %) is far above the average (6 %). Interestingly, their quartz content (5–6 %) remained in the ranges of average (5 %).

5.2.2 Elemental composition

Elemental composition of tufa samples is presented in Appendix 3. The chemistry of analysed tufa (n = 16) is dominated by CaO, SiO_2, Al_2O_3, Fe_2O_3 and MgO (Figure 37a). The presence of Na_2O, K_2O, Sr, Ba and other trace elements was below 0.3 %. The LOI (loss on ignition) was similar for all samples ranging from 39.8 % to 43.1 % (average 41.8 %). The concentrations of Ca were the highest, ranging from 309 to 358 mg/g (average 339 ± 12.8 mg/g). The second most abundant elements are (in the descending order): Mg (4.4 to 22.2 mg/g, average 7.4 mg/g), Si (1.6 to 4.2 mg/g, average 2.7 ± 0.8), Al (0.3 to 0.9 mg/g, average 0.6 ± 0.1 mg/g), Fe (0.2 to 1.0, average 0.2 mg/g), Mn (0.04 to 0.2, average 0.1 ± 0.04 mg/g), Na (0.2 to 0.4 mg/g, average 0.3 ±0.05 mg/g), K (0.6 to 1.3 mg/g, average 0.9 ± 0.2 mg/g), Sr (44 to 58 ppm, average 50 ± 3ppm) and Ba (60 to 95 ppm, average 77 ± 10 ppm). The content of other trace elements was below 50 ppm. Mass variations of major and some trace elements are shown in Figure 37.

The chemistry of bedrock samples (n = 4) is dominated by CaO and MgO ranging from 36.7 to 54.6 % and from 0.9 to 18.6 %, respectively (Appendix 4).

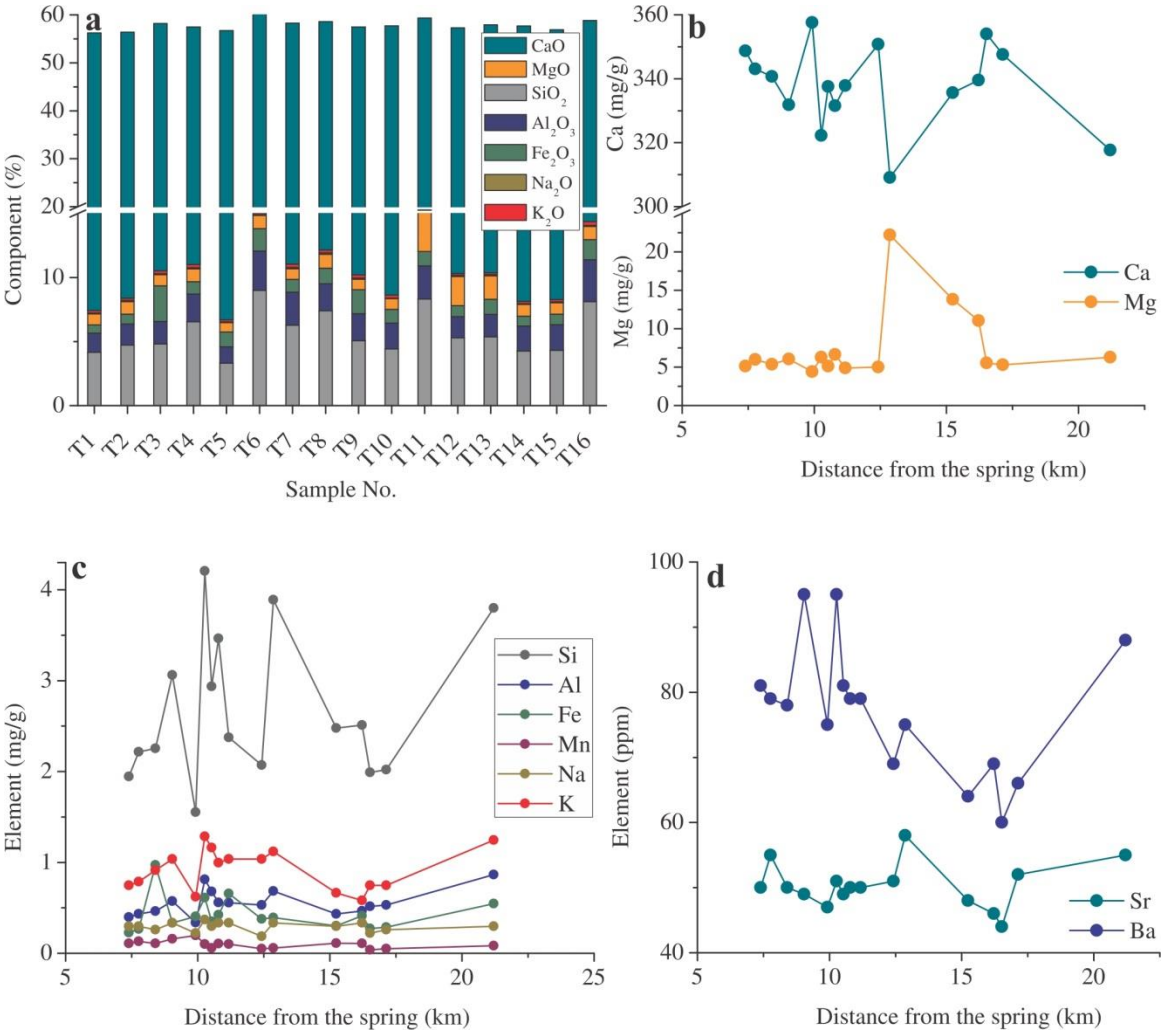

Figure 37: *Elemental composition of tufa samples from Krka River stream.* The plots show percentage of components present in individual tufa samples (**a**) and content variations of Ca and Mg (**b**), minor elements (Si, Al, Fe, Mn, Na, K) (**c**), and trace elements (Sr and Ba) (**d**).

5.2.3 Carbon and nitrogen elemental composition

The total carbon content in tufa samples analysed ranges from 11.0 % to 12.1 % (average 11.6 ± 0.4 %), whereas the content of organic component is much lower; average C_{org} and N_{tot} are 1.1 % and 0.1%, respectively (Appendix 3). Carbon and nitrogen elemental composition does not show any distinctive downstream pattern (Figure 38).

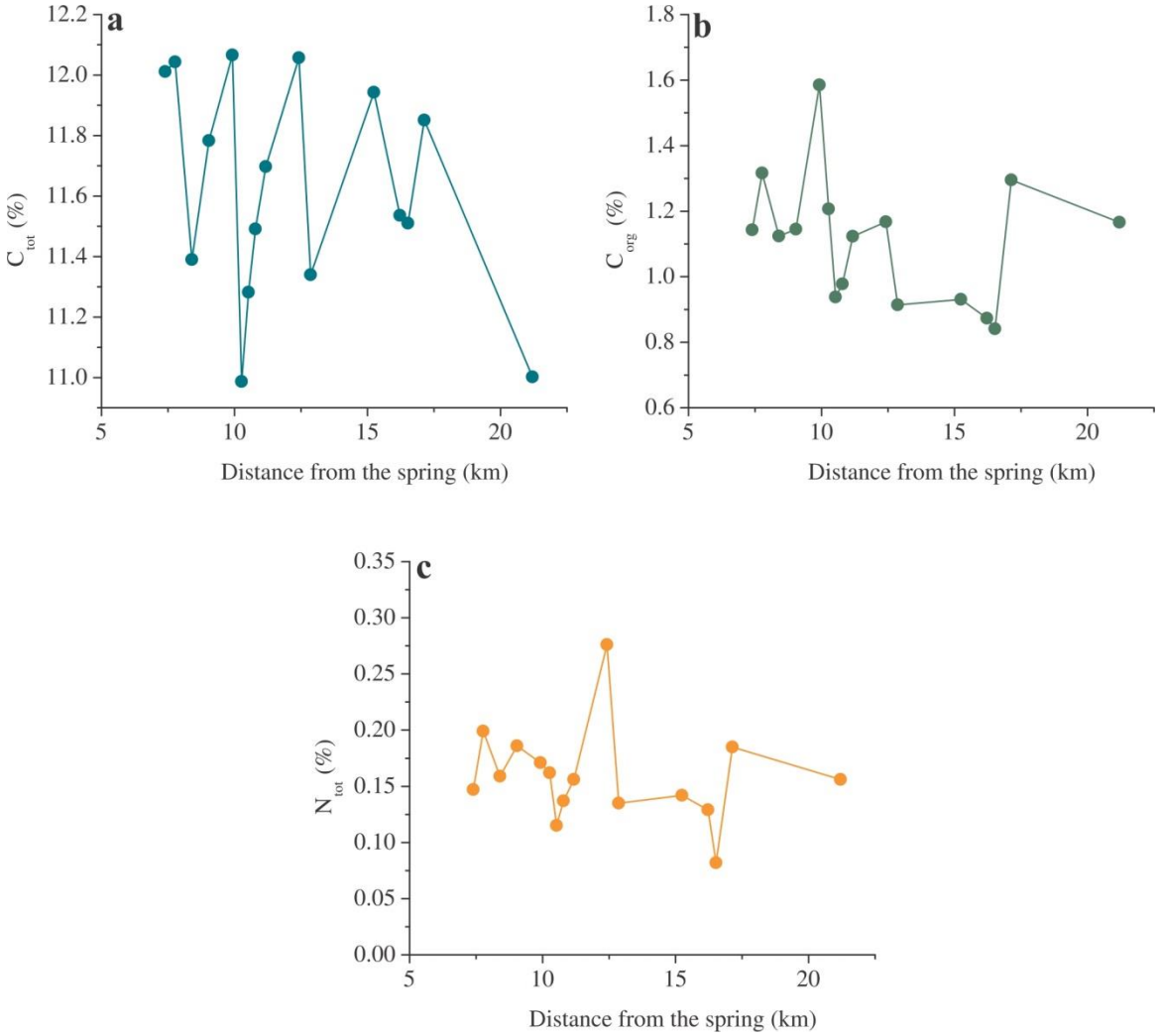

Figure 38: *Carbon and nitrogen elemental composition of tufa samples collected in the Krka River stream.*

5.2.4 Stable isotope composition

The carbon and oxygen isotopic composition of recent tufa precipitated in Krka River show relatively narrow variability (n = 16), with $\delta^{13}C_{tufa}$ and $\delta^{18}O_{tufa}$ ranging from -11.40 ‰ to -6.60 ‰ (average -10.24 ± 0.92 ‰) and from -9.27 to -6.34 ‰ (average -8.76 ± 0.52 ‰), respectively. The majority of samples fall in the range from -11.40 ‰ to -8.71 ‰ and from -9.27 ‰ to -8.16 ‰ in case of C and O isotopic composition, respectively (Appendix 3). No specific downstream trend was observed in oxygen isotopic variability, whereas a decreasing downstream pattern was observed for $\delta^{13}C_{tufa}$ values until T-10 (Figure 39a), followed by a large increase in $\delta^{13}C_{tufa}$ and $\delta^{18}O_{tufa}$ values at T11 (up to 3.6 ‰ for C and 1.9 ‰ for O). Afterwards, the $\delta^{13}C$ and $\delta^{18}O$ values of tufa samples gradually decreased but remained higher in comparison with those determined in tufa samples collected in the upper part. The $\delta^{13}C$ of organic carbon ($\delta^{13}C_{org}$) in bulk tufa

barriers ranged from -31.9 ‰ to -28.5 ‰ (average -30.0 ± 0.9 ‰; Figure 39b).

The carbon isotopic composition of bedrock samples (Appendix 4) ranged from +1.3 ‰ to +1.5 ‰ (average +1.4 ‰).

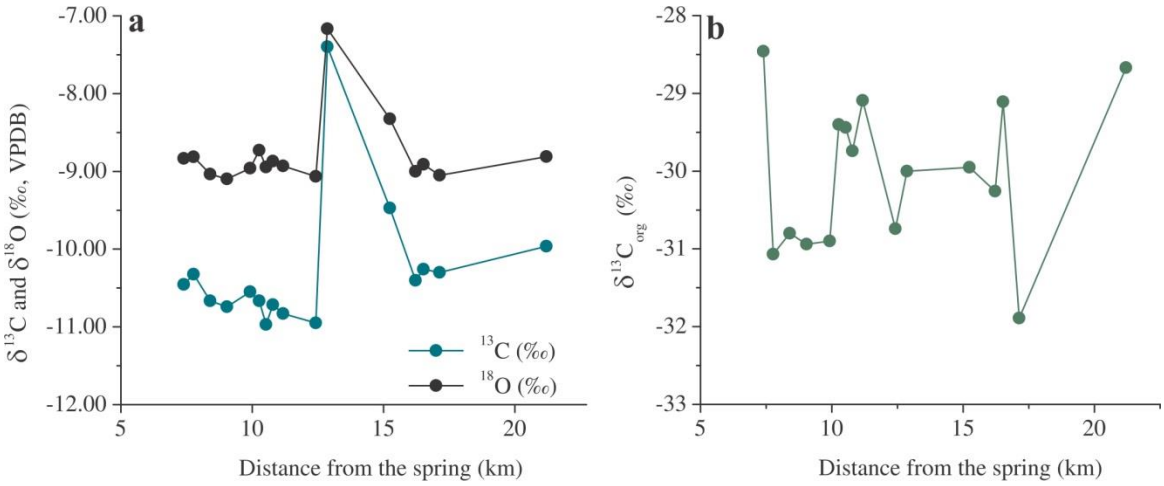

Figure 39: *Stable isotopic composition of tufa samples collected in the Krka River stream.* Plot (**a**) presents stable carbon ($\delta^{13}C_{tufa}$) and oxygen ($\delta^{18}O_{tufa}$) isotopic composition of tufa and plot (**b**) presents stable carbon isotopic composition of organic matter of tufa.

6 Discussion

The following discussion comprehends a set of results obtained in a 3-years long study on weathering processes and carbon cycling in the Krka River watershed and is divided into three major sections. The first section elaborates hydrology, major solute sources, carbonate weathering intensity and CO_2 consumption rates in the watershed. The second section focuses on hydrological and biogeochemical changes of water and DIC in the waters of the Krka watershed using stable isotopes of hydrogen, oxygen and carbon as environmental tracers. In the last section, isotopic fractionation in the carbonate – water system and the use of tufa as environmental indicator is discussed.

6.1 Oxygen isotope tracer and mean residence times in the Krka watershed

Seasonal $\delta^{18}O$ trends observed in precipitation and stream water were investigated quantitatively to estimate residence time of surface water in the Krka watershed. Distinctive monthly variations in $\delta^{18}O$ observed in precipitation at location Dvor (Figure 31) show a typical seasonal pattern, being more depleted during the winter months (average -14.8 ‰) and relatively enriched during the summer (average -7.3 ‰). A fairly narrow range of $\delta^{18}O$ values of Krka stream waters (-11.6 ‰ to -8.0 ‰) with an average decrease of 0.2 ‰ downstream (Figure 31b) and a lack of correlation between $\delta^{18}O$ values and water temperature (R = 0.19) show that evaporation effects have little or no influence on the $\delta^{18}O$ values of Krka stream waters. Hence, the $\delta^{18}O$ imprint of Krka surface waters reflects mixing of groundwater and precipitation within the aquifer.

Therefore, seasonal $\delta^{18}O$ trends observed in precipitation and stream water were used to quantitatively estimate residence time of surface water using periodic regression analysis. Basically, seasonal trends in $\delta^{18}O$ in precipitation and stream water were modelled to fit sine curve of the annual $\delta^{18}O$ variations in precipitation and stream water (cf. De Walle et al., 1997; Rodgers et al., 2005), defined as:

$$\delta^{18}O = \delta^{18}O_{avg} + A\left(\cos(c \cdot t - \theta)\right) \qquad (42)$$

where $\delta^{18}O$ and $\delta^{18}O_{avg}$ are the modelled and the average annual measured $\delta^{18}O$, respectively, A is the calculated $\delta^{18}O$ annual amplitude, c is the radial frequency of annual fluctuations (0.017214 rad/day), t is the time in days after the start of the sampling period and θ is the phase lag or time of the annual peak in $\delta^{18}O$ in radians (0.202114 rad). The mean residence time (T) of water leaving the system was estimated as:

$$T = c^{-1}\left((A_{z1}/A_{z2})^2 - 1\right)^{0.5} \qquad (43)$$

where A_{z1} is the amplitude of precipitation and A_{z2} is the amplitude of the stream water outputs.

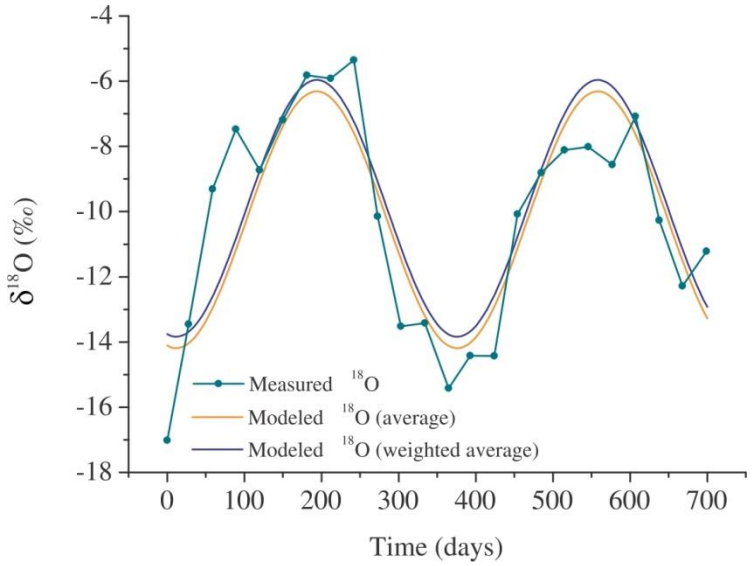

Figure 40: *Fitted annual regression model to measured $\delta^{18}O$ for precipitation collected at Dvor* (Figure 16) for the period 2009–2010. The solid lines represent modeled $\delta^{18}O$ values considering average $\delta^{18}O$ value of -10.3 ‰ (red line) and discharge-weighted $\delta^{18}O$ value of -9.9 ‰ (blue line). Measured $\delta^{18}O$ values ‰ are presented with a cyan colour.

The model with A_{z1} of 3.94‰ described the precipitation data quite well (R = 0.86) (Figure 40). In terms of the Krka stream water the A_{z2} was estimated to be 0.30 but the fit was low (R = 0.47). This is due to a simple nature of the model that assumes steady state condition in the watershed, which is unrealistic for a complex karstic watershed with a diffusive groundwater recharge. Thus, the resulting mean residence time (MRT) must be treated cautiously and be considered as indicative. Nevertheless, given the common approach and evidence from previous studies (e.g. Rodgers et al., 2005; Ogrinc et al., 2008b) it is reasonable to believe that they at least provide meaningful estimates and insight into a complex hydrological behaviour of a karstic Krka watershed.

The obtained results give indication of the degree of mixing of precipitation and groundwater in the Krka watershed. The estimated MRT of stream water are listed in Table 9 and ranged from 1.3 to 4.7 years (average 2.4 years).

Table 9: *Weighted and arithmetic averages, ranges and standard deviations (SD) for $\delta^{18}O$ values together with the estimated mean residence times (MRT) in the Krka River watershed for the period 2007–2010.* The precipitation data is for the period 2009–2010. MRT^1 and MRT^2 are mean residence times calculated using A_{z1} of 3.94 ‰ (estimated in this study) and of 2.92 ‰ (estimated in the study of Ogrinc et al., 2008b).

Sampling point	Weighted average (‰)	Average (‰)	Min (‰)	Max (‰)	SD	MRT^1 (years)	R	MRT^2 (years)	R
P1	-9.90	-10.25	-17.02	-5.35	3.23	-	-	-	-
W1	-	-9.14	-10.13	-8.53	0.41	3.4	0.33	2.5	0.3
W4	-9.18	-9.21	-10.10	-8.62	0.39	3.3	0.54	2.4	0.53
W10	-9.38	-9.4	-10.25	-8.24	0.46	1.9	0.45	1.4	0.45
W18	-9.34	-9.39	-10.60	-8.34	0.58	1.8	0.43	1.4	0.42
W3	-9.08	-9.11	-9.75	-8.54	0.33	4.1	0.35	3.0	0.31
W12	-9.72	-9.72	-11.62	-8.21	0.76	1.3	0.38	1.0	0.37
W14	-9.07	-9.08	-10.25	-8.22	0.38	4.7	0.26	3.5	0.24

In general, the higher is the MRT the weaker is regression fit between the modelled and measured average $\delta^{18}O$ values. The highest MRT values were calculated for the headwaters area (3.4 years) and Višnjica (4.1 years) and Prečna (4.7 years) tributaries (W3 and W14, respectively; Figure 16). In the downstream sections, the MRT ranged from 1.3 to 2.0 years. Such differences imply that waters in the upper reaches reflect isotopic composition of groundwaters that were in longer contact with the aquifer bedrock, which could also explain higher concentrations of dissolved load in the upper reaches compared to lower reaches (see section 6.2). Low MRT values in the lower reaches most likely reflect additional input of groundwater coming from shallow aquifers in the east of the Krka watershed.

Ogrinc et al. (2008b) found that long-term period data of precipitation describe the amplitude better than short-term, thus, we also estimated MRT for the Krka using the A_{z1} of 2.92 ‰ of precipitation collected in Ljubljana in the period 1981–2006. The differences are quite large (Table 9); the average MRT was estimated to be 1.0–3.5 years (average 1.8 years), which is in line with findings from Ogrinc et al. (2008b), who estimated the average MRT to be 1.32 years for the Sava River. However, the MRT range of 1.0–3.5 years clearly shows that residence times in Krka watershed are higher, most likely due to its predominantly karstic nature resulting in longer water-rock interaction times.

6.2 Sources of solutes in the waters of the Krka Watershed

Major mechanisms controlling riverine water chemistry are rock weathering, atmospheric inputs and anthropogenic pollution (e.g. Gibbs, 1970; Gaillardet et al., 1999; Roy et al., 1999; Han and Liu, 2004; Szramek et al., 2007, 2011). The relative importance of various possible sources of major ions in the Krka River watershed is discussed below.

6.2.1 Atmospheric inputs

Despite low concentrations of major ions in rainwater (typically in the range of μM; Liu et al., 2010) the surface river waters are in constant interaction with the atmosphere, thus it is important to evaluate atmospheric inputs. Early studies on surface water chemistry have shown that Cl^- concentrations, very low in surface rocks, can be used as a suitable proxy in calculating atmospheric inputs (Meybeck, 1983 and references therein). However, this approach is valid for riverine systems where Cl^- has no source other than precipitation, but Cl^- is often influenced by anthropogenic activity (Meybeck and Helmer, 1989).

Contribution of major ions from the atmospheric deposition for the Krka watershed was estimated from regional rainwater composition (Table 8). In Krka River waters Cl^- concentrations exceed 20 times those in precipitation; average Cl^- concentration in rainwaters analysed was 11.5 μM (Table 8). Hence, rainwater contribution of major ions to Krka River waters was estimated following the equation of Stallard and Edmond (1987):

$$X_{rain} = (X/Cl)_{rain} \times (Cl_{rain}/f_{ETR}) \quad (44)$$

where X_{rain} are contributions of Ca^{2+}, Mg^{2+}, Na^+, K^+ and SO_4^{2-} from the rainwater and $(X/Cl)_{rain}$ is the molar abundance ratio in rainwater. The evapotranspiration factor (f_{ETR}), the ratio of evapotranspiration (ETR) to precipitation (P), was calculated to be 0.66 using long term data of evapotranspiration and precipitation measurements during 1971 and 2000 (Frantar, 2008). The calculated contribution of atmospheric inputs of major ions in

the Krka waters was less than 3 % of the overall riverine EC. Though atmospheric inputs of Ca^{2+} and Mg^{2+} are negligible (less than 1 %), concentrations of Na^{+}, K^{+}; Cl^{-} and SO_4^{2-} in river waters appear to be more sensitive to rainwater influence; atmospheric inputs of these ions account in average 8 % for Na^{+} 5 % for K^{+} and Cl^{-}, 18 % for sulphate and 25 % for NO_3^{-}. However, these calculations are only rough estimates of rainwater inputs to the Krka waters, thus it is not possible to determine seasonal changes of rainwater influence accurately.

6.2.2 Anthropogenic inputs

Agricultural, animal, municipal and industrial wastes can contribute a considerable amount of Cl^{-}, SO_4^{2-} and NO_3^{-} into the river basin and have therefore been widely used as tracers of anthropogenic inputs (Gaillardet et al., 1999; Roy et al., 1999; Shin et al., 2011; Ogrinc et al., 2008a). Moreover, Gaillardet et al. (1999) stated that variations in total dissolved solids (TDS) in river water are in part related to land use and pollution. Based on water samples collected from December 2009 to November 2010 we estimated TDS content, which varied from 330 to 434 ppm (average 383 ppm) in the main channel and from 309 to 492 ppm (average 383 ppm) in the tributaries. The estimated TDS is in good correlation with electrical conductivity (R = 0.95; Figure 41a), thus we can attribute the variability of the EC in the Krka waters (which was continuously measure during the whole sampling period 2008–2010) to changes in dissolved content.

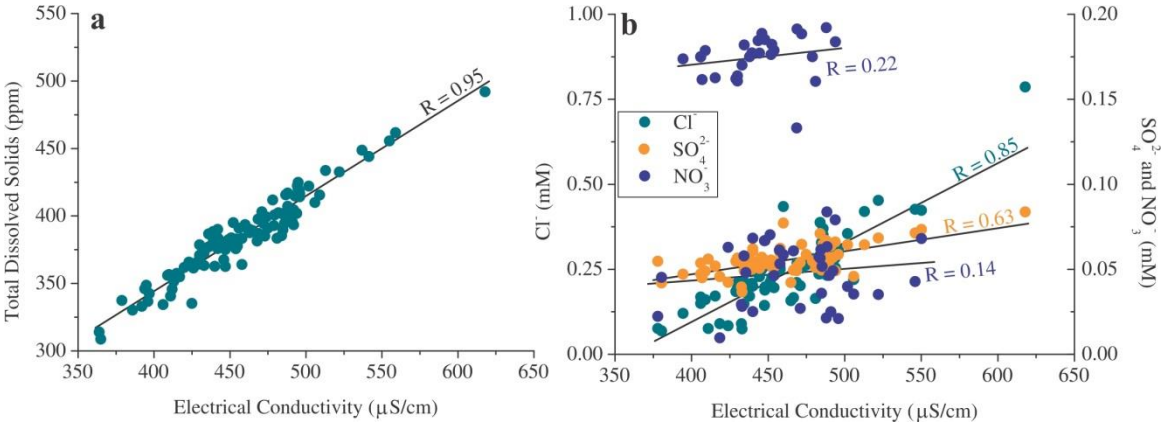

Figure 41: *Relation between electrical conductivity and dissolved solutes in Krka waters.* (**a**) Relationship between total dissolved solids (in ppm) and electrical conductivity (in µS/cm) in water samples collected from December 2009 to November 2010. (**b**) Relationship between electrical conductivity and Cl^{-}, SO_4^{2-} and NO_3^{-} content.

High concentrations of Cl^{-}, SO_4^{2-} and NO_3^{-} in the headwaters of the Krka River (Figures 30–32) indicate contamination of groundwaters in the north-west recharge area of the basin. The river further passes cultivated and moderately populated areas, where the highest nitrate concentrations (average 0.18 mM) in the Krka main channel were observed in spring and autumn 2010, which coincides with increased usage of fertilizers in the area. Interestingly, in the tributaries such high nitrate concentrations were not observed (average 0.04 mM) irrespective of season. A plot in Figure 41b shows that Cl^{-} and SO_4^{2-} correlate positively with the EC (R = 0.85 and R = 0.64, respectively). Though nitrate correlates positively with EC, the correlation is statistically insignificant. Nevertheless, average total contribution of these ions to the overall TDS in the Krka waters is fairly low (~ 2 %). A fairly good correlation of EC with HCO_3^{-}, Mg^{2+} and Na^{+} (R = 0.71, 0.67 and 0.55, respectively; Appendix 1) was observed, implying the variability of EC (and TDS consequently) in Krka waters is more likely a result of dissolved minerals

derived from other sources, such as dissolution of salts (e.g. NaCl) or dissolution of carbonate rocks (Ca^{2+}, Mg^{2+} and HCO_3^-).

A scatter diagram of Na^+ vs. Cl^- relation (Figure 42a) shows that most of the water samples plot on the equilibrium 1:1 line, which is consistent with the stoichiometry of dissolution of NaCl salt. The average Cl/Na molar ratio in Krka waters was 1.2, slightly higher than the Cl/Na ratio of rainwater (1.1; Table 8). The average Cl/Na molar ratios of rainwater (1.1; Table 8) and Krka waters (1.2) are close to the ratio of sea salt (1.0; Roy et al., 1999). Slightly higher values indicate additional input of Cl^-, which can be ascribed to dissolution of chloride salts (NaCl, $CaCl_2$ and $MgCl_2$) that are widely used as de-icer agents during winter months. A positive correlation between Ca^{2+}+Mg^{2+} and Cl^- implies that some of Ca^{2+} and Mg^{2+} ions might originate from an anthropogenic source, such as $CaCl_2$ and $MgCl_2$ salts (Figure 42b).

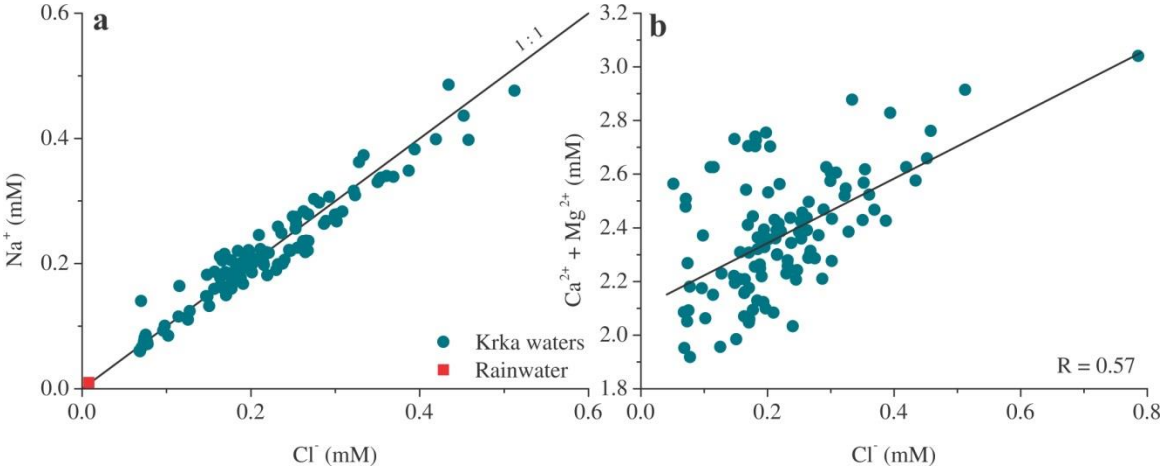

Figure 42: *Relationship between Na^+, Ca^{2+}, Mg^{2+} and Cl^- ions in the Krka waters.* (**a**) Na^+ vs. Cl^-, (**b**) Ca^{2+} + Mg^{2+} vs. Cl^-.

Sulphate concentrations in Krka waters were measured from December 2009 to November 2010 (Table 6). Average SO_4^{2-} content was 0.06 mM, which is lower than the average of 0.11 mM reported in the sampling period 2003–2006 by Szramek et al. (2011) for the Krka River or the average SO_4^{2-} concentration of 0.26 mM reported by Ogrinc et al. (2010) for the Sava watershed. The SO_4^{2-} content in the rainwater collected in 2010 was 0.009 mM (Table 8). Riverine SO_4^{2-} is derived from several sources such as acidic rain, anthropogenic inputs, oxidation of sulphide minerals and evaporite formations etc. (Roy et al., 1999; Ogrinc et al., 2010; Szramek et al., 2011). The average SO_4^{2-}/Cl^- molar ratio in the rainwater is 1.0 (Table 8), whereas the SO_4^{2-}/Cl^- of the Krka waters is lower (average 0.3), which means that SO_4^{2-} concentrations cannot alone explain the source of sulphate.

Szramek et al. (2011) ascribed the origin of sulphate in the waters of Sava watershed to pyrite oxidation rather than atmospheric inputs. However, in the area of Krka watershed only small-size coal mines and numerous localities of iron ore (as limonite FeOOH) are reported but none of sulphides (Buser, 1974; Pleničar and Premru, 1977). In order to determine the sources of sulphate in Krka waters stable isotope analyses of sulphate ($\delta^{34}S_{SO4}$) were performed. The usefulness of stable isotopic analyses of sulphate in terms of clarifying the sulphate origin in the surface waters was proven in several studies, e.g. Kanduč (2006), Ogrinc et al. (2010), Rock and Mayer (2009). Sulphate derived from oxidation of sulphides (e.g. pyrite) or biogenic emissions has strongly negative $\delta^{34}S$ values (Yang et al., 1996). The $\delta^{34}S$ values of sulphide of nearest mine areas that is not drained by Krka waters are very low and range from -10 ‰ to -3 ‰ (Drovenik et al.,

1976). Mean values of $\delta^{34}S$ of atmospheric sulphate in the acid rains of the Central Europe range from +10 ‰ to +12 ‰ (Krouse and Mayer, 2000) indicating the origin of air borne sulphate from fuel combustion. However, lower $\delta^{34}S$ values of atmospheric sulphate were reported in the studies of rains in southern Germany and Austria (average +2.1 ‰ to +3.5 ‰, Mayer, 1998), Poland (+1.4 ‰ to +6.8 ‰ (average +3.8 ‰), Trembaczowski, 1993) and Czech Republic (+7.5 ‰, Novák et al., 2000). Vokal-Nemec et al. (2006) reported $\delta^{34}S$ values of sulphate in rainwater collected in Ljubljana and the Kozina region (Slovenia) ranging from +4.7 ‰ to +5.8 ‰ and concluded that the air borne sulphate originates from combustion of fossil fuels. Additional input of sulphate into the waters can come from fertilizers. The $\delta^{34}S_{SO4}$ values of most widely used fertilizers around the world are reported to vary in a wide range from +0 ‰ to +12 ‰ (Vitòria et al., 2004).

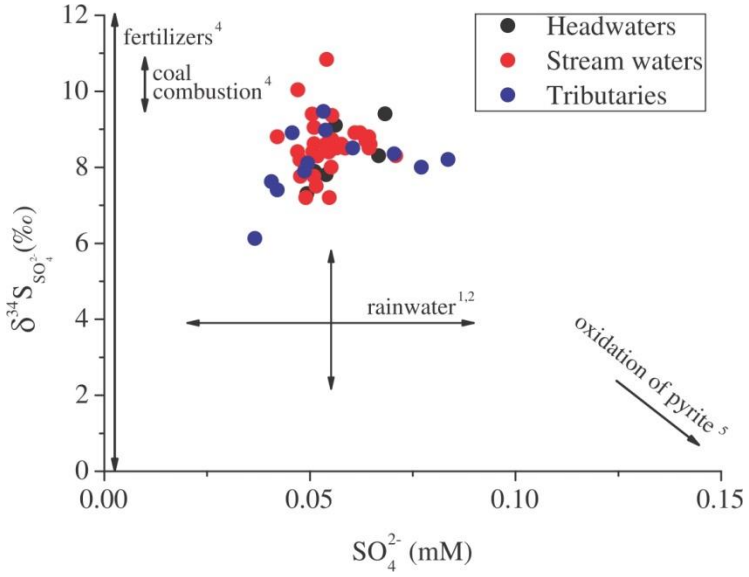

Figure 43: *Scatter diagram of sulphur isotopic composition versus sulphate concentration for the Krka watershed.* The data on end-member isotopic composition is provided from the following studies: **1**, **2** (Mayer, 1998; Vokal-Nemec et al., 2006), **3** (Vitòria et al., 2004), **4** (the $\delta^{34}S$ values of lignite from Velenje Coal Mine ranges from +9.6 ‰ to 10.8 ‰, Šturm et al., 2009) and **5** (Drovenik et al., 1976).

The $\delta^{34}S$ of sulphate in the Krka waters ranges from +6.1 ‰ to +10.8 ‰ indicating different sources of sulphate in the watershed. A scatter diagram of sulphur isotopic composition versus sulphate concentration for the Krka watershed is presented in Figure 43. Based on the isotope data, possible sources are atmospheric inputs, coal combustion and fertilizers. Due to overlapping of the $\delta^{34}S$ values of the possible end-members and lack of $\delta^{18}O$ measurements in sulphate, it is impossible to distinguish between acid rain and fertilizer source. However, concentrations of SO_4^{2+} in Krka waters are up to 10 times lower in comparison to the watersheds where sulphate input is considerably contributing to the cation excess (e.g. Huron watershed, Szramek and Walter, 2004), thus we consider the input of SO_4^{2-} of minor importance regarding water chemistry characterization in Krka watershed.

6.2.3 Carbonate weathering input

The geochemistry of surface waters in the Dinaric karst is dominated by carbonate mineral weathering (Kanduč et al., 2007a; Szramek et al., 2007, 2011) deriving loads of Ca^{2+}, Mg^{2+} and HCO_3^- ions. In the study of Sava and Idrijca watershed Szramek et al.

(2011) showed that while pollution sources from agriculture, industry and atmospheric depositions contribute ions to the studied karstic watersheds, the total contribution to the streams is minimal and can be considered negligible.

Dissolution of calcite and dolomite via carbonic acid produces waters with a molar ratio of $(Ca^{2+}+Mg^{2+}) : HCO_3^- = 1: 2$ (equations 1–2). As discussed in the *Results* section, over 95 % of the total alkalinity constitutes of HCO_3^- ions, thus the total alkalinity is considered as HCO_3^- content hereafter. The $(Ca^{2+}+Mg^{2+})/ HCO_3^-$ molar ratio of Krka waters ranges from 0.44 to 0.75 (average 0.54 ± 0.03) indicating dissolution of carbonate rocks by carbonic acid. Water samples generally plot close at or above the carbonate dissolution line (Figure 44). The low $(Ca^{2+}+Mg^{2+})/HCO_3^-$ ratio (< 0.5) is a result of either HCO_3^- enrichment or $Ca^{2+}+Mg^{2+}$ depletion by cation exchange, whereas the excess of Ca^{2+} and Mg^{2+} ions over HCO_3^- could be attributed to dissolution of carbonates by sulphuric acid (Williams et al., 2007; Szramek et al., 2011).

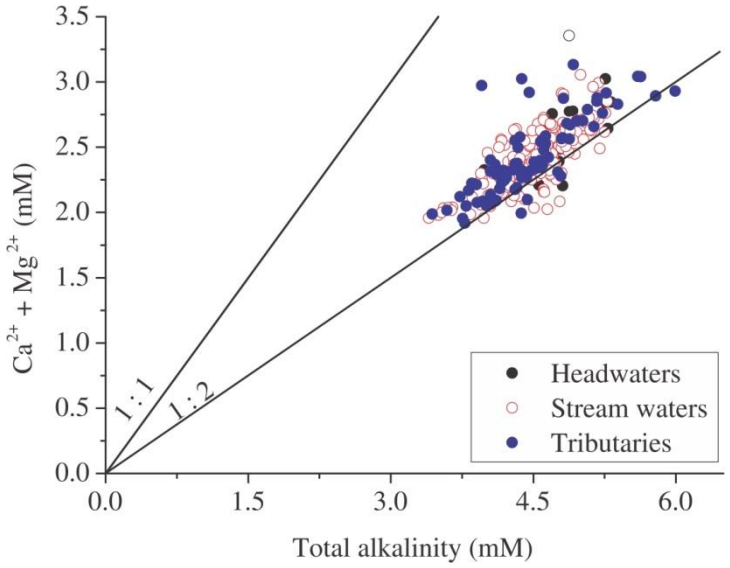

Figure 44: *Scatter plot of $(Ca^{2+}+Mg^{2+})$ versus Total alkalinity.* The dissolution of carbonate minerals (calcite and dolomite) contributes 2 moles of HCO_3^- for every 1 mole of Ca^{2+} and Mg^{2+}. Krka waters plot along the 1:2 line of $Ca^{2+}+Mg^{2+}$: HCO_3^-, indicating carbonate dissolution to be the major control on water geochemistry. The symbols represent waters from the headwaters, stream water and tributaries.

Based on the findings on the sulphate origin the sulphuric acid in the Krka watershed could be produced by the oxidation of atmospheric SO_2 and subsequent weathering of carbonates. Dissolution of carbonates by H_2SO_4 yields stoichiometric molar ratios of Ca^{2+}/ HCO_3^- and $(Ca^{2+}+Mg^{2+})/ HCO_3^-$ for calcite and dolomite to be 1:1:

$$\text{Calcite: } 2CaCO_3+H_2SO_4 \leftrightarrow Ca^{2+}+SO_4^{2-}+2HCO_3^- \quad (45)$$

$$\text{Dolomite: } MgCa(CO_3)_2+H_2SO_4 \leftrightarrow Mg^{2+}+Ca^{2+}+SO_4^{2-}+2HCO_3^- \quad (46)$$

Thus, the difference between the ratios of cation (Ca^{2+} or $Ca^{2+}+Mg^{2+}$) to bicarbonate ion of carbonate weathering by carbonic (1:2) and sulphuric acid (1:1) allows distinguishing between the two weathering types (Hercod et al., 1988). However, the highest Ca^{2+}/ HCO_3^- and $(Ca^{2+}+Mg^{2+})/ HCO_3^-$ ratios were 0.52 and 0.75, respectively, far below unity required for dissolution by sulphuric acid. Nevertheless, as Szramek et al. (2011) already pointed out, in watersheds dominated by carbonate bedrock, the contribution of sulphuric acid weathering can be often lost in the background of carbonic acid dissolution, which most likely holds true in our study case.

6.2.3.1 Dolomite dissolution in the Krka watershed

While Ca^{2+} is a product of calcite and dolomite dissolution, Mg^{2+} is derived mainly from dolomite. Detailed studies of water chemistry in the carbonate watersheds found that dissolution of dolomite contributes the majority of the Mg^{2+} ions into the river waters (Williams et al., 2007; Szramek et al. 2007, 2011). Moreover, the Mg^{2+}/Ca^{2+} molar ratio in carbonate watersheds was found to provide important constraints on relative proportions of calcite and/or dolomite weathering. Dissolution of calcite only produces waters with Mg^{2+}/Ca^{2+} of less than 0.1, while the ratios near 1.0 indicate dolomite dominance. The Mg^{2+}/Ca^{2+} ratio of 0.33 indicates equal calcite and dolomite weathering on a mole basis.

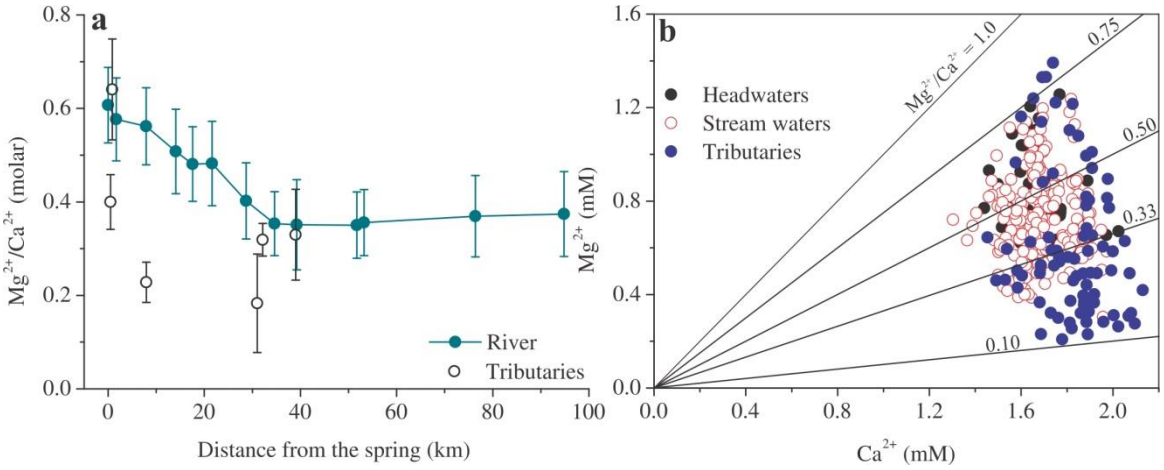

Figure 45: *Variations in the Mg^{2+}/Ca^{2+} molar ratio in Krka waters.* (**a**) Downstream variability of the Mg^{2+}/Ca^{2+} ratio and (**b**) Mg^{2+} versus Ca^{2+} indicates relative contributions of these ions from dolomite and/or calcite dissolution.

Spatial variability of Mg^{2+}/Ca^{2+} ratios in the Krka and relative proportions of Mg^{2+} and Ca^{2+} of Krka waters are shown in Figure 45. The Mg^{2+}/Ca^{2+} molar ratios vary in a wide range from 0.12 to 0.81 with an average value of 0.42, demonstrating that dolomite dissolution contributes 56 % of the total stream dissolved loads of Ca^{2+} and HCO_3^-. Consistently with predominantly dolomitic area in the north-west the proportion of dolomite dissolution is the highest in the main spring of the headwaters (average $Mg^{2+}/Ca^{2+} = 0.62$), and gradually decreases downstream (Figure 45a), following the trend of Mg^{2+} concentrations (Figure 23d) but not of that of total alkalinity (Figure 26b). Due to the fact that Mg^{2+} content decreases downstream, the headwaters seem to be the major source of Mg^{2+} in the watershed. Stream waters exhibit lower average ratio value of 0.44 while the tributaries drain predominantly limestone areas resulting in Mg^{2+}/Ca^{2+} ratios ranging from 0.12 to 0.45 (average 0.26). The highest Mg^{2+}/Ca^{2+} ratios ranging from 0.49 to 0.80 (average 0.65) were determined in the non-karstic Višnjica tributary (W3, Figure 16), which drains dolomite and alluvial sediments. The latter contribute the excess of Mg^{2+} ions into Višnjica.

Relative contributions of Ca^{2+} and bicarbonate ions from dolomite dissolution significantly vary within the watershed due to different lithology of the recharge areas. In the main spring of the headwaters, dolomite weathering contributed from 70 to 97 % of the total carbonate dissolved load, whereas the dissolution of dolomite in the recharge area of the minor spring Poltarca contributed only 45–50 % of the dissolved load. Such differences indicate that (1) the headwaters are recharged by lithologically different aquifers (the bedrock of the recharge area of Poltarca is predominantly of limestone) and (2) the large variability of the amount of Ca^{2+} and bicarbonate ions originating from

dolomite dissolution in the recharge area of the main spring likely results from seasonal changes in discharge conditions. Dolomite dissolution in the majority of the tributaries contributed 56 % of the dissolved load from carbonate rock weathering in their catchments.

6.2.4 Carbonate speciation and carbonate mineral equilibrium in Krka waters

Major ion chemistry and carbonate saturation state parameters of waters reflect carbonate weathering intensity, CO_2 outgassing and in-stream calcium carbonate precipitation within the watershed (e.g. Szramek and Walter, 2004; Williams et al., 2007). Calculated log pCO_2 values in the Krka waters ranged from $10^{-3.1}$ to $10^{-1.8}$ (average $10^{-2.6}$) and were always above atmospheric CO_2 level of 380 ppm ($10^{-3.4}$, Yao et al., 2007). In the headwaters, the log values of pCO_2 values, ranging from $10^{-1.8}$ to $10^{-2.4}$ (average $10^{-2.0}$), were the highest regardless of the season. Even though, we didn't sample groundwaters, such high level of pCO_2 implies that the headwaters have characteristics of water typical for groundwater (low pH, high log pCO_2 values and undersaturation with respect to calcite and dolomite; Cai et al., 2003). Distinctive temporal and spatial differences in the pCO_2 pattern were observed between the headwaters, upper and lower reaches, likely reflecting processes of CO_2 outgassing and in-stream $CaCO_3$ precipitation. Due to outgassing, stream waters had up to 7 times lower pCO_2 depending on turbulence (discharge) and season conditions than the headwaters. Water in the upper reaches was on average by 2000 ppm undersaturated with CO_2 compared to the lower reaches (average log $pCO_2 = 10^{-2.4}$). Such differences can be explained by high turbidity, shallow depth and fast flowing waters in the upper reaches promoting CO_2 outgassing.

The main reason for pCO_2 supersaturation (compared to atmosphere) in river waters is transport of dissolved soil CO_2 to the stream via baseflow and interflow. A thick soil zone in the Krka watershed (on average ~ 70 cm thick, Repe, 2004) provides an ample supply of CO_2 necessary for carbonate dissolution. Mean soil pCO_2 in the watershed was estimated by using equation (43) from Brook et al. (1983) and considering mean annual evapotranspiration (AET) of 765 mm (Frantar, 2008):

$$\log pCO_2 = -3.47 + 2.09(1 - e^{-0.00172 \times AET}) \quad (47)$$

The calculated soil log pCO_2 value was $10^{-1.9}$, equal to the highest log pCO_2 of soil ($10^{-1.9}$) estimated from the CO_2 production rates determined by soil respiration measurements in karst area located in the south-west Slovenia (Čater and Ogrinc, 2011).

In climate regions with clearly distinguished dry and wet period (e.g. monsoon regions) the CO_2 concentrations in water decrease during dry periods due to stable water discharge, low precipitation and weak microbial activities in soil (e.g. Yao et al., 2007). In temperate regions, like in the Krka watershed, precipitation is evenly distributed throughout the year, thus seasonal changes are marked by temperature, sunlight and ecological differences; photosynthesis is most intensive in spring and summer, when air and water temperatures increase and the watershed receives most sunlight, whereas in autumn and winter respiration processes prevail due to lower temperatures and decreasing sunlight availability. Therefore, the lowest pCO_2 in Krka waters would be expected in summer, while the highest should be observed in late autumn and winter. Instead, the highest pCO_2 levels were calculated for summer and autumn (average $10^{-1.9}$). At that time, average discharge was the lowest among all sampling seasons, which means that baseflow was the dominant source of riverine water despite high amounts of precipitation received in the summer. Such circumstances can be explained as a seasonal groundwater discharge

delay; the groundwaters, enriched with large amounts of soil CO_2 produced during cold periods (winter and early spring), were released into the stream during late spring and summer. However, low levels of pCO_2 in early spring (average $10^{-2.2}$) could also be attributed to the input of snowmelt, poor in CO_2. CO_2 concentrations increases in lower reaches in spring and summer most likely respond to slow flow velocity (~ 0.5 m/s), greater depth and higher water temperature that enhance *in-situ* photosynthesis or respiration in colder months.

After groundwaters discharge they become subjected to water-atmosphere interactions and in-stream processes, which in turn affect water chemistry. The saturation states with respect to dolomite versus calcite are presented for the headwaters, stream water and tributaries in Figure 46a. The saturation indices of calcite and dolomite ranged from -0.3 to 1.1 (average 0.6) and from -0.9 to 2.1, respectively. The headwaters of Krka are close at or below the equilibrium with respect to both, indicating thermodynamic conditions for dissolution of calcite and dolomite in the headwaters area. Due to CO_2 outgassing, the downstream sections are relatively supersaturated with respect to calcite and dolomite (Figure 46).

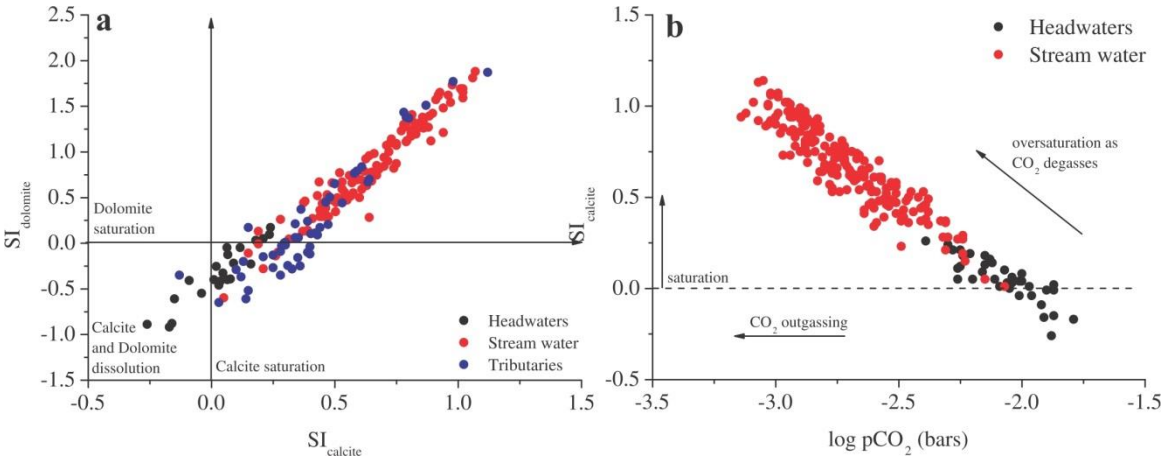

Figure 46: *Saturation indices with respect to CO_2, calcite and dolomite in Krka waters.* (**a**) Saturation indeces of dolomite ($SI_{dolomite}$) versus calcite ($SI_{calcite}$), and (**b**) saturation with respect to calcite ($SI_{calcite}$) versus. log pCO_2.

Increase in calcite saturation resulting from CO_2 outgassing can lead to possible calcium carbonate precipitation in surface waters. Supersaturation with respect to calcite alone does not necessarily imply the occurrence of calcite precipitation, as many waters are stable at high $SI_{calcite}$ values (Jacobson et al., 2002). Nevertheless, in tufa precipitating streams, $CaCO_3$ can precipitate at $SI_{calcite} > 0.6$ (Merz-Preiß and Riding, 1999). The degree of supersaturation with respect to calcite in Krka stream water suggests that losses of Ca^{2+} and HCO_3^- are due to carbonate reprecipitation along the stream.

6.2.5 Factors controlling the variability of the dissolved load in the Krka watershed

Riverine transport of the dissolved load is in principal governed by water mixing, warming/cooling, discharge, CO_2 outgassing and in-stream calcite precipitation (e.g. Herman and Lorah, 1988; Jacobson et al., 2002; Szramek and Walter, 2004; Williams, 2007; Szramek et al., 2007, 2011). Since Krka River is an active tufa precipitating stream, variations in Ca^{2+}, Mg^{2+} and HCO_3^- content, high pCO_2 levels and a wide range of $SI_{calcite}$ values in stream waters are likely subjected to CO_2 outgassing and in-stream calcium carbonate precipitation. A degree of influence of these processes on Krka water

geochemistry is examined in this chapter.

Recent studies have shown the contribution of dolomite to total weathering intensity depends on an inverse temperature dependence of the absolute solubility of calcite and dolomite, greater relative solubility of dolomite at temperatures below 25 °C (Drever, 1997), availability of CO_2 and specific runoff conditions (Szramek et al., 2007). Average Mg^{2+}/Ca^{2+} ratio was the lowest in spring (0.38) and winter (0.41), whereas in summer and autumn it was slightly higher (0.44). An inverse relationship (R = -0.71) between discharge and Mg^{2+}/Ca^{2+} indicates importance not only of the amount of the discharge but also of temperature conditions in the watershed. The water-rock contact times increase during drier conditions (Ihlenfeld et al., 2003) resulting in enhanced dissolution of dolomite relative to calcite and consequently, the Mg^{2+}/Ca^{2+} ratios increase. During warm periods (summer and early autumn), baseflow conditions prevail, which means that groundwaters in the upper reaches contribute the majority of the water into the main channel of the Krka. Thus, in colder period the imprint of dolomite dissolution in the watershed might be interrupted by an input of groundwaters that dissolve limestone lowering the Mg^{2+}/Ca^{2+} ratios of stream water.

In principle, the carbonate mass balance of dissolution and precipitation can be examined by utilizing the concentration relations between Ca^{2+}, Mg^{2+} and HCO_3^- (Herman and Lorah, 1988; Szramek and Walter, 2004; Williams et al., 2007; Szramek et al., 2007), and relations of Ca^{2+}/Mg^{2+} and Ca^{2+}/Sr^{2+} molar ratios to saturation of waters with respect to calcite (Galy and France-Lanord, 1999; Jacobson et al., 2002). The Mg^{2+}/Ca^{2+} and Mg^{2+}/HCO_3^- ratios decrease downstream, indicating the loss of Mg^{2+} but not of Ca^{2+} and HCO_3^-. Average Ca^{2+}/HCO_3^- molar ratio in the Krka headwaters is 0.36 and slightly increases to 0.38 downstream. An increasing pattern shows that HCO_3^- is removed from the water, but since no correlation between Ca^{2+}/HCO_3^- and log pCO_2 or $SI_{calcite}$ was found, variations in HCO_3^- content are likely subjected to other processes rather than only to CO_2 outgassing and subsequent calcite precipitation. Similar to Ca^{2+}/HCO_3^- changes, no correlation was observed between Mg^{2+}/HCO_3^- and log pCO_2 or $SI_{calcite}$. This implies that the loss of HCO_3^- due to in-stream carbonate precipitation is minor and does not significantly affect the geochemistry of Krka waters, which is in line with findings from the study of Dinaric waters of Szramek et al. (2011).

Based on available data of discharges (Appendix 1), the tributaries contribute approximately 30 % of the whole water flux to the Krka River stream. They drain predominantly limestone areas, thus contributing Ca^{2+} and HCO_3^- ions. The catchment area of the headwaters accounts for only 11 % of the whole Krka watershed area, thus the rest of the water flux must originate from additional groundwater input recharging downstream. Most reasonable explanation for the observed changes in Ca^{2+}, Mg^{2+} and HCO_3^- content would be that stream waters are influenced by the input of Mg-poor water from the tributaries and diffusive downstream groundwater discharge (Kogovšek and Petrič, 2002). The latter seem to have different chemical composition than the groundwaters discharging at the main spring, as a result from draining predominantly limestone areas in the southern flanks of the watershed. The input of additional groundwater is so large that processes of CO_2 outgassing and in-stream $CaCO_3$ precipitation are masked by the massive inflow of groundwater.

6.3 Carbonate weathering rates and associated CO_2 consumption rates

Chemical weathering rates of a drainage basin can be estimated by combining the water chemistry, hydrological and surface area data available for the basin (Galy and France-Lanord, 1999). The rate of carbonate weathering (CWR) for the Krka watershed was

calculated using an approach adopted from Roy et al. (1999) and is based on two assumptions: (1) Ca^{2+}, Mg^{2+} and HCO_3^- concentrations are not influenced by local anthropogenic pollution, and (2) during carbonate dissolution by carbonic acid half the amount of HCO_3^- is derived from chemical weathering and the other half from atmospheric/soil CO_2:

$$CWR = (Ca^{2+} + Mg^{2+} + 0.5 \times HCO_3^-) \times \text{discharge} / \text{drainage area} \quad (48)$$

In the calculation, concentrations of Ca^{2+}, Mg^{2+} and HCO_3^- at sampling point W18 (Appendix 1) and discharge data at gauge station 2 (Figure 16) were considered. The calculated estimations of carbonate weathering and CO_2 consumption rates within the Krka watershed showed significant seasonal differences and are presented in Table 10.

Table 10: *Calculated carbonate weathering (CWR) and CO_2 rates (R_{CO2}) at the outflow of the Krka River.*

		Discharge (m^3/month)	CWR (t/km^2/month)	R_{CO2} ($\times 10^3$ mol/km^2/month)
2008	Winter	25.6	-	61
	Spring	47.3	18.4	116
	Summer	20.2	8.0	50
	Autumn	49.0	20.2	123
2009	Winter	165	63.9	396
	Spring	48.8	18.4	114
	Summer	13.1	5.1	32
	Autumn	24.2	10.3	65
2010	Winter	37.9	16.4	103
	Spring	83.8	31.4	195
	Summer	16.3	6.4	41
	Autumn	88.1	34.6	217

The lowest CWR were calculated for summer (average 7 t/km^2/month) and winter (average 8 t/km^2/month), while in spring and autumn similar average weathering rates were observed (23 and 22 t/km^2/month). Such differences may be ascribed to the variability of the discharge amount, which was the highest in spring and autumn. On an annual base, the CWR was 186 t/km^2/yr in 2008, 293 t/km^2/yr in 2009 and 267 t/km^2/yr in 2010. This is similar to reported CWR values from other karstic watersheds, e.g. 133 t/km^2/yr (Li et al., 2010), 131 t/km^2/yr (Xijiang River basin, Sun et al., 2010), or sedimentary basins, e.g. 109 t/km^2/yr in the Rhone River watershed or 126 t/km^2/yr in the Po River watershed (Gaillardet et al., 1999). On a global scale the calculated CWR values for the Krka are 3 to 7 times higher than the mean world CWR value of 24 t/km^2/yr (Gaillardet et al., 1999). Such difference can be explained by enhanced solubility of the carbonte bedrock and high runoff conditions in the Krka watershed. Based on calculated CWR for the Krka watershed and considering a carbonate density of 2.7 g/cm^3 (Galy and France-Lanord, 1999), we estimated that approximately 70 to 110 mm/1000 years of carbonate is being eroded in the Krka basin.

As mentioned before, chemical weathering is the principal processes of removing CO_2 from the atmosphere on the geological time scale (Richey, 2005). For limestone weathering, the removal of 1 mol of $CaCO_3$ consumes 1 mol of CO_2 from the atmosphere and for dolomite weathering, the removal of 1 mol of $CaMg(CO_3)_2$ needs 2 mol of CO_2 from the atmosphere. Assuming that during carbonate dissolution by carbonic acid only half the amount of HCO_3^- is derived from atmospheric/soil CO_2, therefore the total CO_2 (R_{CO2}) consumed by rock weathering can be calculated as:

$$R_{CO_2} = 0.5 \times HCO_3^- \times \text{discharge}/\text{drainage area} \quad (49)$$

The average annual atmospheric CO_2 consumption by carbonate weathering was estimated to be 16×10^5 mol/km^{2}yr in the Krka watershed, twice as much as the estimate of 8×10^5 mol/km^{2}yr for world-scaled CO_2 consumption (Meybeck, 1987).

6.3.1 Relationship between chemical weathering and environmental factors

Chemical weathering is governed by different environmental factors. Millot et al. (2002) proposed that the effect of runoff dominates while others found that temperature is more important (Dalai et al., 2002). Gaillardet et al. (1999) considered both significant, whereas Oliva et al. (2003), Hagedorn and Cartwright (2009) and Sun et al. (2010) consider water-rock interaction more important. The major ion concentrations in Krka River generally decrease exponentially with an increasing discharge (Figure 47). The power of regression fits for Mg^{2+} and total alkalinity range from -0.2 to -0.1, consistent with a range of -0.4 to 0 for majority of the world rivers (Walling and Webb, 1986). Changes in Ca^{2+} content didn't show any correlation with discharge, most likely due to groundwater discharge downstream. Compared with the changes in discharge, Mg^{2+} concentrations and total alkalinity varied with smaller amplitude. Sun et al. (2010) observed similar relation between discharge and solute content and suggested that increasing discharge/runoff must increase chemical weathering.

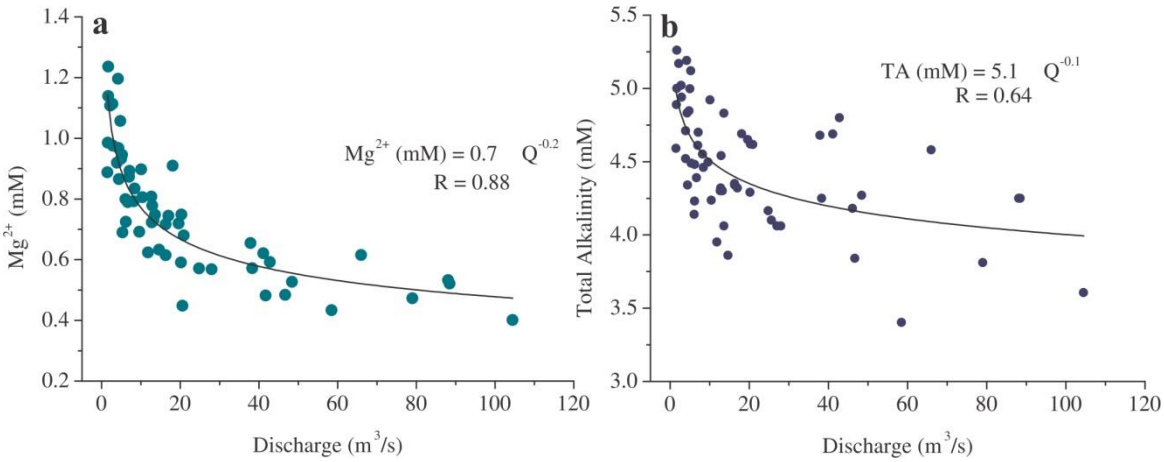

Figure 47: *Relation between discharge and content of Mg^{2+} (**a**) and total alkalinity (**b**) in the main channel of Krka.* A decrease of ion content in the Krka River exponentially decreases with increasing discharge (Q).

A positive but weak correlation between runoff and temperature (R = 0.43) in the Krka watershed suggests that other factors, such as duration of water-rock interaction might control the weathering intensity. Such assumption is supported by the presence of moderately thick (~ 70 cm, Repe, 2004) soil cover in the watershed, which favours mineral weathering due to longer and deeper water circulation prolonging the contact between the water and weatherable minerals (Stallard, 1985).

The calculated CWR values were the lowest for Višnjica tributary (Figure 48), even though it had the highest content of Ca^{2+} and Mg^{2+} ions in comparison with other streams in the watershed. Due to its non-karstic basin, the ion content in water depends on runoff intensity and dissolution of alluvial deposits. However, similar CWR values between the outflow and tributaries Radešca and Prečna (sampling points W11 and W14, respectively, Figure 16) indicate that weathering in the watershed is predominantly controlled by

water-rock interaction and soil CO_2 availability - this is due to their karstic nature with intensive water-rock interaction and thick soil covers in their sub-catchments.

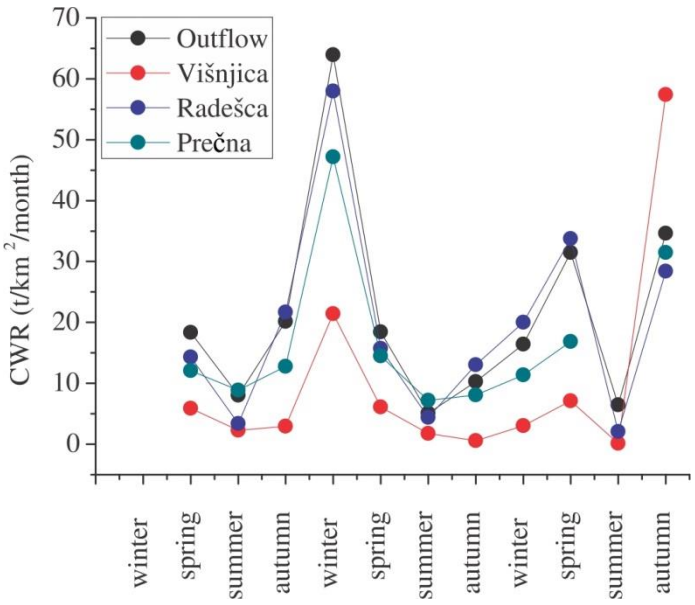

Figure 48: *Calculated carbonate weathering rates (CWR) in Krka watershed.* The lines indicate CWR calculated by combining data on Ca^{2+}, Mg^{2+} and HCO_3^- content, discharge and area of (sub)-watersheds. Diagram represents CWR calculated at the outflow (W18, Figure 16), and tributaries Višnjica, Radešca and Prečna (W3, W11 and W14, respectively, Figure 16).

6.4 Dissolved inorganic carbon in the Krka watershed

6.4.1 Temporal and spatial variability of DIC and its isotopic composition

DIC content in a river watershed is strongly controlled by geology (e.g. Telmer and Veizer, 1999; Kanduč et al., 2007a) and closely related to soil CO_2 (Hope et al., 2004). Low DOC and high DIC and CO_2 concentrations typify waters in the Krka watershed that have been extensively influenced by interaction of soil waters with carbonate bedrock.

The DIC content was measured in water samples collected in year 2008, while the content of DIC in water samples collected in 2009 and 2010 was calculated according to equations (7–9) and (11). A good positive correlation between measured and calculated DIC (Figure 49) allowed us to estimate DIC concentrations based on measured water temperature and pH and calculated log pCO_2.

Temporal and spatial variability of DIC and its carbon isotopic composition ($\delta^{13}C_{DIC}$) are presented in Figures 33 and 36, respectively. DIC content in the Krka waters ranged from 3.61 to 5.94 mM (average 4.63 ± 0.5 mM), reflective of intensive carbonate weathering. A spatial behaviour in the upper reaches showed a decreasing trend followed by a slight increase and remained fairly stable afterwards. The concentrations of DIC were the lowest during spring (average 4.0 mM) when the discharges were the highest (up to 104 m^3/s; average 32 m^3/s), most likely due to snowmelt at higher altitudes.

The $\delta^{13}C_{DIC}$ values in Krka waters ranged from -16.0 ‰ to -10.5 ‰ (average -12.8 ± 1.0 ‰), reflecting variable contributions of different carbon sources (soil pCO_2 and carbonate dissolution) and impacts of processes in the stream that fractionate carbon isotopic composition of DIC (degassing and CO_2 exchange with the atmosphere, dissolution and precipitation of carbonate minerals in the stream, photosynthesis, and

respiration). A clear distinction between the headwaters and stream water can be seen in the carbon chemistry of these waters; in the headwaters the content of DIC and log pCO_2 were the highest, while the $\delta^{13}C_{DIC}$ values were the lowest. The processes influencing the sources of carbon in the Krka watershed and in-stream processes that affect the content of DIC and $\delta^{13}C_{DIC}$ values are discussed below.

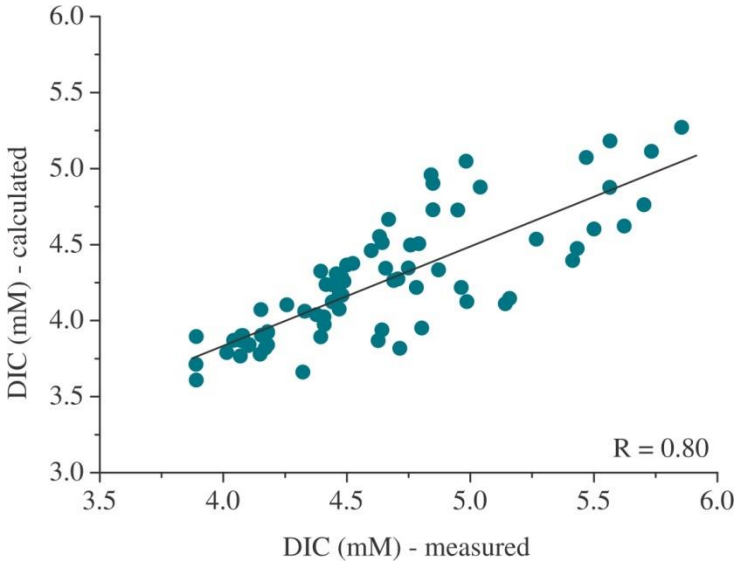

Figure 49: *Calculated versus measured DIC values in Krka waters.* The relation is based on water samples collected in 2008.

6.4.1.1 Sources of carbon

In general, major sources of riverine DIC are soil CO_2 derived from respiration and degradation of organic matter respiration and dissolution of carbonates within the watershed (e.g. Telmer and Veizer, 1999; Barth et al., 2003; Doctor et al., 2008). Due to their difference in carbon isotopic composition, the $\delta^{13}C$ values of DIC in waters can discriminate relative contributions from these sources. Hence, the expected $\delta^{13}C_{DIC}$ values were calculated for the groundwater DIC originating from mixing of soil CO_2 and dissolution of carbonate minerals.

Respiration and microbial degradation of terrestrial plants release CO_2 into the soil. The vegetation in Krka River watershed mostly follows the C_3 photosynthetic pathway, characterized by $\delta^{13}C$ values between -34.8 ‰ and -29.2 ‰ (average -31.6 ± 1.5 ‰, Kanduč et al., 2007b). The presence of C_4 plants with $\delta^{13}C$ values of -13 ‰ (Finlay and Kendall, 2007) in the study area is minor, thus we consider its contribution to the soil carbon imprint negligible. The $\delta^{13}C$ value of biogenic soil CO_2 is derived primarily from $\delta^{13}C$ value of organic material that is being oxidized in soils, thus releasing CO_2. During CO_2 production, little or no fractionation occurs (Peterson and Fry, 1987), but exchange with atmospheric CO_2, diffusion of soil CO_2 and production of CO_2 by carbonate weathering might shift the $\delta^{13}C$ value of soil CO_2.

Soil water essentially represents rainfall as it percolates through the soil enriched with CO_2. In this study, analyses of DIC concentrations and $\delta^{13}C_{DIC}$ in rainwater were not performed, however, hypothetical $\delta^{13}C_{DIC}$ value of rainwater can be estimated using atmospheric carbon dioxide $\delta^{13}C_{CO2}$ composition (-8.1 ‰; White and Vaughn, 2011) and the fractionation between $CO_{2(g)}$ and aqueous carbon species. Carbon fractionation in the $HCO_{3\,(aq)}^-$-$CO_{2(g)}$ system varies between 10.9 ‰ at 0 °C and 7.4 ‰ at 30 °C (Mook et al., 1974), therefore, the $\delta^{13}C_{DIC}$ values of rainwater assuming equilibrium with atmospheric CO_2 yield values between -0.7 ‰ and +2.8 ‰. Nevertheless, the contribution of

atmospheric CO_2 through the soils into rivers is of minor importance (Telmer and Veizer, 1999; Li et al., 2010) due to its low DIC content (0.1 to 0.5 µmol/L; Stumm and Morgan, 1981), low pH (i.e. ~5; Table 8) and high partial pressure of soil CO_2.

A more important isotope shift during CO_2 transfer through the soil horizon is caused by diffusional fractionation between $^{12}CO_2$ and $^{13}CO_2$ leading to enrichment with ^{13}C by up to +4.4‰ relative to the organic source material (Cerling, 1991). Consequently, the $\delta^{13}C$ of soil CO_2 in Krka watershed would range from -30.4 ‰ to -24.8 ‰ (average -27.2 ‰) for C_3 vegetation type. If DIC in Krka River waters would originate solely from respiration CO_2, than at the equilibrium with soil CO_2, the $\delta^{13}C_{DIC}$ of Krka River would be enriched with ^{13}C by +3.5 ‰ to +8.4 ‰ (Vogel et al., 1970), considering water temperature range between 3.0 and 24.3 °C (average 11.6 °C) and pH from 7.10 to 8.52 (average 7.90). Using calculated enrichment factor of C_3 plants respiration, $\delta^{13}C_{DIC}$ should yield values of -26.9 ‰ to -16.4 ‰ (average -21.4 ‰).

The isotopic composition of DIC resulting from carbonate weathering depends on whether dissolution takes place in open or closed conditions (Clark and Fritz, 1997). Both conditions assume the water residence times are long enough to achieve isotopic exchange, which most often holds true in groundwaters due to fast reaction kinetics in the carbonate system relative to residence times (Deines et al., 1974; Doctor et al., 2008). Carbonate mineral dissolution in an open system yields highly depleted $\delta^{13}C_{DIC}$ values due to continual exchange of CO_2 between groundwater and soil atmosphere (i.e. average -31.7 ‰ in the Krka watershed). In a closed system half of the DIC is related to carbonate mineral dissolution, hence the DIC is enriched with ^{13}C; the carbonate bedrock in Krka watershed has an average $\delta^{13}C$ value of +1.4 ‰ (n = 5).

The dissolution of carbonate by carbonic acid is described in the following equation (Telmer and Veizer, 1999):

$$CaC_{carb}O_3 + H_2C_{resp}O_3 \leftrightarrow Ca^{2+} + 2HC_{cw}O_3^- \qquad (50)$$

where C_{carb} ($\delta^{13}C$ = +1.4 ‰) is carbon derived from carbonate dissolution and C_{resp} is derived from soil CO_2 (average $\delta^{13}C_{resp}$ = -27.2 ‰). A 1:1 mixture of DIC derived from carbonate dissolution and soil-derived carbonic acid in the Krka groundwaters is expected to have a $\delta^{13}C_{DIC}$ between -14.5 ‰ and –11.7 ‰ (average -12.9 ‰) for the carbonate weathering end-member (C_{cw}). However, the measured $\delta^{13}C_{DIC}$ values of the headwaters ranged from -15.6 ‰ to -11.3 ‰ (average -13.6 ± 0.9 ‰), suggesting that carbonate mineral dissolution in the watershed occurs primarily under open system conditions. The discrepancy between calculated and measured $\delta^{13}C_{DIC}$ values of the headwaters may be related to outgassing of CO_2 from the water associated with the groundwater discharge (e.g. Doctor et al., 2008). The stoichiometric proportion of carbonate-derived DIC is obviously overestimated; based upon the measured $\delta^{13}C_{DIC}$ values of the headwaters, the average calculated soil derived DIC fraction in the headwaters in Krka watershed is 52 %.

6.4.1.2 Controls on DIC content and $\delta^{13}C_{DIC}$ values in Krka stream waters

After waters discharge they become subjected to processes that occur in the river and further influence the isotopic composition of DIC. The $\delta^{13}C_{DIC}$ values in Krka stream waters ranged from -15.1 ‰ to -10.5 ‰ (average -12.6 ± 0.9 ‰) and from -15.1 ‰ to -10.6 ‰ (average -13.0 ± 1.0 ‰) in the tributaries. As mentioned before, DIC in the main channel and the tributaries had higher $\delta^{13}C_{DIC}$ values in comparison with the headwaters (Figure 36). A negative relation between $\delta^{13}C_{DIC}$ and pCO_2 implies that changes in $\delta^{13}C_{DIC}$ can be attributed to the variability of pCO_2 in the waters; statistically significant correlation between $\delta^{13}C_{DIC}$ and log pCO_2 values was observed (Figure 50a) in all seasons (R = -0.65), except in summer (R < -0.50).

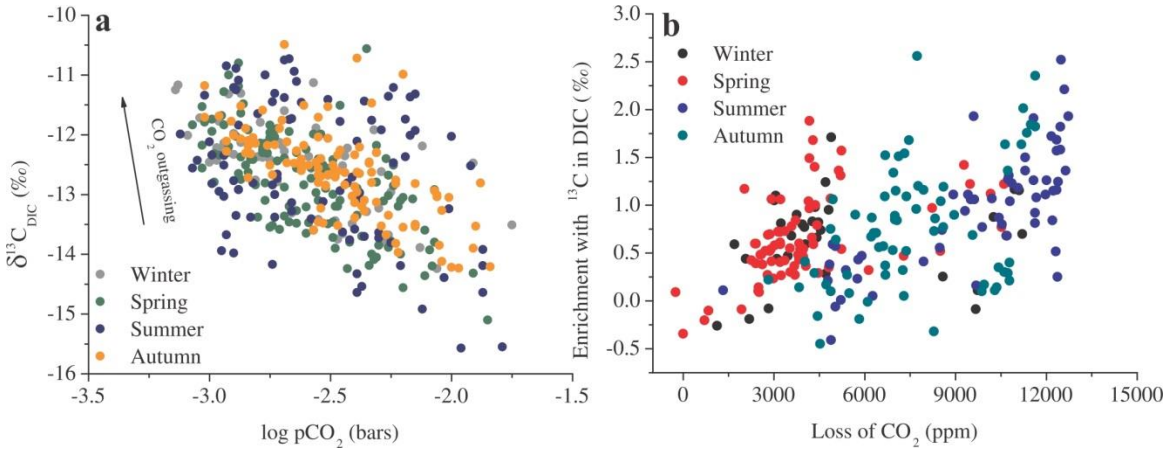

Figure 50: *Relationship between pCO_2 and $\delta^{13}C_{DIC}$.* A negative relationship between log pCO_2 and $\delta^{13}C_{DIC}$ indicates that CO_2 outgassing affects the carbon isotopic composition of DIC (**a**). The enrichment with ^{13}C of DIC is influenced by CO_2 outgassing.

Enrichment of DIC with ^{13}C was estimated as a difference between $\delta^{13}C$ values of DIC in the headwaters and those in stream water ($\delta^{13}C_{DIC\,(HW)}$ - $\delta^{13}C_{DIC\,(SW)}$). Figure 50b shows that the enrichment is positively correlated with CO_2 loss, calculated as a difference between headwaters $pCO_{2(HW)}$ and stream water $pCO_{2(SW)}$ (in ppm). The average magnitude of ^{13}C the enrichment with ^{13}C was the highest in summer (1.0 ‰), whereas in other seasons it ranged from 0.6 ‰ in spring to 0.8 ‰ in autumn. Losses of CO_2 can be ascribed to several processes such as photosynthesis, CO_2 outgassing and authigenic precipitation of $CaCO_3$, whereas *in-situ* respiration produces more CO_2 resulting in depletion with ^{13}C in DIC. Nevertheless, these processes are more pronounced in stagnant surface waters (i.e. lakes) than in fast flowing rivers (Rozanski et al., 2001). Several studies on isotopic composition of DIC in riverine systems have shown that isotopic exchange with the atmospheric CO_2 is a major controlling process on the isotopic composition of in-stream DIC evolution (Aucour et al., 1999; Telmer and Veizer, 1999; Kanduč et al., 2007a; Ferguson et al., 2011), however, transformations of organic to inorganic carbon can have a significant influence on riverine $\delta^{13}C$ (Barth and Veizer, 1999; Brunet et al., 2009). Relative importance of processes contributing to $\delta^{13}C_{DIC}$ variability in Krka River is examined below. The offset in $\delta^{13}C_{DIC}$ values between the sampling years is likely a response to differences in hydrological regimes.

6.4.1.2.1 CO_2 outgassing

The enrichment with ^{13}C of DIC in Krka stream waters ranged from 0.1 ‰ to 2.6 ‰. In general, the amplitude of the enrichment was the highest in parts with more turbulent water (i.e. on cascades), where the gas exchange is most pronounced implying that CO_2 outgassing due to differences in CO_2 levels between the river water and atmosphere significantly affects the isotopic imprint of riverine DIC.

Isotopic equilibration of DIC and atmospheric CO_2 is a relatively slow process in comparison with water transit times (Aucour et al., 1999; Kanduč et al., 2007a). Amiotte-Suchet et al. (1999) found that isotopic exchange between aqueous $CO_{2\,(aq)}$ and atmospheric $CO_{2\,(g)}$ is faster than that between $HCO_{3\,(aq)}$ and $CO_{2\,(g)}$. Average isotopic fractionation between aqueous and atmospheric CO_2 in Krka waters was calculated to be between 1.1 ‰ using the equilibrium equation from Vogel et al. (1970). However, average fraction of $CO_{2\,(aq)}$ in the Krka waters is only 5 %, thus the fractionation of CO_2 between water and gas alone cannot explain the enrichment with ^{13}C in DIC.

Under open system conditions, favourable for rapid CO_2 exchange, kinetic isotope

fractionation can result in greater isotope enrichment. Zhang et al. (1995) reported a kinetic fractionation of ^{13}C between $CO_{2(g)}$ and $HCO_{3\,(aq)}^{-}$ from 0.3 ‰ to 1.5 ‰ in a closed system at low pH ~2. Greater fractionation was observed by Marlier and O'Leary (1984) who determined kinetic fractionation factor for the dehydration of bicarbonate to be α = 1.0147 (in open system conditions at 24 °C and pH ~8.2), thus the enrichment would be 14.7 ‰. In the study of ground-surface water relations in a small-size watershed Doctor et al. (2008) reported an increase in $\delta^{13}C_{DIC}$ of roughly 2.3–2.4 ‰.

6.4.1.2.2 Biogeochemical influences

Aquatic metabolism represents the balance of riverine respiration and photosynthesis. Photosynthesis preferentially consumes $^{12}CO_2$ leaving riverine DIC enriched with ^{13}C. Isotopic fractionation between photosynthetically assimilated CO_2 and riverine DIC varies from 3 ‰ to 10 ‰ (Vogel et al., 1993). In contrast to photosynthesis, *in-situ* respiration as aerobic transformation of organic matter into inorganic carbon, produces DIC enriched with ^{12}C ($\delta^{13}C_{DIC}$ < -25 ‰). The respiration in rivers often exceeds photosynthesis due to large inputs of organic carbon from terrestrial environment (Battin et al., 2008). Nevertheless, transformations of organic to inorganic carbon were found to have a significant influence on riverine $\delta^{13}C_{DIC}$ values (Barth and Veizer, 1999; Brunet et al., 2009). Kanduč et al. (2007b) found that major sources of organic matter in Sava waters are eroded soils from the riparian zones and plant litter, while Junge et al. (2005) showed that freshwater plankton significantly fractionates stable carbon and nitrogen composition of organic matter in the Weisse Elster River (Germany). Such differences may be attributed to different hydrological and runoff intensity conditions in the watersheds.

The isotopic composition of POC in Krka waters ranged from -31.7 ‰ to -25.0 ‰ (average -29.2 ± 1.5 ‰) implying different sources of organic carbon. Major inputs to the organic carbon pool in rivers are allochtonous (terrestrial/riparian vegetation) and autochthonous matter (plankton and detrital organic matter of planktonic origin). Isotopic composition of phytoplankton was not determined in this study, but its carbon isotopic fingerprint can be calculated using measured $\delta^{13}C_{DIC}$ values and estimated isotopic fractionation of 22.3 ‰ between riverine DIC and phytoplankton (Tan and Strain, 1983; Hellings et al., 1999). Given that $\delta^{13}C_{DIC}$ values in Krka River waters range from -16.0 ‰ to -10.5 ‰, the expected $\delta^{13}C$ of phytoplankton would range from -38.3 ‰ to -32.8 ‰ (average -35.1‰). The relative fractions of allochtonous (*allo*) and autochthonous (*auto*) POC can be estimated by applying a two source-mixing model (e.g. Hellings et al., 1999):

$$\delta^{13}C_{POC}=\delta^{13}C_{POC\text{-}\,allo}\times f_{allo}+\delta^{13}C_{POC\text{-}\,auto}\times f_{auto} \qquad (51)$$

where $\delta^{13}C_{POC\,-\,allo}$ values of -30.4 ‰ to -24.8 ‰ (average -27.2 ‰) were considered. The calculation showed that in Krka River watershed the dominant source of POC is terrestrial debris. Autochthonous component contributed up to 45 % in spring in summer to the total POC, whereas in autumn its contribution was minor (< 15 %). To further reconstruct organic carbon sources and processes affecting its isotopic composition in Krka, we plotted $\delta^{15}N_{PN}$ versus $\delta^{13}C_{POC}$ (Figure 51a) and $\delta^{13}C_{DIC}$ values (Figure 51b) supporting the estimation of detrital material being the major contributor to the organic carbon pool in Krka River. The $\delta^{15}N_{PN}$ values ranged from +2.2 ‰ to +6.8 ‰ (average 5.1 ± 1.1 ‰). Additionally, Figure 51b shows that $\delta^{13}C_{POC}$ values are influenced by degradation and photosynthesis in the river. The latter corresponds in lower $\delta^{13}C_{POC}$ values due to intensive bioproductivity during spring and summer.

Moreover, the enrichment with ^{13}C of DIC downstream was the highest in summer

(average 1.0 ‰) and is accompanied with a slight decrease in $\delta^{13}C_{POC}$. A slight decrease in $\delta^{13}C_{POC}$ of OM in Krka waters was observed for summer relative to other seasons and is often ascribed to algal blooms (Finlay and Kendall, 2007). Furthermore, a decrease in $\delta^{13}C_{POC}$ values in Krka is accompanied with the largest enrichment with ^{13}C of DIC downstream, which implies that CO_2 outgassing in Krka is induced by in-stream photosynthesis.

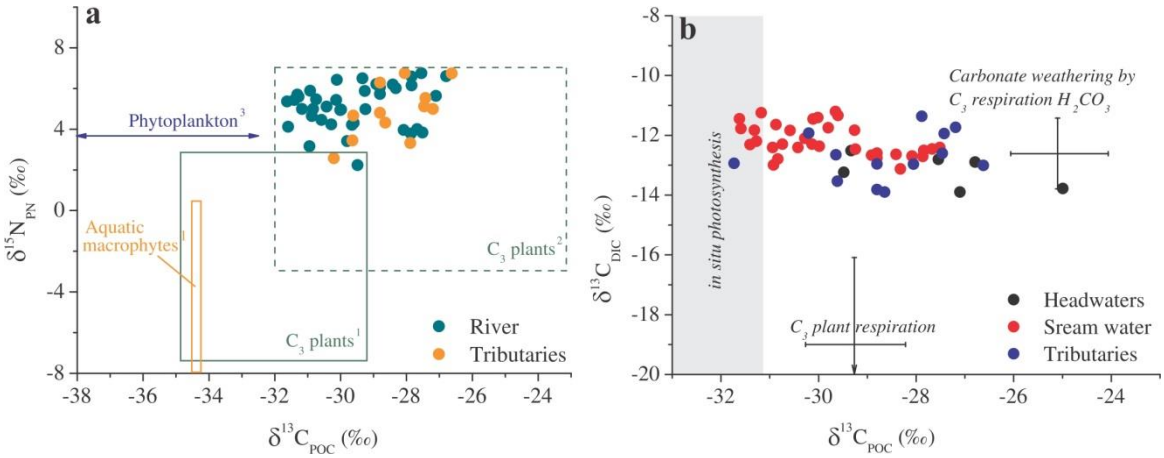

Figure 51: *Isotopic composition of particulate organic matter in Krka waters.* Plots (**a**) $\delta^{15}N_{PN}$ versus $\delta^{13}C_{POC}$ and (**b**) $\delta^{13}C_{DIC}$ and $\delta^{13}C_{POC}$ show source of POC and a relation of carbon isotopic composition between POC and DIC.

Based on positive correlation between $\delta^{13}C_{DIC}$ values and concentrations of dissolved organic carbon (DOC) Barth and Veizer (1999) found that river systems do not only transport carbon but also decompose organic carbon, which results in lowering the $\delta^{13}C$ values of DIC pool. They also stated that relationship between DOC and $\delta^{13}C_{DIC}$ reveals biogeochemical state of the ecosystem. In addition, Shin et al. (2011) found a positive correlation between the enrichment with ^{13}C and dissolved oxygen saturation in the study of surface waters in a carbonate watershed, suggesting that photosynthesis might attribute to the enrichment. On the contrary, Kanduč et al. (2007b) attributed slightly higher $\delta^{13}C$ values of POC relative to organic carbon of C_3 plants in the Sava watershed to biological degradation and anthropogenic influences. Similar pattern was observed for the $\delta^{13}C_{POC}$ in OM of Krka waters.

DOC concentrations in the Krka waters are low (0.02–0.40 mM, average 0.17 mM) in comparison with other rivers (e.g. up to 4.3 mM, Brunet et al., 2009) where DOC contributes largely to total dissolved carbon. There was no significant correlation between $\delta^{13}C_{DIC}$ and DOC concentrations in Krka, therefore we assume that DOC transformations in the water, either by photosynthesis or respiration, have no significant effect on the overall $\delta^{13}C$ of DIC in Krka waters. Additionally, due to the lack of correlation between $\delta^{13}C_{POC}$ and $\delta^{13}C_{DIC}$ in Krka waters, we assume photosynthesis has a negligible effect on the overall DIC.

6.4.1.2.3 In-stream precipitation of authigenic calcite

The carbon in the river waters can be according to the equation (16) lost by calcite precipitation and CO_2 outgassing at the same time, hence the riverine DIC can also be influenced by authigenic precipitation of $CaCO_3$ in the stream. Contribution of in-stream calcite precipitation to carbon budget in rivers is hard to estimate, especially when the pathways of groundwaters recharging the stream are unclear. Given the relatively small isotopic fractionations associated with in-stream carbonate precipitation its influence on

$\delta^{13}C_{DIC}$ should be minor regardless of its scale (Wachniew, 2006). A positive correlation between $SI_{calcite}$ and $\delta^{13}C_{DIC}$ values in the Krka waters (Figure 52) implies that the loss of CO_2 and subsequent enrichment with ^{13}C of DIC could be due to CO_2 outgassing resulting from $CaCO_3$ precipitation. Statistically significant correlation (at $p < 0.05$) was the lowest in autumn ($R = 0.64$), while in spring and winter the correlation was higher ($R = 0.70$ and 0.78, respectively). Interestingly, there was no correlation observed for the summer water samples. Nevertheless, spring and winter months were characterised with the highest discharges leading to high turbidity of the water body. An increased turbidity promotes CO_2 outgassing leaving the water saturated with respect to calcite and depleting the DIC pool with ^{12}C.

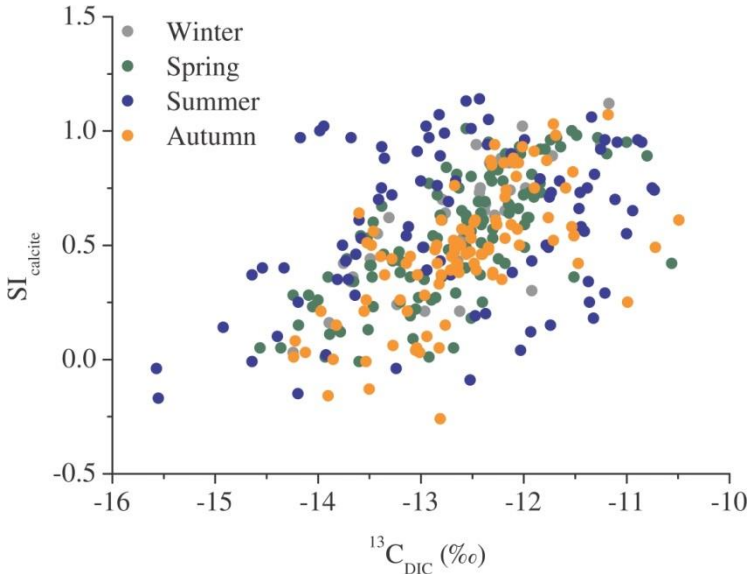

Figure 52: *Relation between $SI_{calcite}$ and $\delta^{13}C_{DIC}$ in Krka stream waters.* Statistically moderate relation indicates that changes $\delta^{13}C$ of DIC could relate to in-stream calcite precipitation.

Moreover, relatively small isotopic effects on the $\delta^{13}C_{DIC}$ values arise from kinetic fractionation between HCO_3^- and $CaCO_3$ (Mickler et al., 2004) that would be in case of rapid calcite precipitation 0.3 ‰ (Turner, 1982). The enrichment of $^{13}\varepsilon_{cc\text{-}HCO3}$ of 1.0 ± 0.2 ‰ and 0.94 ± 0.06 ‰ irrespective of temperature or precipitation rate was found by Romanek et al. (1992) and Jímenez-Lopez et al. (2001), respectively. Considering average $\delta^{13}C_{DIC}$ value of -12.6 ‰ of Krka stream waters and fractionation factors between DIC and $CaCO_3$ mentioned above, the precipitated calcite would range from -12.3 ‰ to -11.6 ‰. These values are up to 2‰ lower than the average measured $\delta^{13}C$ value of -10.2 ‰ for tufa samples collected in the Krka stream. Thus, we conclude that active tufa precipitation in Krka does not affect the $\delta^{13}C$ of DIC significantly. Nevertheless, XRD analyses showed that tufa samples contain a considerable amount of detrital carbonate phase (up to 19 %, Appendix 3) which can influence the isotopic composition of the precipitate resulting in higher δ values of tufa. Potential influence of detrital component on the isotopic composition of tufa is discussed in Chapter 6.6.4 .

To summarize, turbulent and fast flow conditions in Krka River promote CO_2 degassing from water to the atmosphere. The variations in isotopic composition of DIC in stream water show that various in-stream processes influence the $\delta^{13}C$ values of DIC. The contribution of aquatic metabolism and authigenic carbonate precipitation is hard to distinguish. Nevertheless, the overall variation in $\delta^{13}C_{DIC}$ values can be mainly attributed to CO_2 loss due to the CO_2 exchange between atmosphere and riverine water.

6.5 Carbon fluxes, CO_2 outgassing and mass balance calculations

Carbon fluxes for the Krka River and its tributaries were calculated as the product of flow volumes and concentrations of dissolved inorganic carbon in river water. As discussed above, CO_2 outgassing was found to be the major control on the variability of DIC content and $\delta^{13}C_{DIC}$ values in Krka waters. The amount of CO_2 degassed was calculated based on a theoretical diffusion model of CO_2 flux following the equation developed by (Broecker, 1974):

$$F_{CO_2}=\frac{D}{z}\times(CO_{2\,(eq)}-CO_2) \qquad (52)$$

where D is the CO_2 diffusion coefficient, z is the thickness of the boundary layer (a thin film existing at the air-water interface), and $CO_{2(eq)}$ and CO_2 are concentrations of dissolved CO_2 in equilibrium with the atmosphere and measured CO_2, respectively. D/z is the gas exchange rate representing the height of a water column that will equilibrate with the atmosphere per time unit. The thickness of the boundary layer *z* depends largely on wind velocity (Broecker, 1974) and water turbulence (Holley, 1977). In this study, CO_2 fluxes were calculated using a D/z value of 8 cm/h and 28 cm/h at low and moderate turbulence conditions (Mook, 1970).

The DIC fluxes in the Krka ranged from 3.5×10^9 mol/yr in 2008 to 7.0×10^9 mol/yr in 2010, depending on discharge. The lowest fluxes were calculated for summer (average 2.0×10^8 mol/month), while higher fluxes were usually observed in spring and autumn due to increased discharge (average 5.4×10^8 mol/month and 5.5×10^8 mol/month, respectively). DOC fluxes can be calculated only for the sampling year 2008 and are estimated to be 2.1×10^8 mol/yr. Considering the river surface area of 2.9 km^2 (length of 96 km and a mean width of 30 m), the estimated total diffusive loss of CO_2 ranges from 2.0×10^8 to 3.0×10^8 mol/yr. The estimated CO_2 fluxes were in general the highest in autumn (average 2.8×10^7 mol/month) and the lowest in summer (average 1.5×10^7 mol/month). It is important to note that CO_2 degassing estimates are accompanied by uncertainties arising from turbulence of the river water and the groundwater contribution in the downstream section, therefore, our estimates of carbon fluxes here represent conservative values.

A simple isotopic mass balance calculation was performed to quantify different sources of DIC at the outflow of the Krka in sampling period 2010, considering the sum of tributary inputs and biogeochemical processes in the watershed. As discussed in previous sections, the major inputs to the DIC flux (DIC_{river}) and $\delta^{13}C_{DIC}$ are from tributaries (DIC_{trib}), degradation of organic matter (DIC_{org}), exchange with the atmosphere (DIC_{ex}), and dissolution of carbonates (DIC_{carb}). The inputs can be estimated by:

$$DIC_{river} = DIC_{trib}-DIC_{ex}+DIC_{org}+DIC_{carb} \qquad (53)$$

$$DIC_{river}\cdot\delta^{13}C_{river}=DIC_{trib}\cdot\delta^{13}C_{trib}-DIC_{ex}\cdot\delta^{13}C_{ex}+DIC_{org}\cdot\delta^{13}C_{org}+DIC_{carb}\cdot\delta^{13}C_{carb} \qquad (54)$$

DIC_{river}, DIC_{trib} and DIC_{ex} were calculated as a product of DIC concentration and discharge, and the $\delta^{13}C_{river}$, $\delta^{13}C_{trib}$ and $\delta^{13}C_{POC}$ are reported in Table 11. In the equations (53) and (54) the minus sign indicates outgassing of CO_2. The $\delta^{13}C_{ex}$ value was calculated using the equation for equilibrium isotope fractionation between atmospheric CO_2 and carbonic acid in water (Zhang et al., 1995):

$$^{13}\varepsilon_{HCO_3^-\text{-}CO_2}=-(0.141\pm0.003)\cdot T+(10.78\pm0.05) \qquad (55)$$

where $^{13}\varepsilon_{HCO3\text{-}CO2}$ is an enrichment factor between aqueous bicarbonate ion and gaseous

carbon dioxide and temperature (T) is in °C. Considering atmospheric CO_2 as the ultimate source for the CO_2 exchange in the Krka watershed and a $\delta^{13}C$ value of -8.1 ‰ for atmospheric CO_2 (White and Vaughn, 2011), the average isotopic contribution of equilibration between atmospheric CO_2 and DIC ($\delta^{13}C_{ex}$) would then be +1.7 ‰ in winter, +1.3 ‰ in spring, +0.6 ‰ in summer and +1.5 ‰ in autumn. For determining carbonate dissolution contribution average $\delta^{13}C_{carb}$ value of +1.4 ‰ was used in the mass balance equations. The unknowns in equations (53) and (54) are DIC_{org} and DIC_{carb}.

The calculated fluxes for all sampling seasons in 2010 are presented in Table 11. The DIC_{org} and DIC_{carb} values were determined by solving the mass balance equations. The calculated contributions to the average DIC budget from DIC_{trib}:DIC_{ex}:DIC_{org}:DIC_{carb} at the Krka mouth were 21.5:-4.5:37.8:45.3 % in spring, 13.4:-8.3:41.9:52.9 % in summer, 27.0:-3.6:39.7:36.9 % in autumn and 27.9:-2.5:42.4:32.2 % in winter.

Table 11: *Calculated fluxes of dissolved inorganic carbon (F_{DIC}), dissolved organic carbon (F_{DOC}) and outgassed CO_2 (F_{CO2}) in the Krka River for the period 2008–2010.*

	2008 ($\times 10^7$ mol/month)			2009 ($\times 10^7$ mol/month)			2010 ($\times 10^7$ mol/month)		
	F_{DIC}	F_{DOC}	F_{CO2}	F_{DIC}	F_{DOC}	F_{CO2}	F_{DIC}	F_{DOC}	F_{CO2}
Winter	25.9	1.0	1.5	157.6	-	2.8	41.2	-	1.0
Spring	46.8	2.3	2.6	44.5	-	2.4	80.3	-	2.7
Summer	20.0	0.1	1.4	13.1	-	2.2	16.4	-	1.5
Autumn	28.6	2.4	2.4	27.1	-	3.2	89.4	-	3.5

In all sampling seasons, the most important biogeochemical processes are degradation of organic matter and weathering of carbonates. The latter is predominant in spring and summer, whereas degradation of organic matter is more expressed in autumn and winter. In average the tributaries contribute 25.4 % of inorganic carbon to DIC_{river}, however their contribution decreases to 13.4 % in summer due to baseflow conditions in the basin, when groundwater input is the major source of water in the Krka. Kanduč et al. (2007a, 2008) found that dissolution of carbonates contributes the highest proportion to riverine DIC in the Sava and Idrijca watersheds (Slovenia), whereas the contribution of carbon from organic matter degradation is significantly lower leading to more positive $\delta^{13}C_{DIC}$ values. On the contrary, carbonate dissolution and organic matter degradation contribute almost equal proportions to the Krka inorganic carbon mass balance. Such differences among these watersheds are most likely due to different discharge regimes and higher runoff in Sava and Idrijca River.

The least significant process affecting riverine DIC in the Krka is exchange with atmospheric CO_2 accounting for up to 8.3 % of the contribution to the DIC_{river}. By comparison, in carbonate-dominated watersheds the contribution of CO_2 degassing was also found to be minor, i.e. up to 5 % (Shin et al., 2011) or 10 % (Zeng et al., 2010), whereas in silicate watersheds the contribution to the total carbon flux can be greater, ranging from 30–50 % (Telmer and Veizer. 1999; Shin et al., 2011). Amiotte-Suchet et al. (2003) reported that watersheds with 20 % of carbonate bedrock where characterized by DIC fluxes from 4.8 to 27.6 t of C/km^{2}yr, whereas Ferguson et al. (2011) estimated slightly higher DIC fluxes in the predominantly carbonate watershed of the Fly River (Papua New Guinea), concluding that carbon fluxes depend on runoff intensity. Area-normalized DIC fluxes in the Krka ranged from 21 to 42 t of C/km^{2}yr. The lowest values are similar to those reported for the Sava River watershed of 26.4 t of C/km^{2}yr (Ogrinc et al., 2008a), whereas the highest are close to 40 t of C/km^{2}yr estimated for the forested part of the Sava River in Slovenia only (Kanduč et al., 2007a). The Krka watershed is

approximately 4 times smaller than the Slovenian part of the Sava watershed and almost 350 times smaller than the whole Sava watershed, so our estimates of DIC flux emphasize the role of runoff over the watershed scale, enhanced solubility of carbonate bedrock, and high productivity of CO_2 in the soil of a forested Krka watershed.

6.6 Tufa deposits in Krka River

Based on the classification scheme of Pentecost (2005) and findings on water and CO_2 origin in previous chapters, tufas in Krka River are of meteogene type, which form typically in cold-water springs in regions underlain by carbonates. The water source in Krka watershed is groundwater charged with a meteoric carrier. This section discusses potential biotic factors on tufa precipitation in the Krka, kinetic processes in its calcite – water system that influence isotopic composition of tufa and finally, evaluates the use of theoretical temperature equations for reconstructing climate/environmental conditions in the tufa precipitating system of the Krka River.

6.6.1 Mineralogy of tufa

Tufa in the Krka River is dominantly low Mg-calcite, with MgO concentrations of < 3.7 wt. %. Major and trace elements in the tufa samples are generally fixed in the carbonate phase, but can be also fixed in the detrital component. Detrital component in tufa samples consists of mostly dolomite, quartz and Al_2O_3. Quartz and Al_2O_3 are in good correlation (R = 0.79) indicating a common source, most likely originating from the weathering of alluvial sediments. Despite the fact that Krka waters are supersaturated with respect to dolomite, spontaneous precipitation of dolomite is kinetically inhibited (Arvidson and Mackenzie, 2000), thus the only relevant explanation of its source would be detrital material flushed from the riparian zones.

Figure 53 shows downstream variations in mineralogical composition of tufa samples. Samples collected from the first four dams (Figure 17) have similar quantitative mineralogical composition with ~90 % of calcite and almost equal proportions of dolomite and quartz. In the following dams mineralogical composition varies; while sample T5 has 97 % of calcite, samples T6, T7 and T8 have significantly high content of quartz (> 8 %). Mineralogical composition of samples T11, T12 and T13 differentiate the most among all analysed tufa samples; their content of dolomite (12 % to 19 %) is far above the average (6 %). Interestingly, their quartz content (5–6 %) remained in the ranges of average (5 %).

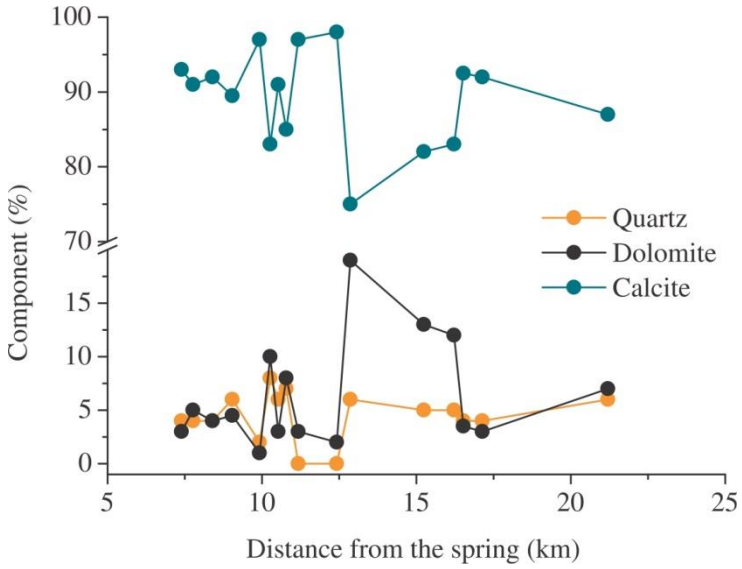

Figure 53: *Downstream variations of calcite, dolomite and quartz content in tufa samples collected in Krka River*. In all samples calcite is the dominant mineral.

6.6.2 Tufa depositional system

The tufa deposits in Krka River are scattered almost continuously along the stream from Zagradec to Otočec, forming a series of barrages or cascades (Figure 54) (cf. barrage model sensu Pedley, 1990). The main succession of barrages occurs in the upper reaches (Mihevc, 1996) in a series along the watercourse of a length of 22 km. The gradient of the riverbed in this section is ~100 m. The barrages in the Krka occur as irregular dams, spanning the channel with a height that varies from few centimetres up to several meters. Each dam is characterized by an upstream ramp and usually several pools. The size of the barrages varies according to the gradient of the riverbed; the largest barrage system occurs at Dvor (Figure 54a) and spans to < 20 m in length. The terminal downstream ramp usually passes into tongue shaped lobes (Mihevc, 1996). Pools vary in size from few decimetres to several meters (Figure 54b) with a water depth that varies from few centimetres just behind the dam or up to few meters on the upstream size of the dam. Such construction leads to differences in water current, depth and turbulence, which are the main physical factors controlling the tufa precipitating system (Janssen et al., 1999).

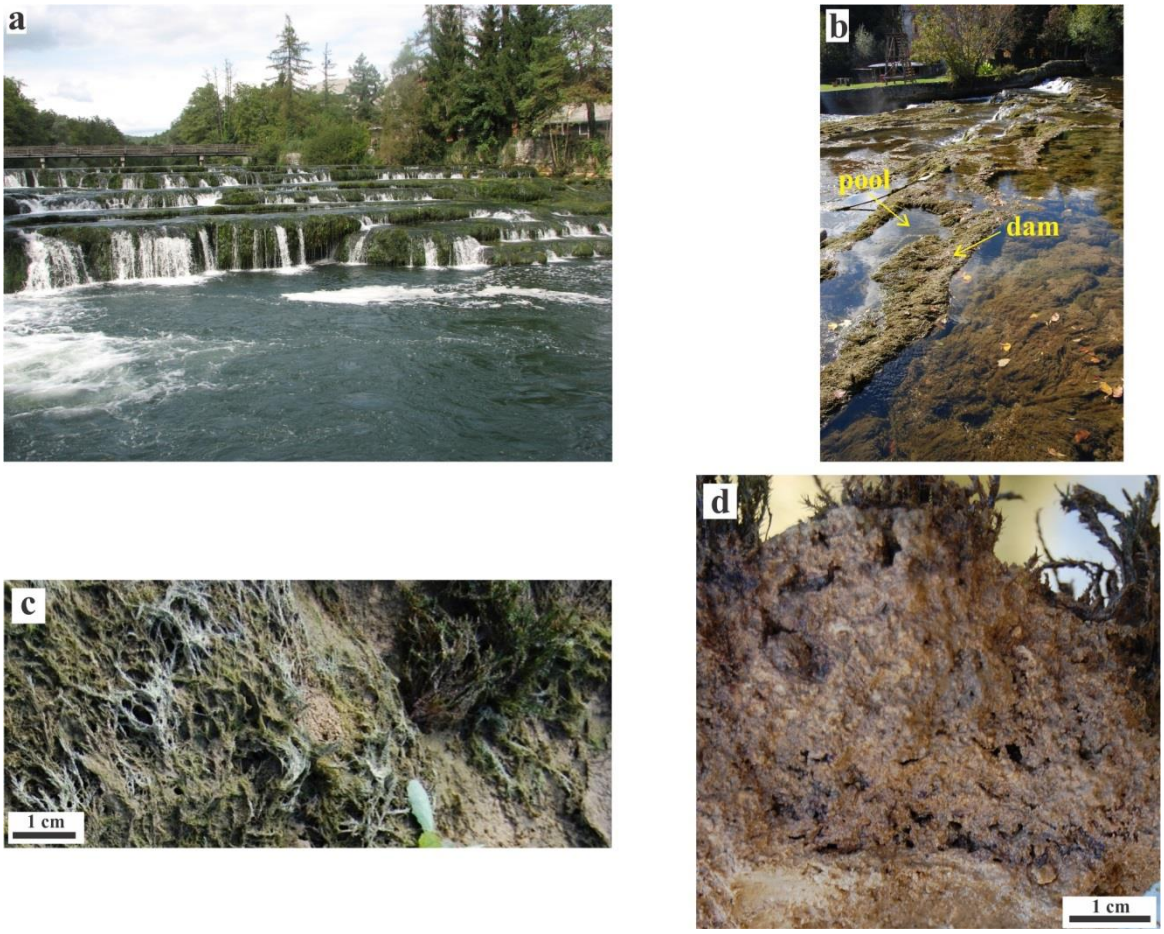

Figure 54: *Depositional system and macroscopic features of tufa in Krka River*. Tufa deposition in the Krka occurs as a series of barrage systems (**a**), comprised of dams and pools (**b**). Both photos were taken at Dvor (T16, Figure 17). (**c**) Organic material (e.g. moss) is a common substrate for tufa precipitation. (**d**) A porous structure of tufa precipitates results from decaying organic material.

The barrages are covered with different biotic communities, predominantly of algae and mosses (Mihevc, 1996). The algae community is predominantly comprised of Bacillariophyceae, Cyanobacteria and Chlorophyceae (Vrhovšek et al., 1996; Krivograd Klemenčič et al., 2004), whereas *Fontinalis antypiretica* and *Cynclidotus fontinaloides*

are the most frequent moss types found on tufa barrages in Krka River (Vrhovšek et al., 1996). Tufas precipitate on organic substrates, such as leaves and mosses and are overgrown with algae (Figure 54c).

6.6.2.1 Macroscopic features and microfacies of tufa

Microscopic features of tufa samples were examined in detail at sampling site T16 (Figure 17), where the barrage system is the largest and consists of 12 major dams and pools (Figure 55a). The internal structure of presently forming tufa deposits in Krka is strongly related to organic particles. Such depositional facies is recognized as vacuolar type (Manzo et al., 2012) characterized by voids between calcified organic matter remains (Figure 55a,c). The voids range in size from ~ 10 μm to over 1.5 mm. Thin sections of tufa deposits showed that calcite is composed of micrite (anhedral opaque calcite crystals, < 5 μm), microsparite (anhedral to subhedral crystals of 5–15 μm) and sparite crystals (euhedral crystals, > 15 μm). Micrite and microsparite crystals are most often associated with laminar, dendrolitic and aphanitic fabric (Figure 55a), whereas the sparry calcite occurs as isolated fan-shaped crystals filling the voids (Figure 55b). Besides sparitic cements, voids contain detrital material, among which quartz and carbonate grains are recognisable (Figure 55b,e). Carbonate grains, including dolomite that was recognized with XRD diffraction method, are sometimes undistinguishable from the surrounding cement. Sizes of detrital grains vary from 20 μm to over 1 mm.

Dendrolitic fabric is composed of filamentous encrusted organic material, mineralized by micrite and/or microsparite. Dendrolitic laminae contain mineralized cyanobacteria filaments, up to 5μm in diameter, forming bush-like fans (Figure 55d). Micrite is mainly present as crust, while microsparite fills the interior. Laminar fabric, surrounding different organic structures, forms 20 to 50 μm thick dark brown to brown laminas (Figure 55e) of micrite and microsparite that passes either to sparry calcite laminas or dendrolitic fabric (Figure 55e,f). Aphanitic fabric is mostly associated with microsparite crystals (Figure 55a) and occasionally it shows indistinctive concentrical laminae (oncoidal texture).

The crystallization of different types of calcite crystals is mediated by organic and/or inorganic activity. Dense micritic and microsparitic fabric cover algal filaments forming anhedral to subhedral calcite crystals, which shows an indication of some biological interference in carbonate precipitation (Janssen et al., 1999). Sparry calcite is typically characterized by sweeping extinction under crossed nicols (Figure 55b) and occurs as intergranular sparitic cement between initial micritic surrounding. Well-developed euhedral crystal forms indicate inorganic calcite precipitation (Janssen et al., 1999), most likely precipitating from porous water filling the voids (Figure 55b).

Laminated structure results from (1) variations in water chemistry (Guo and Riding, 1994; Kano et al., 2003) and/or (2) seasonal variations in growth of the biogenic substrate (Freytet and Plet, 1996; Janssen et al., 1999; Manzo et al., 2012). Variations in water temperature, pH, turbulence, velocity and other factors influence the supersaturation state of water with respect to calcite, which in turn defines the morphology of calcite crystals (Given and Wilkinson, 1985). However, the lamination within the Krka tufa deposits display alternating features of densely calcified micritic to microsparitic layers of encrusted organic filaments passing to a porous layer with radiating filaments (dendrolitic fabric; Figure 55e).

Such different fabrics can be ascribed to seasonal variations in algal growth – during spring, algae show a quick growth resulting in dense lamina, while the porous laminae results from a decreased growth of algae in late summer and autumn (Monty, 1976; Freytet and Plet, 1996; Janssen et al., 1999). In winter only inorganic sparry calcite forms (Irion and Müller, 1968; Janssen et al., 1999) mainly filling the voids in micritic substrate

(Figure 55f). Assuming a combination of dense and porous layer presents a one year cycle of calcite precipitated (Kano et al., 2003), the precipitation rate of tufa in Krka yields from 1 to ~2 mm per year.

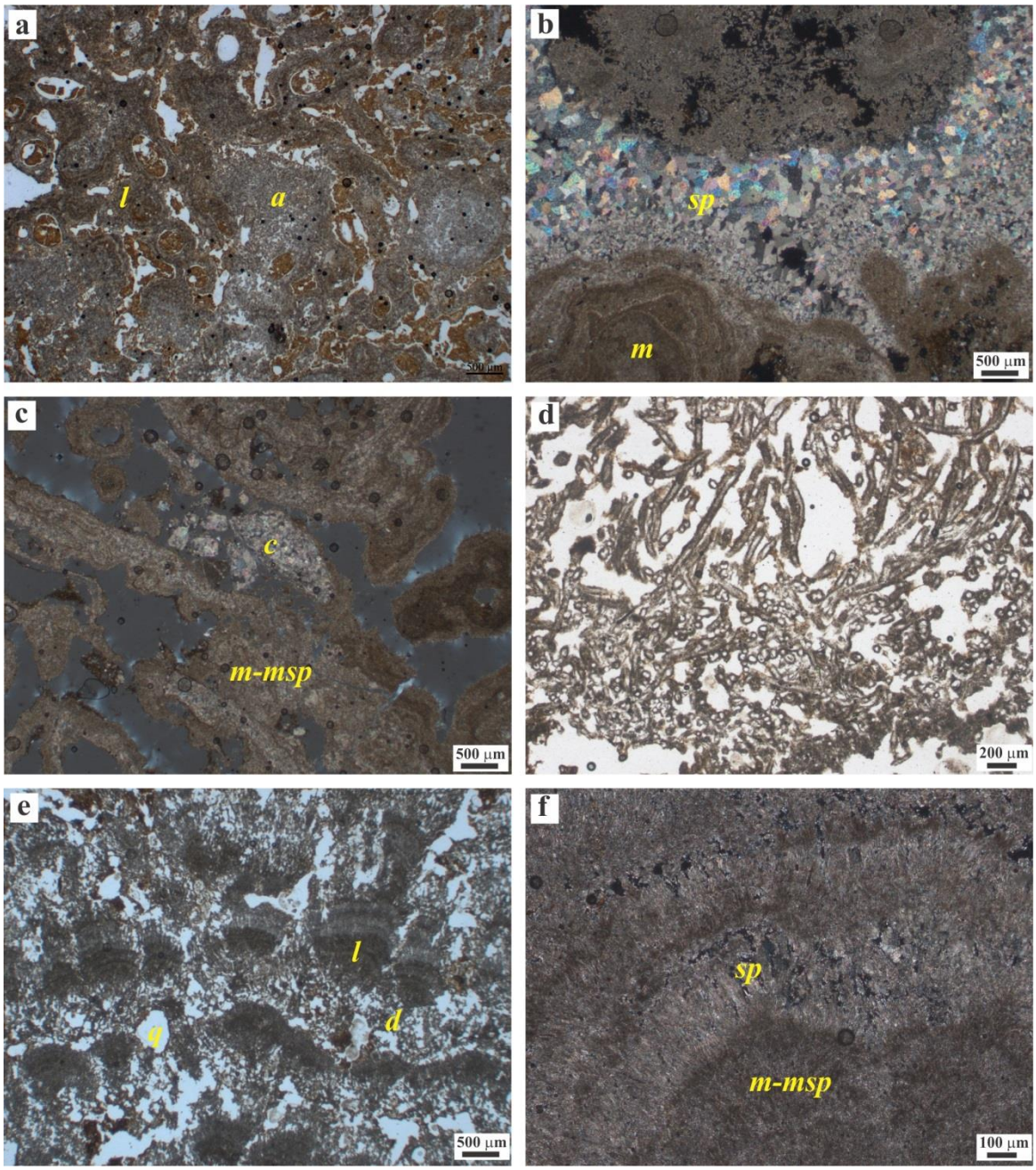

Figure 55: *Thin section photomicrographs of tufa samples (T16, Figure 17) from the Krka River (figures b, c and f are under crossed polars).* (**a**) Typical porous structure with laminated (l) and aphanitic (a) fabric surrounding organic substrates. (**b**) Euhedral sparry crystals (sp) that fill voids in micritic concentrical laminated matrix. (**c**) Porous fabrics formed by subparallel and concentric micrite/microsparite laminae (m-msp). Few sparitic carbonate (c) grains are visible in the centre of microphotograph. (**d**) Cyanobacteria films form dendrolitic fabric. (**e**) A cross section of carbonate crust with laminated fabric (l) and dendrolitic (d) fabric with detrital quartz grain (q). (**f**) Laminaes consist of micrite to microsparite crystals (m-msp) and larger sparitic crystals (sp).

Published studies on tufa deposits report that calcite precipitation occurs only in the presence of organic material (Manzo et al., 2012), while others report that biota acts only as a substrate for $CaCO_3$ deposition (Janssen et al., 1999; Kano et al., 2003). In the

examined thin-sections of the Krka tufas two main types of calcite precipitates are delineated. First is sparry cement calcite filling intergranular space that is clearly of inorganic origin. Second type includes mostly fine-crystalline calcite (micrite, microsparite) with dendrolitic or laminated texture that resembles organic growth, thus giving evidence on biological influences on $CaCO_3$ precipitation in Krka River. Merz (1992) and Arp et al. (2001) suggest that encrustation of organic filaments could occur by photosynthetic uptake of CO_2 directly on organic surfaces; thus, an active biogenic role in tufa precipitation cannot be excluded. Nevertheless, the precipitation of tufa can as well relate to calcite supersaturation of the waters, while the organic structures serve as passive precipitation substrates and define the morphology of the precipitates.

6.6.3 Precipitation rates of calcite in Krka River

Water temperatures in the range of 10 to 20°C, constantly high Ca^{2+} and HCO_3^- content and supersaturation with respect to calcite in Krka waters are ideal conditions for *in-situ* calcite precipitation. A process of an intensive CO_2 outgassing in Krka River, resulting in lowering the CO_2 content (Figure 34b) in the waters and increasing oversaturation with respect to calcite (Figure 35) indicate a clear sign of $CaCO_3$ precipitation downstream (Chafetz and Folk, 1984; Merz-Preiß and Riding, 1999; Chen et al., 2004). Water in the main channel of Krka was oversaturated with respect to calcite (SI > 0) throughout the entire 96 km long stream section and all major tributaries. $SI_{calcite}$ values were always the lowest at the headwaters (average) and increased downstream up to 8.4 (average). The largest tufa barrages in Krka River mainly occur in its upper reaches, where the $SI_{calcite}$ values varied from 0.2 to 1.2 (average 0.7). Generally, calcite precipitates in waters, which are 4 to 10 times supersaturated with respect to calcite (SI = 0.6–1; Herman and Lorah, 1988; Merz-Preiß and Riding, 1999; Zhang et al., 2012), however, active tufa formation was observed in waters with lower saturation (< 4; Lojen et al., 2004). From detailed field measurements of pH, water temperature, Ca^{2+} concentrations and alkalinity, several conclusions were made: (1) photosynthetic uptake of carbon and temperature effects on $CaCO_3$ precipitation at waterfall sites are negligible (Merz-Preiß and Riding, 1999), (2) fastest precipitation occurs at waterfalls, where air-water interface is the largest and the greatest amounts of CO_2 are degassed (Chen et al., 2004), and (3) calcite deposition is sensitive to water temperature and water dilution by rainfall (Vázquez-Urbez et al., 2010 ; Zhang et al., 2012).

The calcite precipitation rates in carbonate-dominated waters can be determined by knowing Ca^{2+} concentration, water temperature and hydrodynamic conditions (Dreybrodt, 1988) and under turbulent flow conditions the precipitation rates can be estimated by the theoretical DBL model (Diffusive Boundary Layer) developed by Buhmann and Dreybrodt (1985) and Dreybrodt et al. (1992). Their sufficiently high accuracy was tested with experimental work in the freshwater streams precipitating $CaCO_3$ (e.g. Liu et al., 1995; Faure et al., 1997; Bono et al., 2001). In practically all natural streams the water flow is turbulent, therefore, the surface of mineral is separated from the turbulent bulk of the solution by a hydrodynamic diffusion boundary layer with a thickness, ε, of between 100 and 300μm (Dreybrodt et al., 1992; Bono et al., 2001). For a H_2O-CO_2-$CaCO_3$ system supersaturated with respect to calcite the precipitation rate of $CaCO_3$ (R) can be calculated as:

$$R = \rho \cdot (C\text{-}C_{eq}) \tag{56}$$

where ρ is a reaction rate constant, C is the actual concentration of Ca^{2+} ions in the water and C_{eq} is the equilibrium Ca^{2+} concentration with respect to calcite and the pCO_2 in the water. The calculation of precipitation rate takes into account the existence of a diffusion

boundary layer (DBL) developed by Dreybrodt and Buhmann (1991); in principal the model assumes DBL of thickness φ that separates the calcite surface from the turbulent bulk of thickness ω. The DBL factor is included in the reaction constant ρ that depends on temperature, the pCO_2 in the solution, on the thickness of the diffusion boundary layer (φ), and because of the slow conversion of HCO_3^- into CO_2, also on thickness of the water layer above the surface (ω) to which calcite is precipitated (Bono et al., 2001).

The precipitation rates of calcite deposition in Krka River were calculated for sampling points W5, W7, W8 and W9 (Figures 16 and 17) in the Krka main channel section where tufa precipitation is most intensive. The thickness of diffusion boundary layer (φ) was set to 50μm and 100μm assuming turbulent conditions, and to 200μm assuming stagnant water conditions. The thickness of the water layer above the precipitated calcite surface (ω) was set to 0.1cm, 1cm, 10 cm and 100cm. The ρ values were experimentally determined by Liu and Dreybrodt (1997) and were considered in our calculations based on measured water temperature at constant pCO_2 (10^{-3} atm).

Maximal rates were obtained assuming a boundary layer of φ = 50 μm and ω = 10 cm (Table 12), which is the best approximation to realistic conditions in turbulent waters (Liu and Dreybrodt, 1997; Bono et al., 2001). The precipitation rates at optimal conditions are presented in Figure 56a and ranged from 5×10^{-8} to 14×10^{-8} mmol/cm^{2}s (average 10×10^{-8} mmol/cm^{2}s). Despite small differences between calculated rates at different φ and ω, we noticed that at lower ω (< 10 cm) the precipitation rates are one order lower, whereas at ω = 100 cm, the rates are very similar to those calculated at ω = 10 cm. The estimated calcite precipitation rates increased downstream; at site W5 the R values were the lowest (average 9.6×10^{-8} mmol/cm^{2}s) and increased to 14.6×10^{-8} mmol/cm^{2}s at site W9 (Figure 16).

Very low correlation between *R* and Ca^{2+} content (R < 0.20) or total alkalinity (R < 0.30) implies that precipitation rates are not controlled by Ca^{2+} and/or HCO_3^- content in the Krka. An increase of deposition rates downstream can be rather ascribed to the gradient of the Krka riverbed (the gradient between W5 and W8 is 57m or 65m in case of W9) resulting in larger water fall leading to more turbulent water conditions. A very good correlation between R and water temperature (R > 0.85; Figure 56b) was observed, which is in satisfactory agreement with the temperature dependence of ρ. Accordingly, the highest R values were calculated for summer (average 12.5×10^{-8} mmol/cm^{2}s) and the lowest for winter (average 7.0×10^{-8} mmol/cm^{2}s). The average R values for spring and autumn were 9.9×10^{-8} mmol/cm^{2}s and 9.0×10^{-8} mmol/cm^{2}s, respectively (Table 12). Similar calculated deposition rates were estimated in other studies of tufa precipitating karst streams worldwide. However, experimentally determined calcite precipitation rates were found to be usually by one order magnitude lower than calculated (Liu et al., 1995; Bono et al., 2001). In the study of tufa precipitates in the stream of Huanlong (China) Liu et al. (1995) reported calcite deposition rates to range from 0.1×10^{-8} to 9.0×10^{-8} mmol/cm^{2}s, while Zhang et al. (2012) found that precipitation rates were below 1.0×10^{-8} mmol/cm^{2}s in 2010. Bono et al. (2001) determined inorganic calcite precipitation in the Tartare karstic spring (Italy) to range from 2.3×10^{-9} to 9.6×10^{-8} mmol/cm^{2}s. Considering density of tufa to be ~2.2 g/cm^3 the rate of calcite precipitation in Krka River ranges from 0.06 to 0.17 mm/month (Table 12), which amounts to 0.7 to 2.1 mm/yr, which is close to the estimation of tufa precipitation (up to 2 mm) examined under microscope. Moreover, our estimates are similar to calculated deposition rates of 1mm/yr in the Huanlong Ravine (China; Yoshimura et al., 2004), or measured rates of 2.2 mm/yr in the Bad Urach stream (Germany, Merz-Preiss and Riding, 1999) or 2.3–4.3 mm/yr in the slow flowing waters of Piedra River (Spain, Vázquez-Urbez et al., 2010). Nevertheless, tufa precipitation rates were found to be even larger, e.g. 2.3–17.5 mm/yr in the fast flowing waters of Piedra

River (Spain, Vázquez-Urbez et al., 2010).

Table 12: *Seasonal averages of calculated precipitation rates of calcite in Krka River at sites W5, W7, W8 and W9 (Figure 16) in 2007–2010 sampling period*. Reported values were calculated according to equation (56) considering thickness of boundary layer φ = 50μm and different thicknesses of the water layer (ω) above the precipitated calcite (0.1 cm < ω < 100cm).

Location	T (°C)	C - C_{eq} (mmol/L)	R ($\times 10^{-8}$ mmol/cm^{2}s) ω (cm)				R (mm/month) ω (cm)			
			0.1	1	10	100	0.1	1	10	100
W5										
Winter	7.5	1.41	3.4	5.9	6.9	6.9	0.04	0.07	0.08	0.08
Spring	12.3	1.32	5.0	8.5	9.6	9.7	0.06	0.10	0.11	0.11
Summer	14.7	1.39	6.1	10.4	11.8	11.9	0.07	0.12	0.14	0.14
Autumn	9.8	1.46	4.5	7.7	8.8	8.9	0.05	0.09	0.10	0.11
W7										
Winter	8.1	1.45	3.8	6.5	7.5	7.6	0.04	0.08	0.09	0.09
Spring	13.1	1.33	5.3	9.0	10.3	10.4	0.06	0.11	0.12	0.12
Summer	15.5	1.40	6.5	11.0	12.4	12.6	0.08	0.13	0.15	0.15
Autumn	10.4	1.47	4.8	8.2	9.4	9.5	0.06	0.10	0.11	0.11
W8										
Winter	8.8	1.46	4.0	7.0	8.0	8.1	0.05	0.08	0.09	0.10
Spring	12.5	1.34	5.1	8.7	9.9	10.0	0.06	0.10	0.12	0.12
Summer	16.0	1.33	6.3	10.7	12.1	12.2	0.07	0.13	0.14	0.14
Autumn	10.3	1.47	4.7	8.1	9.2	9.3	0.06	0.10	0.11	0.11
W9										
Winter	7.9	1.21	3.0	5.3	6.1	6.2	0.04	0.06	0.07	0.07
Spring	12.6	1.38	5.3	9.0	10.2	10.3	0.06	0.11	0.12	0.12
Summer	16.4	1.44	7.1	11.9	13.5	13.6	0.08	0.14	0.16	0.16
Autumn	10.1	1.46	4.6	7.9	9.0	9.1	0.05	0.09	0.11	0.11

Slow deposition rates (below 3mm/yr) are often associated with the presence of cyanobacteria (Pentecost, 2005) or other inhibitors that (1) block surface sites for crystal growth (Zuddas and Mucci, 1994) and (2) present natural energy barrier to calcite nucleation (Berner, 1981). Mg^{2+} has been shown to inhibit calcite growth by substitution for Ca^{2+} into the crystal lattice (Morse, 1983; Liu et al., 1995; Bono et al., 2001). High Mg^{2+}/Ca^{2+} molar ratios in Krka waters (average 0.44) imply that Mg^{2+} potentially inhibits the growth of calcite in Krka. However, a positive and moderately low correlation between Mg^{2+}/Ca^{2+} ratios and precipitation rates ($R < 0.53$) implies that Mg^{2+} content in Krka waters does not play a major role in Krka. High concentrations of phosphates (> 0.15 mg/L, Zhang et al., 2012) can also act as strong growth inhibitors (Morse, 1983; Omelon et al., 2006) but PO_4^{3-} content in the Krka waters was below 0.01 mg/L (ARSO) suggesting that inhibition by phosphate is minor. Another possible inhibitor of calcite precipitation is allochtonous detrital material (Omelon et al., 2006), which in average presents ~ 10 % of the tufa material in Krka estimated by XRD analyses (Appendix 3).

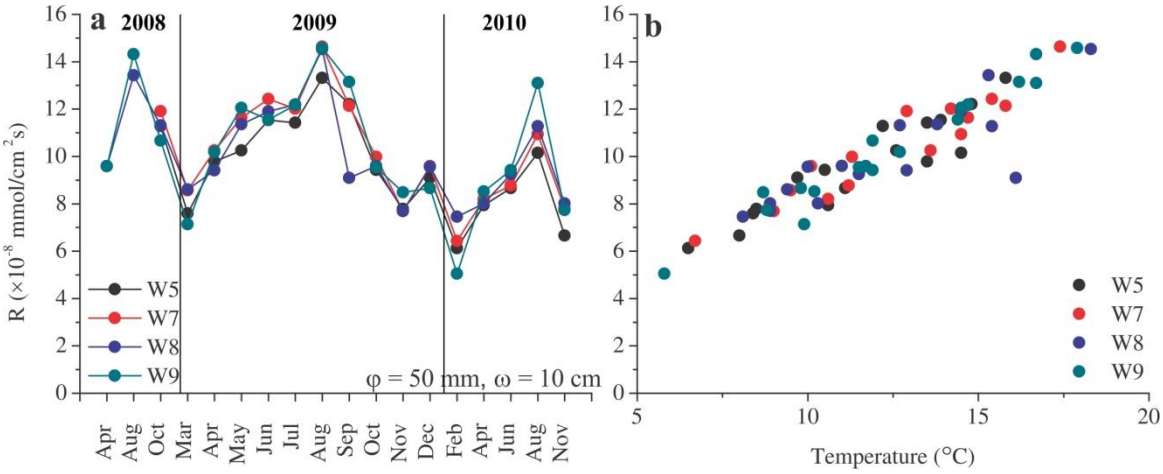

Figure 56: *Calculated precipitation rates of calcite in Krka River.* (**a**) Precipitation rate of calcite was calculated according to the DBL method (Buhmann and Dreybrodt, 1985; Dreybrodt et al., 1992). The φ and ω indicate thicknesses of diffusion boundary layer and water layer above the surface of calcite precipitation, respectively. (**b**) One of the major factors controlling the precipitation of tufa is water temperature.

Considering a range of precipitation rates between 6.1×10^{-8} and 13.5×10^{-8} mmol/cm^{2}s at φ = 50 μm and ω = 10 cm (Table 12) and a surface area of 2.9 km^2 of the river bed where calcite precipitates, we calculated that approximately 0.7×10^7 to 1.5×10^7 mol of C/month (average 1.1×10^7 mol of C/month) is deposited as $CaCO_3$ (F_{CaCO3}) in the Krka River. When comparing to calculated DIC fluxes reported in Table 11 the contribution to the total carbon mass balance in the Krka is in the range of CO_2 fluxes (average 1.5×10^7 mol of C/month). However, calculations show that both of these fluxes (F_{CO2} and F_{CaCO3}) have only minor influence on the overall carbon mass balance in the Krka watershed.

To summarize, the deposition of tufa on dams in Krka River is obviously mostly affected by turbulent conditions at waterfalls and water temperatures rather than by saturation states in water. The presence of biota most likely acts as a substrate for calcite precipitation, which was proven in a set of experimental conditions (e.g. Rogerson et al., 2008). Detrital component seems to only fill the pores lowering the porosity of tufa deposits. Based on carbon and oxygen stable isotopic composition of tufa the extent to which of these factors influence Krka tufa deposits is examined in the following sections.

6.6.4 Stable isotope variations in tufa

As discussed in the *Introduction* section (see chapter 1.4.1.1), stable isotopes of carbon and oxygen in tufa reflect environmental conditions at the time of the precipitation. However, to what extent tufa deposits record variations in environmental parameters, largely depends on the processes that affect the isotopic composition of the water (parent solution) and the precipitates during precipitation. Here we discuss the potential sources and mechanistic controls on the extent of equilibrium and/or kinetic isotope effects that define the isotopic composition of tufa. Several equilibrium equations describing isotopic fractionation between calcite and water are available in the literature, however, their convenience depends on specific situations of the system studied. In this study, we considered most widely used equilibrium equations and isotopic fractionation factors between calcite and water published in the literature (Table 2), in order to (1) determine sources of C and O in tufa precipitates, (2) to test the usefulness of the chosen equilibrium equations, and (3) to evaluate the extent of equilibrium versus kinetic isotopic fractionation in regards to the specific calcite precipitation system of the Krka. Based on

available water chemistry data four tufa-water pairs were considered for calculations of isotopic fractionations (T1-W5, T10-W7, T15-W8, and T16-W9; Figure 17).

Recent tufa precipitates in Krka River have a range of $\delta^{13}C$ and $\delta^{18}O$ values that are consistent with precipitation under isotopic equilibrium to non-equilibrium conditions. The following lines of evidence indicate the influence of kinetic isotope effects:

(1) The $\delta^{13}C$ and $\delta^{18}O$ compositions of tufa samples covariate. This is a proposed criterion for kinetic isotope effects in the formation of speleothems (Hendy, 1971; Mickler et al., 2004) but was recognized in fast-growing $CaCO_3$ dripstones (Zavadlav et al., 2012) and tufas as well (e.g. Matsuoka et al., 2001; Lojen et al., 2004; Leybourne et al., 2009).

(2) The $\delta^{13}C$ and $\delta^{18}O$ composition of recent tufa deviate from equilibrium values calculated from the fraction factors from the literature, the measured water temperatures of Krka River, and $\delta^{13}C$ and $\delta^{18}O$ values of the waters feeding the recent tufa precipitates.

Due to temperature dependence, the calculated fractionation factors varied according to measured water temperatures. In both cases, C and O, the largest deviations from the average fractionation factor value obtained from equilibrium equations and measured water temperatures were for autumn-winter months. This is consistent with the findings from microscopic examination of tufa samples; the largest encrustations occur in spring and summer when algae are most abundant, therefore, we assume that the isotopic imprint of tufa mostly reflects spring-summer hydrogeochemical conditions in the Krka. In this regard, only the spring-summer results were considered suitable for the interpretation of isotope fractionation processes in the Krka $CaCO_3$ – water system.

6.6.4.1 Carbon isotope fractionation

The $\delta^{13}C$ signal of freshwater carbonates results from a complex interplay of abiotic and biotic factors that influence the carbon isotopic fingerprint of DIC (Andrews, 2006; Anzalone et al., 2007). Therefore, the $\delta^{13}C$ values of the $CaCO_3$ provide information about the origin of the CO_2 and DIC in the water. As discussed in previous section (see 6.4.1.1) the inorganic carbon in Krka waters originates from a carbon mixture of soil CO_2 (average $\delta^{13}C$ = -27.7 ‰) and carbonate dissolution ($\delta^{13}C$ = +1.4 ‰) and its carbon isotopic composition is affected by CO_2 outgassing downstream. The $\delta^{13}C_{tufa}$ values ranging from -11.40 ‰ to -6.60 ‰ are higher than measured $\delta^{13}C_{DIC}$ values (-15.1 ‰ to -10.5 ‰, average -12.6 ‰) showing that reconstruction of C source from Krka tufa is not straightforward. Nevertheless, in most temperate systems C_3 plants plant dominate, leading to $\delta^{13}C_{tufa}$ values typically below -8 ‰ (Andrews, 2006). A high $\delta^{13}C$ value of -6.60 ‰ of the T11 sample indicates a different source of DIC originating from predominantly carbonate dissolution and/or possible influence of dolomite component on isotopic composition of tufa. Both hypotheses are quite likely due to near-by groundwater spring occurrence (Figure 17) and high content of dolomite in T11 sample (Figure 36). Interestingly, the additional groundwater discharge is not significantly reflected in the water chemistry of Krka River (Appendix 1) as is in the tufa precipitate.

To further argue the problem of reconstructing C sources from tufa, we first calculated isotopic composition of potential C sources (CO_2 and DIC) using different equilibrium equations (Table 2). Considering a range of $\delta^{13}C_{tufa}$ values and stream water temperatures measured in the upper reaches of the Krka (4.4–18.3 °C, average 11.3 °C) and using the $^{13}\varepsilon_{CaCO3\text{-}CO2}$ of Bottinga et al. (1968), and $^{13}\varepsilon_{cc\text{-}HCO3}$ of Deines et al. (1974) and of Mook (2000) yield average $\delta^{13}C_{CO2}$ values of -22.5 ‰ and -19.5 ‰, and $\delta^{13}C_{HCO3}$ values of -8.2 ‰ and -10.0 ‰, respectively. The calculated $\delta^{13}C$ values of soil CO_2 and DIC were much

higher than the actual ones, indicating (1) possible biological interferences on tufa precipitation and/or (2) kinetic isotope fractionation during calcite precipitation.

The organic matter fills the voids in Krka tufa samples collected on dams (Figure 55a) implying that it might influence the carbon isotopic composition during calcite precipitation. The OM in tufa samples analysed is characterized by $\delta^{13}C_{org}$ values between -31.9 ‰ to -28.5 ‰ (average -30.0 ± 0.9 ‰) and C/N atomic ratios of 9 to 17 (average 13). There are two possible sources of organic matter in Krka tufa: (1) cyanobacteria, algae and mosses that overgrow tufa dams (Mihevc, 1996) and (2) terrestrial organic matter flushed from the riparian zones. Algae have very low $\delta^{13}C$ values of -39.0 ‰ (Janssen et al., 1999) and C/N ratios of 5 to 12 (Finlay and Kendall, 2007), whereas mosses are characterized by $\delta^{13}C$ values -32.3 ‰ and high C/N ratios of 18 to 24 (Kanduč et al., 2007b). Particulate OM in Krka waters is of detrital origin (see 6.4.1.2.2) with average $\delta^{13}C$ value of -29.2 ‰. Thus, we assume that OM in Krka tufa samples is a mixture of macrophyte remains that have not degraded yet and detrital OM that is filling the empty pores. The role of in-stream biological control on tufa $\delta^{13}C$ is still debated. A general view is that mosses and algae provide a framework that aid calcite nucleation (Janssen et al., 1999) but under conditions when cyanobacteria and algae are present in large numbers, the microenvironmental effects of photosynthesis can remove isotopically light $^{12}CO_2$ leaving tufa calcites enriched with ^{13}C (Arp et al., 2001; Lojen et al., 2004). Recently, Shiraishi et al. (2008) found the opposite by studying microbial activity effects on calcite precipitation in thin cyanobacteria-dominated biofilms in the tufa precipitating Westerhöfer Bach creek (Germany). They experimentally proved that despite evident photosynthesis-induced calcite precipitation the stable carbon and oxygen isotopic composition of precipitated calcite were not influenced by photosynthetic activity. Based on the examined sources of OM in Krka tufa and reports from the literature, we assume that isotopic composition of precipitated tufa in Krka is not influenced by in-stream biological activity.

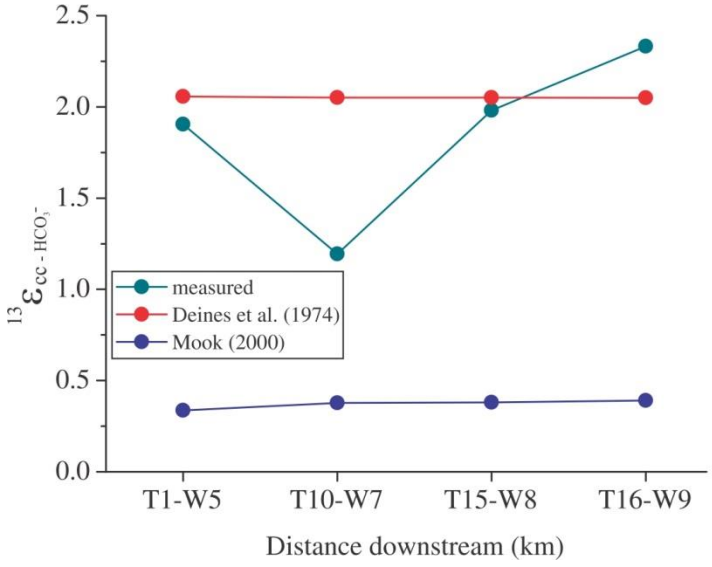

Figure 57: *Carbon isotopic fractionation between modern tufa and DIC in Krka River.* The theoretical equilibrium fractionation factors were calculated using equilibrium equation of Deines et al. (1974) and Mook (2000) and considering measured water temperatures.

Preferential degassing of $^{12}CO_2$ results in higher $\delta^{13}C$ values of DIC and tufa downstream. Degassing of CO_2 results in rapid calcite precipitation and disequilibrium of the carbonate isotope system (Usdowski et al., 1979) evolving towards equilibrium downstream as rates of CO_2 degassing and calcite precipitation decrease (Andrews,

2006). A decreasing downstream trend of $\delta^{13}C_{tufa}$ in Krka (Figure 39) implies that tufa precipitated in equilibrium with water DIC. To test this assumption, we calculated fractionation factors between precipitated tufa and DIC for the Krka $CaCO_3$ – HCO_3^- system using equilibrium equations of Deines et al. (1974) and Mook (2000). Considering the range of water temperatures (4.7 to 18.3 °C) the average calculated $^{13}\varepsilon_{cc\text{-}HCO3}$ was 2.07 ‰, ranging from 2.02 to 2.13 ‰ using the equation of Deines et al. (1974) while the range of $^{13}\varepsilon_{cc\text{-}HCO3}$ calculated using the Mook (2000)'s equation was much lower (-0.12 to 0.59 ‰, average 0.23 ‰).

Table 13 lists calculated average fractionation factors between calcite and DIC ($^{13}\varepsilon_{cc\text{-}HCO3}$) for the tufa-water pairs in Krka and $\delta^{13}C_{CaCO3}$ values for calcite precipitated in equilibrium with DIC using the equations of Deines et al. (1974) and Mook (2000). Based on calculated $\delta^{13}C_{CaCO3}$ values, the equation of Deines et al. (1974) fits well with the measured $\delta^{13}C$ of tufa (Table 13). Similarly, the fractionation factors of tufa-water sample pairs T1-W5, T10-W7, T15-W8 and T16-W9 show very good agreement with theoretically predicted equilibrium fractionation calculated with the equation of Deines et al. (1974) (Figure 57), whereas the $^{13}\varepsilon_{cc\text{-}HCO3}$ calculated with Mook (2000)'s equation were significantly lower for all tufa-water samples. This implies that equilibrium isotopic separation between tufa and DIC in the Krka system is best described by Deines et al. (1974) equation. The deviation of the T10-W7 pair from the predicted equilibrium line towards lower values indicates disequilibrium fractionation. This process likely results from the incorporation of $HCO_{3\ (aq)}^-$ into calcite during rapid mineral precipitation, such that isotopic fractionation is minimized (Mickler et al., 2004).

Table 13: *$\delta^{13}C$ of calcite ($\delta^{13}C_{cc}$) using the water temperature and $\delta^{13}C_{DIC}$ data measured at the downstream section of the Krka River*. The theoretical equilibrium equations used were determined by (a) Deines et al. (1974) and (b) Mook (2000).

Sample	T (°C)	$\delta^{13}C_{DIC}$ (‰)	$^{13}\varepsilon_{cc\text{-}HCO3}$ meas.	$^{13}\varepsilon_{cc\text{-}HCO3}$ calc.[a]	$^{13}\varepsilon_{cc\text{-}HCO3}$ calc.[b]	$\delta^{13}C_{tufa}$ (‰) meas.	$\delta^{13}C_{cc}$ (‰) calc.[a]	$\delta^{13}C_{cc}$ (‰) calc.[b]
T1-W5	13.4	-12.4	1.9	2.1	0.3	-10.45	-10.3	-12.0
T10-W7	14.2	-12.1	1.2	2.1	0.4	-10.95	-11.8	-10.1
T15-W8	14.2	-12.3	2.0	2.1	0.4	-10.30	-10.3	-11.9
T16-W9	14.4	-12.3	2.3	2.0	0.4	-9.97	-10.3	-11.9

Factors that might provoke a shift in $\delta^{13}C$ (and $\delta^{18}O$) of the crust after its formation are recrystallization, isotope exchange with spraying water and an input of detrital material. Sparry calcite filling the voids in micrite – microsparite matrix crystallizes slowly from pore waters, and would potentially have a different isotopic composition. Isotopic exchange between bulk biogenic carbonate and pore waters can produce $\delta^{13}C_{DIC}$ values enriched by +2 ‰ (Walter et al., 2007), leading to depletion of the bulk solid phase. However, the most probable factor that could potentially influence the isotopic composition of Krka tufa is the presence of carbonate detrital component (even up to 20 %). Two facts support the assumption: (1) the δ values of T11 and T12 are significantly higher than other samples, and (2) the amount of dolomite in tufa samples shows statistically significant correlation with both, $\delta^{13}C_{tufa}$ (R = 0.70) and $\delta^{18}O_{tufa}$ (R = 0.79). Using a simple mixing model we calculated what would be bulk δ values of authigenic $CaCO_3$ considering measured δ values of tufa (Appendix 3), a $\delta^{13}C_{carb}$ value of +1.4 ‰ of carbonate rocks (detrital component) and a content of detrital component (Appendix 3), ranging from 1 to 19% based on dolomite. Rough estimations showed that $\delta^{13}C$ values of

authigenic calcite would be on average by 0.8 ‰ depleted with ^{13}C yielding values from -9.5 ‰ to -12.0 ‰. These values are close to average $\delta^{13}C_{DIC}$ values determined in summer and spring water samples (-12.4 ‰). Nevertheless, the contribution of detrital component to the bulk $\delta^{13}C$ values of tufa is very likely higher, which would result in even lower $\delta^{13}C$ values of authigenic $CaCO_3$. Precise estimation of carbonate detrital component is impossible to estimate due to identical mineralogical and elemental composition of authigenic and detrital calcite present in tufa.

6.6.4.2 Oxygen isotope fractionation

The oxygen isotopic composition of tufa is influenced by various factors, the two most important being the temperature-controlled isotope fractionation between $CaCO_3$ and H_2O, and variability of oxygen isotopic composition of waters (Figure 8b; Dorale et al., 1992; Gascoyne et al., 1992). The waters in Krka are recharged by groundwater rather than by surface runoff or snowmelt, resulting in moderate variations of $\delta^{18}O$ in water. Moreover, the $\delta^{18}O$ values ($\delta^{18}O_w$) in the Krka waters are not correlated to water temperatures, thus seasonal and annual variations in $\delta^{18}O_w$ values do not necessarily correspond to changes in temperatures. Therefore, we assume isotopic equilibrium was hardly achieved between tufa and the parent water in our case. Nevertheless, we investigated the deviation from ideal/equilibrium conditions using stable oxygen isotope separation factors ($^{18}\varepsilon_{cc\text{-}w}$).

In principle, the relationship between the oxygen isotopic composition of stream water and calcite is a function of the water temperature during calcite precipitation. Many studies have shown that isotopic equilibrium is rarely maintained under natural conditions during calcite precipitation (Friedman, 1970; Lojen et al., 2004, 2009; Kele et al., 2008, 2011) due to disequilibrium processes that occur during calcite precipitation caused by rapid calcite precipitation (Kele et al., 2008, 2011; Yan et al., 2012) that prevents isotopic equilibration in the calcite – water system. Lojen et al. (2004, 2009) proposed that large water temperature variability also affects isotopic equilibration between calcite and water. Recently, Dietzel et al. (2009) experimentally proved that (1) isotopic equilibrium is not maintained during spontaneous calcite precipitation from the solution and (2) isotopic fractionation between calcite and water is affected by temperature, the pH of the solution, and the precipitation rate of calcite. At constant temperature of 5 °C and a pH of 8.3 the fractionation can be described as a function of the precipitation rate (R) with the following expression:

$$^{18}\varepsilon_{cc\text{-}w} = -1.102 \cdot \log R + 34.56 \quad (57)$$

The calculated $\delta^{18}O_{calcite}$ expectedly varied according to measured water temperatures and $\delta^{18}O_{water}$ values (Table 14). The best approximation to measured $\delta^{18}O_{tufa}$ values was found using the equations of Friedman and O'Neil (1977) and Mook (2000), whereas other equilibrium equations yield up to 0.8 ‰ lower (O'Neil et al., 1969; Kim and O'Neil, 1997; Dietzel et al., 2009) or up to 1.3 ‰ higher in case of using Coplen (2007)'s equation (Table 2). Assuming that both, Friedman and O'Neil (1977)'s and Mook (2000)'s calculated $^{18}\varepsilon_{cc\text{-}w}$ represent equilibrium conditions in the examined calcite – water system, different processes can be recognized that influence the deviations of measured isotopic fractionation between calcite and water (Figure 58). However, the measured $^{18}\varepsilon_{cc\text{-}w}$ (calculated as a difference between $\delta^{18}O_{tufa}$ and $\delta^{18}O_w$) of ~ 31 ‰ (VSMOW) fits better to the calculated $^{18}\varepsilon_{cc\text{-}w}$ using Friedman and O'Neil (1977)'s equation yielding average fractionation factor of 30.8 ‰ (VSMOW). This implies that tufa precipitated in equilibrium with water. An exception can be seen only for the T16-

W9 sample pair, where the difference between measured and calculated fractionation was 0.5 ‰ (VSMOW) approaching the equilibrium value calculated according to Mook (2002)'s equation.

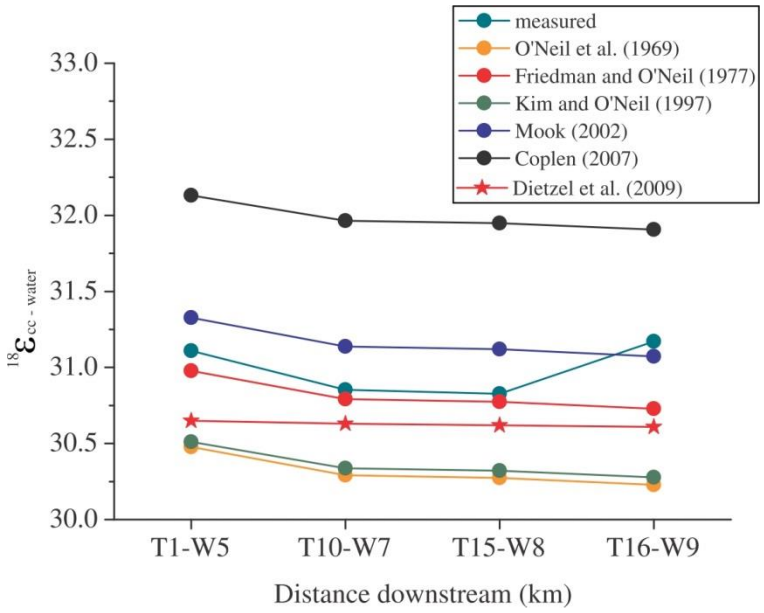

Figure 58: *Oxygen isotopic fractionation between modern tufa and water in Krka River.* The theoretical equilibrium fractionation factors were calculated using theoretical equilibrium equations of O'Neil et al. (1969), Friedman and O'Neil (1977), Kim and O'Neil (1997), Mook (2000), Coplen (2007) and Dietzel et al. (2009). All equations are a function of temperature, except for the Dietzel et al. (2009)'s, which is a function of calcite precipitation rate.

Nevertheless, comparison between measured and calculated $^{18}\varepsilon_{cc\text{-}w}$ using the equation of Mook (2000) provides a different insight into calcite-water isotope exchange in the Krka system. Slightly higher measured fractionation implies that kinetic isotope effects may have controlled the $\delta^{18}O$ values of tufa. This could be due to fast calcite precipitation, especially at upstream sites (Figure 56), that results in incomplete isotopic exchange of the O reservoir (Mickler et al., 2004). The measured fractionation factor at T16-W9 pair is close to the equilibrium value, supporting the assumption of Andrews et al. (1993) that disequilibrium effects diminish downstream as the system re-equilibrates to ambient surface condition. Though no correlation was observed between measured $^{18}\varepsilon_{cc\text{-}w}$ and calculated precipitation rates of calcite (R = 0.22) in Krka stream water, the enrichment factor of 30.6 ‰ estimated using equation (57) of Dietzel et al. (2009) is fairly close to the average measured $^{18}\varepsilon_{cc\text{-}w}$ of 31.0 ‰, which means that variable precipitation rates could also influence the isotopic enrichment in the calcite – water system of the Krka.

As mentioned before, the $\delta^{18}O$ values of tufa can be used as proxies for reconstructing temperatures at the time of their precipitation. Because water samples taken in this study represent "snapshots" and tufa samples represent months of deposition, we considered calculating $\delta^{18}O$ values of calcite rather than water temperatures. For these purpose, we used Anderson and Arthur (1983)'s and Hays and Grossman (1991)'s equations that are most often employed in tufa studies (Andrews, 2006). Consistently with the findings from the fractionation enrichment factor examination, the calculated $\delta^{18}O_{calcite}$ values for spring-summer months fitted best to the measured $\delta^{18}O_{tufa}$ values. Nonetheless, the calculated $\delta^{18}O_{calcite}$ values were in general up to 0.6 ‰ more positive (on average 0.3 ‰) when considering Anderson and Arthur (1983)'s temperature equation. An exception is

the T16-W9 pair where the calculated $\delta^{18}O_{calcite}$ values were up to 0.7‰ more negative. According to Yan et al. (2012) an increase in 1 °C would cause depletion with ^{13}C of 0.2 ‰ in the precipitate. Thus, the calculated water temperature would vary for up to 6.5 °C. The $\delta^{18}O_{calcite}$ values calculated with Hays and Grossman (1991)'s equation showed larger deviation from the measured δ values ranging from -0.9 to +1.8 ‰, which would result in calculated temperature variation of up to 13.5 °C. Lojen et al. (2009) reported similar findings and attributed such deviations to non-equilibrium conditions of carbonate precipitation. Moreover, under non-equilibrium conditions, which usually occur in supersaturated natural systems, isotopically depleted C species incorporate into the crystal lattice, which shifts the $\delta^{18}O$ of calcite toward lower values (Coplen, 2007), yielding higher calculated precipitation temperatures.

Table 14: *Calculations of the measured (meas.) and modelled (calc.) fractionations between calcite (cc) and water (w) ($^{18}\varepsilon_{cc\text{-}w}$) and $\delta^{18}O$ of calcite ($\delta^{18}O_{cc}$) using the water temperature and $\delta^{18}O_w$ water data measured at the downstream section of the Krka River*. The theoretical equilibrium and temperature equations used were determined by (c) O'Neil et al. (1969), (d) Friedman and O'Neil (1977), (e) Kim and O'Neil (1997), (f) Mook (2000), (g) Coplen (2007), (h) Dietzel et al.(2009), (i) Anderson and Arthur (1983), and (j) Hays and Grossman (1991).

Sample	T (°C)	$\delta^{18}O_w$ (‰) (VSMOW)	$^{18}\varepsilon_{cc\text{-}w}$ meas.	$^{18}\varepsilon_{cc\text{-}w}$ calc.[c]	$^{18}\varepsilon_{cc\text{-}w}$ calc.[d]	$^{18}\varepsilon_{cc\text{-}w}$ calc.[e]	$^{18}\varepsilon_{cc\text{-}w}$ calc.[f]	$^{18}\varepsilon_{cc\text{-}w}$ calc.[g]	$^{18}\varepsilon_{cc\text{-}w}$ calc.[h]
T1-W5	13.4	-9.3	31.1	30.5	31.0	30.5	31.3	32.1	30.6
T10-W7	14.2	-9.3	30.9	30.3	30.8	30.3	31.1	32.0	30.6
T15-W8	14.2	-9.2	30.8	30.3	30.8	30.3	31.1	31.9	30.6
T16-W9	14.4	-9.3	31.2	30.2	30.7	30.3	31.1	31.9	30.6

Table 14: *Continued*.

Sample	T (°C)	$\delta^{18}O_{tufa}$ (‰) meas. (VPDB)	$\delta^{18}O_{cc}$ (‰) calc.[c] (VPDB)	$\delta^{18}O_{cc}$ (‰) calc.[d] (VPDB)	$\delta^{18}O_{cc}$ (‰) calc.[e] (VPDB)	$\delta^{18}O_{cc}$ (‰) calc.[f] (VPDB)	$\delta^{18}O_{cc}$ (‰) calc.[g] (VPDB)	$\delta^{18}O_{cc}$ (‰) calc.[h] (VPDB)	$\delta^{18}O_{cc}$ (‰) calc.[i] (VPDB)	$\delta^{18}O_{cc}$ (‰) calc.[j] (VPDB)
T1-W5	13.4	-8.84	-9.3	-8.8	-9.3	-8.4	-7.6	-9.0	-8.7	-9.2
T10-W7	14.2	-9.07	-9.4	-8.9	-9.4	-8.6	-7.8	-9.0	-8.8	-9.3
T15-W8	14.2	-9.05	-9.4	-8.9	-9.4	-8.6	-7.7	-9.0	-8.8	-9.3
T16-W9	14.4	-8.81	-9.6	-9.1	-9.5	-8.7	-7.9	-9.1	-9.0	-9.5

6.6.5 Variations in Mg/Ca and Sr/Ca in tufa

The Mg/Ca and Sr/Ca molar ratios of Krka tufa (Mg/Ca_{tufa} and Sr/Ca_{tufa}, respectively) are lower in comparison with values reported in other studies of similar tufa precipitating systems (e.g. Leybourne et al., 2009). The majority of tufa samples in Krka have average Mg/Ca_{tufa} of 0.03, slightly lower than those reported by Leybourne et al., (2009; Mg/Ca_{tufa} = 0.05–0.17), whereas the Sr/Ca_{tufa} range from 5.7×10^{-5} to 8.6×10^{-5} (average 6.7×10^{-5}), which is one order of magnitude lower than in the study of Leybourne et al. (2009). Nevertheless, samples T11, T12 and T13 show higher Mg/Ca ratios of 0.12, 0.07 and 0.05, respectively (Figure 59). Slightly elevated Sr/Ca_{tufa} were also determined in samples T15 and T16 (Figure 59). A very strong correlation between dolomite content and Mg/Ca_{tufa} (R = 0.92) implies that a significant fraction of Ca and Mg is bound into carbonate detrital phase, which also explains elevated Mg/Ca_{tufa} values in tufa samples.

Similarly, the Sr/Ca_{tufa} values show moderate correlation with dolomite content (R = 0.56) and Mg/Ca_{tufa} (R = 0.57), suggesting its values vary in accordance with the content of detrital component in the sample.

Temperature variation is known to be a key control of Mg partitioning, while partitioning of Sr is temperature and crystal growth rate dependant (Huang and Fairchild, 2001). Moreover, the Mg/Ca and Sr/Ca of tufa generally correlate with Mg/Ca and Sr/Ca ratios in water (Huang and Fairchild, 2001; Leybourne et al., 2009), however, this is not the case in our study. In addition, there was no correlation obtained when correlating water temperatures with water Mg/Ca and Sr/Ca, thus partitioning of Mg and Sr into calcite in the Krka is not straightforward as is assumed by Huang and Fairchild (2001). In a set of *in-vitro* experiments Rogerson et al. (2008) found presence of biofilms importantly alters the behaviour of trace elements. Though the tufa precipitation mechanism was strictly physico-chemical, the incorporation of Sr into solid phase is enhanced, while Mg partitioning is reduced due to chemoselectivity in favour of ions with low charge densities (Rogerson et al., 2008).

Another possible explanation for such discrepancies would be that the fraction of Mg and Sr that is bound to detrital component influences the values of tufa molar ratios. The average Mg/Ca (Sr/Ca) values of dolomite and limestone bedrock in the Krka watershed area are 0.71 (1.3×10^{-4}) and 0.04 (1.6×10^{-4}), respectively. In the case of Sr, the Sr/Ca values of the bedrock are by one order higher than in the tufa (see above). On the contrary, the Mg/Ca of 0.04 of the limestone is similar to average Mg/Ca_{tufa} (0.03) implying that the Mg/Ca_{tufa} partially reflects the Mg/Ca molar ratio of the limestone bedrock. Second explanation would be

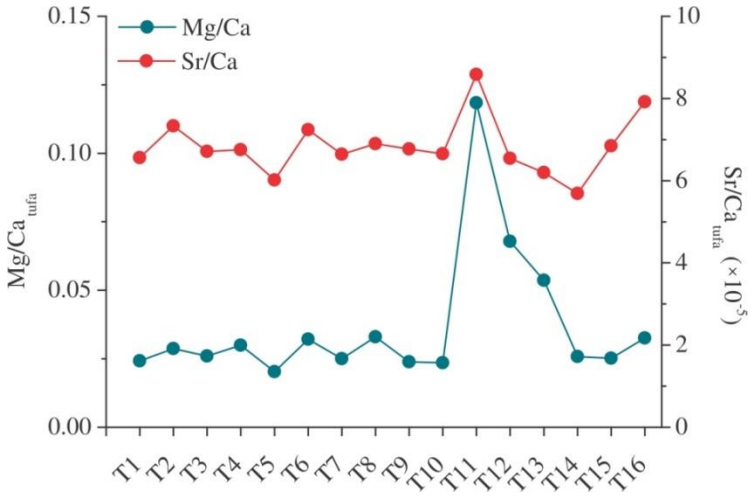

Figure 59: *Molar ratios of Mg/Ca and Sr/Ca in tufa samples.* Spatial variations of the Mg/Ca_{tufa} and Sr/Ca_{tufa} follow a trend of the isotopic composition of tufa (Figure 39a), being the highest in T11, T12 and T13 samples, most likely due to the presence of carbonate detrital component.

Using equation (30) we calculated partitioning coefficients for Mg (D_{Mg}) and Sr (D_{Sr}) considering Mg/Ca and Sr/Ca ratios of water and tufa for T1-W5, T10-W7, T15-W8 and T16-W9 tufa-water sample pairs (Table 15). The calculated D_{Sr} values of 0.27 to 0.30 are significantly higher compared to 0.06 – 0.08 values, determined by Huang and Fairchild (2001). Similar observations were found in the study of Leybourne et al. (2009) who attributed high D_{Sr} values to rapid crystallization of tufa precipitates. The Sr/Ca_{tufa} in Krka correlates with $\delta^{13}C$ and $\delta^{18}O$ of tufa (R = 0.56 and 0.62, respectively), which means that partitioning of Sr was subjected to the same processes as the isotopic imprint of tufa in the Krka. Since the δ values were found to be partially subjected to kinetic processes caused by fast precipitation of $CaCO_3$ from the Krka waters, thus we can assume that

partitioning of Sr was affected by fast precipitation of tufa from the water.

The calculated D_{Mg} values ranging from 0.042 to 0.069 decreased downstream and were in the range of experimentally determined values for karst-analogue conditions (0.057 to 0.078, Huang and Fairchild, 2001). The relationship between D_{Mg} and solution temperature (T) is described with the following relation (Huang and Fairchild, 2001; Lojen et al., 2009) at a temperature range between 15 and 25 °C:

$$D_{Mg} = 0.00120 \cdot T(℃) + 0.001 \quad (58)$$

Table 15*: Calculations of the partitioning coefficient for Mg (D_{Mg}) and Sr (D_{Sr}) between tufa (t) and water using the relations $D_{Mg} = (Mg/Ca)_t/(Mg/Ca)_w$ and $D_{Sr} = (Sr/Ca)_t/(Sr/Ca)_w$.* The temperatures were calculated considering the relation: $D_{Mg} = 0.00120 \times T(°C) + 0.001$ (Huang and Fairchild, 2001).

Sample	T (°C)	Mg/Ca_t	Mg/Ca_w	Sr/Ca_t	Sr/Ca_w	D_{Mg}	D_{Sr}	T (°C) calc.
T1-W5	13.4	0.024	0.57	0.00007	0.0003	0.042	0.27	26.8
T10-W7	14.2	0.024	0.51	0.00007	0.0002	0.047	0.29	30.9
T15-W8	14.2	0.025	0.48	0.00007	0.0003	0.052	0.27	35.1
T16-W9	14.4	0.033	0.48	0.00008	0.0003	0.069	0.30	49.0

Considering the D_{Mg} values for the Krka $CaCO_3$ – water system, we calculated that the water temperature would range from 27 to 49 °C. This is significantly higher than the measured water temperatures; the differences range from 13 to 34 °C. Such deviations were expected due (1) to lack of correlation between water temperature and its Mg/Ca ratio (Zavadlav and Lojen, 2009) and (2) significant fraction of detrital mineralogical component in tufa. Similar findings were obtained by Lojen et al. (2009) who stated that the Mg thermometry can be only used in systems, where the correlation between water temperature and its Mg/Ca ratio is very strong, which is not the case for the Krka waters.

7 Conclusions

Riverine systems are importantly involved in the global carbon biogeochemical cycle. They transport carbon from terrestrial environments to the ocean, consume atmospheric CO_2 via rock dissolution, mineralize and store carbon and also exchange CO_2 with the atmosphere. Despite covering a proportionally small area of 0.004 %, the continental waters account for 29.4 % of the total terrestrial CO_2 sink (Liu et al., 2010).

The study of biogeochemical processes in the Krka River watershed is the first comprehensive study of this area in the context of riverine CO_2 dynamics, thus contributing to the knowledge about weathering intensity, photosynthesis/respiration cycle and in-stream calcium carbonate precipitation in a karstic environment. The Krka drainage basin covers 2,350 km^2 of the north-western part of the Dinaric carbonate platform, a large karst boundary are in the south-east Europe that separates Adriatic Sea in the south-east and the Alps in the north-west. The Krka is 96 km long and is the largest tributary of the Slovenian part of the Sava River, which drains waters into the Danube. Over 80 % of the Krka watershed consists of Mesozoic carbonate sedimentary rocks (Triassic dolomites, and limestones of Jurassic and Cretaceous age) and ~ 17 % of Quaternary sediments (red and brown shale, sandstones and siltstones). The Mesozoic carbonates are highly karstified.

For the purposes of this study we carried out a systematic 3-year long investigation (2007–2010) on the hydrogeochemistry and carbonate system in the Krka River and its major tributaries. Beside field measurements of water temperature, pH and electrical conductivity, we collected water samples for determining the content of major ions (Ca^{2+}, Mg^{2+}, Na^{+}, K^{+}, Sr^{2+}, Ba^{2+}, Cl^{-}, SO_4^{2-}, NO_3^{-}), total alkalinity and stable isotope composition of O in water, C in DIC and POC, N in particulate nitrogen and S in sulphate. In addition, we sampled tufa deposits on 16 largest barrage systems to determine microscopic features and mineralogical, elemental and stable isotope composition of carbon and oxygen in the samples. On the basis of results obtained the following conclusions were drawn:

- The estimated MRT of stream water ranged from 1.3 to 4.7 years (average 2.4 years) showing that waters in the upper reaches reflect isotopic composition of groundwaters that were in longer contact with the aquifer bedrock than those in the lower reaches. Low MRT values in the lower reaches (average 1.6 years) most likely reflect additional input of groundwater coming from shallow aquifers in the east of the Krka watershed.
- The major solute composition of the Krka River and its tributaries is dominated by the input of HCO_3^{-}, Ca^{2+} and Mg^{2+} ions, originating from carbonate rock dissolution via carbonic acid. The major source of Mg^{2+} ions in the watershed is dolomite dissolution, whereas relative contributions of Ca^{2+} and HCO_3^{-} ions from dolomite and/or calcite dissolution significantly vary within the watershed due to different lithology of the recharge areas. We calculated that in the main spring of the headwaters dolomite dissolution contribute over 70 % of the total carbonate dissolved load while in downstream sections and the tributaries dissolution of dolomite contributes only around 50 % of the total dissolved carbonate load.
- The contribution of Cl^{-}, SO_4^{2-} and NO_3^{-} ions in the Krka waters presents less than 5

% of the total dissolved load. Nevertheless, the highest concentrations of Cl^- and NO_3^- were determined in the headwaters indicating contamination of groundwaters in the north-west recharge area of the watershed. The average Cl/Na molar ratio of Krka waters was 1.2 indicating dissolution of NaCl originating from dissolution of salts used as de-icing agents. The excess of Cl^- most likely results from dissolution of Ca- and Mg-chloride salts often used de-icing agents at temperatures below -8 °C.

- On a global scale, the calculated CWR for the Krka watershed were 3 to 7 times higher than the mean world CWR value of 24 t/km^2/yr (Gaillardet et al., 1999), which is due to enhanced solubility of carbonate bedrock and high runoff conditions in the Krka watershed. Accordingly, the CO_2 consumption rates, calculated as a product of HCO_3^- content and discharge and normalized to the surface area of the watershed, were twice as much as the estimate of 8×10^5 mol of C/km^2/yr for world-scale CO_2 consumption determined by Meybeck (1987). Different seasonal CWR values were found to result from seasonal variability of discharge amount being the highest in spring and autumn and prolonged water-rock interaction time due to relatively long retention of groundwater in the karstic aquifer.
- Low dissolved organic carbon content (0.02–0.40 mM), and high dissolved inorganic carbon (3.61–5.94 mM) and pCO_2 (up to $10^{-1.2}$ bars) concentrations characterize Krka River waters influenced by interaction of soil waters with the carbonate bedrock. High pCO_2 levels, low pH and undersaturation with calcite and dolomite (SI < 0) in the headwaters are indicative of high amounts of transported soil CO_2 and carbonate dissolution in the aquifer, suggesting the headwaters reflect characteristics of the groundwaters. A decrease in pCO_2 levels downstream reflects intensive CO_2 outgassing resulting in an increase in SI values (> 0), which in thermodynamical terms meets the conditions for calcite and/or dolomite precipitation.
- A wide range of $\delta^{13}C_{DIC}$ values in Krka (-16.0 ‰ to -10.5 ‰) reflects variable contributions of different carbon sources (soil pCO_2 and carbonate dissolution) and impacts of processes in the stream that fractionate carbon isotopic composition of DIC. Based on the low $\delta^{13}C_{DIC}$ values of the headwaters (average -13.6 ‰) and considering isotopic fractionation factors between dissolved carbonate species we found that DIC in the Krka watershed originates from degradation of organic material dominated by C_3 plants in the soil and carbonate mineral dissolution that primarily occurs under open system conditions.
- In comparison with the $\delta^{13}C_{DIC}$ values in the headwaters, the DIC in the main stream and the tributaries exhibited higher δ values (average -12.6 ‰). In general, the enrichment with ^{13}C was the highest in the upper reaches (> 1.2 ‰) where turbulent water conditions prevail, thus the enrichment can be ascribed to CO_2 outgassing caused by equilibration between dissolved CO_2 and atmospheric CO_2. Aquatic metabolism (photosynthesis and respiration) and in-stream calcium carbonate precipitation were found to be of minor importance influencing the isotopic imprint of the dissolved inorganic carbon pool in the Krka waters. The $\delta^{13}C$ of particulate organic carbon (POC) in the Krka ranged from -31.7 ‰ to -25.0 ‰.
- In all sampling seasons, degradation of organic matter and weathering of carbonates were found to be the most important processes influencing the CO_2 dynamics in the watershed. The process of weathering is predominant in spring and summer, whereas degradation of organic matter was found to be more expressed in autumn and winter. The lowest DIC fluxes were calculated for summer (average 2.0×10^8 mol/month), while higher fluxes were usually observed in spring and autumn due to increased discharge (average 5.4×10^8 mol/month and 5.5×10^8 mol/month, respectively). Similar seasonal changes were observed in the total diffusive loss of CO_2 ranging from

1.5×10^7 mol/month in summer to 2.8×10^7 mol/month in autumn. On average, the tributaries contribute 25.4 % of inorganic carbon to riverine DIC, however their contribution decreases to 13.4 % in summer due to baseflow conditions in the basin, when groundwater input is the major source of water in the Krka. 1.1×10^7 mol of C/month is deposited as $CaCO_3$ (F_{CaCO3}) in the Krka River, which is in the range of CO_2 fluxes. These processes seem to have only minor influence on the overall carbon mass balance in the Krka watershed.

Tufa deposits in Krka River were studied to define relations in the $CaCO_3$ – water system of Krka River. The findings are as follows:

- Tufas in Krka River are dominantly low Mg-calcite. The detrital component consists mostly of dolomite, quartz and allumo-silicates. The most prominent macroscopic feature of Krka tufa is a porous structure with cavities of 5 mm to over 1.5 cm in size. Based on weighing wet and dry samples we estimated rough porosity of ~ 21 %. The internal structure of presently forming tufa deposits in Krka is strongly related to organic particles. The depositional facies was recognized as vacuolar facies characterized by voids between calcified organic matter remains. In the examined thin-sections of the Krka tufas two main types of calcite precipitates are delineated. First is sparry cement calcite filling intergranular space that is clearly of inorganic origin. Second type includes mostly fine-crystalline calcite (micrite, microsparite) with dendrolitic or laminated texture that resembles organic growth, thus giving evidence on biological influences on $CaCO_3$ precipitation. Besides sparitic cements, voids contain detrital material, among which quartz and carbonate grains were recognized.
- Three types of fabric were recognized. Dendrolitic fabric is composed of filamentous encrusted organic material, mineralized by micrite and/or microsparite. Laminar fabric, surrounding different organic structures, forms 20 to 50 μm thick dark brown to brown laminas of micrite and microsparite that passes either to sparry calcite laminas or dendrolitic fabric. Aphanitic fabric is mostly associated with microsparite crystals and occasionally it shows indistinctive concentrical laminae (oncoidal texture, Figure 55a).
- The deposition of tufa in the Krka is enhanced by high turbidity at waterfalls and high water temperatures rather by saturation states with respect to calcite in the water. The presence of biota most likely acts only as a substrate for calcite precipitation, whereas detrital component fills the pores lowering the porosity of tufa deposits.
- The precipitation rates (R) of calcite were calculated to be the highest for summer (average 12.5×10^{-8} mmol/cm^{2}s) and the lowest for winter (average 7.0×10^{-8} mmol/cm^{2}s) indicating that precipitation of tufa is most active during warm months which is consistent with enhanced growth of aquatic biota that serves as a substrate for calcite precipitation. Maximal rates were obtained assuming a boundary layer of thickness ε = 50 μm and thickness of the water layer above the precipitated calcite surface δ = 10 cm, which is the best approximation to realistic conditions in turbulent waters (Liu and Dreybrodt, 1997; Bono et al., 2001). Considering density of tufa to be 2.2 g/cm^3 the rate of calcite precipitation in Krka River ranges from 0.7 to 2.1 mm/yr. This is consistent with the findings from thin section examination, where we observed that growth rate of tufa in the Krka ranges from 1 to ~ 2 mm/yr, assuming a combination of dense and porous layer in the laminated fabric presents a one year cycle of calcite precipitated.
- The isotopic fractionation in the $CaCO_3$ – water system in the Krka was found to be influenced by kinetic isotope effects. In the case of carbon, the deviations from theoretically predicted isotopic fractionation most likely result from isotopically more positive detrital fraction presence in tufa rather than highly negative organic carbon. The

relationship between $\delta^{18}O$ and temperature in Krka waters showed no correlation, suggesting that $\delta^{18}O_{tufa}$ is not only a function of temperature and $\delta^{18}O$ values of water. Calculations of $^{18}\varepsilon$ between calcite and confirmed such assumptions yielding mainly more negative calculated $\delta^{18}O_{calcite}$ values.

- The partitioning of Mg and Sr into Krka tufa give scarce information on environmental conditions in the time of precipitation. While significantly high partitioning coefficient of Sr (D_{Sr}) and positive correlation between Sr/Ca and δ values of carbon and oxygen in tufa can be attributed to fast calcite precipitation, the Mg/Ca_{tufa} molar ratio exhibits lack of any correlation with water temperature and Mg/Ca of water.

Present study gives a detailed overview of CO_2 dynamics in the CO_2 – water – $CaCO_3$ system of a karstic watershed of the Krka River. Due to enhanced solubility of predominantly carbonate bedrock within the watershed we expected that the CO_2 dynamics would be mainly influenced by the intensity of carbonate rock weathering. However, tracing the processes of inorganic carbon transport and transformation by using isotope tracer tools and implementing mass balance calculations revealed that the processes of root respiration and degradation of organic matter in the soil are quantitatively equivalent source of carbon in the Krka watershed. This is due to high soil CO_2 productivity that is particularly pronounced in forested watersheds with thick soil cover as in the case of Krka watershed. The dissolution of carbonate bedrock and CO_2 outgassing in the surface streams are processes that characterize Krka River as a source of CO_2, whereas the in-stream calcium carbonate precipitation has negligible influence on the overall inorganic carbon fluxes.

Due to global concerns on present and past climate changes, tufas have been recognized as important archives of environmental conditions. In this study, we showed that tufas precipitating in groundwater-fed stream water are unsuitable for a straightforward reconstruction of water temperatures using generally-accepted isotopic fractionation equations obtained in laboratory experiments of spontaneous calcite precipitation. These findings open an important question, whether these equations are applicable to natural system conditions. Nevertheless, it is important to note that the Krka tufa contains a significant amount of detrital component, which influences the bulk stable isotopic values and consequently the calculations of isotopic fractionation and water temperatures as well.

Despite its small-size area, the study of a carbonate system in the Krka watershed gives important knowledge on the CO_2 dynamics in watersheds with predominantly carbonate bedrock. This scientific area is yet poorly constrained, since worldwide studies on chemical weathering and carbon fluxes mostly focus on large watersheds with predominantly siliclastic bedrock. Moreover, this study is the first comprehensive research on tufa precipitates in the Krka River in regards to tufa stable isotope geochemistry, mineralogy and microfacies.

8 Acknowledgements

Doctoral dissertation was performed at the Department of Environmental Sciences of the Jožef Stefan Institute. I thank my supervisor Assoc. Prof. Dr. Sonja Lojen for her guidance, encouragement and support during the formation of this work. Thanks are due to the members of the committee for the evaluation of the thesis and their constructive comments and suggestions that greatly improved the final version.

Over the course of my study, I greatly benefited from day-to-day discussions with my colleagues from the Department of Environmental Sciences. I particularly thank Mr. Stojan Žigon for technical support, and the ladies, Assoc. Prof. Dr. Nives Ogrinc, Dr. Polona Vreča, Dr. Tjaša Kanduč and Dr. Martina Burnik Šturm for constructive debates and their generous exchange of knowledge. Maps and figures would not be perfected without Dr. David Kocman's help for which I am very grateful.

Constructive help of colleagues from the Department of Geology at the Faculty of Technical and Engineering Sciences (University of Ljubljana) is much appreciated. Mr. Miran Udovč prepared tufa samples and performed mineralogical analyses. Asst. Prof. Matej Dolenec helped on the interpretation on mineralogical composition of tufa samples and performed XRF analyses on rock samples. Special thanks are given to Asst. Prof. Boštjan Rožič for the assistance with optical microscopy and for the final critical review on the interpretation of microscopic features of tufa samples.

For the assistance in the field work, I am grateful to Mr. Emil Glavič. I also appreciate the administrative help of Mrs. Damjana Nikovski.

Financial support of the Slovenian Research Agency is highly appreciated. The study was performed in the frame of research programme P1-0143, research project J1-9498 and Young Researcher's programme PR-02497.

Finally, I thank my family and friends for all the support during my studies. Samo, thanks for being there for me.

9 References

Amiotte–Suchet, P.; Aubert, D.; Probst, J. L.; Gauthier-Lafaye, F.; Probst, A.; Andreux, F.; Viville, D. $\delta^{13}C$ pattern of dissolved inorganic carbon in a small granitic catchment: the Strengbach case study (Vosges mountains, France). *Chemical Geology* **159**, 129–145 (1999).

Amiotte–Suchet, P.; Probst, J. L.; Ludwig, W. Worldwide distribution of continental rock lithology: Implications for the atmospheric/soil CO_2 uptake by continental weathering and alkalinity river transport to the oceans. *Global Biogeochemical Cycles* **17**, 1891–903 (2003).

Anderson, T. F.; Arthur, M. A. Stable isotopes of oxygen and carbon and their application to sedimentologic and palaeoenvironmental problems. In: *Stable Isotopes in Sedimentary Geology*. Short Course Notes **10**, 1.1–1.151 (Society of Economic Palaeontologists and Mineralogists, USA, 1983).

Andrews, J. E.; Riding, R.; Dennis, P. F. Stable isotopic compositions of Recent freshwater cyanobacterial carbonates from the British Isles: local and regional environmental controls. *Sedimentology* **40**, 303–314 (1993).

Andrews, J. E.; Brimblecombe, P.; Jickells, T. D.; Liss, P. S. The terrestrial environment. In: *An Introduction to Environmental Chemistry*. 46–113 (Blackwell Science Ltd, Oxford, 1996).

Andrews, J. E. Palaeoclimatic records from stable isotopes in riverine tufas: synthesis and review. *Earth-Science Reviews* **75**, 85–104 (2006).

Anzalone, E.; Ferreri, V.; Sprovieri, M.; D'Argenio, B. Travertines as hydrologic archives: The case of the Pontecagnano deposits (southern Italy). *Advances in Water Resources* **30**, 2159–2175 (2007).

Appelo, C. A. J.; Postma, D. *Geochemistry, groundwater and pollution* (Taylor and Francis, Amsterdam, 2009).

Aravena, R.; Schiff, S. L.; Trumbore, S. E.; Dillon, P. I.; Elgood, R. Evaluating dissolved inorganic carbon cycling in a forested lake watershed using carbon isotopes. *Radiocarbon* **34**, 636–645 (1992).

Arp, G.; Wedemeyer, N.; Reitner, J. Fluvial tufa formation in a hard-water creek (Deinschwanger Bach, Franconian Alb, Germany). *Facies* **44**, 1–22 (2001).

ARSO – Agencija Republike Slovenije za okolje (Ministry of Agriculture and Environment) http://www.arso.gov.si/ (last access: February 2013).

Arvidson, R. S.; Mackenzie, F. T. Temperature dependance of mineral precipitation rates along the $CaCO_3$ – $MgCO_3$ join. *Aquatic Geochemistry* **6**, 249–256 (2000).

Atekwana, E. A.; Krishnamurthy, R. V. Seasonal variations of dissolved inorganic carbon and $\delta^{13}C$ of surface waters: application of a modified gas evolution technique. *Journal of Hydrology* **205**, 265–278 (1998).

Aucour, A. M.; Sheppard, S. M. F.; Guyomar, O.; Wattelet, J. Use of ^{13}C to trace origin and cycling of inorganic carbon in the Rhône river system. *Chemical Geology* **159**, 87–105 (1999).

Barth, J. A. C.; Veizer, J.; Mayer, B. Origin of particulate organic carbon in the upper St.

Lawrence: isotopic constraints. *Earth and Planetary Science Letters* **162**, 111–121 (1998).

Barth, J. A. C.; Veizer, J. Carbon cycle in St. Lawrence aquatic ecosystems at Cornwall (Ontario), Canada: seasonal and spatial variations. *Chemical Geology* **159**, 107–128 (1999).

Barth, J. A. C.; Cronin, A. A.; Dunlop, J.; Kalin, R. M. Influence of carbonates on the riverine carbon cycle in an anthropogenically dominated catchment basin: evidence from major elements and stable carbon isotopes in the Lagan River (N. Ireland). *Chemical Geology* **200**, 203–216 (2003).

Battin, T. J.; Kaplan, L. A.; Findlay, S.; Hopkinson, C. S.; Marti, E.; Packman, A. I.; Newbold, J. D.; Sabater, F. (2008). Biophysical controls on organic carbon fluxes in fluvial networks. *Nature Geoscience* **1**, 95–100 (2008).

Battin, T. J.; Luyssaert, S.; Kaplan, L. A.; Aufdenkampe, A. K.; Richter, A.; Tranvik, L. J. The boundless carbon cycle. *Nature Geoscience* **2,** 598–600 (2009).

Berner, R. A. Authigenic mineral formation resulting from organic matter decomposition in modern sediments. *Fortschritte der Mineralogie* **59**, 117–135 (1981).

Bono, P.; Dreybrodt, W.; Ercole, S.; Percopo, C.; Vosbeck, K. Inorganic calcite precipitation in Tartare karstic spring (Lazio, central Italy): field measurements and theoretical prediction on depositional rates. *Environmental Geology* **41**, 305–313 (2001).

Bottinga, Y. Calculation of fractionation factors for carbon and oxygen isotopic exchange in the system calcite-carbon dioxide-water. *The Journal of Physical Chemistry* **72**, 800–808 (1968).

Brasier, A. T. Searching for travertines, calcretes and speleothems in deep time: processes, appearances, predictions and the impact of plants. *Earth-Science Reviews* **104**, 213–239 (2011).

Broecker, W. S. *Chemical oceanography* (Harcourt Brace Jovanovich, New York, 1974).

Brook, G. A.; Folkoff, M. E.; Box, E. O. A world model of soil carbon dioxide. *Earth Surface Processes and Landforms* **8**, 79–88 (1983).

Brunet, F.; Dubois, K.; Veizer, J.; Nkoue Ndondo, G. R.; Ndam Ngoupayou, J. R.; Boeglin, J. L.; Probst, J. L. Terrestrial and fluvial carbon fluxes in a tropical watershed: Nyong basin, Cameroon. *Chemical Geology* **265**, 563–572 (2009).

Buhmann, D.; Dreybrodt, W. The kinetics of calcite dissolution and precipitation in geologically relevant situations of karst areas: 1. Open system. *Chemical Geology* **48,** 189–211 (1985).

Buser, S. Tolmač k osnovni geološki karti SFRJ 1:100 000, list Ribnica (in Slovene) (Zvezni geološki zavod, Beograd, 1974).

Buser, S.; Cajhen, J. Osnovna geološka karta SFRJ 1:100 000, list Ribnica (in Slovene) (Zvezni geološki zavod, Beograd, 1965).

Cao, J.; Yuan, D.; Groves, C.; Huang, F.; Yang, H., Lu, Q. Carbon fluxes and sinks: the consumption of atmospheric and soil CO_2 by carbonate rock dissolution. *Acta Geologica Sinica-English Edition* **86**, 963–972 (2012).

Cerling, T. Carbon dioxide in the atmosphere: evidence from Cenozoic and Mesozoic paleosols. *American Journal of Science* **291**, 377–400 (1991).

Chafetz, H. S.; Folk, R. L. Travertines: depositional morphology and the bacterially constructed constituents. *Journal of Sedimentary Research* **54**, 289–316 (1984).

Chen, J.; Zhang, D. D.; Wang, S.; Xiao, T.; Huang, R. Factors controlling tufa deposition in natural waters at waterfall sites. *Sedimentary geology* **166**, 353–366 (2004).

Clark, I. D.; Fritz, P. *Environmental Isotopes in Hydrogeology* (Lewis Publishers, New York, 1997).

Coplen, T. B. Calibration of the calcite–water oxygen-isotope geothermometer at Devils Hole, Nevada, a natural laboratory. *Geochimica et Cosmochimica Acta* **71**, 3948–3957 (2007).

Craig, H. The measurement of oxygen isotope palaeotemperatures. In: *Stable Isotopes in Oceanographic Studies and Palaeotemperatures*. 161–182 (Consiglio Nazionale Della Richerche Laboratorio de Geologia Nucleare, Pisa, 1965).

Čater, M.; Ogrinc, N. Soil respiration rates and $\delta^{13}C(CO_2)$ in natural beech forest (Fagus sylvatica L.) in relation to stand structure. *Isotopes in Environmental and Health Studies* **47**, 221–237 (2011).

Dalai, T. K.; Krishnaswami, S.; Sarin, M. M. Major ion chemistry in the headwaters of the Yamuna river system: Chemical weathering, its temperature dependence and CO_2 consumption in the Himalaya. *Geochimica et Cosmochimica Acta* **66**, 3397–3416 (2002).

Darling, W. G. Hydrological factors in the interpretation of stable isotopic proxy data present and past: a European perspective. *Quaternary Science Reviews* **23**, 743–770 (2004).

Das, D. K. Decomposition of geological materials for trace elements analysis. In: *Trace Analysis*. 1–29 (Narosa, New Delhi, 2008).

Deines, P.; Langmuir, D.; Harmon, R. S. Stable carbon isotope ratios and the existence of a gas phase in the evolution of carbonate ground waters. *Geochimica et Cosmochimica Acta* **38**, 1147–1164 (1974).

Deines, P. The isotopic composition of reduced organic carbon. In: *Handbook of environmental isotope geochemistry*. 329–406 (Elsevier Sci., New York, 1980).

DeWalle, D. R.; Edwards, P. J.; Swistock, B. R.; Aravena, R.; Drimmie, R. J. Seasonal isotope hydrology of three Appalachian forest catchments. *Hydrological Processes* **11**, 1895–1906 (1997).

Dietzel, M.; Tang, J.; Leis, A.; Köhler, S. J. Oxygen isotopic fractionation during inorganic calcite precipitation – Effects of temperature, precipitation rate and pH. *Chemical Geology* **268**, 107–115 (2009).

Doctor, D. H.; Kendall, C.; Sebestyen, S. D.; Shanley, J. B.; Ohte, N.; Boyer, E. W. Carbon isotope fractionation of dissolved inorganic carbon (DIC) due to outgassing of carbon dioxide from a headwater stream. *Hydrological Processes* **22**, 2410–2423 (2008).

Dolinar, M. Precipitation. In: *Water balance of Slovenia 1971–2000*. 29–34 (Ministry for Environment and Spatial Planning–Environmental Agency of the Republic of Slovenia, Ljubljana, 2008).

Dorale, J. A.; González, L. A.; Reagan, M. K.; Pickett, D. A.; Murrell, M. T.; Baker, R. G. A high-resolution record of Holocene climate change in speleothem calcite from Cold Water Cave, northeast Iowa. *Science* **258**, 1626–1630 (1992).

Drever, J. I. *The Geochemistry of Natural Waters: Surface and Groundwater Environments* (Practise Hall, Sweden, 1997).

Dreybrodt, W. Modelling the Kinetics of Calcite Dissolution and Precipitation in Natural Environments of Karst Areas. In: *Processes in karst systems, physics, chemistry, and geology*. 140–182 (Springer–Verlag, New York, 1988).

Dreybrodt, W.; Buhmann, D. A. Mass transfer model for dissolution and precipitation of calcite from solutions in turbulent motion. *Chemical Geology* **90**, 107–122 (1991).

Dreybrodt, W.; Buhmann, D.; Michaelis, J.; Usdowski, E. Geochemically controlled

calcite precipitation by CO_2 outgassing: Field measurements of precipitation rates in comparison to theoretical predictions. *Chemical Geology* **97**, 285–294 (1992).

Drovenik, M.; Leskovšek, H.; Pezdič, J.; Štrucl, I. Izotopska sestava žvepla v sulfidih nekaterih jugoslovanskih rudišč. *Rudarsko-metalurški zbornik*, **2–3**, 193–246 (1970).

EIONET – European Environment Information and Observation Network. http://nfp-si.eionet.eu.int/ (last access: February 2013).

Epstein, S.; Buchsbaum, R.; Lowenstam, H. A.; Urey, H. C. Revised carbonate-water isotopic temperature scale. *Geological Society of America Bulletin*, **64**, 1315–1326 (1953).

Epstein, S.; Mayeda, T. Variation of O^{18} content of waters from natural sources. *Geochimica et Cosmochimica Acta* **4**, 213–224 (1953).

Esser, G.; Kattge, J.; Sakalli, A. Feedback of carbon and nitrogen cycles enhances carbon sequestration in the terrestrial biosphere. *Global Change Biology* **17**, 819–842 (2011).

Faure, C.; Bonakdar, L.; Dufourc, E. J.; Dreybrodt, W.; Eisenlohr, L.; Madry, B.; Ringer, S. Precipitation kinetics of calcite in the system $CaCO_3$-H_2O-CO_2: The conversion to CO_2 by the slow process $H^+ + HCO_3^- \rightarrow CO_2 + H_2O$ as a rate limiting step. *Geochimica et Cosmochimica Acta* **61**, 3897–3904 (1997).

Ferguson, P. R.; Dubois, K. D.; Veizer, J. Fluvial carbon fluxes under extreme rainfall conditions: Inferences from the Fly River, Papua New Guinea. *Chemical Geology* **281**, 283–292 (2011).

Finlay, J. C.; Kendall, C. Stable isotope tracing of temporal and spatial variability in organic matter sources to freshwater ecosystems. In: *Stable Isotopes in Ecology and Environmental Science*. 283–333 (Blackwell Publishing Ltd, Singapore, 2007).

Frantar, P. *Water balance of Slovenia 1971–2000* (Ministry for Environment and Spatial Planning–Environmental Agency of the Republic of Slovenia, Ljubljana, 2008).

Frantar, P.; Hrvatin, M. Discharge Regimes. In: *Water balance of Slovenia 1971–2000*. 43–50 (Ministry for Environment and Spatial Planning–Environmental Agency of the Republic of Slovenia, Ljubljana, 2008).

Freytet, P.; Plet, A. Modern freshwater microbial carbonates: the Phormidium stromatolites (tufa-travertine) of southeastern Burgundy (Paris Basin, France). *Facies*, **34**, 219–237 (1996).

Friedman, I. Some investigations of the deposition of travertine from hot springs - I. The isotopic chemistry of a travertine-depositing spring. *Geochimica et Cosmochimica Acta*, **34**, 1303–1315 (1970).

Friedman, I.; O'Neil, J. R. Compilation of stable isotope fractionation factors of geochemical interest. In: *Data of Geochemistry*. 1–12 (U. S. Geological Survey, Washington, 1977).

Ford, T. D.; Pedley, H. M. A review of tufa and travertine deposits of the world. *Earth-Science Reviews* **41**, 117–175 (1996).

Gaillardet, J.; Dupre, B.; Louvat, P.; Allegre, C. J. Global silicate weathering and CO_2 consumption rates deduced from the chemistry of large rivers. *Chemical Geology* **159**, 3–30 (1999).

Galy, A.; France-Lanord, C. Weathering processes in the Ganges–Brahmaputra basin and the riverine alkalinity budget. *Chemical Geology* **159**, 31–60 (1999).

Gascoyne, M. Palaeoclimate determination from cave calcite deposits. *Quaternary Science Reviews*, **11**, 609–632 (1992).

Gibbs, R. J. Mechanisms Controlling World Water Chemistry. *Science* **170**, 1088–1090 (1970).

Gieskes, J. M. The alkalinity – total carbon dioxide system in seawater. In: *The Sea. Marine chemistry* **5**. 123–151 (Wiley, New York, 1974).

Given, R. K; Wilkinson, B. H. Kinetic control of morphology, composition, and mineralogy of abiotic sedimentary carbonates. *Journal of Sedimentary Research* **55**, 109–119 (1985).

Guo, L.; Riding, R. Origin and diagenesis of Quaternary travertine shrub fabrics, Rapolano Terme, central Italy. *Sedimentology* **41**, 499–520 (1994).

Hagedorn, B.; Cartwright, I. Climatic and lithologic controls on the temporal and spatial variability of CO_2 consumption via chemical weathering: An example from the Australian Victorian Alps. *Chemical Geology* **260**, 234–253 (2009).

Han, G.; Liu, C. Q. Water geochemistry controlled by carbonate dissolution: a study of the river waters draining karst-dominated terrain, Guizhou Province, China. *Chemical Geology* **204**, 1–21 (2004).

Hays, P. D.; Grossman, E. L. Oxygen isotopes in meteoric calcite cements as indicators of continental paleoclimate. *Geology* **19**, 441–444 (1991).

Hélie, J. F.; Hillaire-Marcel, C.; Rondeau, B. Seasonal changes in the sources and fluxes of dissolved inorganic carbon through the St. Lawrence River - isotopic and chemical constraint. *Chemical Geology* **186**, 117–138 (2002).

Hellings, L.; Dehairs, F.; Tackx, M.; Keppens, E.; Baeyens, W. Origin and fate of organic carbon in the freshwater part of the Scheldt Estuary as traced by stable carbon isotope composition. *Biogeochemistry* **47**, 167–186 (1999).

Hem, J. D. *Study and interpretation of the chemical characteristics of natural water* (US Geological Survey, Alexandria, 1985).

Hendy, C. H. The isotopic geochemistry of speleothems-I. The calculation of the effects of different modes of formation on the isotopic composition of speleothems and their applicability as palaeoclimatic indicators. *Geochimica et Cosmochimica Acta* **35**, 801–824 (1971).

Hercod, D. J.; Brady, P. V.; Gregory, R. T. Catchment-scale coupling between pyrite oxidation and calcite weathering. *Chemical Geology* **151**, 259–276 (1998).

Herman, J. S.; Lorah, M. M. Calcite precipitation rates in the field: measurement and prediction for a travertine-depositing stream. *Geochimica et Cosmochimica Acta* **52**, 2347–2355 (1988).

Hoefs, J. *Stable isotope geochemistry* (Springer–Verlag, Berlin, 2009).

Holley, E. H. Oxygen transfer at the air–water interface. In: *Transport processes in lakes and oceans.* 17–150 (Plenum Press, Atlantic City, 1977).

Hope, D.; Palmer, S. M.; Billett, M. F.; Dawson, J. J. Variations in dissolved CO_2 and CH_4 in a first-order stream and catchment: An investigation of soil–stream linkages. *Hydrological Processes* **18**, 3255–3275 (2004).

Hori, M.; Hoshino, K.; Okumura, K.; Kano, A. Seasonal patterns of carbon chemistry and isotopes in tufa depositing groundwaters of southwestern Japan. *Geochimica et Cosmochimica Acta* **72**, 480–492 (2008).

Huang, Y.; Fairchild, I. J. Partitioning of Sr^{2+} and Mg^{2+} into calcite under karst-analogue experimental conditions. *Geochimica et Cosmochimica Acta* **65**, 47–62 (2001).

Ihlenfeld, C.; Norman, M. D.; Gagan, M. K.; Drysdale, R. N., Maas, R.; Webb, J. Climatic significance of seasonal trace element and stable isotope variations in a modern freshwater tufa. *Geochimica et Cosmochimica Acta*, **67**, 2341–2357 (2003).

Irion, G.; Müller, G. Mineralogy, petrology and chemical composition of some calcareous tufa from the Schwäbische Alb (W. Germany). In: *Recent Developments in Carbonate Sedimentology in Central Europe*. 157–171 (Springer, Berlin, 1968).

Jacobson, A. D.; Blum, J. D.; Walter, L. M. Reconciling the elemental and Sr isotope composition of Himalayan weathering fluxes: Insights from the carbonate geochemistry of stream waters. *Geochimica et Cosmochimica Acta* **66**, 3417–3429 (2002).

Janssen, A.; Swennen, R.; Podoor, N.; Keppens, E. Biological and diagenetic influence in Recent and fossil tufa deposits from Belgium. *Sedimentary Geology* **126**, 75–95 (1999).

Jímenez-López, C.; Caballero, E.; Huertas, F. J.; Romanek, C. S. Chemical, mineralogical and isotope behavior, and phase transformation during the precipitation of calcium carbonate minerals from intermediate ionic solution at 25 °C. *Geochimica et Cosmochimica Acta* **65**, 3219–3231 (2001).

Junge, F. W.; Hanisch, C.; Zerling, L.; Gehre, M. Geochemical signatures (C, N, $\delta^{13}C$, $\delta^{15}N$, metals) of suspended matter in the river Weiße Elster (central Germany): their seasonal and flow-related distribution 1997–2001. *Isotopes in Environmental and Health Studies* **41**, 141–159 (2005).

Kanduč, T. *Hydrogeochemical characteristics and carbon cycling in the Sava River watershed (in Slovene)* (Doctoral dissertation, Universty of Ljubljana, Ljubljana, 2006).

Kanduč, T.; Szramek, K.; Ogrinc, N.; Walter, L. M. Origin and cycling of riverine inorganic carbon in the Sava River watershed (Slovenia) inferred from major solutes and stable carbon isotopes. *Biogeochemistry* **86**, 137–154 (2007a).

Kanduč, T.; Ogrinc, N.; Mrak, T. Characteristics of suspended matter in the River Sava watershed, Slovenia. *Isotopes in Environmental and Health Studies* **43**, 369–386 (2007b).

Kanduč, T.; Kocman, D.; Ogrinc, N. Hydrogeochemical and stable isotope characteristics of the River Idrijca (Slovenia), the boundary watershed between the Adriatic and Black Seas. *Aquatic Geochemistry* **14**, 239–262 (2008).

Kano, A.; Matsuoka, J.; Kojo, T.; Fujii, H. Origin of annual laminations in tufa deposits, southwest Japan. *Palaeogeography, Palaeoclimatology, Palaeoecology* **191**, 243–262 (2003).

Kawai, T.; Kano, A.; Matsuoka, J.; Ihara, T. Seasonal variation in water chemistry and depositional processes in a tufa-bearing stream in SW-Japan, based on 5 years of monthly observations. *Chemical Geology* **232**, 33–53 (2006).

Kele, S.; Demény, A.; Siklósy, Z.; Németh, T.; Tóth, M.; Kovács, M. B. Chemical and stable isotope composition of recent hot-water travertines and associated thermal waters, from Egerszalók, Hungary: Depositional facies and non-equilibrium fractionation. *Sedimentary Geology* **211**, 53–72 (2008).

Kele, S.; Özkul, M.; Fórizs, I.; Gökgöz, A.; Baykara, M. O.; Alçiçek, M. C.; Németh, T. Stable isotope geochemical study of Pamukkale travertines: New evidences of low-temperature non-equilibrium calcite-water fractionation. *Sedimentary Geology* **238**, 191–212 (2011).

Kempe, S.; Emeis, K. Carbonate chemistry and the formation of Plitvice Lakes. In: *Transport of Carbon and Minerals in Major World Rivers*. 351–383 (Mitt. Geol.-Paläontol. Inst. Univ. Hamburg, Hamburg, 1985).

Kendall, C.; Coplen, T. B. Distribution of oxygen-18 and deuterium in river waters across the United States. *Hydrological Processes* **15**, 1363–1393 (2001).

Kendall, C.; McDonnell, J. J. *Isotope tracers in catchment hydrology* (Elsevier Science Ltd, Amsterdam, 1998).

Kim, S. T.; O'Neil, J. R. Equilibrium and nonequilibrium oxygen isotope effects in

synthetic carbonates. *Geochimica et Cosmochimica Acta* **61**, 3461–3475 (1997).

Kogovšek, J.; Petrič, M. Underground water flow from the Tržiščica sinking stream (SE Slovenia). *Acta Carsologica* **3**, 75–91 (2002).

Krivograd Klemenčič, A.; Vrhovšek, D.; Kosi, G. Algae on travertine barriers of the Krka river near Žužemberk, Slovenia. *Natura Croatica* **13**, 371–379 (2004).

Krouse, H. R.; Mayer, B. Sulphur and oxygen isotopes in sulphate. In: *Environmental Tracers in Subsurface Hydrology*. 195–231 (Kluwer Academic Press, Boston, 2000).

Leybourne, M. I.; Betcher, R. N.; McRitchie, W. D.; Kaszycki, C. A.; Boyle, D. R.. Geochemistry and stable isotopic composition of tufa waters and precipitates from the Interlake Region, Manitoba, Canada: Constraints on groundwater origin, calcitization, and tufa formation. *Chemical Geology* **260**, 221–233 (2009).

Li, S. L.; Liu, C. Q.; Li, J.; Lang, Y. C.;, Ding, H.; Li, L. Geochemistry of dissolved inorganic carbon and carbonate weathering in a small typical karstic catchment of Southwest China: Isotopic and chemical constraints. *Chemical Geology* **277**, 301–309 (2010).

Liu, Z.; Svensson, U.; Dreybrodt, W.; Daoxian, Y.; Buhmann, D. Hydrodynamic control of inorganic calcite precipitation in Huanglong Ravine, China: Field measurements and theoretical prediction of deposition rates. *Geochimica et Cosmochimica Acta* **59**, 3087–3097 (1995).

Liu, Z.; Dreybrodt, W. Dissolution kinetics of calcium carbonate minerals in H_2O-CO_2 solutions in turbulent flow: The role of the diffusion boundary layer and the slow reaction $H_2O + CO_2 \rightarrow H^+ + HCO_3^-$. *Geochimica et Cosmochimica Acta* **61**, 2879–2889 (1997).

Liu, Z.; Dreybrodt, W.; Wang, H. A new direction in effective accounting for the atmospheric CO_2 budget: Considering the combined action of carbonate dissolution, the global water cycle and photosynthetic uptake of DIC by aquatic organisms. *Earth-Science Reviews* **99**, 162–172 (2010).

Lojen, S.; Dolenec, T.; Vokal, B.; Cukrov, N.; Mihelčić, G.; Papesch, W. C and O stable isotope variability in recent freshwater carbonates (River Krka, Croatia). *Sedimentology* **51**, 361–375 (2004).

Lojen, S.; Trkov, A.; Ščančar, J.; Vázquez-Navarro, J. A.; Cukrov, N. Continuous 60-year stable isotopic and earth-alkali element records in a modern laminated tufa (Jaruga, river Krka, Croatia): Implications for climate reconstruction. *Chemical Geology* **258**, 242–250 (2009).

Mackenzie, F. T.; Lerman, A. *Carbon in the geobiosphere: Earth's outer shell* (Springer, Dordrecht, 2006).

Manzo, E.; Perri, E.; Tucker, M. E. Carbonate deposition in a fluvial tufa system: processes and products (Corvino Valley–southern Italy), *Sedimentology* **59**, 553–577 (2012).

Marchetto, A.; Bianchi, M.; Geiss, H.; Muntau, H.; Serrini, G.; Serrini-Lanza, G.; Tartari, A.; Mosello, R. Performances of analytical methods for freshwater analysis assessed through intercomparison exercises. I. Total alkalinity. *Memorie Istituto Italiano di Idrobiologia* **56**, 1–14 (1997).

Marlier, J. F.; O'Leary, M. H. Carbon kinetic isotope effects on the hydration of carbon dioxide and the dehydration of bicarbonate ion. *Journal of the American Chemical Society* **106**, 5054–5057 (1984).

Mayer, B. Potential and limitations of using sulfur isotope abundance ratios as an indicator for natural and anthropogenic induced environmental change. In: *Isotope techniques in the study of past and current environmental changes in the hydrosphere*

and the atmosphere. 423–435 (IAEA, Vienna, 1998).

Matsuoka, J.; Kano, A.; Oba, T.; Watanabe, T.; Sakai, S.; Seto, K. Seasonal variation of stable isotopic compositions recorded in a laminated tufa, SW Japan. *Earth and Planetary Science Letters* **192**, 31–44 (2001).

McCrea, J. M. On the isotopic chemistry of carbonates and a paleotemperature scale. *The Journal of Chemical Physics* **18**, 849 (1950).

Merz-Preiß, M.; Riding, R. Cyanobacterial tufa calcification in two freshwater streams: ambient environment, chemical thresholds and biological processes. *Sedimentary Geology* **126**, 103–124 (1999).

Merz, M. U. The biology of carbonate precipitation by cyanobacteria. *Facies* **26**, 81–101 (1992).

Meybeck, M. Atmospheric inputs and river transport of dissolved substances. In: *Proceedings of the Hamburg Symposium on the Dissolved Loads of Rivers and Surface Water Quantity/Quality Relationships*. 173–192 (IAHS, Hamburg, 1983).

Meybeck, M. Global chemical-weathering of surficial rocks estimated from river dissolved loads. *American Journal of Science* **287**, 401–428 (1987).

Meybeck, M.; Helmer, R. The quality of rivers: from pristine stage to global pollution. *Palaeogeography, Palaeoclimatology, Palaeoecology* **75**, 283–309 (1989).

Mickler, P. J.; Banner, J. L.; Stern, L.; Asmerom, Y.; Edwards, R. L.; Ito, E. Stable isotope variations in modern tropical speleothems: Evaluating equilibrium vs. kinetic isotope effects. *Geochimica et Cosmochimica Acta* **68**, 4381–4393 (2004).

Mihevc, A. Morfološke značilnosti lehnjaka na Krki na primeru lehnjaka pri Praprečah in pri Otočcu (in Slovene). In: *Problem varstva in urejanja reke Krke na odsekih z intenzivno rastjo lehnjaka*. 1–9 (Ministrstvo za znanost in tehnologijo, Ljubljana, 1996).

Millot, R.; Gaillardet, J.; Dupré, B.; Allègre, C. J. The global control of silicate weathering rates and the coupling with physical erosion: new insights from rivers of the Canadian Shield. *Earth and Planetary Science Letters* **196**, 83–98 (2002).

Monty, C. L. V. The origin and development of cryptalgal fabrics. *Developments in Sedimentology* **20**, 193–249 (1976).

Mook, W. G. Stable carbon and oxygen isotopes of natural waters in the Netherlands. In: *Proceedings of a Symposium on Use of Isotopes in Hydrology*. 163–189 (IAEA, Vienna, 1970).

Mook, W. G. *Environmental isotopes in the hydrological cycle: principles and applications* (IAEA and UNESCO, Vienna, 2000).

Mook, W. G.; Bommerson, J. C.; Staverman, W. H. Carbon isotope fractionation between dissolved bicarbonate and gaseous carbon dioxide. *Earth and Planetary Science Letters* **22**, 169–176 (1974).

Morse, J. W. The kinetics of calcium carbonate dissolution and precipitation. *Reviews in Mineralogy and Geochemistry* **11**, 227–264 (1983).

Mucci, A. Influence of temperature on the composition of magnesian calcite overgrowths precipitated from seawater. *Geochimica et Cosmochimica Acta* **51**, 1977–1984 (1987).

Mucci, A.; Morse, J. W. The incorporation of Mg^{2+} and Sr^{2+} into calcite overgrowths: influences of growth rate and solution composition. *Geochimica et Cosmochimica Acta* **47**, 217–233 (1983).

Murray, K.; Wade, P. Checking anion-cation charge balance of water quality analyses: Limitations of the traditional method for non-potable waters, *Water SA* **22**, 27–32 (1996).

Novák, M.; Kirchner, J. W.; Groscheová, H.; Havel, M.; Černý, J.; Krejčí, R.; Buzek, F.;

Sulfur isotope dynamics in two central european watersheds affected by high atmospheric deposition of SO_x. *Geochimica et Cosmochimica Acta* **64**, 367–383 (2000).

Ogrinc, N.; Markovics, R.; Kanduč, T.; Walter, L. M.; Hamilton, S. K. Sources and transport of carbon and nitrogen in the River Sava watershed, a major tributary of the River Danube. *Applied Geochemistry* **23**, 3685–3698 (2008a).

Ogrinc, N.; Kanduč, T.; Stichler, W.; Vreča, P. Spatial and seasonal variations in $\delta^{18}O$ and δD values in the River Sava in Slovenia. *Journal of Hydrology* **359**, 303–312 (2008b).

Ogrinc, N.; Kanduč, T.; Globočanin, D.; Kocman, D.; Miljević, N. *A Hydrogeochemical and Isotope Investigation of the River Sava Watershed* (Nova Science Publishers, New York, 2010).

Oliva, P.; Viers, J.; Dupré, B. Chemical weathering in granitic environments. *Chemical Geology* **202**, 225–256 (2003).

Omelon, C. R.; Pollard, W. H.; Andersen, D. T. A geochemical evaluation of perennial spring activity and associated mineral precipitates at Expedition Fjord, Axel Heiberg Island, Canadian High Arctic. *Applied Geochemistry* **21**, 1–15 (2006).

O'Neil, J. R.; Clayton, R. N.; Mayeda, T. K. Oxygen isotope fractionation in divalent metal carbonates. *The Journal of Chemical Physics* **51**, 5547 (1969).

Parkhurst, D. L.; Appelo, C. A. J. User's guide to PHREEQC (version 2)–A computer program for speciation, batch-reaction, one-dimensional transport, and inverse geochemical calculations. In: *Water-Resources Investigations Report 99-4259*. 1–312 (U. S. Geological Survey, Denver, 1999).

Pedley, H. M. Classification and environmental models of cool freshwater tufas, *Sedimentary Geology* **68**, 143–154 (1990).

Pedley, M.; González Martín, J. A.; Ordóñez, S.; García Del Cura, M. A.; Sedimentology of Quaternary perched springline and paludal tufas: criteria for recognition, with examples from Guadalajara Province, Spain. *Sedimentology* **50**, 23–44 (2003).

Pella, E.; Colombo, B. Simultaneous CHN and S microdetermination by combustion and gas chromatography. *Microchimica Acta* **69**, 271–286 (1978).

Pentecost, A. *Travertine* (Springer–Verlag, Berlin, 2005).

Peterson, B. J.; Fry, B. Stable isotopes in ecosystem studies. *Annual review of ecology and systematics* **18**, 293–320 (1987).

Pleničar, M.; Premru, U. Osnovna geološka karta SFRJ 1:100 000, list Novo mesto (Zvezni geološki zavod, Beograd, 1970).

Pleničar, M.; Premru, U. Tolmač k osnovni geološki karti SFRJ 1:100 000, list Novo mesto (in Slovene) (Zvezni geološki zavod, Beograd, 1977).

Plut, D. Vodni viri novomeške občine (in Slovene). In: *Dolenjski zbornik*. 265–289 (Dolenjska založba, Novo mesto, 1990).

Polag, D., Scholz, D., Mühlinghaus, C., Spötl, C., Schröder-Ritzrau, A., Segl, M.; Mangini, A. Stable isotope fractionation in speleothems: Laboratory experiments. *Chemical Geology* **279**, 31–39 (2010).

Repe, B. Vegetation of Slovenia. In: *Slovenia: a Geographical overview*. 57–62 (Association of the Geographical Societies of Slovenia, Ljubljana, 2004).

Richey, J. E. Global River Carbon Biogeochemistry. In: *Encyclopedia of Hydrological Sciences*. 2863–2877 (Wiley, Oxford, 2005).

Rock, L.; Mayer, B. Identifying the influence of geology, land use, and anthropogenic activities on riverine sulfate on a watershed scale by combining hydrometric, chemical

and isotopic approaches. *Chemical Geology* **262**, 121–130 (2009).

Rodgers, P.; Soulsby, C.; Waldron, S.; Tetzlaff, D. Using stable isotope tracers to identify hydrological flow paths, residence times and landscape controls in a mesoscale catchment. *Hydrology and Earth System Sciences Discussions* **2**, 1–35 (2005).

Rogerson, M.; Pedley, H. M.; Wadhawan, J. D.; Middleton, R. New insights into biological influence on the geochemistry of freshwater carbonate deposits. *Geochimica et Cosmochimica Acta* **72**, 4976–4987 (2008).

Romanek, C. S.; Grossman, E. L.; Morse, J. W. Carbon isotopic fractionation in synthetic aragonite and calcite: Effects of temperature and precipitation rate. *Geochimica et Cosmochimica Acta* **56**, 419–430 (1992).

Roy, S.; Gaillardet, J.; Allegre, C. J. Geochemistry of dissolved and suspended loads of the Seine River, France: anthropogenic impact, carbonate and silicate weathering. *Geochimica et Cosmochimica Acta* **63**, 1277–1292 (1999).

Rozanski, K.; Froehlich, K.; Mook, W. G.; Stichler, W. Environmental isotopes in the hydrological cycle-principles and applications. *Technical Documents in Hydrology* **39**, 1–117 (2001).

Ryba, S. A.; Burgess, R. M. Effects of sample preparation on the measurement of organic carbon, hydrogen, nitrogen, sulfur, and oxygen concentrations in marine sediments. *Chemosphere* **48**, 139–147 (2002).

Sharp, Z. *Principles of stable isotope geochemistry* (Pearson Education Inc., New Jersey 2007).

Schidlowski, M. Biologically mediated isotope fractionations: Biochemistry, geochemical significance and preservation in the Earth's oldest sediments. In: *Cosmochemistry and the Origin of Life*. 277–322 (Springer, Dordrecht, 1983).

Schulte, P.; Van Geldern, R.; Freitag, H.; Karim, A.; Négrel, P.; Petelet-Giraud, E.; Probst, A.; Probst, J.-L.; Telmer, K.; Veizer, J.; Barth, J. A. C. Applications of stable water and carbon isotopes in watershed research: Weathering, carbon cycling, and water balances. *Earth-Science Reviews* **109**, 20–31 (2011).

Shin, W. J.; Chung, G. S.; Lee, D.; Lee, K. S. Dissolved inorganic carbon export from carbonate and silicate catchments estimated from carbonate chemistry and $\delta^{13}C_{DIC}$. *Hydrology and Earth System Sciences* **15**, 2551–2560 (2011).

Shiraishi, F. *Microbial metabolisms and calcification in freshwater biofilms* (Doctoral dissertation, Georg-August-Universität Göttingen, Göttingen, 2008).

Shiraishi, F.; Reimer, A.; Bissett, A.; de Beer, D.; Arp, G. Microbial effects on biofilm calcification, ambient water chemistry and stable isotope records in a highly supersaturated setting (Westerhöfer Bach, Germany). *Palaeogeography, Palaeoclimatology, Palaeoecology* **262**, 91–106 (2008).

Soulsby, C.; Tetzlaff, D.; Rodgers, D.; Dunn, S.; Waldron, S. Runoff processes, stream water residence times and controlling landscape characteristics in a mesoscale catchment: An initial evaluation. *Journal of Hydrology* **325**, 197–221 (2005).

Stallard, R. F. (1985). River chemistry, geology, geomorphology, and soils in the Amazon and Orinoco basins. In: *The Chemistry of Weathering*. 293–316 (Springer, Berlin, 1985).

Stallard, R. F.; Edmond, J.M. Geochemistry of the Amazon: 3. Weathering chemistry and limits to dissolved inputs. *Journal of Geophysical Research: Oceans (1978–2012)* **92**, 8293–8302 (1987).

Stumm W.; Morgan, J. J. *Aquatic Chemistry* (Wiley, New York, 1981).

Sun, H.; Han, J.; Zhang, S.; Lu, X. Chemical weathering inferred from riverine water chemistry in the lower Xijiang basin, South China. *Science of the Total Environment*

408, 4749–4760 (2010).

Szramek, K.; Walter, L. M. Impact of Carbonate Precipitation on Riverine Inorganic Carbon Mass Transport from a Mid-continent, Forested Watershed. *Aquatic Geochemistry* **10**, 99–137 (2004).

Szramek, K.; McIntosh, J. C.; Williams, E. L.; Kanduč, T.; Ogrinc, N.; Walter, L. M. Relative weathering intensity of calcite versus dolomite in carbonate-bearing temperate zone watersheds: Carbonate geochemistry and fluxes from catchments within the St. Lawrence and Danube river basins. *Geochemistry, Geophysics, Geosystems* **8**, 1–26 (2007).

Szramek, K.; Walter, L. M.; Kanduč, T.; Ogrinc, N. Dolomite versus calcite weathering in hydrogeochemically diverse watersheds established on bedded carbonates (Sava and Soča Rivers, Slovenia). *Aquatic Geochemistry* **17**, 357–396 (2011).

Šturm, M.; Lojen, S.; Markič, M.; Pezdič, J. Speciation and isotopic composition of sulphur in low-rank coals from four Slovenian coal seams. *Acta Chimica Slovenica* **56**, 989–996 (2009).

Tan, F. C.; Strain, P. M. Sources, sinks and distribution of organic carbon in the St. Lawrence Estuary, Canada. *Geochimica et Cosmochimica Acta* **47**, 125–132 (1983).

Tans, P. P.; Fung, I. Y.; Takahashi, T. Observational constraints on the global atmospheric CO_2 budget. *Science* **247**, 1431–1438 (1990).

Tans, P. Trends in Atmospheric Carbon Dioxide. http://www.esrl.noaa.gov/gmd/ccgg/trends/ (last access: February 2013)

Telmer, K.; Veizer, J. Carbon fluxes, pCO_2 and substrate weathering in a large northern river basin, Canada: carbon isotope perspectives. *Chemical Geology* **159**, 61–86 (1999).

Tipper, E. T.; Bickle, M. J.; Galy, A.; West, A. J.; Pomiès, C.; Chapman, H. J. The short term climatic sensitivity of carbonate and silicate weathering fluxes: insight from seasonal variations in river chemistry. *Geochimica et Cosmochimica Acta*, **70**, 2737–2754 (2006).

Trembaczowski, A.; Halas, S. Sulphur and Oxygen Isotopes in Sulphates in Natural Waters: (1) Surface Waters of Relatively Unpolluted Terrains. *Isotopes in Environmental and Health Studies*, **28**, 215–228 (1993).

Turner, J. V. Kinetic fractionation of carbon-13 during calcium carbonate precipitation. *Geochimica et Cosmochimica Acta* **46**, 1183–1191 (1982).

Usdowski, E., Hoefs, J., Menschel, G. Relationship between ^{13}C and ^{18}O fractionation and changes in major element composition in a recent calcite-depositing spring – a model of chemical variations with inorganic $CaCO_3$ precipitation. *Earth and Planetary Science Letters* **42**, 267–276 (1979).

Vázquez-Urbez, M.; Arenas, C.; Sancho, C.; Osácar, C.; Auqué, L.; Pardo, G. Factors controlling present-day tufa dynamics in the Monasterio de Piedra Natural Park (Iberian Range, Spain): depositional environmental settings, sedimentation rates and hydrochemistry. *International Journal of Earth Sciences* **99**, 1027–1049 (2010).

Vitòria, L.; Otero, N.; Soler, A.; Canals, À. Fertilizer characterization: isotopic data (N, S, O, C, and Sr). *Environmental science & technology* **38**, 3254–3262 (2004).

Vogel, J. C.; Grootes, P. M.; Mook, W. G. Isotopic fractionation between gaseous and dissolved carbon dioxide. *Zeitschrift für Physik* **203**, 225–238 (1970).

Vogel, J. C.; Ehleringer, J. R.; Hall, A. E.; Farquhar, G. D. Variability of carbon isotope fractionation during photosynthesis. In: *Stable isotopes and plant carbon-water relations*. 29–46 (Academic Press Inc., San Diego, 1993).

Vokal-Nemec, B.; Szaran, J.; Trembaczowski, A.; Halas, S.; Dolenec, T.; Lojen, S.

Sulphate sources in the Sava and Ljubljanica Rivers, Slovenia, inferred from sulphur and oxygen isotope compositions. *Aquatic Geochemistry* **12**, 199–220 (2006).

Vrhovšek, D.; Smolar, N.; Krušnik, C.; Kosi, G.; Černač, B. Problemi varstva in urejanja reke Krke na odsekih z intenzivno rastjo lehnjaka – vloga organizmov pri nastajanju lehnjaka (in Slovene). In: *Problem varstva in urejanja reke Krke na odsekih z intenzivno rastjo lehnjaka*. 1–20 (Ministrstvo za znanost in tehnologijo, Ljubljana, 1996).

Wachniew, P. Isotopic composition of dissolved inorganic carbon in a large polluted river: The Vistula, Poland. *Chemical Geology* **233**, 293–308 (2006).

Walling, D. E.; Webb, B. W. Solutes in river systems. In: *Solute Processes*. 251–327 (Wiley, Chichester, 1986).

Walter, L. M.; Ku, T. C.; Muehlenbachs, K.; Patterson, W. P.; Bonnell, L. Controls on the $\delta^{13}C$ of dissolved inorganic carbon in marine pore waters: An integrated case study of isotope exchange during syndepositional recrystallization of biogenic carbonate sediments (South Florida Platform, USA). *Deep Sea Research Part II: Topical Studies in Oceanography* **54**, 1163–1200 (2007).

White, J. W. C.; Vaughn, B. H. Stable Isotopic Composition of Atmospheric Carbon Dioxide (^{13}C and ^{18}O) from the NOAA ESRL Carbon Cycle Cooperative Global Air Sampling Network, 1990 – 2012 (Version: 2013-04-05, 2011) http://ftp.cmdl.noaa.gov/ccg/co2c13/flask/event/ (last access: February 2013).

Williams, E. L.; Szramek, K. J.; Jin, L.; Ku, T. C.; Walter, L. M. The carbonate system geochemistry of shallow groundwater-surface water systems in temperate glaciated watersheds (Michigan, USA): Significance of open-system dolomite weathering. *Geological Society of America Bulletin* **119**, 515–528 (2007).

Yan, H.; Sun, H.; Liu, Z. Equilibrium vs. kinetic fractionation of oxygen isotopes in two low-temperature travertine-depositing systems with differing hydrodynamic conditions at Baishuitai, Yunnan, SW China. *Geochimica et Cosmochimica Acta* **95**, 63–78 (2012).

Yang, W.; Spencer, R. J.; Roy Krouse, H. Stable isotope compositions of waters and sulfate species therein, Death Valley, California, USA: Implications for inflow and sulfate sources, and arid basin climate. *Earth and planetary science letters*, **147**, 69–82 (1996).

Yao, G.; Gao, Q.; Wang, Z.; Huang, X.; He, T.; Zhang, Y.; Jiao, S.; Ding, J. Dynamics of CO_2 partial pressure and CO_2 outgassing in the lower reaches of the Xijiang River, a subtropical monsoon river in China. *Science of the Total Environment* **376**, 255–266 (2007).

Yoshimura, K.; Liu, Z.; Cao, J.; Yuan, D.; Inokura, Y.; Noto, M. Deep source CO_2 in natural waters and its role in extensive tufa deposition in the Huanglong Ravines, Sichuan, China. *Chemical Geology* **205**, 141–153 (2004).

Zavadlav, S.; Lojen, S. Paleoclimate proxies in sub-recent freshwater carbonate system in river Krka, Slovenia. In: *17th International Karstological Schoool "Classical Karst"* 2008. 4 (Karst Research Institute, Postojna, 2009).

Zavadlav, S.; Mazej, D.; Zavašnik, J.; Rečnik, A.; Dominguez-Villar, D.; Cukrov, N.; Lojen, S. C and O stable isotopic signatures of fast-growing dripstones on alkaline substrates : reflection of growth mechanism, carbonate sources and environmental conditions. *Isotopes in Environmental and Health Studies* **48**, 354–371 (2012).

Zavadlav, S.; Kanduč, T.; McIntosh, J.; Lojen, S. Isotopic and chemical constraints on the biogeochemistry of dissolved inorganic carbon and chemical weathering in the karst watershed of Krka river (Slovenia). *Aquatic Geochemistry* **19**, 209–230 (2013).

Zeng, F-W.; Masiello, C. A.; Hockaday, W. C. Controls on the origin and cycling of riverine dissolved inorganic carbon in the Brazos River, Texas. *Biogeochemistry* **104**, 275–291 (2010).

Zhang, J.; Quay, P. D.; Wilbur, D. O. Carbon isotope fractionation during gas-water exchange and dissolution of CO_2. *Geochimica et Cosmochimica Acta* **59**, 107–114 (1995).

Zhang, J.; Wang, H.; Liu, Z.; An, D.; Dreybrodt, W. Spatial–temporal variations of travertine deposition rates and their controlling factors in Huanglong Ravine, China–A world's heritage site. *Applied Geochemistry* **27**, 211–222 (2012).

Zuddas, P.; Mucci, A. Kinetics of calcite precipitation from seawater: I. A classical chemical kinetics description for strong electrolyte solutions. *Geochimica et Cosmochimica Acta* **58**, 4353–4362 (1994).

Index of Figures

Index of Tables

Index of Appendices

Appendix 1: *Results of physico-chemical and geochemical analyse of water samples*: discharge (Q, obtained from ARSO website), temperature (T), pH, electrical conductivity (EC), total alkalinity (TA), dissolved inorganic and organic carbon (DIC and DOC), Ca^{2+}, Mg^{2+}, Na^{+}, K^{+}, Sr^{2+}, Ba^{2+}, Cl^{-}, SO_4^{2-} and NO_3^{-} content, stable isotopes of carbon in DIC ($\delta^{13}C_{DIC}$, VPDB), oxygen in water ($\delta^{18}O$, VSMOW), and particulate organic carbon ($\delta^{13}C_{POC}$, VPDB) and nitrogen ($\delta^{15}N_{PN}$, AIR), partial pressure of CO_2 (log pCO_2), and saturation indices of calcite (SI_c) and dolomite (SI_d). An empty cell designates *no value*.

Date of Sampling	Loc.	Q	T	pH	EC	TA	DIC	DOC	Ca^{2+}	Mg^{2+}	Na^{+}	K^{+}	Sr^{2+}	Ba^{2+}	Cl^{-}	SO_4^{2-}	NO_3^{-}	$\delta^{13}C$ DIC	$\delta^{18}O$	$\delta^{34}S$ sulph.	$\delta^{13}C$ POC	$\delta^{15}N$ PN	log pCO_2	SIc	SId
		m^3/s	°C		µS/cm	mM	mM	mM	mM	mM	mM	mM	µM	µM	mM	mM	mM	‰	‰	‰	‰	‰			
6.11.	Krka River																								
2007	W1		10.1	7.45	528		4.98	0.17	1.54	0.77	0.13	0.03	0.47	0.09				-13.0	-9.2				-2.06	0.05	-0.29
	W4	5.6	10.1	7.71	531		4.85	0.25										-12.6	-9.2				-2.33		
	W5																								
	W7																								
	W8		9.9	8.12	526		4.76	0.18										-12.5	-9.2				-2.75		
	W9		9.5	8.20	528		4.66	0.25										-12.7	-9.3				-2.84		
	W10	20.6	9.4	7.70	487		4.42	0.28	1.56	0.45	0.08	0.02	0.55	0.06				-13.2	-9.5				-2.37	0.26	-0.14
	W13		9.2	7.74	489		4.46	0.11										-12.9	-9.5				-2.40		
	W15		10.0	7.56	520		4.71	0.11	1.82	0.38	0.10	0.02	0.51	0.07				-12.8	-9.1				-2.23	0.33	-0.13
	W16		9.5	7.88	490		4.44	0.18										-13.2	-9.4				-2.54		
	W17																								
	W18	41.7	9.2	7.98	496		4.44	0.21	1.90	0.48	0.09	0.02	0.71	0.07				-12.5	-9.4				-2.65	0.60	0.50
	W19		9.2	8.00	464		4.41	0.16	1.85	0.51	0.10	0.02	0.74	0.08				-12.5	-9.5				-2.68	0.61	0.55
	Krka River tributaries																								
	W2		9.9	7.26	538		5.30	0.19										-14.2	-9.3				-1.84		
	W3	0.1	10.1	7.89	614		5.57	0.13	1.81	0.91	0.21	0.04	0.43	0.09				-12.3	-9.1				-2.46	0.59	0.79
	W6		10.0	7.64	519		4.95	0.17	2.13	0.40	0.05	0.01	0.56	0.07				-13.4	-9.3				-2.26	0.37	-0.08
	W11	4.7	9.5	7.50	503		4.63	0.23	1.97	1.00	0.02	0.01	0.36	0.02				-13.5	-9.3				-2.15	-0.13	-0.35
	W12		9.2	7.85	502		4.60	0.11										-12.5	-9.6				-2.49		
	W14	2.5	10.5	7.60	534		4.84	0.13	2.12	0.42	0.12	0.03	0.55	0.09				-13.6	-9.0				-2.20	0.21	-0.35
24.1.	Krka River																								
2008	W1		8.6	7.26	517	4.54	4.85	0.08										-12.5	-9.5				-1.91		
	W4	3.9	8.1	7.47	500	4.52	4.67	0.09										-12.2	-9.5				-2.12		
	W5																								
	W7																								
	W8		7.5	8.14	534	4.58	4.50	0.13										-11.8	-9.4				-2.79		

Appendix 1: *Continued*.

Date of Sampling	Loc.	Q	T	pH	EC	TA	DIC	DOC	Ca^{2+}	Mg^{2+}	Na^{+}	K^{+}	Sr^{2+}	Ba^{2+}	Cl^{-}	SO_4^{2-}	NO_3^{-}	$\delta^{13}C$ DIC	$\delta^{18}O$	$\delta^{34}S$ sulph.	$\delta^{13}C$ POC	$\delta^{15}N$ PN	log pCO_2	SIc	SId
		m^3/s	°C		µS/cm	mM	mM	mM	mM	mM	mM	mM	µM	µM	mM	mM	mM	‰	‰	‰	‰	‰			
	W9		7.1	8.28	530	4.47	4.47	0.11										-11.8	-9.5				-2.96		
	W10	13.6	8.2	7.88	477	4.06	4.18	0.13										-12.6	-9.5				-2.58		
	W13		8.0	7.88	466	4.00	4.18	0.02										-12.4	-9.7				-2.59		
	W15		9.8	7.76	515	4.32	4.47	0.08										-12.2	-9.4				-2.43		
	W16		8.9	8.09	457	4.25	4.13	0.11										-11.6	-9.7				-2.69		
	W17																								
	W18	25.6	7.0	8.22	450	4.10	4.08	0.16										-11.3	-9.7				-2.92		
	W19		7.0	8.16	460	4.15	4.17	0.19										-11.3	-9.7				-2.87		
	Krka River tributaries																								
	W2		8.9	7.10	473	4.36	4.83	0.13										-13.5	-9.6				-1.75		
	W3	0.04	3.0	7.96	656	5.34	5.47	0.18										-11.1	-9.3				-2.57		
	W6		8.3	7.68	468	4.32	4.48	0.12										-13.3	-9.8				-2.35		
	W11	3.1	8.4	7.76	438	3.91	4.15	0.10										-13.4	-10.1				-2.48		
	W12		8.2	7.86	468	4.05	4.18	0.13										-11.9	-9.9				-2.56		
	W14	2.5	9.7	7.78	525	4.41	4.69	0.17										-12.4	-9.2				-2.44		
25.4.	Krka River																								
2008	W1		10.8	7.60		4.71	4.79	0.28	1.50	0.87	0.19	0.03	0.47	0.09				-12.5	-9.4				-2.24	0.18	0.03
	W4	7.1	11.1	7.90		4.70	4.75	0.30	1.56	0.89	0.20	0.03	0.47	0.09				-12.0	-9.4				-2.54	0.49	0.66
	W5																								
	W7																								
	W8		11.7	8.20		4.70	4.49	0.19	1.64	0.74	0.16	0.02	0.48	0.08				-11.9	-9.5				-2.84	0.81	1.21
	W9		11.7	8.10		4.70	4.48	0.21	1.64	0.69	0.15	0.02	0.46	0.08				-12.0	-9.6				-2.74	0.72	1.00
	W10	28.0	11.0	7.90		4.06	4.01	0.22	1.57	0.57	0.11	0.02	0.58	0.07				-12.2	-9.8				-2.60	0.44	0.36
	W13		11.3	7.80		4.09	3.89	0.17	1.63	0.48	0.10	0.01	0.64	0.06				-12.4	-9.9				-2.49	0.37	0.13
	W15		12.2	7.60		4.33	3.89	0.20	1.81	0.49	0.14	0.03	0.53	0.08				-12.9	-9.8				-2.24	0.27	-0.10
	W16		12.3	8.05		4.03	3.61	0.26	1.63	0.50	0.13	0.02	0.62	0.06				-12.0	-9.7				-2.75	0.62	0.67
	W17																								
	W18	48.4	12.3	8.09		4.27	4.04	0.22	1.62	0.53	0.13	0.02	0.65	0.07				-12.1	-9.7				-2.77	0.68	0.82
	W19		11.7	8.07		4.27	4.07	0.21	1.67	0.54	0.13	0.02	0.70	0.08				-12.1	-9.7				-2.75	0.66	0.77
	Krka River tributaries																								
	W2		10.8	7.50		4.49	4.53	0.23	1.63	0.76	0.13	0.02	0.51	0.07				-13.1	-9.8				-2.16	0.09	-0.22
	W3	0.5	11.7	8.30		5.79	5.73	0.20	1.65	1.24	0.31	0.03	0.41	0.10				-11.5	-9.4				-2.86	0.98	1.77
	W6		10.8	7.80		4.33	4.26	0.17	1.82	0.37	0.06	0.01	0.50	0.06				-13.2	-10.1				-2.47	0.43	0.09
	W11	6.1	11.5	7.80		3.91	3.89	0.15	1.82	0.25	0.08	0.01	0.76	0.05				-12.6	-10.1				-2.51	0.40	-0.12

Appendix 1: *Continued*.

Date of Sampling	Loc.	Q	T	pH	EC	TA	DIC	DOC	Ca^{2+}	Mg^{2+}	Na^{+}	K^{+}	Sr^{2+}	Ba^{2+}	Cl^{-}	SO_4^{2-}	NO_3^{-}	$\delta^{13}C$ DIC	$\delta^{18}O$	$\delta^{34}S$ sulph.	$\delta^{13}C$ POC	$\delta^{15}N$ PN	log pCO_2	SIc	SId
		m^3/s	°C		µS/cm	mM	mM	mM	mM	mM	mM	mM	µM	µM	mM	mM	mM	‰	‰	‰	‰	‰			
	W12		12.4	8.08		3.97	3.89	0.17	1.60	0.48	0.07	0.01	0.80	0.05				-12.1	-10.1				-2.79	0.64	0.70
	W14	3.8	11.5	7.60		4.60	4.48	0.26	1.87	0.49	0.13	0.03	0.49	0.08				-12.4	-9.2				-2.27	0.25	-0.13
24.6.	Krka River																								
2008	W1		14.6	7.24		4.22	4.40	0.15										-14.3	-8.6				-1.91		
	W4	6.2	14.9	7.63		4.23	4.41	0.15										-13.9	-8.8				-2.30		
	W5																								
	W7																								
	W8		16.4	8.13		4.48	4.38	0.14										-13.1	-8.9				-2.77		
	W9		15.7	8.09		4.34	4.40	0.22										-13.6	-8.9				-2.75		
	W10	27.0	13.4	7.70		4.06	4.10	0.15										-13.4	-9.1				-2.39		
	W13		13.0	7.73		4.12	4.11	0.15										-13.8	-9.0				-2.42		
	W15		13.3	7.43		4.60	4.51	0.08										-14.0	-9.0				-2.21		
	W16		15.3	7.85		4.16	4.07	0.16										-12.9	-9.0				-2.52		
	W17																								
	W18	46.1	16.8	8.00		4.18	4.07	0.16										-13.2	-9.1				-2.67		
	W19		16.2	7.89		4.20	4.16	0.11										-13.1	-9.1				-2.55		
	Krka River tributaries																								
	W2		10.4	7.20		4.67	5.04	0.08										-15.1	-9.5				-1.85		
	W3	0.3	18.7	8.07		5.17	5.62	0.08										-12.3	-9.2				-2.64		
	W6		11.3	7.43		4.57	4.64	0.11										-14.2	-9.8				-2.08		
	W11	3.5	12.3	7.70		4.31	4.15	0.19										-13.7	-9.1				-2.37		
	W12		15.9	7.73		4.33	4.33	0.17										-13.1	-9.5				-2.38		
	W14	3.9	14.3	7.54		4.22	4.75	0.07										-13.8	-9.0				-2.07		
12.8.	Krka River																								
2008	W1		13.6	7.22	416	4.38			1.63	0.87	0.22	0.03	0.54	0.13				-14.2	-8.5				-1.87	-0.15	-0.61
	W4	4.4	14.3	7.64	464	4.34			1.70	0.86	0.22	0.03	0.55	0.11				-13.6	-8.7				-2.30	0.28	0.26
	W5																								
	W7																								
	W8		15.3	8.32	469	4.61			1.89	0.83	0.21	0.02	0.57	0.10				-12.9	-8.7				-2.96	1.02	1.69
	W9		16.7	8.30	429	4.55			1.86	0.82	0.22	0.03	0.59	0.09				-12.5	-9.2				-2.94	1.01	1.69
	W10	12.8	14.4	8.22	445	4.32			1.84	0.72	0.18	0.02	0.72	0.09				-13.4	-8.9				-2.89	0.88	1.34
	W13		15.7	8.26	442	4.20			1.83	0.68	0.19	0.02	0.76	0.08				-13.0	-8.8				-2.94	0.91	1.66

Appendix 1: *Continued*.

Date of Sampling	Loc.	Q	T	pH	EC	TA	DIC	DOC	Ca^{2+}	Mg^{2+}	Na^{+}	K^{+}	Sr^{2+}	Ba^{2+}	Cl^{-}	SO_4^{2-}	NO_3^{-}	$\delta^{13}C$ DIC	$\delta^{18}O$	$\delta^{34}S$ sulph.	$\delta^{13}C$ POC	$\delta^{15}N$ PN	log pCO_2	SIc	SId
		m^3/s	°C		µS/cm	mM	mM	mM	mM	mM	mM	mM	µM	µM	mM	mM	mM	‰	‰	‰	‰	‰			
	W15		15.6	7.72	446	4.18												-13.1	-8.7				-2.39		
	W16		17.9	8.08	430	4.30			1.61	0.58	0.20	0.02	0.64	0.08				-13.4	-8.8				-2.73	0.75	1.09
	W17																	-13.5							
	W18	20.2	19.0	8.28	458	4.29			1.69	0.59	0.20	0.01	0.87	0.09				-13.7	-8.7				-2.93	0.97	1.54
	W19		19.9	8.29	409	4.17			1.90	0.65	0.23	0.02	1.09	0.11				-13.9	-8.6				-2.95	1.02	1.65
	Krka River tributaries												0.00	0.00											
	W2		10.3	7.14	479	4.60			2.02	0.67	0.19	0.03	0.63	0.08				-15.6	-9.1				-1.79	-0.17	-0.92
	W3	0.2	18.4	7.99	534	5.45												-13.0	-9.0				-2.54		
	W6		11.9	7.54	471	4.31			2.13	0.42	0.08	0.01	0.57	0.06				-14.2	-9.0				-2.21	0.25	-0.27
	W11	1.1	12.5	7.67	427	4.05			2.08	0.32	0.16	0.01	1.02	0.06				-13.7	-8.7				-2.36	0.35	-0.16
	W12		19.9	7.51	425	4.01												-12.0	-8.8				-2.17		
	W14	2.7	13.4	7.40	459	4.63			1.87	0.65	0.18	0.02	0.66	0.10				-14.4	-8.5				-2.03	0.10	-0.29
7.10.	Krka River																								
2008	W1		12.2	7.31	518	5.26	5.86	0.12	1.77	1.26	0.29	0.04	0.55	0.12				-13.5	-9.0				-1.90	-0.01	-0.22
	W4	1.7	12.8	7.79	507	5.00	5.50	0.13	1.82	1.24	0.28	0.04	0.58	0.13				-12.3	-9.2				-2.40	0.49	0.76
	W5		12.2	8.24	496	5.19	5.27	0.13	1.81	1.18	0.26	0.04	0.57	0.11				-11.9	-9.0				-2.85	0.91	1.57
	W7		12.9	8.40	498	5.13	5.42	0.10	1.83	1.13	0.24	0.03	0.58	0.09				-11.2	-9.1				-3.02	1.07	1.88
	W8		12.7	8.32	489	4.80	5.14	0.15	1.83	1.08	0.23	0.03	0.90	0.11				-11.7	-9.2				-2.96	0.98	1.69
	W9		11.9	8.38	478	4.82	5.16	0.14	1.83	1.07	0.22	0.03	1.08	0.10				-11.7	-9.2				-3.02	1.03	1.77
	W10	7.0	12.2	7.82	463	4.61	4.96	0.22	1.83	0.87	0.19	0.02	0.58	0.09				-12.6	-9.0				-2.44	0.51	0.63
	W13		11.7	7.85	472	4.32	4.80	0.05	1.89	0.74	0.19	0.03	0.83	0.08				-12.8	-9.1				-2.52	0.50	0.52
	W15		12.8	8.08	501	4.68	4.99	0.23	1.85	0.83	0.17	0.02	1.02	0.07				-12.2	-9.2				-2.73	0.74	1.08
	W16		12.5	8.08	452	4.84	4.87	0.40	1.84	0.79	0.25	0.03	1.14	0.08				-11.9	-9.0				-2.71	0.75	1.07
	W17																								
	W18	12.7	13.2	8.23	444	4.30	4.72	0.27	1.82	0.81	0.24	0.03	0.54	0.08				-11.8	-9.0				-2.91	0.87	1.34
	W19		13.1	8.20	448	4.42	4.64	0.27	1.75	0.80	0.23	0.04	0.57	0.10				-11.5	-9.0				-2.87	0.82	1.25
	Krka River tributaries																								
	W2		10.6	7.34	469	4.92	5.57	0.15	1.89	0.89	0.18	0.02	0.67	0.09				-14.2	-9.1				-1.97	0.01	-0.40
	W3	0.02	14.0	8.23	543	5.52	5.70	0.19					0.00	0.00				-12.1	-8.6				-2.81		
	W6		12.2	7.82	428	4.63	4.78	0.10	2.00	0.58	0.07	0.01	0.68	0.07				-13.5	-9.5				-2.47	0.51	0.42
	W11	1.4	10.6	7.56	434	4.04	4.63	0.12										-13.7	-9.1				-2.27		
	W12		15.8	7.64	441	3.87	4.32	0.09										-12.5	-9.6				-2.34		
	W14	1.5	12.3	7.68	462	4.82	5.43	0.04	1.98	0.89	0.17	0.02	0.65	0.09				-12.3	-9.2				-2.31	0.38	0.35

Appendix 1: *Continued*.

Date of Sampling	Loc.	Q	T	pH	EC	TA	DIC	DOC	Ca^{2+}	Mg^{2+}	Na^{+}	K^{+}	Sr^{2+}	Ba^{2+}	Cl^{-}	SO_4^{2-}	NO_3^{-}	$\delta^{13}C$ DIC	$\delta^{18}O$	$\delta^{34}S$ sulph.	$\delta^{13}C$ POC	$\delta^{15}N$ PN	log pCO_2	SIc	SId
		m^3/s	°C		µS/cm	mM	mM	mM	mM	mM	mM	mM	µM	µM	mM	mM	mM	‰	‰	‰	‰	‰			
9.12.	Krka River																								
2008	W1		5.5		421	4.13	4.59	0.28	1.70	0.73	0.20	0.01	0.51	0.10				-15.1	-8.7						
	W4	15.2	4.8		443	4.25	4.71	0.28	1.77	0.74	0.19	0.02	0.52	0.10				-14.7	-8.9						
	W5		4.7		459	4.18	4.47	0.25	1.79	0.71	0.18	0.02	0.52	0.10				-14.3	-8.6						
	W7		4.8		462	4.23	4.53	0.17	1.83	0.64	0.18	0.03	0.51	0.10				-14.0	-8.5						
	W8		5.1		454	4.12	4.53	0.25	1.89	0.63	0.19	0.02	0.55	0.09				-14.3	-8.1						
	W9		5.3		445	4.36	4.49	0.22	1.76	0.57	0.15	0.01	0.55	0.08				-14.2	-8.8						
	W10	64.4	7.7		429	3.82	4.27	0.26	1.81	0.50	0.13	0.01	0.64	0.07				-14.3	-8.0						
	W13		10.3		458	3.66	4.39	0.30										-15.0	-8.1						
	W15		10.0		435	4.18	4.36	0.21										-14.9	-8.2						
	W16		8.2		440	4.01	4.37	0.18	1.93	0.48	0.14	0.02	0.71	0.08				-14.3	-8.3						
	W17		8.1		445	3.96	4.30	0.19	1.96	0.49	0.15	0.02	0.77	0.07				-14.5	-8.5						
	W18	104	8.2		417	4.36	4.38	0.15	1.98	0.50	0.16	0.01	0.80	0.09				-14.1	-8.3						
	W19		11.0		448	4.56	4.39	0.17	1.93	0.48	0.14	0.01	0.71	0.07				-14.1	-8.3						
	Krka River tributaries																								
	W2		6.7		463	4.52	5.19	0.06										-16.0	-8.8						
	W3	0.5	4.7		600	5.09	5.94	0.34										-13.6	-8.9						
	W6																								
	W11	14.3	7.4		504	4.39	4.86	0.23	2.04	0.28	0.10	0.01	0.88	0.05				-15.1	-8.1						
	W12		7.9		462	4.29	4.71	0.26										-14.1	-8.2						
	W14	7.2	9.3		472	4.65	4.95	0.14	2.24	0.47	0.22	0.02	0.59	0.09				-14.8	-8.2						
9.2.	Krka River																								
2009	W1		4.4		357	3.52												-14.2	-10.1						
	W4	51.5	5.0		376	3.55			1.49	0.61	0.29	0.02	0.43	0.08				-14.2	-10.1						
	W5		6.1		366	3.46												-14.3	-10.1						
	W7		6.6		347	3.5												-14.4	-10.0						
	W8		6.8		377	3.54												-14.4	-10.0						
	W9		6.0		387	3.53												-14.4	-10.1						
	W10	130	6.5		344	3.50												-14.5	-10.2						
	W13		6.7		365	3.49												-14.6	-10.3						
	W15		8.2		377	3.96												-14.5	-10.0						
	W16		6.0		422	3.68												-14.2	-10.2						

Appendix 1: *Continued*.

Date of Sampling	Loc.	Q	T	pH	EC	TA	DIC	DOC	Ca^{2+}	Mg^{2+}	Na^{+}	K^{+}	Sr^{2+}	Ba^{2+}	Cl^{-}	SO_4^{2-}	NO_3^{-}	$\delta^{13}C$ DIC	$\delta^{18}O$	$\delta^{34}S$ sulph.	$\delta^{13}C$ POC	$\delta^{15}N$ PN	log pCO_2	SIc	SId
		m^3/s	°C		µS/cm	mM	mM	mM	mM	mM	mM	mM	µM	µM	mM	mM	mM	‰	‰	‰	‰	‰			
	W17		6.5		398	3.68												-14.1	-10.1						
	W18	289	5.7		409	3.6												-14.3	-10.2						
	W19		7.2		379	3.67												-14.3	-10.2						
	Krka River tributaries																								
	W2		5.6		392	3.63												-14.9	-9.9						
	W3	3.3	5.1		498	3.44												-13.6	-9.8						
	W6																								
	W11	35.9	7.5		386	3.83			1.96	0.28	0.14	0.01	0.80	0.05				-14.6	-10.5						
	W12		7.9		356	3.78			1.71	0.46	0.10	0.01	0.67	0.05				-14.7	-10.5						
	W14	28.1	8.3		398	3.82			1.56	0.34	0.22	0.04	0.50	0.11				-14.2	-10.3						
3.3.	Krka River																								
2009	W1		8.0	7.66	508	4.88			1.67	1.10	0.19	0.02	0.41	0.09				-13.2	-9.4				-2.30	0.24	0.17
	W4	4.8	8.3	7.84	506	4.85			1.69	1.06	0.19	0.01	0.41	0.09				-12.6	-9.4				-2.48	0.43	0.52
	W5		8.4	8.23	500	4.94			1.71	1.03	0.18	0.01	0.41	0.10				-12.4	-9.4				-2.97	0.73	1.12
	W7		9.5	8.25	490	4.81			1.78	0.91	0.17	0.01	0.40	0.07				-12.3	-9.2				-2.90	0.86	1.33
	W8		9.4	8.12	484	5.00			1.75	0.86	0.16	0.03	0.39	0.07				-12.4	-9.4				-2.75	0.75	1.08
	W9		9.9	8.34	480	4.70			1.76	0.86	0.16	0.01	0.41	0.08				-12.5	-9.4				-3.00	0.94	1.48
	W10	13.6	9.2	8.07	455	4.83			1.90	0.75	0.14	0.01	0.68	0.06				-12.8	-9.6				-2.81	0.64	0.28
	W13		9.6	7.90	436	4.66			1.89	0.57	0.11	0.01	0.61	0.07				-13.4	-9.8				-2.55	0.55	0.47
	W15		10.3	7.77	478	4.78			1.91	0.60	0.12	0.05	0.45	0.06				-13.5	-9.3				-2.41	0.44	0.29
	W16		9.6	8.00	464	4.63			1.80	0.63	0.14	0.05	0.53	0.06				-13.3	-9.6				-2.66	0.62	0.68
	W17		9.6	8.07	457	4.68			1.82	0.64	0.13	0.05	0.49	0.06				-12.8	-9.3				-2.72	0.70	0.84
	W18	41.1	9.8	8.05	461	4.69			1.66	0.62	0.12	0.05	0.52	0.06				-12.2	-9.6				-2.70	0.65	0.77
	W19		10.5	8.07	459	4.75			1.62	0.63	0.15	0.03	0.66	0.07				-12.1	-9.5				-2.71	0.67	0.85
	Krka River tributaries																								
	W2		9.5	7.40	461	4.56			1.85	0.71	0.10	0.01	0.44	0.05				-14.2	-9.6				-2.06	0.03	-0.46
	W3	0.2	8.0	8.29	582	4.92			1.74	1.39	0.32	0.02	0.34	0.09				-12.2	-9.3				-2.94	0.87	1.51
	W6		10.1	7.79	425	4.32			1.89	0.44	0.05	0.01	0.44	0.05				-13.8	-9.6				-2.47	0.42	0.11
	W11	2.8	9.3	7.61	400	4.44			1.45	0.64	0.12	0.07	0.38	0.05				-13.8	-9.5				-2.28	0.13	-0.20
	W12		12.1	7.63	451	4.37			1.53	0.46	0.19	0.05	1.34	0.09				-12.6	-9.5				-2.29	0.21	-0.15
	W14	2.6	10.1	7.63	484	4.86			2.05	0.63	0.11	0.02	0.45	0.07				-13.7	-9.3				-2.26	0.34	0.06
8.4.	Krka River																								
2009	W1		12.7	7.56	418	3.99			1.53	0.79	0.15	0.02	0.41	0.09				-13.9	-9.5				-2.26	0.11	-0.11
	W4	10.4	12.7	7.83	429	4.24			1.58	0.81	0.15	0.03	0.42	0.07				-13.5	-9.7				-2.51	0.41	0.48

Appendix 1: *Continued*.

Date of Sampling	Loc.	Q	T	pH	EC	TA	DIC	DOC	Ca^{2+}	Mg^{2+}	Na^{+}	K^{+}	Sr^{2+}	Ba^{2+}	Cl^{-}	SO_4^{2-}	NO_3^{-}	$\delta^{13}C$ DIC	$\delta^{18}O$	$\delta^{34}S$ sulph.	$\delta^{13}C$ POC	$\delta^{15}N$ PN	log pCO_2	SIc	SId
		m^3/s	°C		µS/cm	mM	mM	mM	mM	mM	mM	mM	µM	µM	mM	mM	mM	‰	‰	‰	‰	‰			
	W5		13.5	8.20	416	4.18			1.57	0.75	0.14	0.02	0.42	0.08				-12.9	-9.3				-2.88	0.77	1.20
	W7		13.6	7.99	410	4.14			1.67	0.60	0.14	0.02	0.41	0.08				-13.5	-9.2				-2.67	0.60	0.72
	W8		12.9	8.09	402	3.95			1.68	0.57	0.13	0.02	0.44	0.07				-13.4	-9.4				-2.80	0.67	0.82
	W9		12.7	7.99	383	3.83			1.60	0.54	0.12	0.02	0.46	0.06				-13.6	-9.4				-2.71	0.54	0.56
	W10	58.5	13.2	7.84	351	3.40			1.52	0.43	0.10	0.02	0.50	0.05				-13.7	-9.7				-2.60	0.34	0.09
	W13		11.6	7.73	352	3.50			1.59	0.39	0.09	0.02	0.55	0.06				-13.5	-9.9				-2.49	0.23	-0.21
	W15		13.0	7.62	403	3.96			1.96	0.30	0.11	0.02	0.46	0.08				-14.1	-9.8				-2.32	0.28	-0.29
	W16		11.3	7.84	368	3.56			1.65	0.39	0.10	0.01	0.56	0.05				-13.5	-9.8				-2.59	0.36	0.02
	W17		11.1	7.89	370	3.65			1.62	0.42	0.10	0.01	0.53	0.05				-13.5	-9.8				-2.64	0.41	0.15
	W18	104	12.3	7.90	368	3.61			1.63	0.40	0.09	0.02	0.61	0.07				-13.3	-9.9				-2.64	0.43	0.20
	W19		12.0	8.00	371	3.64			1.62	0.40	0.09	0.01	0.62	0.06				-13.5	-9.7				-2.74	0.53	0.39
	Krka River tributaries																								
	W2		11.1	7.49	395	3.92			1.67	0.56	0.09	0.02	0.43	0.05				-14.6	-9.8				-2.20	0.05	-0.46
	W3	1.1	13.8	8.14	535	3.96			1.75	1.22	0.21	0.03	0.38	0.08				-12.8	-9.3				-2.98	0.61	1.04
	W6		12.0	7.71	364	3.80			1.68	0.37	0.06	0.01	0.45	0.05				-14.2	-10.0				-2.43	0.28	-0.17
	W11	13.7	13.1	7.58	358	3.44			1.78	0.21	0.07	0.02	0.70	0.05				-14.2	-9.3				-2.34	0.15	-0.67
	W12		12.7	7.94	355	3.59			1.59	0.43	0.06	0.02	0.74	0.04				-13.4	-9.8				-2.69	0.46	0.32
	W14	10.1	12.8	7.60	415	3.86			1.90	0.33	0.10	0.02	0.47	0.07				-14.1	-9.2				-2.31	0.23	-0.34
12.5.	Krka River																								
2009	W1		11.5	7.57	469	4.64			1.65	1.00	0.19	0.02	0.45	0.08				-13.1	-9.2				-2.21	0.19	0.08
	W4	4.3	12.9	7.91	469	4.83			1.67	0.97	0.18	0.02	0.44	0.10				-12.5	-9.2				-2.53	0.56	0.84
	W5		12.6	8.22	458	4.64			1.67	0.93	0.17	0.02	0.44	0.09				-12.8	-9.2				-2.87	0.84	1.38
	W7		14.7	8.37	436	4.48			1.67	0.81	0.16	0.03	0.42	0.07				-11.5	-9.2				-3.03	1.00	1.68
	W8		13.8	8.37	448	4.55			1.73	0.77	0.15	0.02	0.44	0.08				-12.6	-9.2				-3.03	1.01	1.64
	W9		14.5	8.33	431	4.40			1.68	0.76	0.15	0.02	0.44	0.08				-11.7	-9.4				-2.99	0.96	1.56
	W10	11.8	12.6	8.06	406	3.95			1.67	0.62	0.12	0.01	0.54	0.07				-12.8	-9.6				-2.77	0.63	0.79
	W13		15.5	8.32	387	3.97			1.63	0.59	0.12	0.01	0.57	0.05				-11.8	-9.7				-3.02	0.92	1.39
	W15		14.9	7.91	412	4.17			1.97	0.58	0.12	0.03	0.48	0.08				-12.6	-9.9				-2.58	0.61	0.68
	W16		11.3	7.84	368	3.56			1.65	0.39	0.10	0.01	0.56	0.05				-13.5	-9.8				-2.59	0.36	0.02
	W17		15.7	7.97	411	4.17			1.73	0.58	0.13	0.02	0.57	0.07				-12.6	-9.6				-2.64	0.63	0.78
	W18	24.8	17.9	8.10	419	4.17			1.74	0.57	0.13	0.02	0.71	0.07				-12.3	-9.7				-2.76	0.78	1.13
	W19		18.3	8.22	412	4.14			1.73	0.58	0.13	0.02	0.73	0.07				-12.0	-9.7				-2.89	0.90	1.37

Appendix 1: *Continued*.

Date of Sampling	Loc.	Q	T	pH	EC	TA	DIC	DOC	Ca^{2+}	Mg^{2+}	Na^{+}	K^{+}	Sr^{2+}	Ba^{2+}	Cl^{-}	SO_4^{2-}	NO_3^{-}	$\delta^{13}C$ DIC	$\delta^{18}O$	$\delta^{34}S$ sulph.	$\delta^{13}C$ POC	$\delta^{15}N$ PN	log pCO_2	SIc	SId
		m^3/s	°C		µS/cm	mM	mM	mM	mM	mM	mM	mM	µM	µM	mM	mM	mM	‰	‰	‰	‰	‰			
	Krka River tributaries																								
	W2		10.0	7.43	422	4.28			1.83	0.57	0.10	0.01	0.46	0.06				-14.4	-9.4				-2.11	0.05	-0.52
	W3	0.2	15.0	8.17	542	4.38			1.69	1.33	0.25	0.03	0.36	0.09				-12.3	-9.0				-2.83	0.80	1.49
	W6		11.2	7.80	398	4.19			1.92	0.40	0.06		0.46	0.05				-13.7	-9.9				-2.49	0.44	0.13
	W11	2.1	12.0	7.87	371	3.73			1.89	0.23	0.10	0.01	0.82	0.05				-13.2	-10.1				-2.60	0.47	-0.03
	W12		17.2	7.86	390	3.90			1.69	0.53	0.09	0.03	1.38	0.07				-12.4	-9.6				-2.55	0.51	0.53
	W14	2.1	13.1	7.58	456	4.52			1.76	0.57	0.12	0.01	0.53	0.08				-13.2	-9.1				-2.22	0.25	-0.04
3.6.	Krka River																								
2009	W1		12.2	7.52	498	4.70			1.63	1.13	0.19	0.02	0.48	0.10				-12.7	-9.1				-2.26	0.05	-0.12
	W4	2.8	12.8	7.96	497	5.02			1.55	1.11	0.18	0.02	0.48	0.09				-12.0	-9.2				-2.57	0.59	0.99
	W5		13.9	8.17	492	4.94			1.65	1.08	0.18	0.03	0.47	0.09				-12.3	-9.1				-2.78	0.83	1.45
	W7		15.4	8.32	478	4.70			1.66	1.01	0.18	0.03	0.44	0.07				-11.7	-9.0				-2.95	0.97	1.74
	W8		14.5	8.32	469	4.84			1.66	0.98	0.17	0.02	0.46	0.08				-11.3	-9.1				-2.94	0.97	1.71
	W9		14.4	8.26	469	4.93			1.66	0.96	0.17	0.02	0.47	0.08				-11.6	-9.2				-2.87	0.93	1.60
	W10	6.7	13.6	8.01	432	4.39			1.61	0.79	0.13	0.01	0.62	0.06				-12.0	-9.2				-2.67	0.62	0.90
	W13		14.6	8.28	421	4.35			1.64	0.72	0.13	0.02	0.68	0.04				-11.5	-9.5				-2.46	0.36	-0.15
	W15		15.3	8.06	437	4.34			1.69	0.72	0.13	0.01	0.63	0.06				-11.9	-9.4				-2.72	0.71	1.05
	W16		17.6	8.23	427	4.29			1.67	0.68	0.17	0.00	0.66	0.05				-11.2	-9.2				-2.88	0.90	1.44
	W17		16.4	8.10	432	4.38			1.69	0.69	0.15	0.02	0.64	0.05				-11.8	-9.3				-2.75	0.77	1.16
	W18	17.0	18.2	8.23	423	4.32			1.61	0.74	0.15	0.01	0.71	0.06				-10.8	-9.0				-2.88	0.89	1.49
	W19		18.8	8.27	431	4.34			1.67	0.75	0.17	0.02	0.75	0.08				-11.0	-9.4				-2.92	0.95	1.61
	Krka River tributaries																								
	W2		10.2	7.50	453	4.63			1.77	0.75	0.10	0.01	0.54	0.07				-13.5	-9.4				-2.15	0.13	-0.20
	W3	0.1	16.3	8.18	557	5.63			1.71	1.33	0.29	0.03	0.39	0.09				-12.0	-9.0				-2.73	0.93	1.77
	W6		12.1	7.84	416	4.38			1.84	0.48	0.06	0.02	0.53	0.04				-12.6	-9.7				-2.50	0.49	0.35
	W11	1.4	12.5	7.74	388	3.82			1.89	0.28	0.09	0.01	0.83	0.05				-13.1	-9.9				-2.46	0.36	-0.15
	W12		20.6	7.70	438	4.10			1.72	0.64	0.20	0.03	3.70	0.12				-10.6	-9.3				-2.35	0.42	0.49
	W14	1.6	13.0	7.70	480	4.89			1.88	0.78	0.12	0.03	0.49	0.08				-12.2	-9.1				-2.31	0.42	0.41
6.7.	Krka River																								
2009	W1		13.7	7.54	493	4.85			1.56	1.09	0.21	0.03	0.50	0.10				-11.3	-8.9				-2.15	0.18	0.18
	W4	2.9	13.0	7.63	487	4.94			1.65	0.98	0.20	0.04	0.52	0.09				-11.2	-9.2				-2.24	0.29	0.31
	W5		13.5	8.03	479	4.96			1.68	0.93	0.19	0.02	0.52	0.09				-11.1	-9.2				-2.64	0.70	1.11
	W7		14.2	8.06	473	4.89			1.70	0.88	0.18	0.03	0.49	0.07				-10.7	-9.1				-2.67	0.74	1.17

Appendix 1: *Continued*.

Date of Sampling	Loc.	Q	T	pH	EC	TA	DIC	DOC	Ca^{2+}	Mg^{2+}	Na^{+}	K^{+}	Sr^{2+}	Ba^{2+}	Cl^{-}	SO_4^{2-}	NO_3^{-}	$\delta^{13}C$ DIC	$\delta^{18}O$	$\delta^{34}S$ sulph.	$\delta^{13}C$ POC	$\delta^{15}N$ PN	log pCO_2	SIc	SId
		m^3/s	°C		µS/cm	mM	mM	mM	mM	mM	mM	mM	µM	µM	mM	mM	mM	‰	‰	‰	‰	‰			
	W8		14.7	8.07	467	4.77			1.69	0.82	0.18	0.03	0.55	0.08				-10.8	-9.1				-2.69	0.75	1.17
	W9		14.7	8.01	454	4.44			1.71	0.78	0.16	0.04	0.56	0.07				-10.9	-9.1				-2.65	0.65	0.97
	W10	13.2	16.3	8.00	439	4.30			1.65	0.73	0.17	0.03	0.69	0.06				-11.0	-9.2				-2.77	0.55	0.76
	W13		17.2	8.28	427	4.37			1.69	0.66	0.16	0.03	0.74	0.04				-10.9	-9.4				-2.93	0.95	1.52
	W15		17.1	8.06	434	4.52			1.69	0.66	0.16	0.01	0.67	0.07				-11.4	-9.3				-2.69	0.75	1.13
	W16		19.7	8.10	433	4.37			1.67	0.66	0.20	0.01	0.74	0.07				-11.3	-9.2				-2.73	0.81	1.28
	W17		18.8	8.03	436	4.39			1.66	0.65	0.17	0.03	0.72	0.07				-11.7	-9.3				-2.66	0.73	1.11
	W18	16.3	21.4	8.25	428	4.34			1.60	0.72	0.20	0.02	0.79	0.09				-11.1	-9.2				-2.88	0.95	1.65
	W19		21.6	8.26	452	4.34			1.58	0.72	0.19	0.02	0.81	0.08				-10.9	-9.2				-2.89	0.96	1.67
	Krka River tributaries																								
	W2		12.1	7.37	460	4.74			1.77	0.74	0.14	0.03	0.55	0.08				-12.0	-9.4				-2.00	0.04	-0.36
	W3	0.4	14.6	7.80	548	4.46			1.91	1.01	0.27	0.04	0.45	0.11				-11.4	-8.5				-2.36	0.58	0.87
	W6		12.3	7.53	419	4.38			1.87	0.39	0.14	0.01	0.52	0.05				-12.4	-9.7				-2.19	0.20	-0.33
	W11	2.1	13.5	7.76	417	4.20			1.88	0.37	0.15	0.03	0.93	0.05				-12.8	-9.7				-2.43	0.43	0.12
	W12		24.3	7.72	441	4.22			1.64	0.62	0.25	0.05	4.64	0.14				-11.8	-9.4				-2.33	0.49	0.68
	W14	2.3	15.6	7.68	470	4.81			1.89	0.68	0.13	0.04	0.52	0.08				-11.9	-9.0				-2.29	0.43	0.42
6.8.	Krka River																								
2009	W1		13.5	7.29	506	5.23			1.68	1.15	0.21	0.02	0.47	0.11				-14.6	-9.0				-1.87	-0.01	-0.22
	W4	2.2	15.1	7.82	516	5.17			1.69	1.11	0.21	0.02	0.48	0.10				-13.6	-9.0				-2.40	0.53	0.88
	W5		15.8	8.23	514	5.07			1.67	1.06	0.20	0.02	0.47	0.09				-13.4	-8.9				-2.83	0.93	1.67
	W7		17.4	8.44	473	4.96			1.70	1.01	0.17	0.03	0.44	0.07				-12.4	-9.0				-3.05	1.14	2.09
	W8		18.3	8.38	457	4.77			1.62	0.95	0.17	0.02	0.44	0.08				-12.8	-9.0				-2.99	1.07	1.95
	W9		17.9	8.27	451	4.82			1.65	0.96	0.17	0.02	0.46	0.07				-12.9	-9.1				-2.88	0.97	1.75
	W10	6.1	17.5	8.33	395	4.14			1.70	0.80	0.16		0.59	0.06				-12.1	-9.0				-3.00	0.90	1.60
	W13		17.7	7.98	425	4.74			1.67	0.71	0.14	0.01	0.68	0.08				-13.4	-8.9				-2.58	0.70	1.06
	W15		15.3	7.75	465	4.25			1.56	0.67	0.15	0.01	0.64	0.07				-12.7	-8.9				-2.41	0.37	
	W16		20.2	8.02	441	4.23			1.65	0.65	0.17	0.03	0.62	0.09				-13.3	-8.7				-2.66	0.72	
	W17		19.6	7.92	436	4.16			1.66	0.66	0.18	0.02	0.62	0.08				-13.6	-8.6				-2.57	0.61	
	W18	14.6	21.4	8.05	404	3.86			1.48	0.63	0.19	0.03	0.84	0.09				-12.7	-8.4				-2.72	0.69	
	W19		21.7	7.96	398	3.54			1.37	0.63	0.16	0.04	0.89	0.11				-13.1	-8.3				-2.66	0.54	

Appendix 1: *Continued*.

Date of Sampling	Loc.	Q	T	pH	EC	TA	DIC	DOC	Ca^{2+}	Mg^{2+}	Na^{+}	K^{+}	Sr^{2+}	Ba^{2+}	Cl^{-}	SO_4^{2-}	NO_3^{-}	$\delta^{13}C$ DIC	$\delta^{18}O$	$\delta^{34}S$ sulph.	$\delta^{13}C$ POC	$\delta^{15}N$ PN	log pCO_2	SIc	SId
		m^3/s	°C		µS/cm	mM	mM	mM	mM	mM	mM	mM	µM	µM	mM	mM	mM	‰	‰	‰	‰	‰			
	Krka River tributaries																								
	W2		10.6	7.32	460	4.64			1.77	0.77	0.15	0.00	0.55	0.07				-15.6	-9.0				-1.96	-0.04	
	W3	0.01	21.7	8.29	456	4.58			1.58	0.96	0.34	0.02	0.38	0.11				-14.0	-9.2				-2.90	1.00	
	W6		11.9	7.72	421	4.57			1.90	0.49	0.05		0.53	0.05				-14.5	-9.6				-2.37	0.40	
	W11	1.4	13.4	7.71	382	4.11			2.02	0.26	0.12	0.01	1.01	0.06				-14.3	-9.3				-2.39	0.40	
	W12		19.4	7.62	426	4.28			1.73	0.59	0.13	0.02	2.08	0.09				-13.8	-9.2				-2.25	0.35	
	W14	2.5	20.0	8.16	404	4.96			1.90	0.80	0.16	0.03	0.50	0.10				-14.2	-8.8				-2.74	0.97	
7.9.	Krka River																								
2009	W1		14.9	7.30	525	5.32			1.64	1.20	0.17	0.06	0.45	0.11				-13.9	-9.0				-1.87	0.02	
	W4	1.7	14.4	7.82	511	5.26			1.62	1.14	0.16	0.07	0.43	0.11				-13.0	-9.1				-2.38	0.49	
	W5		14.8	8.47	491	5.19			1.61	1.11	0.15	0.07	0.42	0.10				-12.6	-9.1				-3.07	1.13	
	W7		15.8	8.42	489	5.20			1.49	0.99	0.14	0.07	0.33	0.07				-12.3	-9.0				-2.99	1.05	
	W8		16.1	8.48	431	4.53			1.50	0.85	0.16	0.06	0.29	0.07				-12.0	-8.8				-3.12	0.96	
	W9		16.2	8.30	478	5.05			1.64	1.05	0.14	0.03	0.41	0.11				-12.8	-9.0				-2.90	0.99	
	W10	3.9	17.0	8.15	448	4.71			1.65	0.92	0.13	0.03	0.61	0.09				-12.8	-9.0				-2.82	0.89	
	W13		15.9	7.81	444	4.60			1.72	0.77	0.13	0.01	0.69	0.09				-13.8	-9.0				-2.42	0.50	
	W15		18.9	8.14	425	4.29			1.54	0.77	0.13	0.04	0.62	0.07				-12.8	-8.8				-2.74	0.76	
	W16		19.0	8.09	436	4.42			1.57	0.75	0.17	0.03	0.62	0.06				-13.0	-8.7				-2.73	0.78	
	W17		18.0	7.94	431	4.44			1.58	0.76	0.15	0.02	0.63	0.07				-13.1	-8.8				-2.53	0.58	
	W18	8.4	20.2	8.13	434	4.46			1.52	0.83	0.17	0.03	0.71	0.07				-12.7	-8.7				-2.72	0.78	
	W19		20.1	8.34	417	4.31			1.47	0.83	0.15	0.02	0.71	0.07				-12.4	-8.6				-2.94	0.94	
	Krka River tributaries																								
	W2		10.6	7.48	469	4.89			1.70	0.89	0.12	0.04	0.55	0.09				-14.9	-9.3				-2.12	0.14	
	W3	0.01																							
	W6		12.1	7.75	424	4.53			1.80	0.56	0.05	0.07	0.54	0.04				-13.6	-9.2				-2.45	0.46	
	W11	0.8	12.6	7.74	398	4.05			2.00	0.31	0.07	0.00	0.86	0.06				-14.6	-9.3				-2.39	0.37	
	W12		18.7	7.58	414	4.05			1.54	0.59	0.29	0.04	4.03	0.14				-11.4	-8.3				-2.26	0.25	
	W14	1.4	13.3	7.73	479	5.02			1.88	0.82	0.10	0.03	0.45	0.07				-13.7	-8.9				-2.30	0.43	
14.10.	Krka River																								
2009	W1		11.6	7.43	474	5.29			1.60	1.04	0.19	0.04	0.35	0.09				-13.1	-8.7				-2.01	0.04	
	W4	4.2	11.4	7.71	469	5.19			1.69	1.20	0.21	0.03	0.50	0.12				-12.3	-8.8				-2.31	0.37	
	W5		10.5	8.23	460	5.28			1.69	1.16	0.21	0.02	0.51	0.11				-12.3	-8.8				-2.83	0.87	
	W7		11.3	8.29	445	5.14			1.70	1.02	0.17	0.01	0.49	0.10				-12.0	-8.8				-2.90	0.93	
	W8		11.0	8.31	438	5.12			1.67	0.99	0.17	0.01	0.49	0.10				-12.3	-8.8				-2.93	0.94	

Appendix 1: *Continued*.

Date of Sampling	Loc.	Q	T	pH	EC	TA	DIC	DOC	Ca^{2+}	Mg^{2+}	Na^{+}	K^{+}	Sr^{2+}	Ba^{2+}	Cl^{-}	SO_4^{2-}	NO_3^{-}	$\delta^{13}C$ DIC	$\delta^{18}O$	$\delta^{34}S$ sulph.	$\delta^{13}C$ POC	$\delta^{15}N$ PN	log pCO_2	SIc	SId
		m^3/s	°C		µS/cm	mM	mM	mM	mM	mM	mM	mM	µM	µM	mM	mM	mM	‰	‰	‰	‰	‰			
	W9		11.5	8.23	440	5.10			1.64	0.99	0.17	0.01	0.48	0.10				-12.2	-8.8				-2.84	0.86	
	W10	10.1	11.0	7.89	430	4.92			1.65	0.90	0.17	0.01	0.69	0.09				-12.7	-9.0				-2.51	0.52	
	W13		10.8	7.84	418	4.80			1.72	0.77	0.15	0.01	0.71	0.08				-12.3	-9.1				-2.47	0.48	
	W15		12.9	7.91	438	5.03			1.68	0.88	0.15	0.07	0.45	0.08				-11.5	-8.9				-2.51	0.58	
	W16		12.4	7.92	416	4.68			1.53	0.76	0.15	0.07	0.59	0.08				-11.7	-8.8				-2.55	0.52	
	W17		12.1	7.99	412	4.78			1.39	0.69	0.15	0.08	0.52	0.06				-12.5	-9.0				-2.62	0.56	
	W18	20.3	12.7	7.97	410	4.62			1.41	0.75	0.15	0.09	0.61	0.09				-11.5	-9.1				-2.61	0.54	
	W19		13.8	8.06	405	4.65			1.30	0.72	0.17	0.09	0.57	0.06				-10.5	-9.0				-2.69	0.61	
	Krka River tributaries																								
	W2		10.1	7.42	417	4.81			1.52	0.69	0.11	0.09	0.42	0.06				-13.9	-9.1				-2.05	0.00	
	W3	0.01	9.8	7.96	471	5.17			1.91	0.94	0.29	0.08	0.39	0.11				-13.6	-8.6				-2.57	0.64	
	W6		10.2	7.75	392	4.66			1.93	0.49	0.06		0.57	0.06				-13.1	-9.3				-2.40	0.42	
	W11	2.1	10.4	7.73	379	4.31			1.92	0.37	0.09		0.91	0.06				-13.0	-9.4				-2.41	0.37	
	W12		14.8	7.56	420	4.47			1.77	0.55	0.26	0.08	3.60	0.13				-11.0	-9.0				-2.20	0.25	
	W14	1.7	12.1	7.76	446	5.14			1.74	0.92	0.15	0.06	0.45	0.09				-13.1	-8.8				-2.36	0.45	
2.11.	Krka River																								
2009	W1		11.3	7.43	449	4.98			1.61	1.04	0.21	0.02	0.52	0.11				-13.3	-8.8				-2.04	0.06	
	W4	1.6	10.6	7.76	443	4.89			1.64	0.99	0.19	0.09	0.49	0.11				-12.6	-8.8				-2.39	0.38	
	W5		8.5	8.24	430	5.25			1.67	0.94	0.16	0.07	0.48	0.10				-12.3	-8.9				-2.85	0.85	
	W7		9.0	8.13	439	4.94			1.61	0.84	0.18	0.07	0.40	0.09				-12.2	-9.1				-2.76	0.71	
	W8		8.9	8.29	431	4.88			1.64	0.81	0.19	0.08	0.42	0.08				-12.1	-9.1				-2.93	0.87	
	W9		8.7	8.22	432	4.85			1.67	0.84	0.20	0.09	0.45	0.10				-12.1	-9.3				-2.87	0.80	
	W10	5.3	9.4	7.87	396	4.49			1.70	0.69	0.13	0.05	0.70	0.08				-12.4	-9.3				-2.54	0.46	
	W13		7.8	7.87	391	4.41			1.84	0.63	0.13		0.95	0.08				-12.6	-9.0				-2.55	0.46	
	W15		9.7	7.72	445	4.52			1.87	0.69	0.14	0.05	0.79	0.09				-12.2	-9.2				-2.38	0.35	
	W16		8.4	7.93	405	4.46			1.87	0.64	0.19	0.03	0.86	0.09				-12.2	-9.0				-2.61	0.53	
	W17		7.7	8.00	402	4.46			1.88	0.64	0.17	0.06	0.85	0.08				-12.1	-9.2				-2.68	0.59	
	W18	9.6	8.1	8.02	416	4.50			1.87	0.69	0.17	0.06	0.89	0.09				-11.8	-9.2				-2.70	0.62	
	W19		9.5	8.12	410	4.61			1.90	0.71	0.16	0.02	0.90	0.10				-11.6	-9.2				-2.78	0.75	
	Krka River tributaries																								
	W2		9.8	7.40	425	4.78			1.73	0.75	0.17	0.01	0.57	0.09				-14.1	-8.9				-2.04	0.03	
	W3	0.01	5.6	7.83	531	5.99			1.85	1.08	0.49	0.04	0.45	0.11				-10.7	-8.9				-2.39	0.49	

Appendix 1: *Continued*.

Date of Sampling	Loc.	Q	T	pH	EC	TA	DIC	DOC	Ca^{2+}	Mg^{2+}	Na^{+}	K^{+}	Sr^{2+}	Ba^{2+}	Cl^{-}	SO_4^{2-}	NO_3^{-}	$\delta^{13}C$ DIC	$\delta^{18}O$	$\delta^{34}S$ sulph.	$\delta^{13}C$ POC	$\delta^{15}N$ PN	log pCO_2	SIc	SId
		m^3/s	°C		µS/cm	mM	mM	mM	mM	mM	mM	mM	µM	µM	mM	mM	mM	‰	‰	‰	‰	‰			
	W6		8.7	7.91	398	4.79			1.90	0.38	0.06	0.04	0.44	0.06				-13.5	-9.2				-2.55	0.56	
	W11	0.7	8.9	7.61	387	4.34			2.07	0.31	0.15	0.01	1.12	0.06				-13.5	-9.3				-2.29	0.26	
	W12		14.2	7.70	421	4.61			1.91	0.65	0.17		3.15	0.14				-11.5	-9.4				-2.33	0.42	
	W14	1.3	8.5	7.89	405	5.07			1.98	0.81	0.14	0.02	0.53	0.09				-12.1	-9.0				-2.51	0.57	
2.12.	Krka River																								
2009	W1		10.4	7.46	496	5.04			1.68	1.02	0.20	0.01	0.47	0.10	0.20	0.07		-12.9	-8.7				-2.07	0.10	
	W4	5.0	10.3	7.71	493	5.00			1.77	0.93	0.18	0.01	0.48	0.11	0.18	0.05		-12.8	-9.0				-2.33	0.37	
	W5		9.7	8.11	487	5.01			1.82	0.88	0.17	0.01	0.49	0.10	0.17	0.05		-12.7	-8.8				-2.74	0.76	
	W7		10.1	8.20	495	5.08			1.84	0.89	0.17	0.01	0.46	0.10	0.15	0.05		-12.1	-9.3				-2.82	0.86	
	W8		10.0	8.22	495	5.13			1.85	0.89	0.17	0.02	0.47	0.09	0.18	0.05		-12.1	-8.9				-2.84	0.88	
	W9		9.8	8.20	494	5.09			1.84	0.89	0.17	0.02	0.47	0.09	0.18	0.06		-12.1	-9.1				-2.82	0.86	
	W10	20.9	9.5	7.79	453	4.62			1.83	0.68	0.13	0.01	0.64	0.08	0.07	0.06		-12.8	-9.2				-2.44	0.42	
	W13		9.4	7.77	443	4.49			1.95	0.68	0.13	0.03	0.79	0.06	0.11	0.06		-13.4	-9.1				-2.40	0.45	
	W15		10.4	7.75	479	4.80			1.87	0.67	0.13	0.07	0.50	0.08	0.17	0.05		-12.7	-8.9				-2.38	0.42	
	W16		9.2	7.86	456	4.53			1.85	0.56	0.14	0.07	0.66	0.07	0.17	0.05		-12.9	-9.0				-2.52	0.48	
	W17		9.2	7.85	454	4.53			1.86	0.58	0.13	0.08	0.66	0.08	0.18	0.05		-12.7	-9.0				-2.51	0.47	
	W18	42.8	9.3	8.00	469	4.80			1.71	0.59	0.14	0.08	0.82	0.08	0.27	0.06		-12.3	-8.9				-2.64	0.61	
	W19		9.3	7.90	463	4.67			1.71	0.61	0.15	0.07	0.66	0.06	0.19	0.07		-12.0	-8.9				-2.55	0.50	
	Krka River tributaries																								
	W2		9.9	7.38	478	5.01			1.97	0.65	0.10		0.53	0.08	0.11	0.05		-14.2	-9.0				-2.00	0.08	
	W3	0.1	9.6	7.94	542	5.17			1.88	0.99	0.33	0.04	0.40	0.09	0.33	0.08		-12.8	-8.6				-2.55	0.61	
	W6		10.3	7.73	452	4.80			2.07	0.49	0.05		0.53	0.05	0.05	0.04		-13.3	-9.4				-2.36	0.44	
	W11	9.5	9.5	7.54	430	4.31			2.10	0.28	0.09	0.01	0.85	0.05	0.10	0.06		-14.0	-9.4				-2.22	0.21	
	W12		9.0	7.87	439	4.61			1.89	0.59	0.06	0.00	1.02	0.06	0.07	0.05		-13.5	-9.5				-2.53	0.50	
	W14	3.8	10.6	7.72	509	4.90			1.98	0.77	0.16	0.06	0.48	0.08	0.20	0.05		-12.5	-8.9				-2.34	0.42	
9.2.	Krka River																								
2010	W1		7.5	7.62	522	5.02			1.66	1.00	0.41	0.03	0.48	0.10	0.45	0.07	0.04	-13.0	-9.1	9.4			-2.25	0.21	
	W4	5.2	8.0	7.88	513	5.12			1.68	0.94	0.37	0.03	0.47	0.10	0.42	0.06		-12.5	-8.9	8.8			-2.45	0.53	
	W5		6.5	8.27	502	4.95			1.70	0.92	0.31	0.03	0.47	0.10	0.35	0.06	0.04	-12.3	-9.0	8.5			-2.92	0.83	
	W7		6.7	8.29	496	4.95			1.74	0.86	0.26	0.03	0.36	0.07	0.31	0.06		-12.1	-9.0	8.5			-2.94	0.86	
	W8		8.1	8.44	496	4.91			1.74	0.83	0.25	0.03	0.38	0.07	0.30	0.06	0.02	-12.0	-8.6				-3.09	1.02	
	W9		5.8	8.32	488	4.94			1.77	0.84	0.25	0.03	0.38	0.07	0.30	0.06	0.02	-12.2	-8.7	8.6			-2.97	0.88	
	W10	19.6	6.3	8.13	475	4.65			1.72	0.72	0.21	0.02	0.51	0.07	0.26	0.06		-12.4	-9.3	8.5			-2.80	0.68	
	W13		6.4	8.10	458	4.52			1.77	0.61	0.25	0.02	0.59	0.06	0.25	0.06		-12.4	-9.4	8.9			-2.78	0.65	

Appendix 1: *Continued*.

Date of Sampling	Loc.	Q	T	pH	EC	TA	DIC	DOC	Ca^{2+}	Mg^{2+}	Na^{+}	K^{+}	Sr^{2+}	Ba^{2+}	Cl^{-}	SO_4^{2-}	NO_3^{-}	$\delta^{13}C$ DIC	$\delta^{18}O$	$\delta^{34}S$ sulph.	$\delta^{13}C$ POC	$\delta^{15}N$ PN	log pCO_2	SIc	SId
		m^3/s	°C		µS/cm	mM	mM	mM	mM	mM	mM	mM	µM	µM	mM	mM	mM	‰	‰	‰	‰	‰			
	W15		7.3	8.03	490	4.71			1.82	0.61	0.23	0.02	0.48	0.07	0.24	0.06	0.05	-12.3	-9.2	8.4			-2.69	0.63	
	W16		5.3	8.19	486	4.59			1.81	0.62	0.30	0.03	0.58	0.06	0.35	0.07		-12.1	-9.2	8.6			-2.87	0.74	
	W17		4.7	8.22	491	4.64			1.78	0.65	0.25	0.02	0.52	0.07	0.30	0.06	0.03	-12.0	-9.0	8.7			-2.90	0.75	
	W18	37.9	4.1	8.36	486	4.68			1.81	0.65	0.31	0.03	0.68	0.07	0.37	0.06		-11.7	-9.1	8.9			-3.04	0.89	
	W19		3.4	8.44	484	4.62			1.78	0.64	0.32	0.03	0.68	0.07	0.39	0.07	0.06	-11.3	-9.2	8.3			-3.14	0.94	
	Krka River tributaries																								
	W2		9.6	7.50	471	4.81			1.86	0.67	0.17	0.02	0.50	0.06	0.20	0.05	0.03	-13.9	-9.3	7.8			-2.13	0.16	
	W3	0.2	5.5	8.52	568	5.60			1.83	1.22	0.43	0.04	0.32	0.08	0.79	0.08		-11.2	-9.0	8.2			-3.13	1.12	
	W6																								
	W11	6.5	8.4	7.75	440	4.19			1.96	0.28	0.20	0.02	0.80	0.05	0.25	0.06	0.02	-13.7	-9.7	8.5			-2.45	0.36	
	W12		10.3	7.66	485	4.51			1.83	0.55	0.34	0.03	2.24	0.09	0.33	0.05	0.04	-11.9	-9.2	8.1			-2.32	0.30	
	W14	3.3	8.7	7.87	506	4.88			1.96	0.61	0.16	0.02	0.47	0.06	0.22	0.05	0.04	-12.6	-8.8	8.9			-2.51	0.53	
3.4.	Krka River																								
2010	W1		9.4	7.73	436	4.56			1.44	0.77	0.24	0.02	0.32	0.07	0.29	0.06		-12.9	-9.9		-26.8	6.6	-2.39	0.26	
	W4	12.9	9.4	7.83	442	4.54			1.50	0.78	0.24	0.03	0.33	0.07	0.30	0.06	0.18	-13.0	-9.9		-30.9	5.9	-2.49	0.37	
	W5		10.6	8.39	436	4.48			1.51	0.77	0.28	0.03	0.33	0.07	0.28	0.06	0.18	-11.8	-9.9		-31.3	5.7	-3.07	0.92	
	W7		10.6	8.35	439	4.40			1.59	0.70	0.21	0.03	0.32	0.06	0.27	0.05	0.17	-12.2	-9.9			5.6	-3.03	0.90	
	W8		10.3	8.30	430	4.41			1.60	0.66	0.18	0.02	0.33	0.06	0.23	0.05	0.18	-12.3	-10.1		-31.4	5.4	-2.98	0.85	
	W9		10.2	8.23	430	4.31			1.59	0.64	0.17	0.02	0.34	0.06	0.23	0.05	0.18	-12.2	-10.1		-31.3	5.6	-2.92	0.78	
	W10	46.7	10.1	8.04	386	3.84			1.50	0.48	0.12	0.01	0.38	0.05	0.15	0.05	0.17	-12.3	-10.8		-30.7	5.5	-2.77	0.53	
	W13		10.1	8.06	379	3.98			1.54	0.42	0.10	0.01	0.43	0.05	0.13	0.05	0.17	-12.3	-11.0		-30.1	5.4	-2.78	0.57	
	W15		11.5	8.00	442	4.51			1.57	0.46	0.18	0.03	0.38	0.06	0.24	0.05	0.18	-12.8	-10.3		-30.8	5.0	-2.80	0.36	
	W16		10.2	8.11	395	4.05			1.59	0.48	0.20	0.02	0.42	0.05	0.16	0.05	0.17	-12.4	-10.7		-30.9	3.2	-2.82	0.64	
	W17		9.8	8.16	394	4.05			1.60	0.45	0.13	0.02	0.45	0.05	0.17	0.05	0.15	-12.4	-10.6		-30.0	5.0	-2.87	0.69	
	W18	79.0	9.5	8.09	406	3.81			1.62	0.47	0.14	0.02	0.53	0.06	0.18	0.05	0.16	-12.4	-10.6		-30.4	5.1	-2.83	0.59	
	W19		9.8	8.22	397	3.95			1.59	0.47	0.14	0.02	0.55	0.06	0.17	0.05	0.18	-11.8	-10.6		-29.3	5.9	-2.94	0.73	
	Krka River tributaries																								
	W2		9.4	7.57	425	4.31			1.60	0.62	0.15	0.02	0.34	0.05	0.19	0.05	0.08	-13.8	-10.4		-25.0		-2.25	0.12	
	W3	0.6	9.9	8.35	537	5.23			1.60	1.16	0.37	0.03	0.28	0.08	0.46	0.07	0.07	-12.3	-9.5				-2.96	0.95	
	W6		10.2	7.78	425	4.05			1.76	0.30	0.07	0.02	0.32	0.00	0.10	0.04		-13.9	-10.9		-28.6	4.3	-2.48	0.36	
	W11	9.5	10.2	7.75	364	3.78			1.69	0.23	0.06	0.01	0.54	0.00	0.09	0.06		-12.7	-11.5		-29.6	3.4	-2.48	0.29	
	W12		10.5	8.25	365	3.76			1.49	0.46	0.05	0.01	0.50	0.00	0.07	0.04		-11.9	-11.6		-27.4	5.5	-2.99	0.73	

Appendix 1: *Continued*.

Date of Sampling	Loc.	Q	T	pH	EC	TA	DIC	DOC	Ca^{2+}	Mg^{2+}	Na^{+}	K^{+}	Sr^{2+}	Ba^{2+}	Cl^{-}	SO_4^{2-}	NO_3^{-}	$\delta^{13}C$ DIC	$\delta^{18}O$	$\delta^{34}S$ sulph.	$\delta^{13}C$ POC	$\delta^{15}N$ PN	log pCO_2	SIc	SId
		m^3/s	°C		µS/cm	mM	mM	mM	mM	mM	mM	mM	µM	µM	mM	mM	mM	‰	‰	‰	‰	‰			
	W14	5.9	11.3	7.71	442	4.38			1.83	0.46	0.19	0.03	0.37	0.07	0.27	0.05	0.08	-13.0	-9.4		-28.1	6.8	-2.38	0.35	
2.6.	Krka River																								
2010	W1		10.9	7.63	456	4.58			1.53	0.83	0.18	0.03	0.36	0.08	0.21	0.06	0.19	-13.1	-9.7	9.1			-2.28	0.21	
	W4	8.2	10.9	7.42	462	4.55			1.60	0.79	0.18	0.02	0.37	0.08	0.21	0.05	0.17	-12.9	-9.9	8.6			-2.07	0.01	
	W5		11.1	8.17	451	4.46			1.60	0.75	0.18	0.02	0.37	0.07	0.20	0.05	0.19	-12.6	-9.9	8.3			-2.84	0.75	
	W7		11.2	8.14	450	4.44			1.61	0.66	0.15	0.02	0.34	0.06	0.19	0.04	0.18	-12.8	-10.0	7.8			-2.81	0.72	
	W8		11.5	8.21	449	4.45			1.68	0.68	0.16	0.02	0.36	0.07	0.19	0.05	0.18	-12.7	-10.0	8.2			-2.88	0.81	
	W9		11.9	8.19	439	4.51			1.69	0.70	0.17	0.03	0.37	0.07	0.20	0.05	0.19	-12.5	-10.0	8.4			-2.85	0.80	
	W10	38.3	11.0	7.90	426	4.25			1.65	0.57	0.13	0.02	0.48	0.06	0.15	0.05	0.19	-12.7	-10.4	8.4			-2.58	0.48	
	W13		10.9	7.79	410	4.18			1.70	0.45	0.10	0.02	0.54	0.05	0.11	0.05	0.17	-13.2	-11.0	10.0			-2.48	0.38	
	W15		12.4	7.61	463	4.47			1.81	0.62	0.19	0.03	0.39	0.08	0.21	0.05	0.19	-13.0	-9.3	9.0			-2.26	0.27	
	W16		11.6	7.88	423	4.24			1.72	0.49	0.14	0.02	0.55	0.06	0.16	0.05	0.19	-13.0	-10.5	9.4			-2.56	0.49	
	W17		11.6	7.93	420	4.23			1.68	0.51	0.13	0.02	0.51	0.06	0.15	0.04	0.17	-12.8	-10.5	8.8			-2.61	0.53	
	W18	88.5	12.3	7.95	425	4.25			1.69	0.52	0.14	0.02	0.61	0.06	0.16	0.05	0.17	-12.6	-10.5	8.6			-2.63	0.56	
	W19		13.1	8.01	415	4.14			1.67	0.49	0.14	0.02	0.67	0.07	0.16	0.05	0.17	-12.4	-10.4	8.6			-2.69	0.61	
	Krka River tributaries																								
	W2		9.9	7.42	446	4.40			1.70	0.61	0.14	0.02	0.38	0.06	0.17	0.05	0.02	-13.9	-10.3	7.3			-2.09	0.01	
	W3	0.4	12.7	7.96	555	5.39			1.69	1.14	0.35	0.04	0.39	0.09	0.39	0.07	0.02	-12.6	-9.3	8.3			-2.54	0.65	
	W6		10.2	7.64	412	4.15			1.86	0.32	0.06	0.01	0.37	0.04	0.08	0.05	0.01	-14.0	-10.9	7.9			-2.33	0.26	
	W11	14.4	10.3	7.41	392	4.01			1.73	0.32	0.06	0.01	0.57	0.00	0.07	0.05	0.02	-13.6	-11.5	9.0			-2.11	-0.01	
	W12		10.8	7.99	396	4.10			1.58	0.50	0.05	0.01	0.60	0.00	0.07	0.04	0.05	-12.9	-11.1	7.6			-2.69	0.54	
	W14	4.8	12.4	7.56	473	4.57			1.76	0.59	0.17	0.03	0.42	0.07	0.24	0.05	0.05	-13.1	-9.6	9.5			-2.20	0.22	
14.8.	Krka River																								
2010	W1		13.4	7.30	488	4.77			1.46	0.93	0.25	0.04	0.35	0.28	0.26	0.07	0.19	-12.5	-9.1	8.3	-29.3	6.5	-1.92	-0.09	
	W4	1.5	13.2	7.60	472	4.59			1.47	0.89	0.24	0.04	0.36	0.30	0.25	0.07	0.19	-12.5	-9.2		-29.2	5.0	-2.24	0.19	
	W5		14.5	8.22	454	4.36			1.46	0.82	0.22	0.03	0.36	0.30	0.23	0.05	0.18	-11.8	-9.2	10.8	-30.6	4.5	-2.88	0.79	
	W7		14.5	7.75	479	4.54			1.55	0.82	0.26	0.03	0.34	0.29	0.28	0.06	0.18	-12.1	-9.2	7.2	-30.3	4.2	-2.39	0.38	
	W8		15.4	8.16	469	4.48			1.52	0.79	0.25	0.03	0.36	0.32	0.27	0.05	0.19	-11.7	-9.3	7.5	-30.9	4.6	-2.80	0.78	
	W9		16.7	8.27	494	4.72			1.53	0.85	0.24	0.03	0.37	0.29	0.25	0.05	0.18	-11.3	-9.3	7.2	-31.2	5.0	-2.89	0.92	
	W10	6.2	15.7	8.10	448	4.48			1.52	0.72	0.18	0.02	0.53	0.30	0.19	0.06	0.19	-11.5	-9.7	8	-31.6	5.4	-2.74	0.73	
	W13		16.6	7.84	438	4.61			1.53	0.64	0.16	0.03	0.60	0.24	0.17	0.06	0.18	-11.8	-9.9	8.7	-31.6	4.1	-2.46	0.50	
	W15		16.9	7.89	481	4.61			1.55	0.61	0.15	0.03	0.54	0.32	0.16	0.05	0.16	-11.4	-9.7	7.8	-30.0	4.9	-2.51	0.56	
	W16		20.0	7.99	430	4.27			1.50	0.58	0.21	0.04	0.56	0.25	0.21	0.06	0.16	-11.5	-9.7	9.4	-30.1	6.4	-2.62	0.66	
	W17		19.2	8.04	433	4.41			1.51	0.59	0.19	0.03	0.55	0.32	0.20	0.05	0.17	-11.8	-9.8	8.6	-29.8	3.4	-2.67	0.71	

Appendix 1: *Continued*.

Date of Sampling	Loc.	Q	T	pH	EC	TA	DIC	DOC	Ca^{2+}	Mg^{2+}	Na^{+}	K^{+}	Sr^{2+}	Ba^{2+}	Cl^{-}	SO_4^{2-}	NO_3^{-}	$\delta^{13}C$ DIC	$\delta^{18}O$	$\delta^{34}S$ sulph.	$\delta^{13}C$ POC	$\delta^{15}N$ PN	log pCO_2	SIc	SId
		m^3/s	°C		µS/cm	mM	mM	mM	mM	mM	mM	mM	µM	µM	mM	mM	mM	‰	‰	‰	‰	‰			
	W18	16.3	21.7	8.27	430	4.35			1.51	0.61	0.18	0.03	0.65	0.25	0.19	0.06	0.16	-11.2	-9.6	8.5	-29.7	4.2	-2.90	0.96	
	W19		21.8	8.38	429	4.30			1.53	0.60	0.17	0.03	0.68	0.31	0.18	0.06	0.16	-11.3	-9.6	8.5	-29.6	4.3	-3.02	1.06	
	Krka River tributaries																								
	W2		10.4	7.36	454	4.54			1.64	0.68	0.16	0.04	0.43	0.10	0.20	0.05	0.05	-13.2	-9.6	7.9	-29.5	2.2	-2.01	-0.04	
	W3	0.01	18.0	7.56	460	4.36			1.69	0.88	0.47	0.02	0.27	0.39	0.43	0.08	0.06	-11.7	-9.7	8.0	-27.2	5.0	-2.19	0.15	
	W6		11.1	7.49	433	4.43			1.74	0.52	0.06	0.02	0.47	0.26	0.07	0.04	0.03	-11.9	-10.2	6.1	-30.2	2.6	-2.15	0.12	
	W11	0.7	11.5	7.77	411	4.11			1.81	0.28	0.07	0.01	0.75	0.26	0.08	0.06		-12.9	-10.6		-31.7		-2.46	0.39	
	W12		18.2	7.58	465	4.76			1.77	0.54	0.16	0.03	2.38	0.33	0.16	0.04		-11.4	-9.8	7.4	-27.9	3.3	-2.17	0.34	
	W14	1.4																							
9.11.	Krka River																								
2010	W1		7.5	7.21	492	4.50			1.60	0.93	0.31	0.03	0.33	0.11	0.36	0.06	0.08	-12.8	-9.3		-27.5	6.8	-1.88	-0.26	
	W4	18.1	7.8	7.58	492	4.69			1.66	0.91	0.30	0.03	0.28	0.11	0.35	0.06	0.05	-12.8	-9.3		-28.8	5.7	-2.23	0.15	
	W5		8.0	7.93	484	4.41			1.67	0.87	0.28	0.03	0.00	0.00	0.32	0.06	0.05	-12.5	-9.3		-27.8	6.1	-2.61	0.47	
	W7		8.9	7.93	482	4.65			1.74	0.78	0.29	0.03	0.34	0.11	0.32	0.06	0.08	-12.5	-9.1		-27.8	6.6	-2.59	0.53	
	W8		8.9	7.96	474	4.58			1.84	0.79	0.28	0.03	0.00	0.00	0.29	0.05	0.06	-12.6	-9.4		-28.8	6.1	-2.62	0.57	
	W9		8.8	7.89	472	4.63			1.75	0.72	0.24	0.02	0.35	0.12	0.29	0.05	0.06	-12.7	-9.3		-28.9	6.2	-2.55	0.49	
	W10	66.0	8.8	7.83	442	4.58			1.69	0.61	0.18	0.02	0.42	0.10	0.22	0.05	0.07	-12.6	-9.4		-28.4	6.2	-2.49	0.41	
	W13		9.1	7.62	426	4.25			1.78	0.47	0.15	0.02	0.48	0.12	0.18	0.05	0.06	-13.1	-9.8		-28.3	6.0	-2.31	0.21	
	W15		9.5	7.44	458	4.02			1.95	0.50	0.20	0.03			0.26	0.05	0.13	-12.8	-9.3			6.3	-2.15	0.05	
	W16		8.7	7.79	447	4.29			1.87	0.56	0.23	0.03			0.25	0.05	0.07	-12.7	-9.3		-27.9	3.8	-2.48	0.39	
	W17		8.5	7.86	442	4.36			1.81	0.60	0.20	0.02			0.22	0.05	0.07	-12.7	-9.6		-28.1	4.0	-2.54	0.45	
	W18	88.1	8.0	7.92	447	4.25			1.67	0.53	0.20	0.02	0.54	0.09	0.25	0.06	0.05	-12.4	-9.4		-27.5	3.8	-2.62	0.46	
	W19		7.9	7.85	417	4.08			1.74	0.56	0.18	0.02	0.58	0.07	0.22	0.06	0.07	-12.5	-9.6		-27.7	4.0	-2.56	0.39	
	Krka River tributaries																								
	W2		9.1	7.24	455	4.43			1.75	0.63	0.20	0.02	0.36	0.14	0.22	0.05	0.06	-13.9	-9.6		-27.1	5.6	-1.91	-0.16	
	W3	4.0	8.0	7.86	559	5.27			1.81	1.10	0.44	0.04	0.33	0.16	0.51	0.07	0.07	-12.6	-9.3		-27.5	5.1	-2.47	0.50	
	W6		9.8	7.54	413	4.17			1.87	0.35	0.11	0.02	0.36	0.08	0.13	0.04	0.03	-13.8	-9.6		-28.8	6.3	-2.23	0.15	
	W11	12.7	9.2	7.44	415	4.06												-13.5	-10.0		-29.6	4.7	-2.15		
	W12		9.0	7.71	409	4.31			1.68	0.49	0.08	0.01	0.56	0.08	0.10	0.04	0.06	-13.0	-10.0		-28.8	4.8	-2.39	0.28	
	W14	10.0	9.6	7.38	468	4.34			1.99	0.50	0.21	0.03	0.38	0.15	0.27	0.05	0.06	-13.0	-9.3		-26.6	6.7	-2.06	0.03	

Appendix 2: Stable oxygen isotopic composition of precipitation collected in 2009 and 2010 at precipitation monitoring station Dvor (Figure 16).

Date	$\delta^{18}O$ (‰)
31.1.2009	-17.02
28.2.2009	-13.45
31.3.2009	-9.31
30.4.2009	-7.47
31.5.2009	-8.73
30.6.2009	-7.19
31.7.2009	-5.82
31.8.2009	-5.92
30.9.2009	-5.35
31.10.2009	-10.14
30.11.2009	-13.52
31.12.2009	-13.42
31.1.2010	-15.42
28.2.2010	-14.42
31.3.2010	-14.43
30.4.2010	-10.08
31.5.2010	-8.81
30.6.2010	-8.11
31.7.2010	-8.01
31.8.2010	-8.56
30.9.2010	-7.08
31.10.2010	-10.27
30.11.2010	-12.28
31.12.2010	-11.22

Appendix 3: Geochemical and mineralogical results of elemental, XRD, C, N and stable isotope analyses of tufa samples collected in the Krka River.

	Elemental Analyses																	
Sample No.	SiO_2 (%)	Al_2O_3 (%)	Fe_2O_3 (%)	MgO (%)	CaO (%)	Na_2O (%)	K_2O (%)	LOI (%)	Ca (mg/g)	Mg (mg/g)	Si (mg/g)	Al (mg/g)	Fe (mg/g)	Mn (mg/g)	Na (mg/g)	K (mg/g)	Sr (ppm)	Ba (ppm)
T1	4.16	1.50	0.65	0.85	48.79	0.08	0.18	42.79	348.7	5.1	1.9	0.4	0.2	0.1	0.3	0.7	50	81
T2	4.74	1.64	0.76	0.99	48.00	0.08	0.19	42.51	343.1	6.0	2.2	0.4	0.3	0.1	0.3	0.8	55	79
T3	4.82	1.75	2.78	0.89	47.67	0.07	0.22	42.05	340.7	5.4	2.3	0.5	1.0	0.1	0.3	0.9	50	78
T4	6.55	2.17	0.96	1.00	46.43	0.09	0.25	41.41	331.8	6.0	3.1	0.6	0.3	0.2	0.3	1.0	49	95
T5	3.32	1.27	1.16	0.73	50.03	0.06	0.15	43.05	357.6	4.4	1.6	0.3	0.4	0.2	0.2	0.6	47	75
T6	9.00	3.07	1.75	1.04	45.09	0.10	0.31	39.78	322.3	6.3	4.2	0.8	0.6	0.1	0.4	1.3	51	95
T7	6.28	2.57	1.00	0.85	47.23	0.08	0.28	41.1	337.5	5.1	2.9	0.7	0.3	0.1	0.3	1.2	49	81
T8	7.41	2.11	1.21	1.10	46.39	0.09	0.24	40.85	331.5	6.6	3.5	0.6	0.4	0.1	0.3	1.0	50	79
T9	5.08	2.10	1.88	0.81	47.27	0.09	0.25	42.13	337.8	4.9	2.4	0.6	0.7	0.1	0.3	1.0	50	79
T10	4.43	2.01	1.08	0.83	49.08	0.05	0.25	42.3	350.8	5.0	2.1	0.5	0.4	0.0	0.2	1.0	51	69
T11	8.32	2.59	1.12	3.68	43.25	0.09	0.27	40.72	309.1	22.2	3.9	0.7	0.4	0.1	0.3	1.1	58	75
T12	5.30	1.64	0.86	2.29	46.96	0.08	0.16	42.15	335.6	13.8	2.5	0.4	0.3	0.1	0.3	0.7	48	64
T13	5.37	1.76	1.18	1.83	47.51	0.09	0.14	41.9	339.6	11.0	2.5	0.5	0.4	0.1	0.3	0.6	46	69
T14	4.26	1.95	0.78	0.92	49.53	0.06	0.18	42.17	354.0	5.5	2.0	0.5	0.3	0.0	0.2	0.7	44	60
T15	4.32	2.01	0.82	0.88	48.63	0.07	0.18	42.78	347.6	5.3	2.0	0.5	0.3	0.1	0.3	0.7	52	66
T16	8.13	3.27	1.56	1.04	44.45	0.08	0.30	40.3	317.7	6.3	3.8	0.9	0.5	0.1	0.3	1.2	55	88

Appendix 3: *Continued.*

XRD Analyses				C/N Analyses				Stable Isotope Analyses		
Sample No.	Calcite (%)	Dolomite (%)	Quartz (%)	C_{tot} (%)	C_{org} (%)	N_{tot} (%)	C/N	$\delta^{13}C_{CaCO3}$ (‰)	$\delta^{18}O_{CaCO3}$ (‰)	$\delta^{13}C_{org}$ (‰)
T1	93	3	4	12.0	1.1	0.1	14	-10.5	-8.8	-28.5
T2	91	5	4	12.0	1.3	0.2	9	-9.8	-8.8	-31.1
T3	92	4	4	11.4	1.1	0.1	14	-10.7	-9.0	-30.8
T4	89.5	4.5	6	11.8	1.1	0.1	12	-10.7	-9.1	-30.9
T5	97	1	2	12.1	1.6	0.2	10	-10.6	-9.0	-30.9
T6	83	10	8	11.0	1.2	0.1	14	-10.7	-8.7	-29.4
T7	91	3	6	11.3	0.9	0.1	13	-11.0	-8.9	-29.4
T8	85	8	7	11.5	1.0	0.1	17	-10.7	-8.9	-29.7
T9	97	2	1	11.7	1.1	0.1	16	-10.8	-8.9	-29.1
T10	98	2		12.1	1.2	0.1	11	-11.0	-9.1	-30.7
T11	75	19	6	11.3	0.9	0.1	15	-7.4	-7.2	-30.0
T12	82	13	5	11.9	0.9	0.1	14	-9.5	-8.3	-30.0
T13	83	12	5	11.5	0.9	0.1	9	-10.4	-9.0	-30.3
T14	92.5	3.5	4	11.5	0.8	0.1	10	-9.6	-8.7	-29.1
T15	92	3	4	11.9	1.3	0.2	9	-10.3	-9.1	-31.9
T16	87	7	6	11.0	1.2	0.1	15	-10.0	-8.8	-28.7

Appendix 4: Elemental and stable carbon isotope results of geochemical analyses of carbonate bedrock samples.

Sample No.	SiO_2 (%)	Al_2O_3 (%)	Fe_2O_3 (%)	MgO (%)	CaO (%)	Ca (mg/g)	Mg (mg/g)	Sr (ppm)	Mg/Ca	Sr/Ca	$\delta^{13}C_{CaCO3}$ (‰)
R 1	0.48	0.22	0.15	18.62	36.74	262.6	112.3	72.0	0.71	1.3E-04	+1.5
R 2	0.17	-	0.03	0.92	54.59	390.1	5.5	147.5	0.02	1.7E-04	+1.3
R 3	0.18	-	0.03	1.50	53.70	383.8	9.1	131.9	0.04	1.6E-04	+1.4
R 4	0.31	0.16	0.05	1.07	53.84	384.8	6.4	151.5	0.03	1.8E-04	+1.3

Appendix 5: Results of XRD analyses of tufa samples T1, T6, T9, T11 and T16.

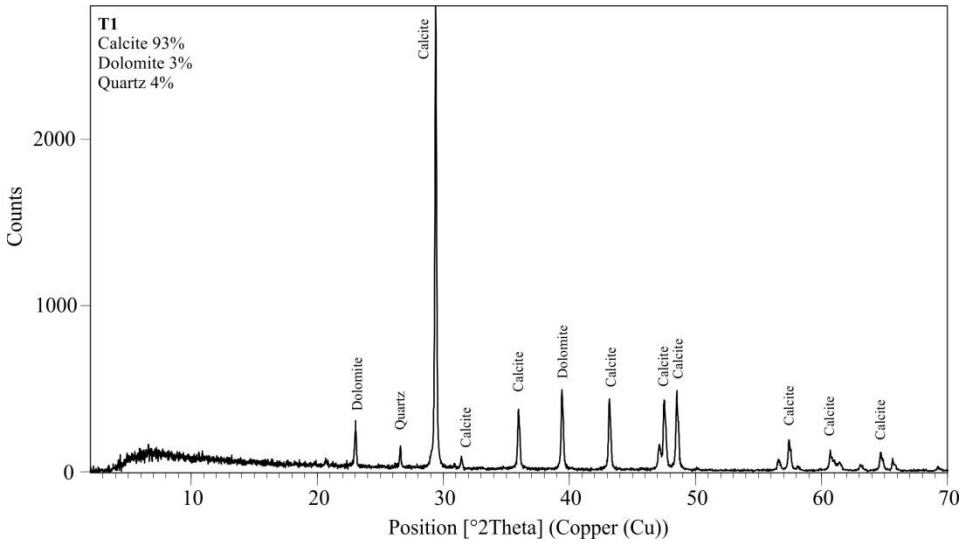

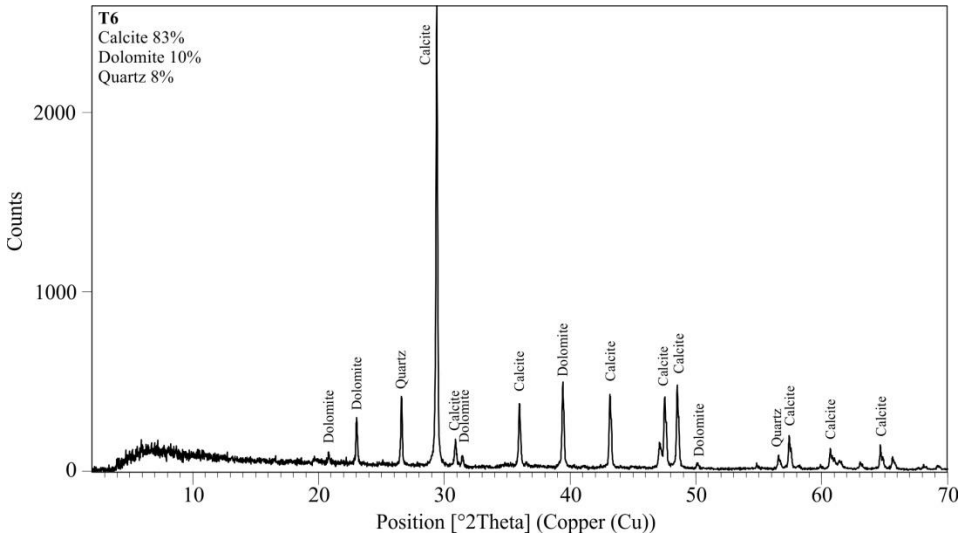

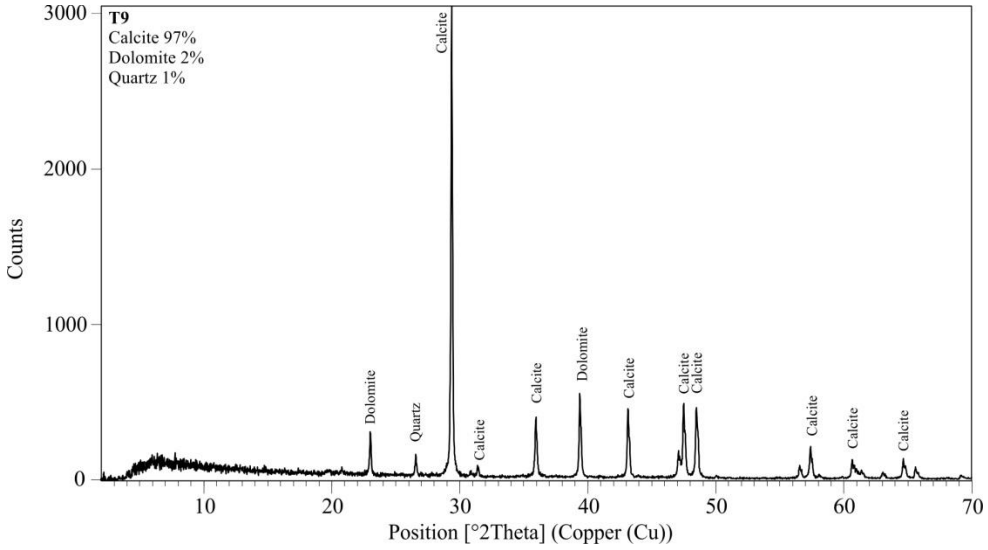
T9
Calcite 97%
Dolomite 2%
Quartz 1%
Counts
Position [°2Theta] (Copper (Cu))
Calcite
Dolomite
Quartz
Calcite
Calcite
Dolomite
Calcite
Calcite
Calcite
Calcite
Calcite
Calcite

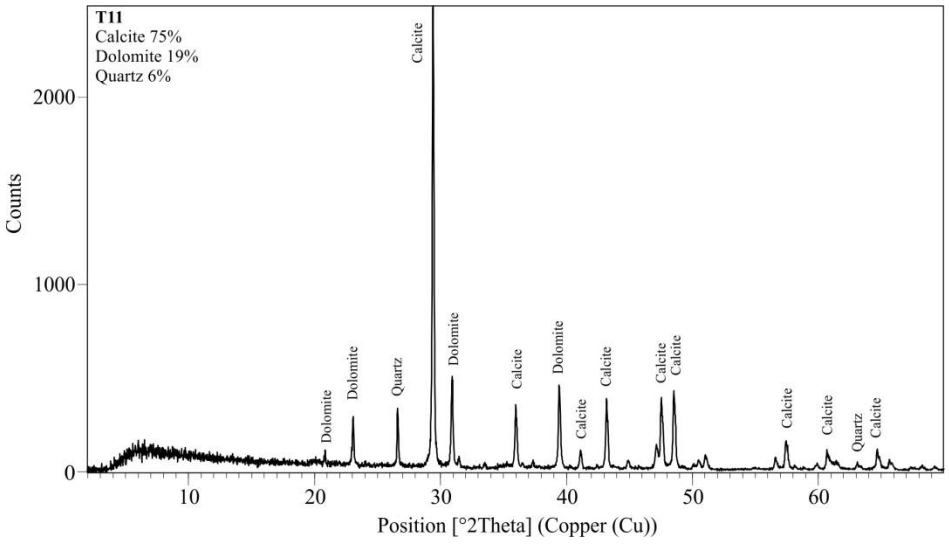
T11
Calcite 75%
Dolomite 19%
Quartz 6%
Counts
Position [°2Theta] (Copper (Cu))
Calcite
Dolomite
Dolomite
Quartz
Dolomite
Calcite
Dolomite
Calcite
Calcite
Calcite
Calcite
Calcite
Quartz
Calcite

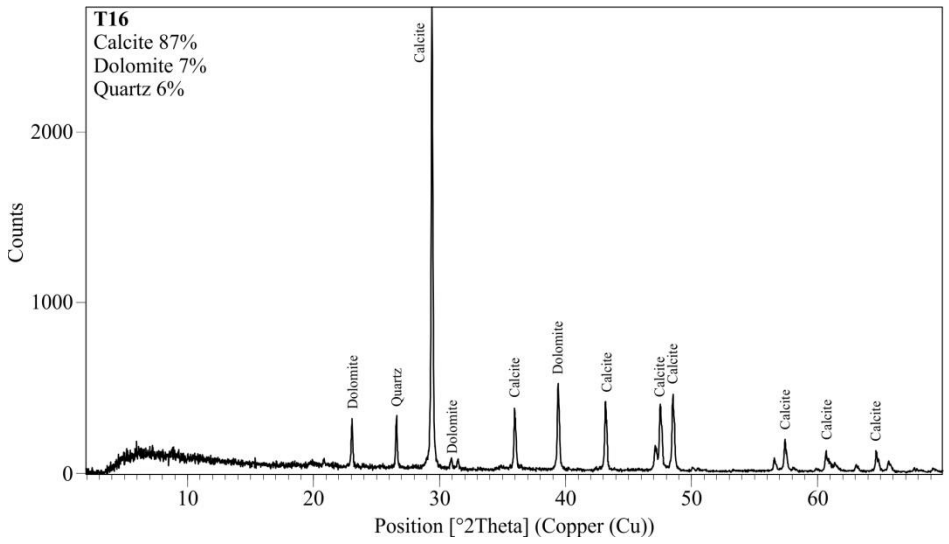
T16
Calcite 87%
Dolomite 7%
Quartz 6%
Counts
Position [°2Theta] (Copper (Cu))
Calcite
Dolomite
Quartz
Dolomite
Calcite
Dolomite
Calcite
Calcite
Calcite
Calcite
Calcite
Calcite

Appendix 6: Personal bibliography for the period 2006–2013.

SAŠA ZAVADLAV [30892]

Original scientific article

Zavadlav, S.; Kanduč, T.; McIntosh, J.; Lojen, S. Isotopic and chemical constraints on the biogeochemistry of dissolved inorganic carbon and chemical weathering in the karst watershed of Krka river (Slovenia). *Aquatic Geochemistry* **19**, 209–230 (2013).

Zavadlav, S.; Mazej, D.; Zavašnik, J.; Rečnik, A.; Dominguez-Villar, D.; Cukrov, N.; Lojen, S. C and O stable isotopic signatures of fast-growing dripstones on alkaline substrates: reflection of growth mechanism, carbonate sources and environmental conditions. *Isotopes in Environmental and Health Studies* **48**, 354–371 (2012).

Published scientific conference contribution

Zavadlav, S.; Kanduč, T.; Lojen, S. Carbonate weathering and biogeochemical carbon cycle in the Krka river watershed. In: *21st Meeting of Slovenian Geologists*. 178–181 (University of Ljubljana, Ljubljana, 2013).

Zavadlav, S.; Lojen, S. Paleoclimate proxies in sub-recent freshwater carbonate system in river Krka, Slovenia. In: *17th International Karstological Schoool "Classical Karst"* 2008. 4 (Karst Research Institute, Postojna, 2009).

Published scientific conference contribution abstract

Vrzel, J.; Zavadlav, S.; Tamše, S.; Solomon, K.; Ogrinc, N. Evaluating the vulnerability of groundwater resources using groundwater tracers. In: *Proceedings of the 7th Young Researchers Day*. 55 (Institut "Jožef Stefan", Ljubljana, 2013).

Zavadlav, S.; Kanduč, T.; Lojen, S. Water geochemistry controlled by carbonate weathering and associated CO_2 consumption. In: *Proceedings of the 7th Young Researchers Day*. 55 (Institut "Jožef Stefan", Ljubljana, 2013).

Zavadlav, S.; Lojen, S. Seasonal variations of dissolved inorganic carbon and $\delta^{13}C$ of tufa precipitating water (Krka river, Slovenija). In: *Proceedings of the 8th International Conference on Applications of Stable Isotope Techniques to Ecological Studies*. 82 (CNRS, Brest, 2012).

Ogrinc, N.; Zavadlav, S.; Tamše, S., Solomon, K. The use of tracers to evaluate the vulnerability of groundwater resources in Ljubljana. In: *Report RER/8/016 of the Final Workshop on "Assessment of Groundwater Resources Affected by Rivers in Danube Basin"*. 1 (IAEA, Ljubljana, 2012).

Zavadlav, S.; Lojen, S. Seasonal variation in stable isotopic and hydrogeochemical composition of tufa-depositing water in river Krka, Slovenia. In: *Proceedings of the International School of Travertine and Tufa.* 43 (Società Geologica Italiana, Sienna, 2011).

Zavadlav, S.; Lojen, S. Hydrogeochemical and isotopic characteristics of tufa precipitating waters : a case study of river Krka (Slovenia). In: *Proceedings of the International Symposium on Isotopes in Hydrology, Marine Ecosystems, and Climate Change Studies*. 141 (IAEA, Monaco, 2011).

Zavadlav, S.; Cukrov, N.; Lojen, S. Recent tufa and lacustrine sediments of river Krka (Croatia) : reflection of recent environmental conditions. In: *Proceedings of the Network in solid waste and water treatment between Europe and Mediterranean countries. Case study I, Monitoring of water and lake semident quality in natural environment : programme and abstracts.* 21 (Ruđer Bošković Institute, Zagreb, 2011).

Zavadlav, S.; Lojen, S. The relevance of Mg as palaeotemperature proxie in tufa sediments: a case study from river Krka (Slovenia). In: *Ion-partitioning in ambient temperature aqueous systems: from fundamentals to applications in climate proxies and environmental geochemistry : EMU school 2010: program and abstracts*. 37 (University of Oviedo, Oviedo, 2010).

Zavadlav, S.; Lojen, S. Hidrogeokemične značilnosti precipitacije lehnjaka v reki Krki (in Slovene). In: *Zbornik 4. Dan Mladih Raziskovalcev KMBO*. 69 (Institut "Jožef Stefan", Ljubljana, 2010).

Lojen, S.; Trkov, A.; Zavadlav, S.; Dolenec, M.; Váquez-Navarro, J., A.; Cukrov, N. Comparison of tufas as geochemical environmental proxies in continental Mediterranean Dinaric Karst. In: *Proceedings of the 27th Meeting of Sedimentary Environments of Mediterranean Island(s)*. 252 (IAS, Alghero, 2009).

Zavadlav, S.; Mazej, D.; Rečnik, A.; Lojen, S. Isotopic and chemical study of recent dripstones on alkaline substrates. In: *Proceedings of the 27th Meeting of Sedimentary Environments of Mediterranean Island(s)*. 724 (IAS, Alghero, 2009).

Zavadlav, S.; Lojen, S. Paleoklimatske raziskave na primeru lehnjaka reke Krke (in Slovene). In: *Zbornik* 3. *Dan mladih raziskovalcev 2009*. 1 (Institut "Jožef Stefan", Ljubljana, 2009) .

Zavadlav, S.; Zavašnik, J.; Rečnik, A.; Dolenec, T.; Bermanec, T. Baritno-tennantitna mineralizacija v žilah spodnje permskega apnenca nad Dolžanovo sotesko (in Slovene). In: *Zbornik 2. slovenski geološki kongres*. 62–63 (Rudnik živega srebra v zapiranju, Idrija, 2006).

Independent scientific component part or a chapter in a monograph

Zavadlav, S.; Zavašnik, J.; Rečnik, A.; Bermanec, V.; Dolenec, T. Kristali azurita s Počivalnika nad Dolžanovo sotesko (in Slovene). In: *Nahajališča mineralov v Sloveniji*. 115–120 (Institut "Jožef Stefan", Ljubljana, 2007).

Podgoršek, V.; Zavašnik, J.; Zavadlav, S.; Rečnik, A. Nahajališče epidota v Frajhajmu na Pohorju (in Slovene). In: *Nahajališča mineralov v Sloveniji*. 331–336 (Institut "Jožef Stefan", Ljubljana, 2007).

Zavašnik, J.; Zavadlav, S.; Schmidt, G. Piritne konkrecije in zviti kristali pirita iz Lemberga pri Dobrni (in Slovene). In: *Nahajališča mineralov v Sloveniji*. 336–344 (Institut "Jožef Stefan", Ljubljana, 2007).

Undergraduate thesis

Zavadlav, S. *Non-equilibrium precipitation of carbonates on alkaline substrates* (in Slovene) (University of Ljubljana, Ljubljana, 2008).

Selected format of bibliographic unit: ISO 690

Source of bibliographic records: shared data base COBISS.SI/COBIB.SI, 19. 4. 2013

Appendix 7: Article: Isotopic and chemical constraints on the biogeochemistry of dissolved inorganic carbon and chemical weathering in the karst watershed of Krka River (Slovenia). *Aquatic Geochemistry* **19**, 209–230 (2013).

Aquat Geochem
DOI 10.1007/s10498-013-9188-5

ORIGINAL PAPER

Isotopic and Chemical Constraints on the Biogeochemistry of Dissolved Inorganic Carbon and Chemical Weathering in the Karst Watershed of Krka River (Slovenia)

Saša Zavadlav · Tjaša Kanduč · Jennifer McIntosh · Sonja Lojen

Received: 25 September 2012 / Accepted: 2 February 2013

Abstract The hydrogeochemical and carbon isotope characteristics of the Krka River, Slovenia, were investigated to estimate the carbon transfer from the land ecosystem in the watershed. During the 3-year sampling period (2008–2010), temperature, pH, electrical conductivity, major ion content, dissolved inorganic carbon (DIC) and dissolved organic carbon content, and the isotopic composition of DIC ($\delta^{13}C_{DIC}$) were monitored in the main stream of the Krka River and its tributaries. The major solute composition of analysed waters is dominated by an input of HCO_3^-, Ca^{2+} and Mg^{2+} originating from carbonate dissolution. The Mg^{2+}/Ca^{2+} and Mg^{2+}/HCO_3^- molar ratio values ranging from 0.24 to 0.71 and 0.05 to 0.30, respectively, indicate a high degree of dolomite dissolution relative to calcite. Dissolved CO_2 concentrations in the river were up to tenfold supersaturated relative to the atmosphere, resulting in supersaturation with respect to calcite and degassing of CO_2 downstream. The $\delta^{13}C$ values in river water range from −15.6 to −9.4 ‰ and are controlled by the input of tributaries, exchange with atmospheric CO_2, degradation of organic matter, and dissolution of carbonates. The mass balance calculations for riverine DIC suggest that the contribution from carbonate dissolution and degradation of organic matter have major influence, whereas the exchange with atmospheric CO_2 has minor influence on the inorganic carbon pool in the Krka River.

Keywords River · Carbonate weathering · Biogeochemical processes · Dissolved inorganic carbon · Stable carbon isotopes

Electronic supplementary material The online version of this article (doi:10.1007/s10498-013-9188-5) contains supplementary material, which is available to authorized users.

S. Zavadlav (✉) · T. Kanduč · S. Lojen
Department of Environmental Sciences, Jožef Stefan Institute, Ljubljana, Slovenia
e-mail: sasa.zavadlav@ijs.si

J. McIntosh
Department of Hydrology and Water Resources, University of Arizona, Tucson, AZ, USA

Published online: 20 February 2013

1 Introduction

Riverine systems are an important linkage between the terrestrial, oceanic and atmospheric environments. Numerous studies have investigated influences on river water chemistry to understand the biogeochemical dynamics of the dissolved load in their basin and found that it is controlled by rock weathering, atmospheric input, anthropogenic pollution, and biological activity (Gibbs 1970; Meybeck 1987; Roy et al. 1999; Zhang et al. 2009). Chemical rock weathering and associated CO_2 consumption within the watershed are important issues related to global climate change (Gaillardet et al. 1999; Amiotte Suchet et al. 2003; Sun et al. 2010). Natural factors, particularly lithological variations, exert dominant control over water chemistry in both carbonate and silicate basins (Gaillardet et al. 1999), but some studies also emphasise the importance of other factors, such as runoff, air temperature and human activity (Meybeck 1987; Roy et al. 1999; Tipper et al. 2006; Szramek et al. 2011). Most of these studies have focused on silicate-rock dominated watersheds, whereas studies of river basins dominated by carbonate bedrock provide us also with important information on calcite and dolomite dissolution (Williams et al. 2007; Szramek et al. 2011).

Measurements of concentrations and the stable isotope composition ($\delta^{13}C$) of dissolved inorganic carbon (DIC) are frequently used in studies of carbon dynamics in waters. Along with measurements of water temperature and pH, the concentrations of DIC and $\delta^{13}C_{DIC}$ values provide information on carbon fluxes, sources and biogeochemical processes involved in the riverine carbon cycle (Atekwana and Krishnamurthy 1998; Aucour et al. 1999; Telmer and Veizer 1999; Pawellek et al. 2002; Brunet et al. 2005; Kanduč et al. 2007; Ferguson et al. 2011). Rivers transport 0.8–1.2 Gt of dissolved and particulate carbon per year to the oceans (Ludwig et al. 1996). The largest riverine carbon pool is DIC, which originates from dissolution of atmospheric CO_2, organic matter degradation and weathering of rocks in the watershed area. Most surface waters in carbonate areas have a high partial pressure of CO_2 (pCO_2) compared to atmospheric pCO_2, which makes surface water bodies (rivers and lakes) act as a local source of CO_2. Therefore, it is essential to understand the sources, sinks and transformations of carbon in aquatic systems in order to provide additional constraints on the global carbon cycle (Schulte et al. 2011).

Because of transformation of dissolved and particulate organic carbon (DOC and POC) and DIC during the transfer from soils to the river and in the river itself, the carbon isotopic signature of DIC can change significantly downstream the river depending on watershed characteristics (e.g. geological and geomorphological characteristics, land cover/use, etc.). In rivers draining predominantly carbonate watersheds, like the Danube, upper Rhine, Rhone or Houzhai, $\delta^{13}C_{DIC}$ values reflect a mixture of carbon of carbonate and organic origin (Hartmann et al. 2007; Li et al. 2010; Pawellek et al. 2002). $\delta^{13}C_{DIC}$ values are further influenced by several biogeochemical processes, such as organic matter degradation, respiration and photosynthesis of phytoplankton and exchange of CO_2 with the atmosphere. In the water column, photosynthesis preferentially selects the lighter carbon (^{12}C) leaving the remaining DIC enriched in ^{13}C. A positive shift in $\delta^{13}C_{DIC}$ is also caused by CO_2 equilibration with or evasion to the atmosphere, whereas respiration of organisms and oxidation of organic matter release CO_2 leading to increased DIC concentrations and decreased $\delta^{13}C_{DIC}$ values.

Not much research has been done on the variability of carbon dynamics and the effects of carbonate weathering on water chemistry in karstic areas (Li et al. 2010). This paper represents the first comprehensive background investigation of the chemical and isotopic composition of dissolved and suspended constituents in the Krka watershed, which is a typical karstic river with local tufa occurrences. The objectives of our study were (1) to

analyse seasonal and spatial patterns of major ion concentrations in river water, (2) to evaluate seasonal and spatial variations in the concentration and isotopic composition of DIC using chemical and isotopic techniques, (3) to quantify carbonate weathering rates and the associated CO_2 consumption and (4) to identify the main biogeochemical processes governing carbon geochemistry in the karst river.

2 Site Description

The Krka River drainage basin covers about 2,350 km^2 of the north-western part of the Dinaric carbonate platform, a large karst boundary area in southeastern Europe that separates the Adriatic Sea in the southeast and the Alps in the northwest (Fig. 1). The Krka River is 96 km long and is the largest tributary of the Slovenian part of the Sava River, which drains waters into the Danube River basin.

The geology of the basin covers lithological units ranging in age from Permian quartz sandstones and conglomerates to Quaternary alluvial deposits (Buser 1974; Buser and Cajhen 1965; Pleničar and Premru 1977; Pleničar and Premru 1970). Over 80 % of the watershed consists of Mesozoic carbonate sedimentary rocks (Triassic dolomites, and limestones of Jurassic and Cretaceous age) and approximately 17 % of Quaternary sediments (red and brown shale, sandstones and siltstones). The Mesozoic carbonates are highly karstified; in the western part of the watershed, a 100-m-thick fractured-rock aquifer

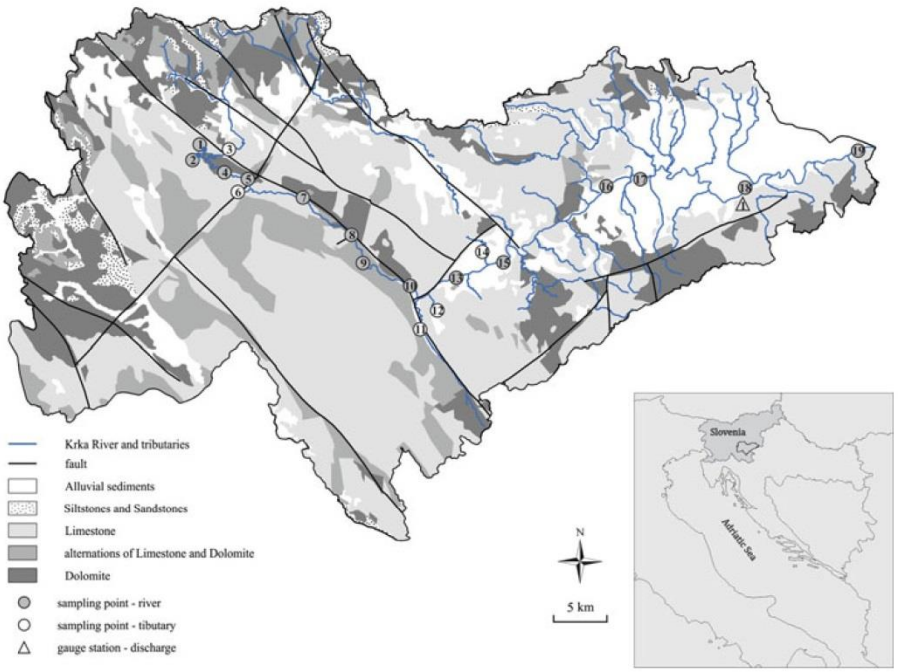

Fig. 1 Geological framework of the Krka River watershed with a detailed location map of sampling sites in the watershed. Sample sites are described in Table 1. The thicknesses of major lithological units are: dolomite (750–1,200 m), limestone (200–1,600 m), dolomite–limestone alternation (140–410 m), siltstones and sandstones (50–300 m), and alluvial (10–150 m)

is present, whereas in the eastern part, close to the confluence with the Sava River, the aquifer is shallower and of intergranular-rock type. Quaternary deposits are distributed in the plain area in the eastern part of the watershed surrounded by limestone and dolomite hills.

The river drains a sparsely populated area with extensive agricultural activities in the eastern part. The headwaters of the Krka are fed by groundwater from the broad karst hinterland in the north- and south-western areas. The waters rise to the surface at two main springs, at an elevation of 238 m. After almost 30 km of flow through a narrow, up to 100-m-deep canyon, the river enters a wide plain area where it discharges into the Sava River at the elevation of 139 m. The river is recharged by groundwater in the headwater catchment area, which accounts for about 11 % of the whole watershed area, the tributaries that drain approximately 700 km^2 of the watershed and from the diffused groundwater input throughout the course of the river (Kogovšek and Petrič 2002). The Višnjica and Prečna tributaries (sampling points No. 3 and 14, respectively; Table 1) drain mostly alluvial deposits and are the only non-karst streams in the watershed (Buser and Cajhen 1965).

In the watershed, a continental climate prevails. Hydrological and climatic characteristics during the study period (2008–2010) are summarised in Table 1. Mean annual temperatures in the watershed were between 10 and 12 °C. The average annual amount of precipitation (1971–2000) in the area is 1,147 mm (Frantar 2008). During the sampling period, the precipitation amounted to 1,115, 1,070 and 1,340 mm in 2008, 2009 and 2010, respectively. The precipitation was almost evenly distributed throughout the year, but was nevertheless higher during the summer (monthly average 350 mm through downpours and storms) than in winter (average 234 mm). The discharge regime in the Krka River is of Dinaric pluvial–nival type, with the highest discharge in spring and autumn, and the lowest in summer (Frantar 2008). The lowest average discharge of 18.9 m^3/s occurred in the summer months, whereas in autumn and winter, similar average discharges were observed (69.5 and 64.1 m^3/s, respectively).

3 Materials and Methods

3.1 Sampling Scheme and Procedures

Water samples from the main stream and major tributaries of the Krka River were collected between November 2007 and November 2010 on 23 sampling campaigns. The sampling locations, 13 in the main stream of the Krka River and 6 in its tributaries, are shown in Fig. 1. Sampling sites were selected on the basis of the spatial distribution of bedrock, tufa barrier occurrence and population density and in the main stream set before and after the confluence with the tributaries. Where possible, the water samples were collected in the channel centre below the water surface, mostly from road bridges. If access was difficult, the water samples were taken as far as possible from the river bank.

Water samples were collected for major ion analysis (Ca^{2+}, Mg^{2+}), alkalinity, dissolved organic carbon (DOC) and stable isotopic composition of dissolved inorganic carbon ($\delta^{13}C_{DIC}$) and particulate organic carbon ($\delta^{13}C_{POC}$). Samples for major ion analysis were filtered through 0.45-μm pore-size filters with SFCA membranes, then poured into 60 mL HDPE bottles (Nalgene, USA) and acidified with Suprapur HNO_3 acid (Merck, Germany) until the pH was below 2. 12 mL aliquots of water samples for $\delta^{13}C_{DIC}$ analyses were filtered through 0.20-μm pore-size glass-filters with SFCA membranes to suppress bacterial activity and stored in glass septum vials (Labco Ltd., UK) filled with no headspace.

Table 1 Hydrological characteristics of the Krka River watershed

Sampling points		Coordinates		Drainage area[a] (km^2)	Height above sea[a] level (m)	Distance from the spring (km)
Krka River						
1	Gradiček (spring)	N 45°53′22.98″	E 14°46′18.41″		283	0.0
4	Krka	N 45°53′12.24″	E 14°46′4.89″	321	272	1.7
5	Zagradec	N 45°53′19.39″	E 14°46′59.64″		251	8.0
7	Vrhovo	N 45°52′57.26″	E 14°46′54.38″		200	14.5
8	Žužemberk	N 45°51′35.61″	E 14°49′52.32″		194	18.1
9	Dvor	N 45°51′31.24″	E 14°49′48.52″		186	22.2
10	Soteska	N 45°51′1.31″	E 14°53′57.35″	534	173	28.4
13	Straža	N 45°49′46.06″	E 14°55′42.88″		169	34.4
15	Češča vas	N 45°48′35.78″	E 14°57′44.78″	1,313	168	39.1
16	Otočec	N 45°46′44.69″	E 15° 1′8.88″		165	51.5
17	za Otočcem	N 45°45′35.16″	E 15° 2′7.32″		164	53.0
18	Kostanjevica na Krki	N 45°45′36.68″	E 15° 3′19.65″	2,238	150	76.2
19	Velike Malence	N 45°46′51.72″	E 15° 4′34.00″	2,346	143	95.0
Krka River tributaries						
2	Poltarica	N 45°47′43.80″	E 15° 7′17.42″		282	0.5
3	Višnjica	N 45°47′41.73″	E 15° 7′36.80″	76	274	0.9
6	Globočec	N 45°49′57.92″	E 15°13′19.85″		252	8.5
11	Radešca	N 45°50′16.97″	E 15°14′16.17″	287	171	30.8
12	Sušica	N 45°50′53.90″	E 15°25′3.98″	35	174	31.9
14	Temenica (Prečna)	N 45°53′34.27″	E 15°35′9.40″	294	168	38.9

[a] Data obtained from Environmental Agency of the Republic of Slovenia (http://www.arso.gov.si/vode/podatki/)

All water samples were stored at 4 °C until analysis. Alkalinity and $\delta^{13}C_{DIC}$ values of water samples were measured within 24 h of sample collection. 3-L water samples were collected in pre-washed HDPE bottles for particulate organic carbon (POC) analyses.

3.2 Field and Laboratory Analysis

Temperature, pH and electric conductance (EC) were measured on site using a WTW 340 I pH/Cond meter. Replicate measurements produced an analytical error (1σ) of ± 0.1 °C for temperature, ±0.01 unit for pH and ±0.5 % for conductivity. The pH and EC electrodes were calibrated using 7.00 and 9.21 pH buffer solutions (Mettler Toledo, Ohio, USA) for pH and KCl solutions of 200 and 500 µS/cm for conductivity.

The alkalinity was determined by Gran titration using 0.01 M HCl (Gieskes 1974). The analytical error estimated by replicate measurements of water samples was determined to be less than 5 %. Major ion concentrations (Ca^{2+}, Mg^{2+}) were determined using a Jobin–Yvon Horiba ICP-OES at the University of Michigan (samples collected in 2008) and a PerkinElmer Optima 5300 DV ICP-OES instrument at the University of Arizona (samples collected in 2009 and 2010). In both cases, the analytical precision was estimated to be ±2 %, determined by multiple analyses of standards. Dissolved organic carbon (DOC) content was determined using Teledyne Tekmar TOC/TN analyser at the National Institute of Chemistry (Slovenia). The analytical precision was ±2 %.

3.2.1 Stable Isotope Analysis

The carbon isotopic composition of DIC ($\delta^{13}C_{DIC}$) in water samples collected during 2008 was determined using a Europa Scientific 20-20 IRMS with an ANCA-TG preparation module, while samples collected in 2009 and 2010 were analysed on an IsoPrime mass spectrometer with a MultiFlow Bio module. Water samples were injected into H_3PO_4-containing septum vials, purged with He (6.0) and left for 24 h at room temperature. The evolved CO_2 was then analysed for stable carbon isotope composition. Standard sample solutions of 4.8 mM Na_2CO_3 (Carlo Erba, Italy, and Fisher Scientific, UK) with $\delta^{13}C_{DIC}$ of −10.8 ‰ and −4.5 ‰ ± 0.2, respectively, were used as working standards. For isotope analysis of POC, 3 L of water was filtered through a pre-combusted GF/F glass filter (Whatman, UK, pore size 0.7 µm) immediately upon arrival at the laboratory. Afterwards, the filters were first treated with 1 M HCl to remove the inorganic carbon fraction and dried at 60 °C for 24 h. $\delta^{13}C_{POC}$ values were determined using a Europa Scientific 20-20 IRMS with an ANCA-SL preparation module at the Jožef Stefan Institute. IAEA CH-3, IAEA CH-6 and IAEA CH-7 standards were used to check the accuracy of the measurements.

Carbonate rocks collected in the watershed ($n = 5$) were crushed to powder and afterwards reacted for 24 h with orthophosphoric acid in He-flushed vials. The CO_2 released was then used for measuring the carbon isotopic composition of carbonates ($\delta^{13}C_{carb}$) using a Europa Scientific 20-20 IRMS with an ANCA-TG preparation module. IAEA CO-1, IAEA CO-9, NBS-18 and NBS-19 were used to calibrate the measurements, with KH-2 as a working standard.

All isotope analyses were performed at the Jožef Stefan Institute. The results of stable isotope analyses are reported in relative δ values in ‰, as the difference in parts per mil of the isotopic ratio $^{13}C/^{12}C$ of the samples from those of the reference materials VPDB (Vienna Pee Dee Belemnite).

CO_2 partial pressure (pCO_2), DIC content and DIC species activity were calculated from the empirical expressions for the equilibrium constants K_{CO2}, K_1 and K_2 (Clark and Fritz 1997) using the measured water temperature, pH and total alkalinity values. The saturation indices (SI) for calcite and dolomite were calculated by definition: $SI_{calcite} = \log([Ca^{2+}][CO_3^{2-}]/K_{calcite})$ and $SI_{dolomite} = \log([Ca^{2+}][Mg^{2+}][CO_3^{2-}]/K_{dolomite})$, where $[Ca^{2+}]$, $[Mg^{2+}]$ and $[CO_3^{2-}]$ are their activities in aqueous solution and K is the solubility product of calcite and dolomite, respectively. All the calculations were performed using the hydrogeochemical computer software PHREEQC v.2 (Parkhurst and Appelo 1999), using the PHREEQC database. The correlation coefficients presented are based on Pearson Product Moment correlations, significant at $p < 0.05$, unless otherwise stated.

4 Results

Physicochemical parameters, major solute chemistry, DIC and DOC concentrations and stable isotope composition of DIC are presented as ranges in Table 2 (a complete data set is provided in Supplementary Table 2), and Figs. 2 and 3. The major solute composition of the Krka River and its tributaries is dominated by Ca^{2+}, Mg^{2+} and HCO_3^- ions. In the main stream, Ca^{2+} concentrations ranged from 1.44 to 1.97 mM (average 1.71 ± 0.12 mM; where ± applies to 1σ) without any noticeable seasonal or spatial differences (Fig. 2A–D). In contrast, Mg^{2+} content, ranging from 0.42 to 1.26 mM (average 0.74 ± 0.18 mM), decreased downstream until sampling point 9 and remained fairly stable thereafter (Fig. 2E–H). In comparison to river water, the Ca^{2+} concentrations were slightly higher in the tributaries during all seasons, whereas the Mg^{2+} content was lower. The Ca^{2+} content was the highest in those that drain limestone bedrock (i.e. sampling points 6 and 14, Fig. 1), whereas Mg^{2+} content was the highest in the Višnjica tributary (average 1.12 ± 0.23 mM) that drains alluvial deposits. The Mg^{2+}/Ca^{2+} molar ratios varied from 0.26 to 0.71 (average 0.44 ± 0.11) in the main stream and from 0.12 to 0.80 mM (average 0.35 ± 0.17 mM) in the tributaries (Fig. 2I–L).

Water temperatures in the Krka River ranged from 3.0° in winter to 24.3 °C in summer (average 11.6 ± 3.7 °C). The water pH values varied from 7.1 to 8.5, with a mean value of 7.9. pH was the lowest in the headwaters. Only slight seasonal changes were observed, but pH was up to 0.2 units lower in the warm part of the year (Fig. 3A–D). Electrical conductivity (EC) in stream water samples ranged from 364 to 542 µS/cm (average 424 µS/cm) and decreased downstream. Similar EC values were found in tributaries draining carbonates, whereas in tributary draining alluvial deposits (sampling point 3, Fig. 1), the EC reached up to 656 µS/cm. On the temporal scale, the highest EC values were measured in autumn and winter.

Seasonal variations of total alkalinity are shown in Fig. 3I–L. Speciation calculations identified HCO_3^- as the most abundant dissolved carbonate species, accounting for up to 95 % of DIC. The alkalinity ranged from 3.81 to 5.26 mM (average 4.53 ± 0.31 mM) in the main stream and from 3.73 to 5.79 mM (average 4.50 ± 0.46 mM) in the tributaries.

The calculated partial pressure of surface water CO_2 (pCO_2) in the headwaters was the lowest during spring (average 6,300 ppm) and increased to 17,800 ppm in autumn. pCO_2 concentrations in the main stream varied from 720 to 8,400 ppm (average 2,400 ± 1,300 ppm) and showed minor seasonal changes. pCO_2 generally increased during summer and autumn and markedly decreased in winter and spring (Fig. 3E–H).

Dissolved organic carbon (DOC) concentrations ranged from 0.02 to 0.40 mM (average 0.17 ± 0.08 mM). Concentrations in the tributaries were generally lower than in the main

Table 2 Ranges of chemical and isotopic data for the Krka River watershed in the sampling period from 2008 to 2010; data in parenthesis indicate average values; a complete data set is provided in Supplementary Table 2

Date of sampling	Location	Discharge (m^3/s)	T (°C)	pH	EC (µS/cm)	Total Alkalinity (mM)	DIC (mM)	DOC (mM)
Spring								
4/25/2008	River	48.4	10.8–12.3 (11.6)	7.60–8.20 (7.93)		4.03–4.71 (4.39)	3.61–4.79 (4.20)	0.17–0.30 (0.23)
	Tributaries	0.5–6.1 (3.5)	10.8–12.4 (11.5)	7.50–8.30 (7.85)		3.91–5.79 (4.52)	3.89–5.73 (4.46)	0.17–0.40 (0.24)
5/12/2009	River	24.8	11.5–18.3 (14.6)	7.57–8.37 (8.11)	387–469 (428.3)	3.95–4.71 (4.39)		
	Tributaries	0.2–2.1 (1.5)	10.0–17.2 (13.1)	7.43–8.17 (7.79)	371–542 (430)	3.73–4.52 (4.17)		
4/3/2010	River	79.0	9.4–11.5 (10.1)	7.69–8.39 (8.09)	379–442 (416)	3.81–4.81 (4.25)		
	Tributaries	0.6–9.5 (5.3)	9.4–11.3 (10.3)	7.57–8.35 (7.90)	364–537 (426)	3.76–5.23 (4.25)		
Summer								
8/12/2008	River	20.2	13.6–19.9 (16.2)	7.22–8.32 (8.00)	409–489 (443)	4.17–4.61 (4.33)		
	Tributaries	0.2–2.7 (1.3)	10.3–19.9 (14.4)	7.14–7.99 (7.54)	425–534 (466)	4.01–5.45 (4.51)		
7/6/2009	River	16.3	13.0–21.6 (16.6)	7.54–8.28 (8.02)	427–493 (454)	4.30–4.96 (4.58)		
	Tributaries	0.4–2.3 (1.6)	12.1–24.3 (15.4)	7.37–7.80 (7.64)	417–548 (459)	4.20–4.81 (4.47)		
8/14/2010	River	16.3	13.2–21.8 (16.9)	7.30–8.38 (7.99)	388–494 (450)	4.27–4.77 (4.50)		
	Tributaries	0.01–1.4 (0.70)	10.4–18.2 (13.8)	7.36–7.77 (7.55)	411–465 (445)	4.11–4.76 (4.44)		
Autumn								
10/7/2008	River	12.7	11.7–13.2 (12.5)	7.31–8.40 (8.06)	444–518 (481)	4.30–5.26 (4.78)	4.64–5.86 (5.11)	0.05–0.40 (0.18)
	Tributaries	0.02–1.5 (0.97)	10.6–15.8 (12.6)	7.34–8.23 (7.71)	428–543 (463)	3.87–5.52 (4.63)	4.32–5.70 (5.07)	0.04–0.19 (0.12)
12/2/2009	River	42.8	9.2–10.4 (9.7)	7.46–8.22 (7.91)	443–496 (475)	4.49–5.13 (4.83)		
	Tributaries	0.1–9.5 (4.5)	9.0–10.6 (9.8)	7.38–7.94 (7.70)	430–542 (476)	4.31–5.17 (4.80)		
09.11.2010	River	88.1	7.5–9.5 (8.5)	7.21–7.96 (7.75)	417–492 (460)	4.02–4.69 (4.41)		
	Tributaries	4.0–12.7 (8.9)	8.0–9.8 (9.1)	7.24–7.86 (7.53)	409–559 (453)	4.06–5.27 (4.43)		
Winter								
1/24/2008	River	25.6	7.0–9.8 (8.0)	7.26–8.28 (7.91)	450–534 (491)	4.00–4.58 (4.30)	4.08–4.85 (4.37)	0.02–0.91 (0.37)
	Tributaries	0.04–3.1 (1.9)	3.0–9.7 (7.8)	7.10–7.96 (7.69)	438–656 (505)	3.91–5.34 (4.40)	4.15–5.47 (4.63)	0.10–0.80 (0.34)
3/3/2009	River	41.1	8.0–10.5 (9.4)	7.66–8.34 (8.03)	436–509 (475)	4.63–5.00 (4.78)		
	Tributaries	0.2–2.8 (1.9)	8.0–12.1 (9.9)	7.40–8.29 (7.73)	400–582 (467)	4.32–4.92 (4.58)		
2/9/2010	River	37.9	3.4–8.1 (6.2)	7.62–8.44 (8.18)	186–522 (468)	4.52–5.12 (4.79)		
	Tributaries	0.2–6.5 (3.3)	5.5–10.3 (8.5)	7.50–8.52 (7.86)	440–618 (504)	4.19–5.60 (4.80)		

Table 2 continued

Date of sampling	Location	Ca^{2+} (mM)	Mg^{2+} (mM)	δ^{13}C-DIC (‰)	δ^{13}C-POM (‰)	log pCO_2	SI calcite	SI dolomite
Spring								
4/25/2008	River	1.50–1.81 (1.63)	0.48–0.89 (0.63)	−12.9 to −11.9 (−12.2)		−2.8 to −2.2 (−2.6)	0.2–0.8 (0.5)	−0.1 to 1.2 (0.6)
	Tributaries	1.60–1.87 (1.73)	0.25–1.24 (0.60)	−13.2 to −11.5 (−12.5)		−2.9 to −2.2 (−2.5)	0.1–1.0 (0.5)	−0.2 to 1.8 (0.4)
5/12/2009	River	1.63–1.97 (1.72)	0.54–1.00 (0.72)	−13.1 to −12.0 (−12.6)		−3.0 to −2.2 (−2.8)	0.2–1.0 (0.8)	0.1–1.7 (1.1)
	Tributaries	1.69–1.92 (1.80)	0.23–1.33 (0.60)	−14.4 to −12.3 (−13.2)		−2.8 to −2.1 (−2.5)	0.1–0.8 (0.4)	−0.5 to 1.5 (0.3)
4/3/2010	River	1.44–1.77 (1.57)	0.42–1.77 (1.57)	−13.0 to −11.8 (−12.4)	−31.4 to −26.8 (−30.3)	−3.1 to −2.3 (−2.8)	0.3–0.92 (0.6)	0.1–1.5 (0.7)
	Tributaries	1.49–1.83 (1.66)	0.23–1.16 (0.54)	−13.9 to −12.0 (−12.9)	−29.6 to −25.0 (−27.8)	−3.0 to −2.3 (−2.6)	0.1–1.0 (0.5)	−0.4 to 1.7 (0.3)
Summer								
8/12/2008	River	1.61–1.90 (1.77)	0.58–0.87 (0.73)	−14.2 to −12.5 (−13.4)		−3.0 to −1.9 (−2.7)	−0.2 to 1.0 (0.7)	−0.6 to 1.7 (0.9)
	Tributaries	1.87–2.13 (2.03)	0.32–0.67 (0.51)	−15.6 to −12.0 (−13.8)		−2.5 to −1.8 (2.2)	−0.2 to 0.4 (0.1)	−0.9 to 0.2 (−0.4)
7/6/2009	River	1.56–1.71 (1.66)	0.65–1.09 (0.79)	−11.7 to −10.7 (−11.1)		−2.9 to −2.2 (−2.7)	0.2–1.0 (0.7)	0.2–1.7 (1.1)
	Tributaries	1.64–1.91 (1.83)	0.37–1.01 (0.64)	−12.8 to −8.8 (−11.6)		−2.4 to −2.0 (−2.3)	0.0–0.6 (0.4)	−0.4 to 0.9 (0.2)
8/14/2010	River	1.46–1.55 (1.51)	0.58–0.93 (0.73)	−12.5 to −11.2 (−11.7)		−3.0 to −1.9 (−2.6)	−0.1 to 1.1 (0.6)	−0.4 to 1.8 (1.0)
	Tributaries	1.29–1.81 (1.65)	0.28–0.88 (0.58)	−13.2 to −11.4 (−12.2)		−2.5 to −2.0 (−2.2)	0.0–0.4 (0.2)	−0.6 to 0.2 (−0.1)
Autumn								
10/7/2008	River	1.75–1.89 (1.82)	0.74–1.26 (0.98)	−13.5 to −11.2 (−12.1)		−3.0 to −1.9 (−2.7)	0.0–1.1 (0.7)	−0.2 to 1.9 (1.1)
	Tributaries	1.89–2.00 (1.96)	0.58–0.89 (0.79)	−14.2 to 9.5 (−12.6)		−2.8 to −2.0 (−2.4)	0.0–0.5 (0.3)	−0.4 to 0.4 (0.1)
12/2/2009	River	1.68–1.95 (1.81)	0.56–1.02 (0.76)	−13.4 to −12.0 (−12.6)		−2.8 to −2.1 (−2.5)	0.1–0.9 (0.6)	−0.1 to 1.4 (0.6)
	Tributaries	1.88–2.10 (1.98)	0.28–0.99 (0.63)	−14.2 to −12.5 (−13.4)		−2.6 to −2.0 (−2.3)	0.1–0.6 (0.4)	−0.6 to 0.9 (0.1)
09/11/2010	River	1.60–1.95 (1.75)	0.47–0.93 (0.68)	−13.1 to −12.4 (−12.7)	−28.9 to −27.5 (−28.1)	−2.6 to −1.9 (−2.4)	−0.3 to 0.6 (0.3)	−0.9 to 0.7 (0.1)
	Tributaries	1.68–1.99 (1.82)	0.35–1.10 (0.62)	−13.9 to −12.6 (−13.3)	−29.6 to −26.6 (−28.1)	−2.5 to −1.9 (−2.2)	−0.2 to 0.5 (0.2)	−0.9 to 0.7 (−0.3)
Winter								
1/24/2008	River			−12.6 to −11.3 (−12.0)		−3.0 to −1.9 (−2.6)		
	Tributaries			−13.5 to −11.1 (−12.6)		−2.6 to −1.8 (−2.4)		
3/3/2009	River	1.62–1.91 (1.77)	0.55–1.10 (0.77)	−13.5 to −12.1 (−12.7)		−3.0 to −2.3 (−2.7)	0.2–0.9 (0.63)	0.2–1.5 (0.8)
	Tributaries	1.45–2.05 (1.75)	0.44–1.39 (0.71)	−14.2 to −12.2 (−13.4)		−2.9 to −2.1 (−2.4)	0.0–0.9 (0.3)	−0.5 to 1.5 (0.2)
2/9/2010	River	1.66–1.82 (1.75)	0.61–1.00 (0.76)	−13.0 to −11.3 (−12.2)		−3.1 to −2.3 (−2.8)	0.2–1.0 (0.7)	0.1–1.6 (0.9)
	Tributaries	1.83–1.96 (1.89)	0.28–1.22 (0.67)	−13.9 to −11.2 (−12.7)		−3.1 to −2.1 (−2.5)	0.2–1.1 (0.5)	−0.3 to 1.9 (0.4)

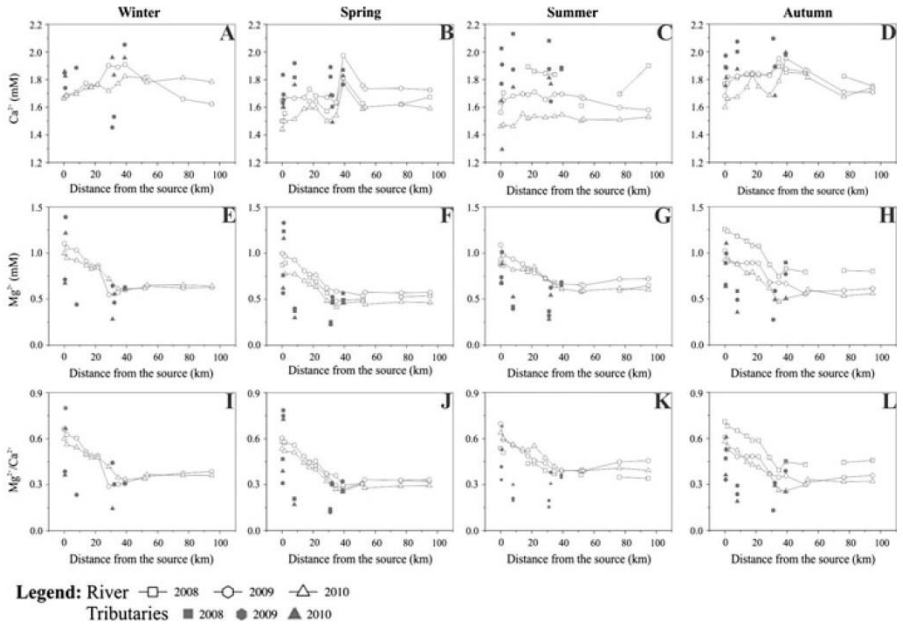

Fig. 2 Seasonal variation in Ca^{2+} (**A–D**) and Mg^{2+} (**E–H**) contents, and the Mg^{2+}/Ca^{2+} molar ratios (**I–L**) in the main stream of Krka River watershed

channel and ranged from 0.04 to 0.23 mM. Lowest concentrations were found in winter and increased during spring.

$\delta^{13}C$ values of DIC in stream water ranged from −14.2 to −10.7 ‰ with an average value of −12.3 ± 0.7 ‰. $\delta^{13}C_{DIC}$ values were the lowest in the headwaters and generally increased downstream for 0.1 ‰ in summer to 2.4 ‰ in autumn (Fig. 3M–P). In 2009 and 2010, $\delta^{13}C_{DIC}$ values were the lowest during spring and autumn and increased in summer. The seasonal pattern in 2008 was slightly different; the lowest $\delta^{13}C_{DIC}$ values were found in summer (average −12.0 ‰) and the highest in the winter. $\delta^{13}C_{DIC}$ values of water samples collected from tributaries followed the same seasonal pattern and ranged from −15.6 to −8.8 ‰ (average −12.9 ± 1.6 ‰).

5 Discussion

5.1 Carbonate Weathering Input

The geochemistry of surface waters in the Dinaric karst is dominated by carbonate mineral weathering (Kanduč et al. 2007; Szramek et al. 2011). Szramek et al. (2011) also showed that while pollution sources from agriculture, industry and atmospheric depositions contribute ions to the studied karstic watersheds, the total contribution to the streams is minimal and can be considered negligible.

Dissolution of calcite and dolomite produces waters with a molar ratio of $(Ca^{2+}+Mg^{2+})$: HCO_3^-=1:2 (Eqs. 1 and 2):

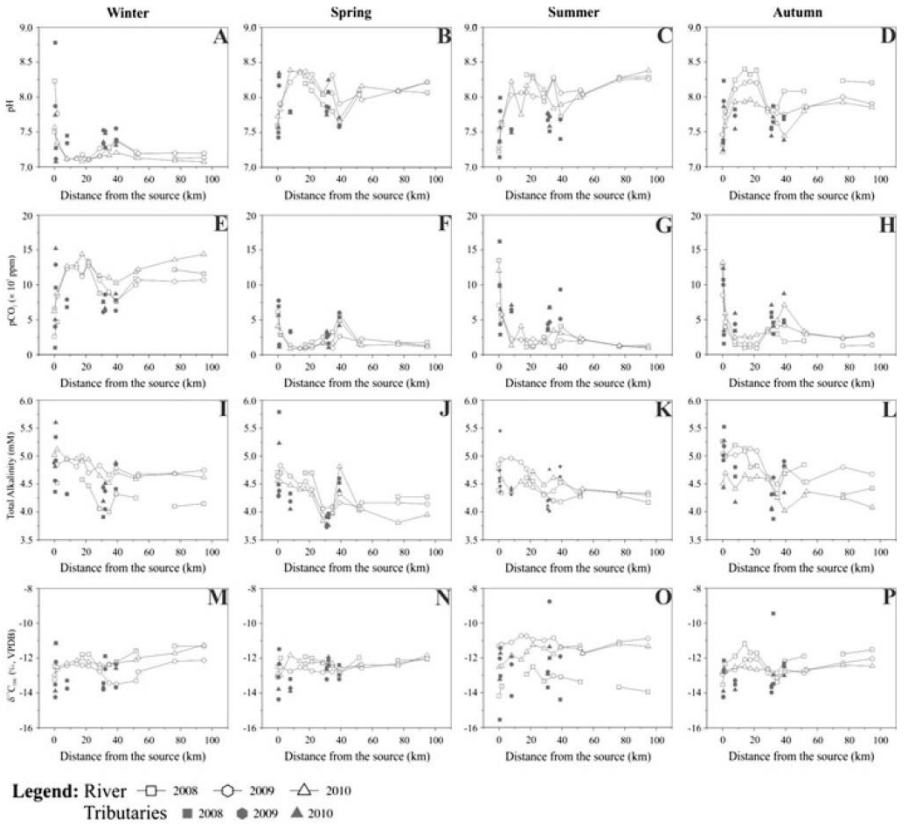

Fig. 3 Seasonal variation in pH (**A–D**), pCO_2 (**E–H**), total alkalinity (**I–L**) and $\delta^{13}C_{DIC}$ (**M–P**) versus distance from the source in the main stream of the Krka River

$$\text{Calcite} \quad CaCO_3 + H_2CO_3 \leftrightarrow Ca^{2+} + 2HCO_3^- \tag{1}$$

$$\text{Dolomite} \quad Ca_xMg_{1-x}CO_3 + H_2CO_3 \leftrightarrow xCa^{2+} + (1-x)Mg^{2+} + 2HCO_3^- \tag{2}$$

The weathering of dolomite in carbonate watersheds contributes the majority of Mg^{2+} to the river waters, in which the Mg^{2+}/Ca^{2+} and Mg^{2+}/HCO_3^- molar ratios indicate the relative proportions of calcite and/or dolomite dissolution (Szramek and Walter 2004; Williams et al. 2007). Dissolution of calcite produces waters with a Mg^{2+}/Ca^{2+} molar ratio of less than 0.1, 0.33 in the case of congruent dissolution of calcite and dolomite, and equal to 1 if only dolomite is dissolving (Szramek et al. 2011). On a mass basis, dissolution of dolomite equal to calcite yields a Mg^{2+}/HCO_3^- ratio of 0.125 and a ratio of 0.08 and 0.16 would indicate dissolution of dolomite of half or twice that of calcite, respectively (Williams et al. 2007).

Analysed waters in the Krka plot close to or above the carbonate dissolution line (Fig. 4A). A low $(Ca^{2+} + Mg^{2+})/HCO_3$ ratio (<0.5) is a result of either HCO_3^- enrichment or $Ca^{2+} + Mg^{2+}$ depletion by cation exchange, whereas an excess of Ca^{2+} and Mg^{2+} ions over HCO_3^- could be attributed to the dissolution of carbonates by sulphuric acid (Hercod et al. 1998; Williams et al. 2007). However, in watersheds dominated by

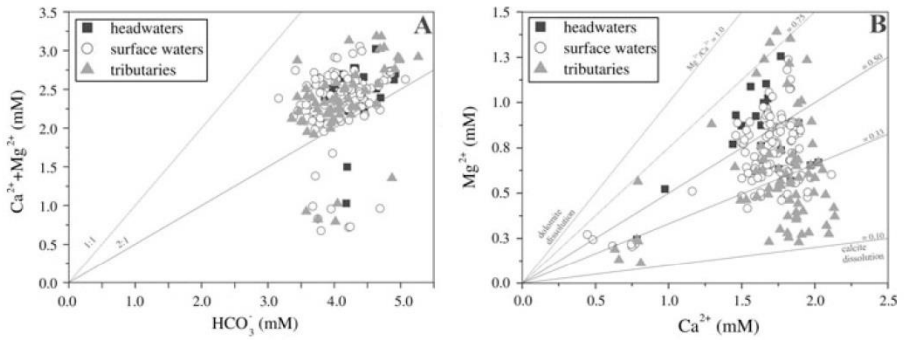

Fig. 4 **A** Plot of HCO_3^- versus $Ca^{2+} + Mg^{2+}$ for the Krka River watershed. The $2HCO_3^-$: $1(Ca^{2+} + Mg^{2+})$ relationship is shown as a line (2:1). **B** Ca^{2+} versus Mg^{2+} for the Krka River watershed; the *lines* represent Mg^{2+}/Ca^{2+} ratios indicating dolomite and/or calcite dissolution

carbonate bedrock, the contribution of sulphuric acid to the overall weathering can often be lost in the background of carbonic acid weathering (Szramek et al. 2011). The waters in the Krka have an average $(Ca^{2+} + Mg^{2+})/HCO_3^-$ ratio of 0.57 ± 0.1 mM indicating dissolution of carbonate rocks predominantly by carbonic acid.

The relative proportions of Mg^{2+} and Ca^{2+} in the Krka waters are shown in Fig. 4B. Relatively high average Mg^{2+}/Ca^{2+} and Mg^{2+}/HCO_3^- molar ratios of 0.44 and 0.22, respectively, demonstrate significant contribution of dolomite dissolution in the watershed. The tributaries drain predominantly limestone areas resulting in Mg^{2+}/Ca^{2+} ratios ranging from 0.12 to 0.32. Higher Mg^{2+}/Ca^{2+} (average 0.68) was determined in the non-karstic Višnjica tributary, draining alluvial deposits.

The proportion of dolomite dissolution is higher in the headwaters and upper reaches ($Mg^{2+}/Ca^{2+} \sim 0.71$) than in the lower reaches ($Mg^{2+}/Ca^{2+} \sim 0.34$), which is consistent with the dominance of dolomite bedrock in the north-western part of the watershed. The Mg^{2+}/Ca^{2+} and Mg^{2+}/HCO_3^- ratios decrease downstream, indicating the "loss" of Mg^{2+} but not of Ca^{2+} and HCO_3^-. Such decrease, especially in the lower reaches, might result from an additional source of waters dissolving mostly calcite, and/or in-stream carbonate precipitation (Szramek and Walter 2004; Williams et al. 2007), which is evident from tufa occurrence in the river. Since the decrease in Mg^{2+} concentrations is not accompanied by a significant decrease in HCO_3^-, the influence of in-stream carbonate precipitation is minor without a significant effect on the carbonate mass balance in the Krka waters. Thus, the observed Mg^{2+}/Ca^{2+} and Mg^{2+}/HCO_3^- variations can be attributed to the input of Mg-poor water from the tributaries and diffusive groundwater recharge (Kogovšek and Petrič 2002). These waters are obviously depleted in Mg^{2+} compared to the groundwater discharging at the main spring, which is reasonable since they drain predominantly limestone areas on the southern flanks of the watershed.

5.2 Carbonate Weathering Intensity and Associated CO_2 Consumption

The chemical weathering rates of a drainage basin can be estimated by combining the water chemistry, hydrological and surface area data available for the basin (Galy and France-Lanord 1999). The rate of carbonate weathering (CWR) for the Krka River watershed was calculated using an approach adopted from Roy et al. (1999) and is based on two assumptions: (1) Ca^{2+}, Mg^{2+} and HCO_3^- concentrations are not influenced by local

anthropogenic pollution, and (2) during carbonate dissolution by carbonic acid, half the amount of HCO_3^- is derived from chemical weathering and the other half from atmospheric/soil CO_2:

$$\mathrm{CWR} = (\mathrm{Ca}^{2+} + \mathrm{Mg}^{2+} + 0.5 \times \mathrm{HCO}_3^-) \times \text{discharge/drainage area} \quad (3)$$

The data from sampling site 18, where water discharge data were available (Table 1), represent the dissolved load from chemical weathering of 85 % of the Krka basin. The highest weathering rates were calculated for autumn (up to 24 t/km^2/month) and the lowest in summer (up to 5.7 t/km^2/month). The calculated CWR ranged from 84 in 2008 to 179 t/km^2/year in 2010 (average 121 t/km^2/year), similar to reported CWR values from other karstic watersheds [133 t/km^2/year (Li et al. 2010) and from 117.1 to 394.9 t/km^2/year (Sun et al. 2010)] or sedimentary basins (109 t/km^2/year for the Rhone River and 126 t/km^2/year for the Po River reported in Gaillardet et al. 1999). On a global scale, the calculated CWR values for the Krka are 3–7 times higher than the mean world CWR value of 24 t/km^2/year (Gaillardet et al. 1999). Such difference is explained by the predominance of carbonate bedrock and high runoff in the case of our study.

Assuming that during carbonate dissolution by carbonic acid, only half the amount of HCO_3^- is derived from atmospheric/soil CO_2; therefore, the total CO_2 (R_{CO2}) consumed by rock weathering can be calculated as:

$$R_{CO2} = 0.5 \times \mathrm{HCO}_3^- \times \text{discharge/drainage area} \quad (4)$$

The average annual atmospheric CO_2 consumption by carbonate weathering was estimated to be 12×10^5 mol/km^2/year at the outflow of the Krka River (sampling point 18; Fig. 1), reasonably close to the estimate of 8×10^5 mol/km^2/year for world-scaled CO_2 consumption (Meybeck 1987).

5.3 Seasonal Variations in the Carbonate System of the Krka River

Low DOC content ranging from 0.02–0.40 mM, and high alkalinity (3.30–5.71 mM, Fig. 3I–L) and pCO_2 (720–17,800 ppm; Fig. 3E–H) typify water in the Krka River watershed that has been extensively influenced by interaction of soil waters with the carbonate bedrock. The spatial and temporal variability of DIC, pCO_2 and $\delta^{13}C_{DIC}$, and the basic processes that affect carbon of water in the Krka are discussed below in the context of determining sources of carbon and processes controlling the carbon transfer.

5.3.1 Controls on Carbonate Saturation States

The thick soil zone in the Krka River watershed (on average over 70 cm thick; Repe 2004) provides an ample supply of CO_2 necessary for carbonate dissolution. A mean soil pCO_2 in the watershed was estimated using Eq. (5) from Brook et al. (1983) and considering a mean annual evapotranspiration (AET) of 765 mm (Frantar 2008):

$$\log(pCO_2) = -3.47 + 2.09(1 - e^{-0.00172 \times \mathrm{AET}}) \quad (5)$$

The calculated soil pCO_2 was 11,500 ppm, which is similar to the highest soil CO_2 concentrations (11,406 ppm) estimated from the CO_2 production rates determined by soil respiration measurements in a karst area (Čater and Ogrinc 2011) located in the western part of Slovenia. Concentrations of CO_2 calculated in the Krka ranged from 720 to 17,800 ppm and were always above the atmospheric CO_2 level (380 ppm, Yao et al. 2007).

The pCO_2 in the headwaters was the highest in summer and autumn (average 11,500 ppm) reflecting high soil CO_2 productivity in the watershed and implying that the headwaters are fed only by water that was extensively in contact with soil CO_2. Distinctive temporal and spatial differences in the pCO_2 pattern were observed between the upper and lower reaches most probably due to different processes influencing the pCO_2 evolution in the stream. Constantly higher pCO_2 levels ($\sim$2,000 ppm) were calculated for the upper reaches, whereas in the lower reaches, pCO_2 levels generally decreased for 500–1,000 ppm, respectively. An unclear seasonal pattern was observed for the stream water. In general, the highest pCO_2 were calculated for autumn and summer, probably due to more intensive degradation of organic matter in the river (Dever et al. 1983), whereas high pCO_2 levels in winter result from greater solubility of CO_2 at low temperatures (Atkins 1994).

The headwaters of the Krka are close to or below equilibrium with respect to both calcite and dolomite, which means that calcite and dolomite dissolve in the headwaters (Fig. 5A). Decreasing pCO_2 levels indicate CO_2 loss downstream, resulting in increase in the carbonate saturation state in stream water. This leads to carbonate back precipitation in surface waters; however, calcite precipitation from surface waters requires a high oversaturation of $SI_{calcite}$ >0.6 (Merz-Preiß and Riding 1999), which is likely to occur in the Krka in summer and autumn. However, the trend of increasing Ca^{2+} concentrations downstream and the weak correlation between Ca^{2+} and DIC imply that CO_2 losses in the Krka River could not be attributed only to calcite precipitation.

5.3.2 Carbon Sources and Controls on $\delta^{13}C_{DIC}$ in the Krka Watershed

Calculated DIC concentrations in the Krka River and its tributaries ranged from 3.3 to 5.9 mM (average 4.7 ± 0.40 mM) and were the lowest during spring, most likely due to snowmelt, when the water discharge was high (up to 80 m^3/s). The $\delta^{13}C_{DIC}$ values ranged from −15.6 to −8.8 ‰ (Table 2), reflecting variable contributions of different carbon sources (soil CO_2 and carbonate dissolution) and the impacts of processes such as CO_2 evasion, photosynthesis and respiration that fractionate carbon isotopic composition (Telmer and Veizer 1999; Barth 2003; Doctor et al. 2008).

The carbon isotopic composition of soil CO_2 depends on the type of vegetation in the watershed area (Finlay and Kendall 2007) and fractionation processes during CO_2 transfer through the soil horizon (Cerling 1991). The vegetation in the Krka watershed mostly follows the C_3 photosynthetic pathway, characterised by $\delta^{13}C$ values between −34.8 and −29.2 ‰ (average −31.6 ± 1.5 ‰; Kanduč et al. 2007). The presence of C_4 plants with $\delta^{13}C$ values of −13 ‰ (Finlay and Kendall 2007) in the area is minor; thus, we consider its contribution to the soil carbon imprint negligible. During CO_2 transfer through the soil horizon, an isotopic shift occurs caused by diffusional fractionation between $^{12}CO_2$ and $^{13}CO_2$, leading to ^{13}C-enrichment by up to +4.4 ‰ relative to the organic source material (Cerling 1991). Consequently, the $\delta^{13}C$ value of soil CO_2 in the Krka watershed would range from −30.8 to −24.8 ‰ (average −27.2 ‰). If DIC in Krka waters would originate solely from respiration CO_2, then at equilibrium with soil CO_2, the $\delta^{13}C_{DIC}$ value of the Krka River would be enriched with ^{13}C by +3.5 to +8.4 ‰ (average +6.1 ‰; Vogel et al. 1970), considering average water temperature of 11.6 °C and average pH of 7.9. Using the calculated enrichment factor, the $\delta^{13}C_{DIC}$ should yield values of −26.9 to −16.4 ‰ (average −21.1 ‰). The isotopic composition of DIC resulting from carbonate rock dissolution depends on whether the dissolution takes place in open or closed conditions (Clark and Fritz 1997). Carbonate mineral dissolution in an open system yields highly depleted $\delta^{13}C_{DIC}$ values due to continual exchange of CO_2 between groundwater and the soil (i.e.

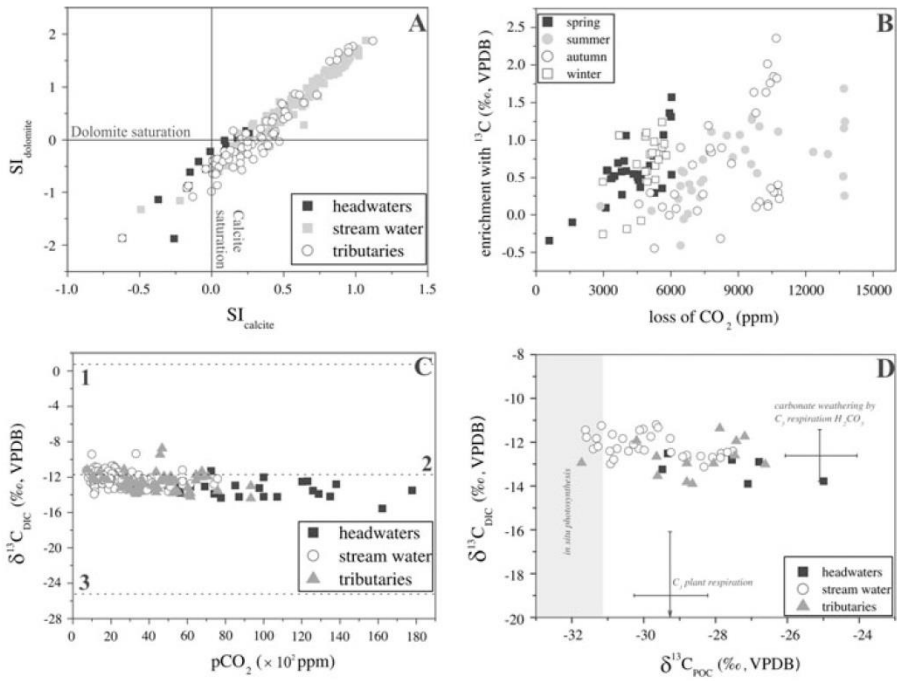

Fig. 5 Variations of the carbonate system in the Krka River watershed: **A** saturation indexes (SI) of headwaters, stream water and tributaries ($SI_{calcite}$ versus $SI_{dolomite}$). The saturation indices (SI) for calcite and dolomite were calculated by definition: $SI_{calcite} = \log([Ca^{2+}][CO_3^{2-}]/K_{calcite})$ and $SI_{dolomite} = \log([Ca^{2+}][Mg^{2+}][CO_3^{2-}]/K_{dolomite})$, where $[Ca^{2+}]$, $[Mg^{2+}]$ and $[CO_3^{2-}]$ are their activities in aqueous solution and K is the solubility product of calcite and dolomite, respectively. **B** Relationship between enrichment of DIC with ^{13}C and loss of CO_2; **C** plot of variation in the $\delta^{13}C_{DIC}$ of water with lines indicating processes occurring in the watershed (*1*—open system DIC in equilibrium with the atmosphere, *2*—non-equilibrium carbonate dissolution by carbonic acid produced from soil zone CO_2 and *3*—open system equilibration of DIC with soil CO_2); **D** plot of $\delta^{13}C_{DIC}$ versus $\delta^{13}C_{POC}$ with indicated processes affecting the carbon in the river

−27.2 ‰ in the Krka watershed). In a closed system, half of the DIC is derived from carbonate dissolution, and hence, DIC is enriched with ^{13}C. In this case, $\delta^{13}C_{DIC}$ values would be between −14.5 and −11.7 ‰ (average −12.9 ‰). However, $\delta^{13}C_{DIC}$ values of the headwaters in the Krka ranged from −15.6 to −11.3 ‰ (average −13.4 ± 0.9 ‰), suggesting that carbonate mineral dissolution in the watershed occurs primarily under open system conditions (Fig. 5D).

The $\delta^{13}C_{DIC}$ values in Krka stream water ranged from −13.9 to −10.7 ‰ (average −12.2 ‰) and increased downstream for 0.1 ‰ in summer to 2.4 ‰ in autumn (Fig. 3M–P). The average magnitude of ^{13}C enrichment of 0.7–0.8 ‰ was similar regardless of season. The downstream enrichment of DIC with ^{13}C was calculated as the difference between $\delta^{13}C_{DIC}$ values of the headwaters and stream water and is positively correlated with the CO_2 loss (Fig. 5B). Losses of CO_2 can be ascribed to several processes such as photosynthesis, CO_2 evasion and authigenic precipitation of carbonate, whereas in situ respiration adds ^{13}C-depleted CO_2 to the water.

Isotopic fractionation during the exchange between aqueous and atmospheric CO_2 in the Krka was calculated to be between 1.3 and 1.4 ‰ using the equilibrium equation from

Vogel et al. (1970). However, rapid CO_2 exchange can result in kinetic isotope fractionation in which the dehydration of HCO_3^- results in ^{13}C-enrichment of 1 ‰ (at pH ~ 2; Zhang et al. 1995) or 14.7 ‰ in open system conditions at 24 °C (pH ~ 8.2; Marlier and O'Leary 1984). In general, the amplitude of enrichment with ^{13}C was the highest in parts with more turbulent water (i.e. at cascades in the upper reaches, Fig. 1), where gas exchange is the most pronounced, implying that CO_2 degassing due to differences in CO_2 levels between river water and the atmosphere significantly affects the isotopic imprint of riverine DIC.

Transformations of organic to inorganic carbon can have a significant influence on riverine $\delta^{13}C_{DIC}$ values (Barth and Veizer 1999; Brunet et al. 2009). Major inputs to the organic carbon pool in rivers are allochtonous (terrestrial vegetation) and autochtonous matter (plankton and detrital organic matter of planktonic origin). The isotopic composition of particulate organic carbon (POC) in the Krka ranged from −31.7 to −25.0 ‰ (average −29.2 ‰). The isotopic composition of phytoplankton was not estimated in this study; however, it can be calculated using measured $\delta^{13}C_{DIC}$ values and the isotopic fractionation of 22.3 ‰ between riverine DIC and phytoplankton (Tan and Strain 1983). Given the average $\delta^{13}C_{DIC}$ value in Krka waters is −12.5 ‰, the expected $\delta^{13}C$ of phytoplankton would be −34.8 ‰. As shown in Fig. 5D, POC in Krka River is ^{13}C-enriched in comparison with the estimated $\delta^{13}C$ values of phytoplankton, indicating that the majority of POC in the river is originally terrestrial debris flushed from the riparian zones. DOC concentrations in the Krka River watershed are low (0.02–0.40 mM) in comparison with other watersheds (e.g. up to 4.3 mM; Brunet et al. 2009), where DOC contributes largely to total dissolved carbon. There was no significant correlation between the $\delta^{13}C_{DIC}$ values and DOC concentrations in our case; therefore, we assume that DOC transformations, either by photosynthesis or respiration, have no significant effect on the overall $\delta^{13}C$ of DIC. Moreover, the degree of enrichment in the watershed during the study period was the highest in autumn (up to 2.4 ‰), whereas in spring and summer, it did not exceed 1.7 ‰. If photosynthesis was a major control on CO_2 loss, then the enrichment would be greatest in spring and summer when photosynthetic activity is highest.

The contribution of in-stream carbonate precipitation to the carbon budget in rivers is hard to estimate. Given the relatively small isotopic fractionations associated with in-stream carbonate precipitation (with $\varepsilon_{CaCO_3-HCO_3}$ of 1.0 ± 0.2 ‰ irrespective of temperature and precipitation rate, Romanek et al. 1992; Jímenez-López et al. 2001), its influence on $\delta^{13}C_{DIC}$ should be minor regardless of its scale (Wachniew 2006), and thus, we conclude that active carbonate precipitation in the Krka does not affect the $\delta^{13}C$ of DIC significantly.

5.4 Carbon Fluxes, CO_2 Degassing and Mass Balance Calculations

Carbon fluxes for the Krka River and its tributaries were calculated as the product of flow volumes and concentrations of DIC and DOC in river water. River discharge data were obtained from the Environmental Agency of the Republic of Slovenia gauge station (sampling site 18, Fig. 1) located about 10 km upstream of the river mouth. The amount of CO_2 degassed was calculated based on a theoretical diffusion model of CO_2 flux following the equation developed by (Broecker 1974):

$$F_{CO_2} = \frac{D}{z} \times (CO_{2(eq)} - CO_2) \quad (6)$$

where D is the CO_2 diffusion coefficient, z is the thickness of the boundary layer at the air–water interface, and $CO_{2(eq)}$ and CO_2 are concentrations of dissolved CO_2 in equilibrium with the atmosphere and calculated CO_2, respectively. D/z is the gas exchange rate representing the height of a water column that will equilibrate with the atmosphere per time unit. The thickness of the boundary layer z depends largely on wind velocity (Broecker 1974) and water turbulence (Holley 1977). In this study, CO_2 fluxes were calculated using a D/z value of 8 and 28 cm/h at low and moderate turbulence conditions (Mook 1970).

The DIC fluxes in the Krka ranged from 3.5×10^9 mol/year in 2008 to 7.0×10^9 mol/year in 2010, depending on discharge. The lowest fluxes were calculated for summer (average 2.0×10^8 mol/month), while higher fluxes were usually observed in spring and autumn due to increased discharge (average 5.4×10^8 mol/month and 5.5×10^8 mol/month, respectively). DOC fluxes can be calculated only for the sampling year 2008 and are estimated to be 2.1×10^8 mol/year. Considering the river surface area of 2.9 km^2 (length of 96 km and a mean width of 30 m), the estimated total diffusive loss of CO_2 ranges from 2.0×10^8 to 3.0×10^8 mol/year. The estimated CO_2 fluxes were in general the highest in autumn (average 2.8×10^7 mol/month) and the lowest in summer (average 1.5×10^7 mol/month). It is important to note that CO_2 degassing estimates are accompanied by uncertainties arising from turbulence of the river water and the groundwater contribution in the downstream sections, and therefore, our estimates of carbon fluxes here represent conservative values.

A simple isotopic mass balance calculation was performed to quantify different sources of DIC at the Krka River in sampling period 2010, considering the sum of tributary inputs and biogeochemical processes in the watershed. As discussed in previous section, the major inputs to the DIC flux (DIC_{RI}) and $\delta^{13}C_{DIC}$ are from tributaries (DIC_{trib}), degradation of organic matter (DIC_{org}), exchange with the atmosphere (CO_2 degassing, DIC_{ex}) and dissolution of carbonates (DIC_{carb}). The inputs can be estimated by:

$$DIC_{RI} = DIC_{trib} - DIC_{ex} + DIC_{org} + DIC_{carb} \tag{7}$$

$$DIC_{RI} \cdot \delta^{13}C_{RI} = DIC_{trib} \cdot \delta^{13}C_{trib} - DIC_{ex} \cdot \delta^{13}C_{ex} + DIC_{org} \cdot \delta^{13}C_{POC} + DIC_{carb} \cdot \delta^{13}C_{carb} \tag{8}$$

DIC_{RI}, DIC_{tri} and DIC_{ex} were calculated as explained above. In Eqs. (2) and (3), the minus sign indicates outgassing of CO_2. The $\delta^{13}C$ values of DIC_{RI} and DIC_{trib} are reported in Table 2, whereas the $\delta^{13}C_{ex}$ value was calculated according to the equation for equilibrium isotope fractionation between atmospheric CO_2 and carbonic acid in water (Zhang et al. 1995), where a $\delta^{13}C$ value of −7.8 ‰ for atmospheric CO_2 was considered (Levin et al. 1987). Considering atmospheric CO_2 as the ultimate source for the CO_2 exchange in the Krka River drainage basin, the isotopic composition of the contribution of equilibration between atmospheric CO_2 and DIC ($\delta^{13}C_{ex}$) would then be +1.6 ‰ in spring, +0.7 ‰ in summer, +1.8 ‰ in autumn and +2.1 ‰ in winter 2010. For $\delta^{13}C_{POC}$ and $\delta^{13}C_{carb}$, average values of −27.2 ‰ and +1.4 ‰ were used in the mass balance equations.

The calculated fluxes for all sampling seasons in 2010 are presented in Table 3. The DIC_{org} and DIC_{carb} values were determined by solving the mass balance equations. The calculated contributions to the average DIC budget from DIC_{trib}:DIC_{ex}:DIC_{org}:DIC_{carb} at the Krka mouth were 21.5:−4.5:37.8:45.3 % in spring, 13.4:−8.3:41.9:52.9 % in summer, 27.0:−3.6:39.7:36.9 % in autumn and 27.9:−2.5:42.4:32.2 % in winter. In all sampling seasons, the most important biogeochemical processes are degradation of organic matter and weathering of carbonates. The latter is predominant in spring and summer, whereas

Table 3 Calculated dissolved inorganic carbon fluxes in 2010 of different factors affecting the DIC at the Krka River mouth (DIC_{RI}): tributaries (DIC_{trib}), degradation of organic matter (DIC_{org}), CO_2 flux to the atmosphere (DIC_{ex}) and dissolution of carbonates (DIC_{carb})

Sampling season	DIC_{trib} (mol/day)	DICex (mol/day)	DIC_{org} (mol/day)	DIC_{carb} (mol/day)	DIC_{RI} (mol/day)
Spring	5.6E+06	−1.2E+06	9.9E+06	1.2E+07	2.6E+07
Summer	8.0E+05	−5.0E+05	2.5E+06	3.2E+06	6.0E+06
Autumn	8.7E+06	−1.2E+06	1.3E+07	1.2E+07 5.8E+06	3.2E+07
Winter	3.8E+06	−3.4E+05	4.4E+06		1.4E+07

degradation of organic matter is more expressed in autumn and winter. In average, the tributaries contribute 25.4 % of inorganic carbon to DIC_{RI}; however, their contribution decreases to 13.4 % in summer due to baseflow conditions in the basin, when groundwater input is the major source of water in the Krka. Kanduč et al. (2007, 2008) found that dissolution of carbonates contributes the highest proportion to riverine DIC in the Sava and Idrijca River watersheds (Slovenia), whereas the contribution of carbon from organic matter degradation is significantly lower leading to more positive $\delta^{13}C_{DIC}$ values. On the contrary, carbonate dissolution and organic matter degradation contribute almost equal proportions to the Krka River inorganic carbon mass balance. Such differences among these watersheds are most likely due to different discharge regimes and higher runoff in Sava and Idrijca River.

The least significant process affecting riverine DIC in the Krka is exchange with atmospheric CO_2 accounting for up to 8.3 % of the contribution to the DIC_{RI}. By comparison, in carbonate-dominated watersheds, the contribution of CO_2 degassing was also found to be minor, i.e., up to 5 % (Shin et al. 2011) and 10 % (Zeng et al. 2010), whereas in silicate watersheds, the contribution to the total carbon flux can be greater, reaching from 30 to 50 % (Telmer and Veizer 1999; Shin et al. 2011).

Amiotte Suchet et al. (2003) reported that watersheds with 20 % of carbonate bedrock were characterised by DIC fluxes from 4.8 to 27.6 t of C/km^2/year, whereas Ferguson et al. (2011) estimated slightly higher DIC fluxes in the predominantly carbonate watershed of the Fly River (Papua New Guinea), concluding that carbon fluxes depend on runoff intensity. Area-normalised DIC fluxes in the Krka ranged from 21 to 42 t of C/km^2/year, which is similar to those reported for the Sava River of 40 t of C/km^2/year (Kanduč et al. 2007). The Krka watershed is approximately 4 times smaller than the Sava watershed, so our estimates of DIC flux emphasise the role of runoff over the watershed scale.

6 Conclusions

The water chemical composition and carbon isotopic composition of dissolved inorganic carbon were used to evaluate the origin and dynamics of carbon and carbonate weathering intensity in a small karstic watershed of Krka River in southeastern Slovenia. The downstream variability of physicochemical parameters and major solute chemistry of the Krka River reflect differences between headwaters and in-stream processes that influence water chemistry downstream.

The major solute composition of the Krka River and its tributaries is dominated by the input of HCO_3^-, Ca^{2+} and Mg^{2+} ions, originating from carbonate rock weathering. The proportions of calcite and/or dolomite dissolution were examined by the Mg^{2+}/Ca^{2+} and

Mg^{2+}/HCO_3^- molar ratios in the water. The Mg^{2+}/Ca^{2+} ratio ranged from 0.24 to 0.71, indicating mixing of waters showing different proportions of calcite and dolomite dissolution. The highest Mg^{2+}/Ca^{2+} ratios were in the headwaters and upper reaches, indicating that weathering of dolomite prevails over calcite in the north-western part of the watershed. Similar variation was observed in the Mg^{2+}/HCO_3^- ratios ranging from 0.05 to 0.30, also indicating a high degree of dolomite dissolution relative to calcite. The CO_2 consumption during weathering was estimated to be 12×10^5 mol/km^2/year, comparable to world-scaled CO_2 consumption. However, on a global scale, the calculated weathering rates for the Krka are 3–7 times higher due to high runoff in the watershed.

Low DOC (0.02–0.40 mM) and high DIC (3.3–5.9 mM) and pCO_2 (up to 17,800 ppm) concentrations characterise Krka River waters influenced by the interaction of soil waters with the carbonate bedrock. According to the calculated pCO_2 levels (up to ten times supersaturated relative to atmospheric pCO_2), the Krka represents a source of CO_2 to the atmosphere during all sampling seasons. In the course of the stream, the pCO_2 levels decrease by up to 10 times in comparison with those at the headwaters, which results in increased saturation states for calcite and dolomite.

Concentrations of CO_2 and DIC in the Krka River were consistently the highest in the headwaters and decreased downstream, whereas the isotopic composition of DIC increased downstream, indicating equilibration with atmospheric CO_2. The biogeochemical processes affecting DIC concentrations and its isotopic composition were quantified by total C and ^{13}C mass balance calculations. The calculations showed that most important processes at the Krka mouth are carbonate dissolution comprising 36.9 % in autumn to 52.9 % in summer, and degradation of organic matter comprising 32.2 % in winter to 41.9 % in summer. The tributaries and exchange of CO_2 with the atmosphere have minor impact on the Krka riverine carbon cycle. The study also confirms that geological composition and degradation of organic matter are the most important processes controlling the biogeochemistry of the carbon in the river.

Acknowledgments This study was financially supported by the Slovenian Research Agency, contract PR-02497 of the Young Researchers Programme, research project J1-9498 and research programme P1-0143. The authors thank Mr. Stojan Žigon and Dr. Martina B. Šturm for analytical support. Special thanks are given to Mr. Anthony Byrne for linguistic corrections and two anonymous reviewers for the critical and constructive comments on the manuscript.

References

Amiotte Suchet P, Probst JL, Ludwig W (2003) Worldwide distribution of continental rock lithology: implications for the atmospheric/soil CO_2 uptake by continental weathering and alkalinity river transport to the oceans. Glob Biogeochem Cy 17:1038–1051. doi:10.1029/2002GB001891

Atekwana EA, Krishnamurthy RV (1998) Seasonal variations of dissolved inorganic carbon and δ13C of surface waters: application of a modified gas evolution technique. J Hydr 205:265–278. doi:10.1016/S0022-1694(98)00080-8

Atkins PW (1994) Physical chemistry. Oxford University press, Oxford

Aucour AM, Sheppard SMF, Guyomar O, Wattelet J (1999) Use of 13C to trace origin and cycling of inorganic carbon in the Rhône river system. Chem Geol 159:87–105. doi:10.1016/S0009-2541(99)00035-2

Barth JAC (2003) Influence of carbonates on the riverine carbon cycle in an anthropogenically dominated catchment basin: evidence from major elements and stable carbon isotopes in the Lagan River (N. Ireland). Chem Geol 200:203–216. doi:10.1016/S0009-2541(03)00193-1

Barth JAC, Veizer J (1999) Carbon cycle in St. Lawrence aquatic ecosystems at Cornwall (Ontario), Canada: seasonal and spatial variations. Chem Geol 159:107–128. doi:10.1016/S0009-2541(99)00036-4

Broecker WS (1974) Chemical oceanography. Harcourt Brace Jovanovich, New York

Brook GA, Folkoff ME, Box EO (1983) A world model of soil carbon dioxide. Earth Surf Process Land 8:79–88. doi:10.1002/esp.3290080108

Brunet F, Gaiero D, Probst JL et al (2005) $\delta^{13}C$ tracing of dissolved inorganic carbon sources in Patagonian rivers (Argentina). Hydrol Process 19:3321–3344. doi:10.1002/hyp.5973

Brunet F, Dubois K, Veizer J et al (2009) Terrestrial and fluvial carbon fluxes in a tropical watershed: Nyong basin, Cameroon. Chem Geol 265:563–572. doi:10.1016/j.chemgeo.2009.05.020

Buser S (1974) Tolmač lista Ribnica, Osnovna geološka karta SFRJ 1: 100 000 (in Slovene)

Buser S, Cajhen J (1965) Osnovna geološka karta SFRJ 1: 100 000, list Ribnica

Čater M, Ogrinc N (2011) Soil respiration rates and $\delta^{13}C(CO_2)$ in natural beech forest (Fagus sylvatica L.) in relation to stand structure. Isotopes Environ Health Stud 47:221–237. doi:10.1080/10256016.2011.578214

Cerling T (1991) Carbon dioxide in the atmosphere: evidence from Cenozoic and Mesozoic paleosols. Am J Sci 291:377–400. doi:10.2475/ajs.291.4.377

Clark ID, Fritz P (1997) Environmental isotopes in hydrogeology. Lewis, New York

Dever L, Durand R, Fontes JC, Vachier P (1983) Etude pedogenetique et isotopique des neoformations de calcite dans un sol sur craie: Caracteristiques et origines. Geochim Cosmochim Acta 47:2079–2090. doi:10.1016/0016-7037(83)90033-9

Doctor D, Kendall C, Sebestyen S et al (2008) Carbon isotope fractionation of dissolved inorganic carbon (DIC) due to outgassing of carbon dioxide from a headwater stream. Hydrol Process 2423:2410–2423. doi:10.1002/hyp.6833

Ferguson PR, Dubois KD, Veizer J (2011) Fluvial carbon fluxes under extreme rainfall conditions: inferences from the Fly River, Papua New Guinea. Chem Geol 281:283–292. doi:10.1016/j.chemgeo.2010.12.015

Finlay JC, Kendall C (2007) Stable isotope tracing of temporal and spatial variability in organic matter sources to freshwater ecosystems. In: Michener R, Lajtha K (eds) Stable isotopes in ecology and environmental science. Blackwell, New York, pp 283–333

Frantar P (2008) Vodna bilanca Slovenije 1971–2000. Water balance of Slovenia 1971–2000. Ministry for Environment and Spatial Planning—Environmental Agency of the Republic of Slovenia, Ljubljana

Gaillardet J, Dupre B, Louvat P, Allegre CJ (1999) Global silicate weathering and CO_2 consumption rates deduced from the chemistry of large rivers. Chem Geol 3–30. doi:10.1016/S0009-2541(99)00031-5

Galy A, France-Lanord C (1999) Weathering processes in the Ganges—Brahmaputra basin and the riverine alkalinity budget. Chem Geol 159:31–60. doi:10.1016/S0009-2541(99)00033-9

Gibbs RJ (1970) Mechanisms controlling world water chemistry. Science 170:1088–1090. doi:10.1126/science.170.3962.1088

Gieskes JM (1974) The alkalinity-total carbon dioxide system in seawater. In: Goldberg ED (ed) Marine chemistry of the sea, vol 5. Wiley, New York, pp 123–151

Hartmann J, Jansen N, Kempe S, Dürr HH (2007) Geochemistry of the River Rhine and the Upper Danube: recent trends and lithological influence on baselines. JESSS 1:39–46

Hercod DJ, Brady PV, Gregory RT (1998) Catchment-scale coupling between pyrite oxidation and calcite weathering. Chem Geol 151:259–276. doi:10.1016/S0009-2541(98)00084-9

Holley EH (1977) Oxygen transfer at the air–water interface. In: Gibbs R (ed) Transport processes in lakes and oceans. Proceedings of the symposium on transport processes in the ocean held at the 82nd Nat. Meet of the AICE, N.J., August 29–September 1, 1976. Plenum Press, Atlantic City, pp 117–150

Jímenez-López C, Caballero E, Huertas FJ, Romanek CS (2001) Chemical, mineralogical and isotope behavior, and phase transformation during the precipitation of calcium carbonate minerals from intermediate ionic solution at 25 °C. Geochim Cosmochim Acta 65:3219–3231. doi:10.1016/S0016-7037(01)00672-X

Kanduč T, Szramek K, Ogrinc N, Walter LM (2007) Origin and cycling of riverine inorganic carbon in the Sava River watershed (Slovenia) inferred from major solutes and stable carbon isotopes. Biogeochem 86:137–154. doi:10.1007/s10533-007-9149-4

Kanduč T, Kocman D, Ogrinc N (2008) Hydrogeochemical and stable isotope characteristics of the River Idrijca (Slovenia), the boundary watershed between the Adriatic and Black Seas. Aquat Geochem 14:239–262. doi:10.1007/s10498-008-9035-2

Kogovšek J, Petrič M (2002) Underground water flow from the Tržiščica sinking stream (SE Slovenia). Acta Carsologica 3:75–91

Levin I, Kromer B, Wagenbach D, Munnich KO (1987) Carbon isotope measurements of atmospheric CO_2 at a coastal station in Antarctica. Tellus, pp 89–95. doi:10.1111/j.1600-0889.1987.tb00273.x

Li S-L, Liu C-Q, Li J et al (2010) Geochemistry of dissolved inorganic carbon and carbonate weathering in a small typical karstic catchment of Southwest China: isotopic and chemical constraints. Chem Geol 277:301–309. doi:10.1016/j.chemgeo.2010.08.013

Ludwig W, Amiotte-Suchette P, Probst J-L (1996) River discharges of carbon to the world's oceans: determining local inputs of alkalinity and of dissolved and particulate organic carbon. In Comptes Rendus De L Academie Des Sciences Serie Ii Fascicule a-Sciences De La Terre Et Des Planetes 323:1007–1014

Marlier JF, O'Leary MH (1984) Carbon kinetic isotope effects on the hydration of carbon dioxide and the dehydration of bicarbonate ion. J Am Chem Soc 8:5054–5057. doi:10.1021/ja00330a003

Merz-Preiß M, Riding R (1999) Cyanobacterial tufa calcification in two freshwater streams: ambient environment, chemical thresholds and biological processes. Sediment Geol 126:103–124. doi:10.1016/S0037-0738(99)00035-4

Meybeck M (1987) Global chemical-weathering of surficial rocks estimated from river dissolved loads. Am J Sci 287:401–428. doi:10.2475/ajs.287.5.401

Mook WG (1970) Stable carbon and oxygen isotopes of natural waters in the Netherlands. In: IAEA (ed) Isotope hydrology: proceedings of a symposium on use of isotopes in hydrology. IAEA, Vienna, pp 163–189

Parkhurst DL, Appelo CA (1999) User's guide to PHREEQC (version 2)–A computer program for speciation, batch-reaction, one-dimensional transport, and inverse geochemical calculations: U.S. Geological Survey Water-Resources Investigations Report 99-4259. 312

Pawellek F, Frauenstein F, Veizer J (2002) Hydrochemistry and isotope geochemistry of the upper Danube River. Geochim Cosmochim Acta 66:3839–3853. doi:10.1016/S0016-7037(01)00880-8

Pleničar M, Premru U (1970) Osnovna geološka karta SFRJ 1: 100 000, list Novo mesto

Pleničar M, Premru U (1977) Tolmač lista Novo mesto, Osnovna geološka karta SFRJ 1: 100 000 (in Slovene)

Repe B (2004) Vegetation of Slovenia. In: Orožen Adamič M (ed) Slovenia: a Geographical overview. Association of the Geographical Societies of Slovenia, Ljubljana, pp 57–62

Romanek CS, Grossman EL, Morse JW (1992) Carbon isotopic fractionation in synthetic aragonite and calcite: effects of temperature and precipitation rate. Geochim Cosmochim Acta 56:419–430. doi:10.1016/0016-7037(92)90142-6

Roy S, Gaillardet J, Allegre CJ (1999) Geochemistry of dissolved and suspended loads of the Seine River, France: anthropogenic impact, carbonate and silicate weathering. Geochim Cosmochim Acta 63:1277–1292. doi:10.1016/S0016-7037(99)00099-X

Schulte P, Van Geldern R, Freitag H et al (2011) Applications of stable water and carbon isotopes in watershed research: weathering, carbon cycling, and water balances. Earth-Sci Rev 109:20–31. doi:10.1016/j.earscirev.2011.07.003

Shin WJ, Chung GS, Lee D, Lee KS (2011) Dissolved inorganic carbon export from carbonate and silicate catchments estimated from carbonate chemistry and $\delta^{13}C_{DIC}$. Hydrol Earth Sys Sci 15:2551–2560. doi:10.5194/hess-15-2551-2011

Sun H, Han J, Li D et al (2010) Chemical weathering inferred from riverine water chemistry in the lower Xijiang basin, South China. Sci Total Environ 408:4749–4760. doi:10.1016/j.scitotenv.2010.06.007

Szramek K, Walter LM (2004) Impact of carbonate precipitation on riverine inorganic carbon mass transport from a mid-continent, forested watershed. Aquat Geochem 10:99–137. doi:10.1023/B:AQUA.0000038960.63501.5b

Szramek K, Walter LM, Kanduč T, Ogrinc N (2011) Dolomite versus calcite weathering in hydrogeochemically diverse watersheds established on bedded carbonates (Sava and Soča Rivers, Slovenia). Aquat Geochem 17:357–396. doi:10.1007/s10498-011-9125-4

Tan FC, Strain PM (1983) Sources, sinks and distribution of organic carbon in the St. Lawrence Estuary, Canada. Geochim Cosmochim Acta 47:125–132. doi:10.1016/0016-7037(83)90096-0

Telmer K, Veizer J (1999) Carbon fluxes, pCO_2 and substrate weathering in a large northern river basin, Canada: carbon isotope perspectives. Chem Geol 159:61–86. doi:10.1016/S0009-2541(99)00034-0

Tipper ET, Bickle MJ, Galy A et al (2006) The short term climatic sensitivity of carbonate and silicate weathering fluxes: insight from seasonal variations in river chemistry. Geochim Cosmochim Acta 70:2737–2754. doi:10.1016/j.gca.2006.03.005

Vogel JC, Grootes PM, Mook WG (1970) Isotopic fractionation between gaseous and dissolved carbon dioxide. Z Phys 203:225–238. doi:10.1007/BF01394688

Wachniew P (2006) Isotopic composition of dissolved inorganic carbon in a large polluted river: The Vistula, Poland. Chem Geol 233:293–308. doi:10.1016/j.chemgeo.2006.03.012

Williams EL, Szramek KJ, Jin L et al (2007) The carbonate system geochemistry of shallow groundwater-surface water systems in temperate glaciated watersheds (Michigan, USA): significance of open-system dolomite weathering. Geol Soc Am Bull 119:515–528. doi:10.1130/B25967.1

Yao G, Gao Q, Wang Z et al (2007) Dynamics of CO_2 partial pressure and CO_2 outgassing in the lower reaches of the Xijiang River, a subtropical monsoon river in China. Sci Total Environ 376:255–266. doi:10.1016/j.scitotenv.2007.01.080

Zeng F-W, Masiello CA, Hockaday WC (2010) Controls on the origin and cycling of riverine dissolved inorganic carbon in the Brazos River, Texas. Biogeochemistry 104:275–291. doi:10.1007/s10533-010-9501-y

Zhang J, Quay PD, Wilbur DO (1995) Carbon isotope fractionation during gas-water exchange and dissolution of CO2. Geochim Cosmochim Acta 59:107–114. doi:10.1016/0016-7037(95)91550-D

Zhang S, Lu XX, Sun H et al (2009) Major ion chemistry and dissolved inorganic carbon cycling in a human-disturbed mountainous river (the Luodingjiang River) of the Zhujiang (Pearl River), China. Sci Total Environ 407:2796–2807. doi:10.1016/j.scitotenv.2008.12.036

Appendix 8: Article: C and O stable isotopic signatures of fast-growing dripstones on alkaline substrates: reflection of growth mechanism, carbonate sources and environmental conditions. *Isotopes in Environmental and Health Studies* **48**, 354–371 (2012).

Isotopes in Environmental and Health Studies
2012, 1–18, iFirst

C and O stable isotopic signatures of fast-growing dripstones on alkaline substrates: reflection of growth mechanism, carbonate sources and environmental conditions

Saša Zavadlav[a]*, Darja Mazej[a], Janez Zavašnik[b], Aleksander Rečnik[b], David Dominguez-Víllar[c], Neven Cukrov[d] and Sonja Lojen[a]

[a]*Department of Environmental Sciences, Jožef Stefan Institute, Ljubljana, Slovenia;* [b]*Department for Nanostructured Materials, Jožef Stefan Institute, Ljubljana, Slovenia;* [c]*Department of Geology, University of Alcalá de Henares, Madrid, Spain;* [d]*Division for Marine and Environmental Research, Ruđer Bošković Institute, Zagreb, Croatia*

(*Received 15 June 2011; final version received 16 November 2011*)

Secondary carbonate precipitates (dripstones) formed on concrete surfaces in four different environments – Mediterranean and continental open-space and indoor environments (inside a building and in a karstic cave) – were studied. The fabric of dripstones depends upon water supply, pH of mother solution and carbonate-resulting precipitation rate. Very low $\delta^{13}C$ (average −28.2‰) and $\delta^{18}O$ (average −18.4‰) values showed a strong positive correlation, typical for carbonate precipitated by rapid dissolution of CO_2 in a highly alkaline solution and consequent disequilibrium precipitation of $CaCO_3$. The main source of carbon is atmospheric or biogenic CO_2 in the poorly ventilated karstic cave, which is reflected in even lower $\delta^{13}C$ values. Statistical analysis of $\delta^{13}C$ and $\delta^{18}O$ values of the four groups of samples showed that the governing factor of isotope fractionation is not the temperature, but rather the precipitation rate.

Keywords: carbon-13; concrete; dripstones; isotope ecology; isotope hydrogeology; oxygen-18; secondary carbonates; trace elements

1. Introduction

Secondary carbonate formations on concrete structures often occur as dripstones or flowstones along beam junctions and cracks in the material, and are believed to accelerate concrete degradation, which is a worldwide concern with enormous economic implications [1,2]. They resemble speleothems in many characteristics, such as seasonal or annual alternation of porous and dense laminae, distribution of trace elements, and are believed to record environmental conditions during their formation [3]. The origin of carbonates, the environment and the mechanisms of their formation are, however, different. Calcium is usually provided by the concrete substrate, where calcium oxide reacts with water dripping through the concrete structure or condensing on its surface to form calcium hydroxide [4]. This process yields a strongly alkaline solution with pH values reaching around 9 for carbonated concrete, or even >13 for alkaline cements without

*Corresponding author. Email: sasa.zavadlav@ijs.si

ISSN 1025-6016 print/ISSN 1477-2639 online

http://dx.doi.org/10.1080/10256016.2012.645540
http://www.tandfonline.com

carbonate additives [5]. The predominant carbon source is atmospheric CO_2, rapidly dissolving in the alkaline solution; the higher the pH, the higher is the CO_2 dissolution rate [6]. Compared with dripping waters in karstic caves, the Ca^{2+} concentration in the pore water or in the water film on concrete may be as much as four times higher [7], making the solution highly supersaturated with respect to calcite even at very low concentrations of dissolved inorganic carbon (DIC). This initiates rapid precipitation and growth of dripstone with various features. $CaCO_3$ usually precipitates in the form of calcite, at rates several orders of magnitude larger than those of the precipitation of speleothems [8–15]. The C and O stable isotope ratios of these carbonates show a strong depletion in heavy isotopes, which is attributed to the large kinetic isotope fractionation related to the non-equilibrium conditions during their precipitation [1,14].

In this paper, we investigate whether the environmental, in particular climatic conditions and different sources of C and O (atmospheric versus biogenic CO_2) are reflected in the stable isotopic compositions of C and O of secondary carbonates, or whether the environmental influence is completely masked by the large kinetic isotope fractionation related to the disequilibrium effects during the processes of their precipitation. Therefore, dripstones (soda straws, flowstone, stalactites and stalagmites) formed on concrete surfaces in four different environments were compared with respect to their C and O stable isotope composition. Elemental (Mg, Sr, Ba) distributions were determined in the case of a bigger stalagmite and the dripstone fabric was studied using electron microscopy. The sampling locations differed from each other with respect to temperature, precipitation, humidity, ventilation rate and pCO_2. Two of them were located in Mediterranean climate (in an open space under the underpass and in a closed space in an old fortress) and two in continental climate (in an open space under a bridge and underpass, and in a closed space of a karstic cave).

2. Regional setting

Dripstone samples were collected at two sites in the Mediterranean region and several continental sites (Figure 1): inside the fortress of St Nikola (central Adriatic, Croatia), in an underpass at a nearby regional road close to the shoreline (approximately 5 km airline distance from the fortress of St Nikola, Croatia), in the continental area of central Slovenia (northwest of Ljubljana) and in a continental karstic cave (Postojna Cave, Slovenia). Some specific characteristics of the sampling sites are listed in Table 1.

In the Mediterranean area, soda straws and stalagmites were taken from a fortress from the sixteenth century (St Nikola). It is preserved in full and was partly renovated in 1987–1989. The flat roof is now covered with concrete slabs, where rainwater leaks through junctions and cracks and seeps into the main hall through the clay masonry bound with cement mortar. The dripstone formation started after the reconstruction; however, no reliable records are available about its first occurrence. As reported by local people, its rapid growth started about 10 years ago (around 2000). The ceiling of the hall is now overgrown by up to 20 cm long soda straws, whereas the floor is covered with unbound calcite mud with sporadic laminated stalagmites. Since access to the fortress is open, most of them are broken or trampled down by tourists. Further, soda straws were collected in an underpass on the Zadar–Šibenik regional road, about 5 km north of the fortress of St Nikola.

In the continental area, dripstones were collected on vaults and concrete beams of bridges and passages over roads and a railway. Stalactites occurred on junctions or on mechanically damaged concrete surfaces along cracks exposed to leaking meteoric water. At one of these locations (Žerovnik, Figure 1), a stalactite was collected from a steel beam of a bridge. In most cases, only stalactites were available, whereas at Polhov Gradec (Figure 1), also small stalagmites and some flowstone on the side wall of a bridge were found.

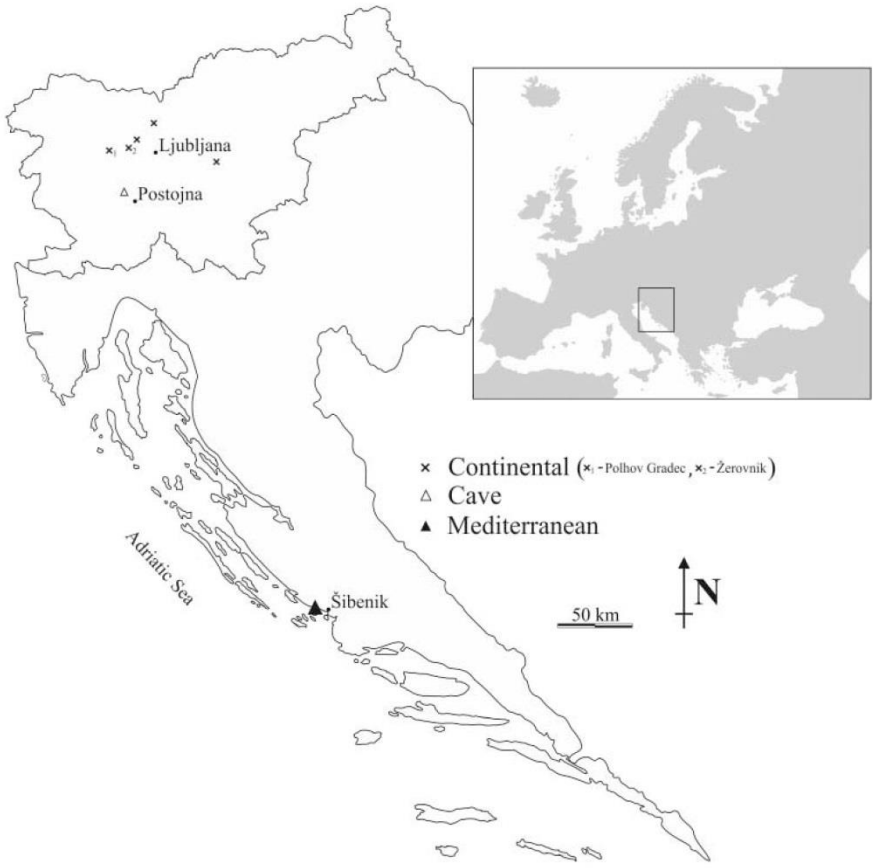

Figure 1. Sampling sites.

Table 1. Hydrometeorological characteristics of the sampling sites and number of samples.

Site	Environment	Mean annual temperature (°C)	Mean annual precipitation (mm)	Weighted mean annual $\delta^{18}O$ of precipitation (‰ VSMOW)	Number of samples, size
Ljubljana, Slovenia	Outdoor (bridge, underpass)	11.1[a]	1366[a]	−8.6[b]	28 stalactites (<20 cm) 2 stalagmites (2 and 13 cm)
Postojna, Slovenia	Outdoor Cave	9.4[a] 8.5	1542[a]	−8.5	6 stalactites (2–6 cm), 7 stalagmites (1.5–2 cm)
Šibenik, Croatia	Indoor (fortress) Outdoor (underpass)	15.4[a]	790[a]	−5.6[c]	12 stalactites (5–20 cm) 17 stalagmites (>4 cm) 4 stalactites (5–10 cm)

[a]Data from national monitoring programmes of the Environmental Agency of Slovenia and National Hydrometeorological Survey of Croatia for 1990–2010.
[b]Vreča *et al.* [19].
[c]Estimate based on data from Vreča *et al.* [18].

In Postojna Cave, only a few dripstones occurred on concrete substrates in the tourist part of the cave, on beams and the vault of a bridge, as well as on the concrete kerbs of walkways. As reported by the staff, they appear continuously, but are regularly removed during maintenance work.

Precipitation was sampled at the Postojna monitoring station at the southwest outskirts of the town, being part of the national precipitation monitoring network managed by the Slovenian Environmental Agency. Data for the isotopic composition of precipitation in Ljubljana were obtained from the regular Global Network of Isotopes in Precipitation monitoring programme.

3. Methods

3.1. *Sampling and sample handling*

Dripstones were carefully removed from the substrate and dried at room temperature. Soda straws are extremely fragile, so many of them were damaged during handling and transport. These were analysed whole as a composite sample. Subsamples from preserved straws were taken from the base and from the tips of the straws, crushed and powdered manually using an agate mortar and pestle.

Entire stalagmites were extracted from the muddy substrate. Subsamples from the largest stalagmite were taken from individual growth layers along the growth axis and from the growth surface symmetrically at different distances from the apex. They were collected using a hand drill fitted with a tungsten carbide WC bit (diameter 0.8 mm). In small stalagmites, only the surface layer of the apex was analysed.

Dripping water was collected monthly in Postojna Cave from January 2009 to December 2010 at nine sites with various drip rates (from <1 to >20 drops min^{-1}). Precipitation has been collected daily since the beginning of 2009 near Postojna Cave. The O isotopic composition of precipitation was analysed in monthly composite samples. Samples of the cave atmosphere for isotopic analyses of C and O in CO_2 were collected by flushing 10 ml evacuated septum vials (Labco Exetainer®) with 10 times the amount of air using a plastic syringe.

3.2. *Analyses*

The pH of dripping water was measured using a Myron 6PII Ultrameter, and the pH of the water film was measured on wet apices of stalagmites and at exposed masonry surfaces using a Mettler Toledo Inlab surface flat electrode. The cave temperature was recorded using a Tinytag PLUS2 data logger.

The morphology and elemental composition of samples was examined using a JEOL JSM-5800 scanning electron microscope equipped with a Link ISIS-300 EDS analyser (Oxford Instruments). For scanning electron microscopy (SEM) analyses, cross-sections of samples were mounted in glycol methacrylate resin (Technovit 7100), polished and coated with 3 nm of amorphous carbon to improve electron conductivity.

The C and O stable isotopic composition of carbonate was measured in the CO_2 released from 20 mg aliquots after reaction with 100% H_3PO_4 for 3 h at 60 °C, using a Varian MAT 250 dual inlet isotope ratio mass spectrometer. IAEA-CO1, IAEA-CO8, NBS-18 and NBS-19 reference materials prepared simultaneously in the same batch were used for calibration. The reproducibility of the isotopic analyses of the reference materials was equal to or better than ±0.05‰, while the standard uncertainty of the entire analytical procedure for the samples was 0.1‰ for both $\delta^{13}C$ and $\delta^{18}O$.

The results of the stable isotopic analyses are reported in relative δ values in per mil, i.e. the difference in parts per mil of the isotopic ratios $^{18}O/^{16}O$ and $^{13}C/^{12}C$ from those of the Vienna

Standard Mean Ocean Water (VSMOW) reference materials for O in water, and Vienna Pee Dee Belemnite (VPDB, defined by NBS-19) reference materials for C and O in carbonate and DIC.

The $\delta^{18}O$ of water was determined using an IsoPrime continuous-flow isotope ratio mass spectrometer with a MultiflowBio equilibration module (GV Instruments), after equilibration with CO_2 [16,17] with a standard uncertainty of 0.1‰. Working standards (water) were calibrated versus the IAEA SMOW and Greenland Ice Sheet Precipitation (GISP) calibration materials.

The stable isotopic composition of DIC in water was determined in 5 ml samples injected into He-flushed septum vials containing 100% H_3PO_4. The CO_2 released was then analysed using a continuous-flow Europa 20–20 Stable Isotope Analyser with an ANCA TG separation module. The standard uncertainty of the analysis was 0.2‰. The same instrument was used for the analysis of $\delta^{13}C$ of atmospheric CO_2. It is noteworthy, however, that only samples with CO_2 concentrations larger than 1000 ppmv could be measured, and therefore no data are available for the colder part of the year when the CO_2 concentrations in the cave were typically below 1000 ppmv.

The analyses of trace metal (Mg, Sr and Ba) concentrations were performed on a stalagmite from the Mediterranean site only. Analysis of the largest stalagmite was performed on subsamples taken from individual growth layers, as well as along the growth surface symmetrically at different distances from the apex. Thirty milligrams of homogenised sample were decomposed in 1 ml of 65% supra-pure HNO_3 and diluted to 10 ml with water (Milli-Q). Before measurement, an additional dilution was made. Solutions were analysed by an inductively coupled plasma mass spectrometer (7500ce, Agilent) equipped with an ASX-510 Autosampler (Cetac), a micro mist nebuliser, a Scott-type spray chamber and an octapole reaction system using helium as reaction gas. The radio frequency power was 1500 W. Torch position and gas flow rates were optimised daily to give maximum sensitivity. Isotopes monitored were ^{24}Mg, ^{88}Sr and ^{137}Ba. An XXI multielement standard solution CertiPUR® (Merck) was used for external calibration.

All chemical and isotopic analyses were performed at the Department of Environmental Sciences of Jožef Stefan Institute. The electron microprobe analyses and X-ray diffraction (XRD) analyses were performed at the Department of Nanostructured Materials of Jožef Stefan Institute, Ljubljana, Slovenia. The phase composition of samples was determined by the XRD method, using the X'Pert Graphic & Identify (Phillips Analytical) program package. The Statistica 6.0 (StatSoft) package was used for data treatment.

4. Results

4.1. *Mineralogy and fabrics*

XRD analysis revealed no other phases than calcite, except in samples collected from steel beams and traverses, where the presence of small amounts of lepidocrocite (iron oxyhydroxide) was identified.

SEM analysis of both forms of open-space stalactites from the continental climate (soda straws and a cone-shaped massive stalactite) revealed that they consisted of several calcitic bands (Figure 2(a)), where the void surfaces were overgrown by calcite crystals. The morphology of individual bands was defined by rhombohedric (Figure 2(b)) and spherulitic fabrics (Figure 2(c)). Both fabrics exhibited an alternation of light and dark laminae, which were thinner in spherulitic areas (up to 5 μm). Hollow spaces between calcitic rings were often filled with second-generation calcite (Figure 2(d)). In samples with lepidocrocite, an up to 4 μm thick layer of iron-rich coating was found to enclose a monocrystalline calcite grain, embedded in a calcite matrix. The light and the dark laminae contained about 2 and 10% of iron oxyhydroxide, respectively. In the Mediterranean stalactites, sporadic grains enriched in sulphur occurred. They were not observed in any of the continental specimens.

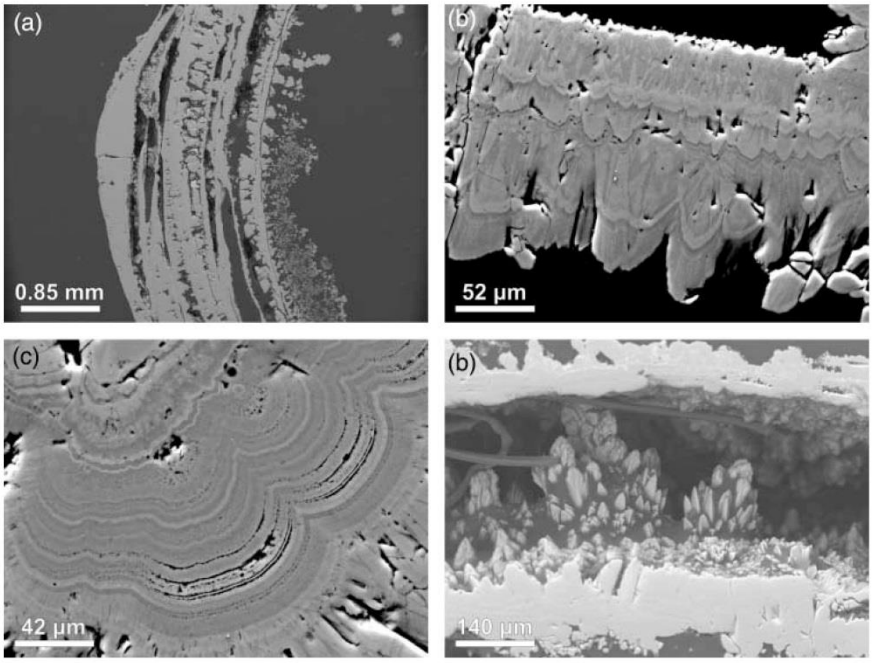

Figure 2. SEM photographs of a cone-shaped stalactite formed in open space in continental climate: (a) calcitic rings of stalactite formed in open space in continental climate at low magnification; (b) rhombohedric ring structure; (c) spherulitic ring structure; (d) second-generation calcite crystals filling hollow spaces between individual rings.

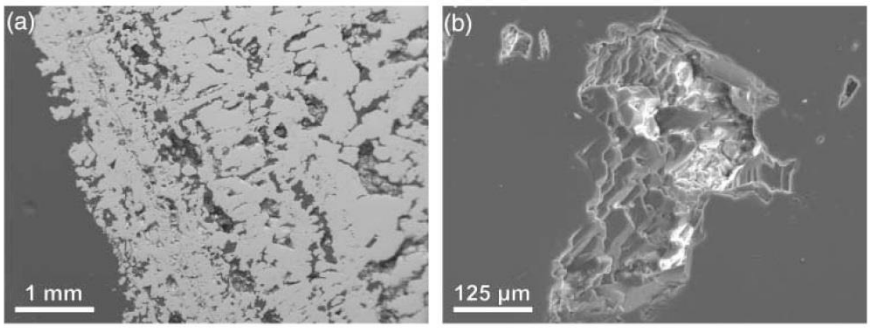

Figure 3. SEM photographs of stalagmite formed in open space in continental climate: (a) alteration of porous and dense layers; (b) rhombohedric crystals filling the voids between layers.

Stalagmites exhibited less variable morphology, with alternation of porous (dark) and dense (light) laminae (Figure 3(a)), where voids were partially filled with large rhombohedric crystals, elongated along the *b* and *c* axes, pointing in the growth direction (Figure 3(b)). No impurities were found in the matrix, e.g. they were uniformly distributed throughout the analysed surface and present at levels below the detection limits of the method.

In contrast to dripstones formed in open spaces, the cave dripstones (both stalactites and stalagmites) were rather dense (although some of them showed some increased porosity). No impurities could be detected using SEM–energy dispersive spectroscopy.

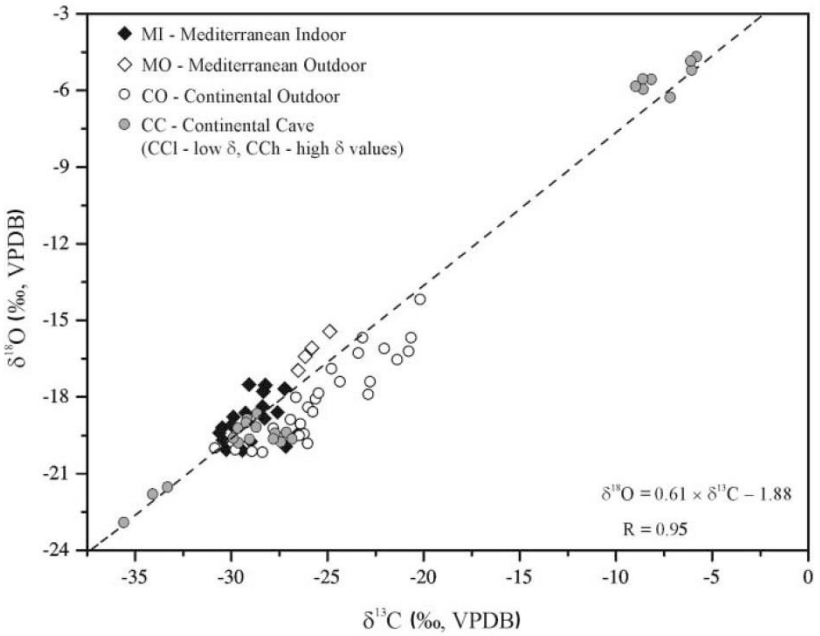

Figure 4. Relation between $\delta^{13}C$ and $\delta^{18}O$ values of all analysed samples.

4.2. *pH*

pH measurements were performed on the solutions collected on concrete walls and at apices of larger stalagmites, where exposed flat surfaces were large enough to perform the measurement. On concrete and brick surfaces the solution had pH values between 9.6 and 9.9, whereas the water film at the apices of stalagmites had a pH between 8.5 and 8.6. The pH of dripping water in Postojna Cave varied from site to site between 6.8 and 8.4, averaging 7.6.

4.3. *Stable isotopes*

4.3.1. *Dripstones*

Stable isotope compositions of dripstones are presented in Figure 4.

Mediterranean samples from the fortress of St Nikola form a relatively uniform group with respect to both $\delta^{13}C$ and $\delta^{18}O$, with average $\delta^{13}C$ and $\delta^{18}O$ values of -29.4 and -18.6‰ VPDB, respectively. $\delta^{13}C$ and $\delta^{18}O$ values of samples taken along the growth axis scattered irregularly ($R = 0.50$) within 1.3 and 0.4‰ for $\delta^{13}C$ and $\delta^{18}O$, respectively (Figure 5(a)), whereas the differences on the surface were even larger, up to 1.8‰ in $\delta^{13}C$ and 1.1‰ in $\delta^{18}O$, and increased with increasing distance from the growth axis. Samples taken from the same growth layer of the large stalagmite showed increasing δ values for both C and O with increasing distance from the apex (Figure 5(b)) and were correlated with an R value of 0.70, whereas the correlation between $\delta^{13}C$ and $\delta^{18}O$ values along the growth axis was even weaker ($R = 0.60$). Samples collected in the underpass a few kilometres away from the fortress were enriched in heavy C and O by a few per mil compared with samples from the fortress (average $\delta^{13}C$ and $\delta^{18}O$ values were -25.8 and -16.2‰ VPDB, respectively).

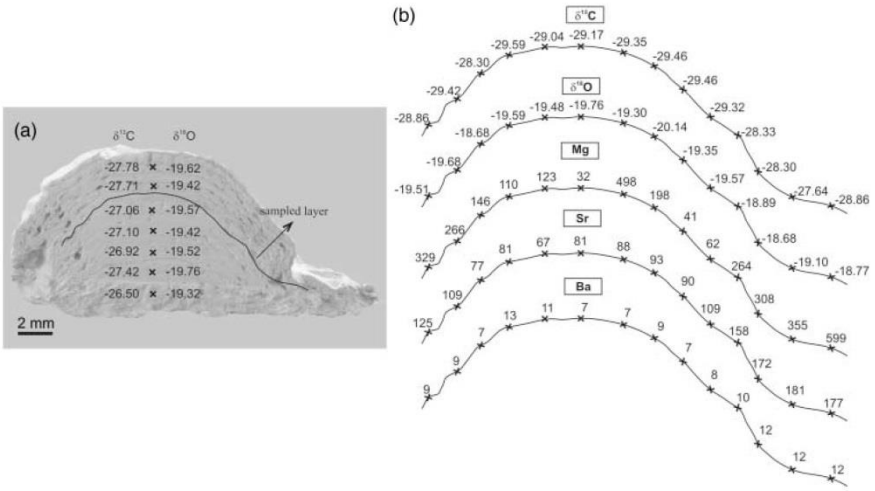

Figure 5. Stable isotopic and trace element composition in the largest stalagmite collected from the fortress of St Nikola in the Mediterranean environment: (a) distribution of $\delta^{13}C$ and $\delta^{18}O$ along the growth axis; (b) distribution of $\delta^{13}C$, $\delta^{18}O$ and trace elements (Mg, Sr and Ba) along the growth layer. δ values are reported in per mil relative to VPDB, and concentrations of Mg, Sr and Ba in mg/kg.

Continental outdoor (CO) stalactites collected at several locations show a larger range of values than the Mediterranean ones (−30.9 to −20.2‰ VPDB for $\delta^{13}C$ and −20.2 to −14.2‰ VPDB for $\delta^{18}O$, with average values of −25.4 and −18.1‰ VPDB, respectively). The two stalagmites were depleted in heavy isotopes compared with stalactites for both elements, with $\delta^{13}C$ values on average −30.9‰ VPDB (−31.7 to −30.0‰) and $\delta^{18}O$ values on average −20.8‰ VPDB (−20.1 to −21.6‰).

Continental cave samples exhibited the largest range of δ values of all groups. They, in fact, represent two distinct groups, one with very negative δ values (on average -32.1 ± 3.2‰ VPDB for $\delta^{13}C$ and -20.6 ± 1.6‰ VPDB for $\delta^{18}O$), and the other with average $\delta^{13}C$ and $\delta^{18}O$ values of -8.75 ± 1.6‰ and -5.6 ± 0.5‰, respectively.

A strong positive correlation existed between $\delta^{13}C$ and $\delta^{18}O$ values of all forms of dripstone. Combining the results of all analysed samples in all environments, a correlation line $\delta^{18}O = (0.61 \pm 0.02) \times \delta^{13}C - (1.88 \pm 0.43)$ with $R = 0.95$ was found (Figure 4). Looking at individual groups of samples, good linear correlations were found in all groups ($0.72 < R < 0.99$), except in Mediterranean indoor (MI) samples from the fortress, where no significant correlation between $\delta^{13}C$ and $\delta^{18}O$ could be observed ($R = 0.26$).

Similarities between groups of samples from different locations were tested using the unequal N Tukey HSD test (Tukey-Kramer evaluation) at $p < 0.05$ (Table 2). Samples were grouped into five groups: MI (from the fortress), Mediterranean outdoor (MO, from the underpass), CO, continental cave low (CCl, cave specimen with low δ values) and continental cave high (CCh, cave specimen with high δ values). The CCh group differed statistically significantly from all other groups with respect to both $\delta^{13}C$ and $\delta^{18}O$. No statistically significant differences were found between the MI and CCl groups and between MO and CO groups with respect to both elements. MI samples differed statistically significantly from MO samples with respect to $\delta^{13}C$, but not to $\delta^{18}O$. The same applies for MO versus CO and CCl. The t-test for MO and MI groups, however, showed a statistically significant difference between them with respect to both elements, which was not detected by a more conservative unequal N Tukey HSD test. Grouping samples by hierarchical tree clustering showed that the CCh samples form a separate group, while

Table 2. Comparison of the four groups of dripstones from different environments using Tukey HSD test ($p < 0.05$).

group	MO	CO	CCl	CCh
MI	C	***	C,O	***
MO		C,O	***	***
CO			***	***
CCl				***

Note: MI, Mediterranean indoor; MO, Mediterranean outdoor; CO, continental outdoor; CCl, continental cave dripstones with low δ values; CCh, continental cave with high δ values; C, not significant at $p < 0.05$ for $\delta^{13}C$; O, not significant at $p < 0.05$ for $\delta^{18}O$.
***Significant at $p < 0.05$.

others were clustered into two groups – indoor (MI and CCl) and outdoor sites (CO and MO, Figure 4).

4.3.2. *Atmosphere, dripping water and precipitation*

The atmospheric CO_2 in Postojna Cave had $\delta^{13}C$ values between −26.8 and −15.1‰ VPDB (on average −22.8‰, with lower values measured in the summer and higher in the winter months), and $\delta^{18}O$ values between −16 and −2.9‰ (on average −11.4‰ VPDB). Dripping water in Postojna Cave had $\delta^{18}O$ values which changed seasonally, between −9.7 and −7.2‰ VSMOW (mean −8.47‰), whereas $\delta^{13}C$-DIC varied between −15.6 and −7.2‰ VPDB (mean −13.0‰).

The weighted average $\delta^{18}O$ of precipitation in Postojna in 2009–2010 was −8.35‰ VSMOW (ranging from −13.01 to −4.00‰ VSMOW for monthly averages). The stable isotopic composition of precipitation for other locations was taken or estimated from the literature [18,19] (Table 1).

4.4. *Elemental concentrations*

Mg and Sr concentrations in the carbonate were determined only in the large stalagmite from the Mediterranean environment and were found to be very low (up to 600 mg kg^{-1} Mg and up to 180 mg kg^{-1} Sr) and highly variable (Figure 5(b)), both along the growth axis, as well as along a single growth layer. No correlation between Sr and Mg ($R < 0.10$) was found; however, some positive correlation between Mg and $\delta^{13}C$ existed ($R = 0.66$). Analysis of carbonate samples taken from the same growth layer (Figure 5(b)) showed that, like δ values, all trace element concentrations generally increased along the flanks of the stalagmite, whereas at the flat surface of the apex, they were highly variable.

5. Discussion

5.1. *Fabrics*

The phenomenon of rhombohedric and spherulitic carbonate fabrics, which were mainly found in open-space dripstones, has been extensively discussed by Boistelle and Astier [20], who found that spherulitic structures result from rapid precipitation from supersaturated solutions, followed by crystallisation of $CaCO_3$ rhombohedra, when the saturation of the solution decreases. In all analysed samples, the pores inside calcitic bands and between individual layers were often filled with small aggregates of calcite crystals (Figure 2(d)), which occurred in two stages, precipitated

in different morphologies. Saturation of the mother solution thus plays an important role for the habitus of the precipitates: porous calcite crystals are formed from supersaturated solutions entering the pores, whereas the crystals with smooth surfaces, which fill up the rest of pore space, are formed later, when the saturation of the solution has already decreased. Formation of different fabrics can thus be related to changing weather conditions in the area, e.g. the dynamics of seepage dripping.

It was also found that dripstones with higher δ values (on average 7‰ for C and 3‰ for O) respond to denser fabric and thus mark slower growth of dripstones. To support this assumption, high-resolution $\delta^{18}O$ profiling of dripstones would be necessary. However, with the instrumentation available, we were not able to analyse such thin (<1 mm) layers.

The presence of sulphur in Mediterranean samples is explained as marine sulphate deriving from seaspray.

Stalagmites exhibit alterations of dense and porous layers, similar to the speleothems found in caves, representing wet and dry growth periods ([21] and references therein). In caves, these laminations usually represent annual growth cycles. The Mediterranean stalagmites analysed in this study have growth rates of up to 1 cm y^{-1}, so that the lamination is most probably sub-annual. Dense layers are formed from fast dripping water in the wet seasons [22,23], while porous layers represent the crystallisation of residual carbonate material and eventually re-crystallisation of the carbonate surface in the water film.

The most obvious difference in the fabrics of dripstones formed in a cave and in open space is the higher density of the cave formations. This could be caused by various factors. First, the dynamics of cave dripping water is much slower, but also much less prone to short-term (daily or even diurnal) variations than in open space. In contrast to open space (e.g. the fortress or bridges), dripping water must first find its way through a complex system of seepage channels and fissures in the approximately 40 m thick karstic aquifer forming the cave ceiling [9] before it reaches the cave. Second, the outdoor is better ventilated compared with cave space, which has a constant temperature of 8–9 °C and a humidity of >99% [9]. Nevertheless, even in the cave, some individual dripstones with high porosity were found, rather typical of open-space locations. It is noteworthy that the cave dripstones had rather variable fabrics with respect to porosity, and that the difference in their isotopic composition is related to their fabric differences, where more porous specimens generally exhibited much lower $\delta^{13}C$ (−32.1‰) and $\delta^{18}O$ (−20.6‰) values than dense samples with average $\delta^{13}C$ and $\delta^{18}O$ values of −8.75 and −5.6‰, respectively. The fabrics and isotopic composition of denser samples resemble the 'natural' speleothems found in Postojna Cave [9,24]. At least for these samples, differences in the δ values could be directly related to fabric characteristics (in terms of porosity), which in turn reflect the mechanism of their formation, meaning more porous fabric responds to higher supersaturation of the solution and faster growth. It is therefore assumed that specimens with more denser and relatively high δ values were formed by the same mechanism as 'natural' speleothems, and the locus of their formation rather incidentally occurred at a concrete surface.

5.2. *Isotopic signals*

The very low $\delta^{13}C$ and $\delta^{18}O$ (below −20‰ for carbon and below −15‰ for oxygen, respectively) values of secondary carbonates occurring in degraded mortars or those growing as dripstones on concrete structures were not yet fully explained in the literature, either by a single process, or by a combination of different fractionation processes, such as the incorporation of atmospheric ^{13}C-depleted CO_2 [1,25–28]. Krishnamurthy *et al.* [1] suggested that not even the incorporation of ^{13}C-depleted fossil fuel-derived CO_2 can be ruled out, nor can the effects of microbial activity. Based on previous work by Dietzel *et al.* [6], Kosednar-Legenstein *et al.* [14] showed that low δ values are related to the formation mechanism, e.g. the rapid dissolution of atmospheric CO_2 in a

highly alkaline solution, and the high precipitation rate directly related to its pH, related to large isotope fractionation for both C and O isotopes.

The large range of $\delta^{13}C$ and $\delta^{18}O$ values of dripstones found in this study ($-35.6‰ < \delta^{13}C < -6.0‰$ VPDB and $-23.0‰ < \delta^{18}O < -5.0‰$ VPDB) is comparable to the $\delta^{13}C$ and $\delta^{18}O$ values obtained for carbonate in historical cements and mortars by Kosednar-Legenstein *et al.* [14] ($-30.9‰ < \delta^{13}C < -0.1‰$ VPDB and $-23.8‰ < \delta^{18}O < -2.6‰$ VPDB) and Dotsika *et al.* [2] ($-19.6‰ < \delta^{13}C < -9.54‰$ VPDB and $-16.8‰ < \delta^{18}O < -9.7‰$ VPDB) who used them for diagnosis of the degradation of the calcite matrix. It should to be pointed out, however, that their results apply to the bulk carbonate in mortars, which represent a mixture of secondary precipitate and the residual fraction of possible original carbonate used as mortar additive, whereas in our study, only pure secondary carbonates from concrete surfaces were analysed. In our case, the highest δ values were recorded in dripstones formed on concrete surfaces in the cave environment, which resemble the isotopic composition of natural speleothems with $\delta^{13}C$ values between -10.2 and $-9.2‰$ and $\delta^{18}O$ values between -7.5 and $-4.9‰$ VPDB [9,24,28], whereas the highest values obtained by Kosednar-Legenstein *et al.* [14] in mortars apply to the carbonate additive in mortars deriving from marine carbonate formations [29,30]. Krishnamurthy *et al.* [1] measured the isotopic composition of dripstones growing under concrete structures (bridge, overpass) in the northern USA and obtained a narrower range of values ($-31.4‰ < \delta^{13}C < -21.6‰$ VPDB, $-18.25‰ < \delta^{18}O < -14.75‰$ VPDB), which match well with the continental and Mediterranean samples, as well as with the cave samples exhibiting low δ values.

In the following sections, we attempt to explain the range of values and variability of C and O isotopic compositions of dripstones in the light of carbonate sources and processes affecting their stable isotope signatures. First, the correlation between $\delta^{13}C$ and $\delta^{18}O$ values is examined so as to estimate whether the isotopic signatures are governed by equilibrium or disequilibrium processes. Second, $\delta^{13}C$ and $\delta^{18}O$ values are discussed in terms of possible C and O sources and fractionation processes, i.e. atmospheric CO_2 versus substrate-derived DIC for C and seeping water for O.

5.2.1. *Correlation between $\delta^{13}C$ and $\delta^{18}O$*

Statistical evaluation of obtained data (Tukey HSD test and hierarchical tree clustering) indicates that the climatic conditions (continental versus Mediterranean) influence the C and O isotopic compositions of dripstones to a lesser extent than other environmental factors, such as the ventilation (indoor versus outdoor): MI samples exhibit more similarity with CCl samples than with MO samples, which are closer to the CO than to MO samples. Assuming the temperature-dependent isotope fractionation coefficients, the temperature difference had obviously less influence than other environmental factors (ventilation, sources of C and O).

The bulk dripstones analysed in our study comply in most cases with the criteria set for the speleothems formed under disequilibrium conditions [30–33], showing a positive correlation between $\delta^{13}C$ and $\delta^{18}O$ both along the growth axis and along individual growth layers with distance from the apex. The correlation line $\delta^{18}O = (0.61 \pm 0.02) \times \delta^{13}C - (1.88 \pm 0.43)$ (Figure 4) yields a parallel to that found by Kosednar-Legenstein *et al.* [14] in progressively degraded Roman mortars ($\delta^{18}O = 0.61 \times \delta^{13}C - 3.3$), which is almost parallel to the experimentally determined correlation line for carbonates formed in a CO_2 absorption experiment in alkaline $Ca(OH)_2$ solution ($\delta^{18}O = 0.67 \times \delta^{13}C - 6.4$) at an initial pH of 12.1. The identity of the slope of the line correlating the $\delta^{13}C$ and $\delta^{18}O$ indicates that the processes separating C and O isotopes in all environments were basically similar (resulting in a similar isotopic separation of the two isotopes, e.g. the same dominant reaction mechanism), whereas the different intercept indicates that the source material for carbonate precipitation in the different environments could be different.

5.2.2. *Carbon sources*

Secondary carbonates precipitated in or on concrete surfaces from strongly alkaline solutions receive their CO_2 almost exclusively from the atmosphere [6], since no soil horizon or aquifer occurs at structures such as bridges and vaults. Concrete itself is hardly significant as a carbon source, since CO_2 is generally released during the calcination process. If carbonate is present as an additive, its dissolution in a highly alkaline solution could not contribute significantly to the overall carbon in the precipitate. Liu and He [7] and Letolle *et al.* [27] found that with increasing pH of the water solution, carbonate precipitates become depleted in ^{13}C because of secondary diffusion of $CO_{2(aq)}$ through crusts of rapidly precipitating $CaCO_3$. Dietzel *et al.* [6] claimed that carbonates precipitated from drainage water at neutral or slightly alkaline pH are formed in isotopic equilibrium with water, where the carbon isotopic composition of calcite should approach equilibrium with recent DIC in the solution, i.e. towards a value about 1‰ higher than that of DIC in water [34,35]. At high pH, however, large kinetic isotope fractionation occurs since in aquatic solution $^{12}CO_{2(aq)}$ and $^{13}CO_{2(aq)}$ diffuse and react with other ionic species independently. Nevertheless, the CO_2 hydroxylation affects the overall kinetic fractionation to a much greater extent than diffusion [6,36].

Although all samples analysed in this study were collected from alkaline (concrete) substrates with pH $\leq$ 9.9, a large range of $\delta^{13}C$ values was observed, especially in samples collected in continental areas: open-space continental dripstones had $\delta^{13}C$ values within a range of 10.7‰, whereas in the cave, the range of values was even larger (29.4‰). Generally, the $\delta^{13}C$ values varied much more than the $\delta^{18}O$ values. Due to high pH values of mother solutions, the formation mechanism of all samples with low δ values was the same, e.g. the adsorption of atmospheric CO_2 into the highly alkaline solution. The large range of δ values can be explained by precipitation at different rates, considering the differences in the measured pH of water film and drip water (Section 4.) or sources other than atmospheric CO_2 must have been involved in their formation. The difference in the pH of the mother solution at the locus of precipitation can be related either to the varying residence time of water within the concrete or mortar matrix (seepage rate), or to the degree of equilibration with atmospheric CO_2 with prolonged time of exposure of the dripping water or the water film to the atmosphere. In any case, it is proportional to the $[pOH]^{1/2}$ value of the solution [6].

Neglecting the group of cave dripstones with high δ values, which obviously were not formed by the same processes as the majority of the other analysed samples, the mean $\delta^{13}C$ values of different groups of samples decrease from continental surface (−25.4‰), MO (−25.8‰), MI (−29.4‰) to the continental cave (−32.1‰) environment. Evidently, dripstones formed in outdoor conditions are very similar in both Mediterranean and continental climates, indicating that the mean annual temperature difference of 4.3 °C did not affect their isotopic composition significantly. Therefore, the precipitation rate and CO_2 sources must have played a more important role than the temperature.

The two continental environments – outdoors and in the cave – are distinguished by several factors: (1) the mean annual temperature is similar, but the diurnal temperature variation in the cave is negligible, and seasonal variation is very small compared with that at the surface, where daily and seasonal temperature variations often exceed 10 °C, (2) air circulation in the cave is very limited compared with that in open space and (3) CO_2 sources for carbonate precipitation in the cave and at the surface are different, since the contribution of biogenic CO_2 is considerably larger in the cave environment.

While atmospheric CO_2 in the area of Postojna had $\delta^{13}C$ values roughly between −9 and −8‰ VPDB [9], CO_2 in the Postojna Cave can have a large range of $\delta^{13}C$ values (between −26.8 and −15.1‰ VPDB), closely related to its concentration. In the winter ventilation mode, when the temperature in the cave is higher than outside, the CO_2 concentrations in the cave are

slightly above the surface atmospheric CO_2 concentrations, between 500 and 600 ppmv with $\delta^{13}C$ values only slightly lower than in the atmosphere in open space. In the warmer part of the year, when the air flux through the cave is very low, CO_2 can accumulate up to 5000 ppmv, with $\delta^{13}C$ values as low as −26.8‰ VPDB. Since no continuous measurements could be made, the values measured in this study are only momentary snapshots hardly representative of the annual average values. Considering the annual average $\delta^{13}C$ of soil CO_2 (the main source of CO_2 degassing from dripping water [9]) to be about -21.4 ± 3.4‰ VPDB [37] and the average concentration of CO_2 in the cave around 1000 ppm (information obtained from the cave management), the average $\delta^{13}C$ of atmospheric CO_2 (using a linear mixing model) could be estimated to be around −16‰ VPDB. Comparing the $\delta^{13}C$ values of dripstones analysed in this study, the continental open-space samples had average $\delta^{13}C$ values about 7‰ more positive than the cave samples, clustering at low $\delta^{13}C$ values (on average –32.1‰ VPDB), which fits well with the average difference between $\delta^{13}C$ values of the cave and surface atmospheric CO_2. This indicates that the difference in $\delta^{13}C$ between continental open-space and cave secondary dripstones is at least in part related to the different sources of CO_2.

Comparing the two groups of samples from the Mediterranean environment – those formed in semi-closed space in the fortress and in an underpass on the regional road – the difference is obvious. The samples from the underpass have average $\delta^{13}C$ values about 3.5‰ higher than those from the fortress. Along the road, the atmosphere can be enriched in CO_2 derived from fuel combustion (with $\delta^{13}C$ around −25‰) and to a lesser extent in biogenic CO_2 with $\delta^{13}C$ around −28‰ VPDB [38]. Nevertheless, in open space, these differences would only be subtle and strongly dependent upon the atmospheric conditions. Therefore, the different CO_2 sources as the reason for measured differences in $\delta^{13}C$ of dripstone for these locations can be ruled out. Since in both climates (continental and Mediterranean), the outdoor samples are depleted in ^{13}C compared with those formed in closed or poorly ventilated space, the most obvious reason for different C isotope fractionation would be the ventilation, i.e. the air flow, which affects the CO_2 dissolution rate in the alkaline solution.

5.2.3. *Oxygen sources*

While O in speleothems is derived predominantly from water, secondary dripstones on concrete substrates receive O from both water and atmospheric CO_2 [1,6]. O'Neil and Barnes [26] found that two-thirds of the oxygen atoms are derived from atmospheric CO_2 and one-third from water. Since in highly alkaline solutions CO_2 preferentially reacts with OH^- ions in solution [6], the isotopic composition of oxygen in the carbonate precipitate represents a mixture:

$$\delta^{18}O_{CaCO_3} = 2/3 \times \delta^{18}O_{CO_2} + 1/3 \times \delta^{18}O_{OH^-} \quad (1)$$

O isotopic fractionation factors for the $H_2O - OH^-$ exchange reaction are available only for a few discrete temperature values [39], being 1.040 and 1.045 ± 0.003 at 25 °C and 15 °C, respectively [39,40]. Linear extrapolation to the actual measured ambient temperatures (15.4 °C in Šibenik, 11.1 °C in Ljubljana and 9.5 °C in Postojna) gave values which are within the range of analytical uncertainty. Taking into account the average temperature and $\delta^{18}O$ of precipitation, we assumed a $\delta^{18}O_{OH^-}$ value of −82.2‰ for the continental and −77.3‰ VPDB for the Mediterranean area. Atmospheric $\delta^{18}O_{CO_2}$ is reported to be around +41‰ VSMOW with seasonal and spatial variations of only a few per mil [41–44]. Photosynthetic uptake of CO_2, plant and soil respiration and fossil fuel burning, however, may alter the isotopic composition of both C and O in CO_2. Seasonal analyses of $\delta^{18}O_{CO_2}$ in urban areas of Krakow, Poland [38], and Bern, Switzerland [45], showed considerably lower values (−8 to −3‰ VPDB and −5 to +2‰ VPDB). As no measurements of open-space atmospheric CO_2 oxygen isotopic composition were made, the

average value of −3.5‰ VPDB was taken, considering that the sampling locations were mostly along roads. The calculated mean $\delta^{18}O_{CaCO_3}$ value using Equation (1) was −27.9‰ VPDB for the Mediterranean site and −29.5‰ VPDB for the continental open-space samples, which are about 10‰ lower than the measured mean δ values. However, assuming the average atmospheric $\delta^{18}O_{CO_2}$ of +41‰ VSMOW, the measured and calculated mean $\delta^{18}O$ values of carbonates were much closer. For the continental samples, the calculated and mean measured $\delta^{18}O$ values for dripstones were within ±2.6‰, whereas for the Mediterranean samples the difference was negligible (−19.12‰ VPDB, yielding a difference within analytical uncertainty).

The $\delta^{18}O$ values of isotopically light dripstones from Postojna Cave were within -20.6 ± 1.6‰ VPDB. Using Equation (1), the $\delta^{18}O$ of dripstone formed from cave air CO_2 with an average measured $\delta^{18}O$ value of −11.4‰ VPDB and the OH^- of dripping water with $\delta^{18}O$ of −82.2‰ VPDB; the average $\delta^{18}O$ of speleothems should be −34.9‰ VPDB, which is over 14‰ lower than the mean measured value. This implies that the rapid disequilibrium precipitation of carbonate at high pH values may incorporate variable fractions of oxygen deriving from water (OH^-) and atmospheric CO_2 and does not apply for all conditions and CO_2 dissolution, as well as $CaCO_3$ precipitation rates. Moreover, Dietzel *et al.* [46] proved that for calcite precipitation, the O isotope fractionation factor critically depends not only upon the temperature, but also on the pH and the precipitation rate, which may additionally increase the isotope separation between the C and O sources and the $CaCO_3$ precipitate.

5.3. *Variability of isotopic and elemental composition along the growth layer and the growth axis*

The variability of C and O isotopic composition and elemental concentrations was also studied along the single growth layer of a larger stalagmite from the MI environment. The $\delta^{13}C$ and $\delta^{18}O$ values generally increased with distance from the apex (Figure 5(b)). A similar variation was observed in the elemental composition, where the concentrations of trace elements (Mg, Sr and Ba) generally increased on the slope along the flanks (Figure 5(b)). At the apex, however, all measured parameters varied irregularly, most probably due to the morphology of the stalagmite, where some structures similar to dissolution pits occurred. pH measurement of stalagmite surfaces gave values around 8.5 both for natural cave speleothems and for the Mediterranean stalagmite formed from the alkaline solution, which indicates that the water film on the stalagmite surface was already much closer to equilibrium with atmospheric CO_2 and $CaCO_3$, compared with the initial stages of dripstone formation in solutions with pH $\geq$ 9.6. Romanov *et al.* [47,48] calculated the variation of $\delta^{13}C_{CaCO_3}$ along the growth layer of speleothems (assuming growth from a continuously flowing water film and irreversible CO_2 degassing and calcite precipitation), showing precipitation of carbonate increasingly enriched in ^{13}C along the growth layers. The same trend also occurs from the decreasing calcite precipitation rate because of the decreasing pH of the solution by absorption of atmospheric CO_2 into the water film slowly flowing down the flanks of the stalagmites formed from (initially) highly alkaline solutions. Both mechanisms result in increasing $\delta^{13}C$ values with time due to decreased supersaturation of the solution and a decreased precipitation rate. All the stalagmites analysed in this study had irregular shapes, which make a constant flow rate of the water film impossible. However, uneven shapes explain the irregular ^{13}C and elemental (Mg, Sr) profiles.

The concentrations of Mg and Sr in the samples were much lower than typically found in natural karstic systems, where the source of metals (Ca, Mg, Sr) is the carbonate rock with typically some molar percent of $MgCO_3$. In our sample, the source material for metals is mortar, where the Mg and Sr are present mainly in the carbonate additive, which is hardly soluble in the highly alkaline Ca^{2+}-rich solution.

The spatial distribution of Mg and Sr at the apex of the stalagmite was highly irregular (Figure 5(b)). A possible explanation for this irregularity is the morphology of the apex, with several voids and pits where water was retained, so that re-dissolution and re-crystallisation of carbonate could occur (note that the pH value of the water film at the apex was rather low, between 8.5 and 8.6). The increase in trace metal concentrations along the flanks (along an individual growth layer) with increasing distance from the apex is easily explained by rapid precipitation of $CaCO_3$ in a dynamic continuously flowing water film, constantly interacting with the atmosphere and the carbonate substrate, and the resulting gradual enrichment of the water film in trace elements, which then co-precipitated with carbonate.

The distribution of Mg and Sr between the solution and precipitating carbonate has been extensively studied in marine systems [49] and in laboratory systems in karst-analogous conditions [50], where, however, the physicochemical conditions are different from those in the studied environment. It was also found that the incorporation of alien cations into the calcite depends upon the morphology of the growing crystals and is different at different faces of a single crystal, so that this can hardly be considered as an equilibrium process [51]. The trace metal distribution coefficients (D_{Me}, defined as the ratio between the Me/Ca molar ratio of carbonate and mother solution) for Mg, Sr and Ba are generally known, though their relation to the metal concentrations, temperature and precipitation rates is not yet clear. D_{Mg} is thought to depend exclusively upon the temperature in karst-analogous conditions at concentration levels close to those found in karst conditions [50], though the uncertainties are still rather large [52]. For Sr and Ba, concentration levels in the mother solution and precipitation rate influence the distribution coefficient by an order of magnitude or more [50,53]. In the case of rapid non-equilibrium precipitation of a stalagmite from the strongly alkaline solution, only the temperature can be considered as stable, whereas the metal concentration in the solution, pH and precipitation rate in open-space conditions change constantly in a rather unpredictable way. Rapid precipitation of calcite results in a rapid increase in Mg/Ca and Sr/Ca ratios in the solution, which in turn results in gradual enrichment of the precipitate in Mg and Sr with increasing distance from the apex. The highest Mg/Sr ratios were recorded at the apex of the stalagmite and along the vertical growth axis (between 5.2 and 34.6, on average 20.9), whereas along the flanks the ratio was much lower, but constantly increasing with increasing distance from the apex (from 1.6 to 12). The increasing trend of the Mg/Sr ratio in carbonate along the flanks is the result of the accumulation of Mg and Sr in the residual solution after preferential crystallisation of pure $CaCO_3$ and low-Mg calcite.

6. Conclusions

Secondary calcium carbonate precipitates in various forms of dripstones formed in open and closed space (fortress, cave) in continental (Slovenia) and Mediterranean (Croatia) areas were studied. The formation of different fabrics (porous calcite crystals, spherulitic and rhombohedric fabrics, and porous and dense layers) in studied dripstones largely depends on the saturation state of the mother solution. Porous layers and calcite crystals result from fast calcite precipitation from highly saturated solutions, followed by slow crystallisation of smooth-surface calcite crystals and denser layers from less saturated solutions. Differences in C and O isotopic compositions are related to different fabrics, both elements being isotopically heavier in denser, slowly growing formations. This implies that the precipitation rate affects the isotope separation between the solution and the carbonate precipitate.

The $\delta^{13}C$ and $\delta^{18}O$ of bulk dripstones analysed in our study show a positive correlation along the growth axis and along individual growth layers, indicating $CaCO_3$ precipitation in non-equilibrium conditions. Based on the identity of the slope of the correlation line $\delta^{18}O = (0.61 \pm 0.02) \times \delta^{13}C - (1.88 \pm 0.43)$ found in our samples and that obtained for carbonate precipitates obtained

by precipitation from a highly alkaline solution with initial pH around 12 in controlled laboratory conditions [14], we conclude that the basic mechanism of formation of highly depleted dripstones on concrete structures in all investigated environments is the fast $CaCO_3$ precipitation from highly alkaline solutions, induced by rapid CO_2 dissolution in the solution, resulting in a large isotopic separation between source materials (CO_2, water) and precipitates.

Statistically significant differences were found between dripstones formed in outdoor (open space) conditions and those formed in rather closed space of a karstic cave and inside the building, whereas the differences in climatic conditions, e.g. temperature, obviously did not play a relevant role in the isotope fractionation processes. On the other hand, sources of CO_2 can be estimated from the isotopic fingerprints, as indicated in the case of the cave samples with very low $\delta^{13}C$ and $\delta^{18}O$ values, precipitated by dissolution of ^{13}C- and ^{18}O-depleted biogenic CO_2 in the water film on concrete surfaces. Further, the assumption that one-third of O in the precipitate is contributed by water (OH^-) and two-thirds by atmospheric CO_2 [6] was not confirmed in the cave environment.

The variability of carbon and oxygen isotopic composition and elemental concentrations along the single growth layer of a larger stalagmite from an MI environment showed a trend of increasing $\delta^{13}C$ and $\delta^{18}O$ values as a result of decreasing saturation of the solution and decreasing precipitation rate. This enrichment is accompanied by increasing trace metal concentrations (Mg, Sr and Ba) on the slope along the flanks, resulting from the accumulation of trace metals in the residual solution after preferential crystallisation of pure $CaCO_3$ and low-Mg calcite. As the pH of the surface water film on the analysed stalagmite was already low (in the range typical for water film on natural speleothems in karstic caves), the effect of the specific formation mechanism and the precipitation rate stopped playing the critical role in the isotope fractionation, so it followed the trends occurring in common environments of dripstone formations [47,48].

Acknowledgements

The study was financially supported by the Slovenian Research Agency (ARRS) research programme P-0143 and the Ministry of Science, Education and Sports of the Republic of Croatia under Projects 098-0982934-2720 S. Hydrometeorological data were kindly provided by the Environmental Agency of Slovenia and National Hydrometeorological Survey of Croatia. Sincere thanks are due to the management of the Postojna Kras Turizem enterprise and in particular to Mr Stanislav Glažar for assistance and support during sampling. The authors also thank Dr Anthony R. Byrne for linguistic revision and two anonymous reviewers for thoughtful comments and suggestions.

References

[1] R.V. Krishnamurthy, D. Schmitt, E.A. Atekwana, and M. Baskaran, Isotopic Investigation of Carbonate Growth on Concrete Structures, *Appl. Geochem.* **18**, 435 (2003).
[2] E. Dotsika, D. Psomiadis, D. Poutoukis, B. Raco, and P. Gamaletsos, Isotope Analysis for Degradation Diagnosis of Calcite Matrix in Mortar, *Anal. Bioanal. Chem.* **395**, 2227 (2009).
[3] A. Kuczumow, D. Genty, P. Chevallier, J. Nowak, M. Florek, and A. Bucyńska, X-Ray Electron Microprobe Investigation of Speleothems from Godarville Tunnel, *X-ray Spectrom.* **34**, 502 (2005).
[4] G.E. Troxell, H.E. Davis, and J. Kelly, *Composition and Properties of Concrete*, McGraw-Hill Civil Engineering Series (McGraw-Hill Book Company, New York, 1968).
[5] M.B. Valcarce and M. Vázquez, Carbon Steel Passivity Examined in Solutions with a Low Degree of Carbonation: The Effect of Chloride and Nitrite Ions, *Mater. Chem. Phys.* **115**, 313 (2009).
[6] M. Dietzel, E. Usdowski, and J. Hoefs, Chemical and $^{13}C/^{12}C$- and $^{18}O/^{16}O$-Isotope Evolution of Alkaline Drainage Waters and the Precipitation of Calcite, *Appl. Geochem.* **6**, 177 (1992).
[7] Z. Liu and D. He, Special Speleothems in Cement-Grouting Tunnels and Their Implications of the Atmospheric CO_2 Sink, *Environ. Geol.* **35**, 258 (1998).
[8] W. Dreybrodt, Deposition of Calcite from Thin Films of Natural Calcareous Solution and the Growth of Speleothems, *Chem. Geol.* **29**, 89 (1980).
[9] B. Vokal, *The Carbon Transfer in Karst Areas – an Application to the Study of Environmental Changes and Paleoclimatic Reconstruction*, Ph.D. thesis, University of Nova Gorica, Slovenia, 1999.
[10] A. Baker, C.J. Proctor, and W. Barnes, Variations in Stalagmite Luminescence Laminae Structure at Poole's Cavern, England, AD 1910 ± 1996: Calibration of a Palaeoprecipitation Proxy, *Holocene* **9**, 683 (1999).

[11] P.J. Mickler, J.L. Banner, L. Stern, Y. Asmerom, R.L. Edwards, and E. Ito, Stable Isotope Variations in Modern Tropical Speleothems: Evaluating Equilibrium vs. Kinetic Isotope Effects, *Geochim. Cosmochim. Acta* **68**, 4381 (2004).

[12] P.J. Mickler, L.A. Stern, and J.L. Banner, Large Kinetic Isotope Effects in Modern Speleothems, *GSA Bull.* **118**, 65 (2006).

[13] I.J. Fairchild, S. Frisia, A. Borsato, and A.F. Tooth, Speleothems, in *Geochemical Sediments and Landscapes*, edited by D.J. Nash and S.J. McLaren (Blackwell, Oxford, 2006), pp. 200–245.

[14] B. Kosednar-Legenstein, M. Dietzel, A. Leis, and K. Stingl, Stable Carbon and Oxygen Isotope Investigation in Historical Lime Mortar and Plaster – Results from Field and Experimental Study, *Appl. Geochem.* **23**, 2425 (2008).

[15] A. Hartland, I.J. Fairchild, J.R. Lead, D. Domínguez-Villar, A. Baker, J. Gunn, M. Baalousha, and Y. Ju-Nam, The Dripwaters and Speleothems of Poole's Cavern: A Review of Recent and Ongoing Research, *Cave Karst Sci.* **36**, 37 (2010).

[16] S. Epstein and T. Mayeda, Variations of ^{18}O Contents of Water from Natural Resources, *Geochim. Cosmochim. Acta* **4**, 213 (1953).

[17] J.R. O'Neil, R.N. Clayton, and T.K. Mayeda, Oxygen Isotope Fractionation in Divalent Metal Carbonates, *J. Chem. Phys.* **51**, 5547 (1969).

[18] P. Vreča, I. Krajcar-Bronić, N. Horvatinčić, and J. Barešić, Isotopic Characteristics of Precipitation in Slovenia and Croatia: Comparison of Continental and Maritime Stations, *J. Hydrol.* **330**, 457 (2006).

[19] P. Vreča, I. Krajcar-Bronić, A. Leis, and M. Brenčič, Isotopic Composition of Precipitation in Ljubljana (Slovenia), *Geologija* **51**, 169 (2008).

[20] R. Boistelle and J.-P. Astier, Crystallization Mechanisms in Solution, *J. Cryst. Growth* **90**, 14 (1988).

[21] I.J. Fairchild and P.C. Treble, Trace Elements in Speleothems as Recorders of Environmental Change, *Quart. Sci. Rev.* **28**, 449 (2009).

[22] S. Frisia, A. Borsato, I.J. Fairchild, and F. McDermott, Calcite Fabrics, Growth Mechanisms, and Environment of Formation in Speleothems from the Italian Alps and Southwestern Ireland, *J. Sediment. Res.* **70**, 1183 (2000).

[23] D. Genty, A. Baker, and B. Vokal, Intra- and Inter-Annual Growth Rate of Modern Stalagmites, *Chem. Geol.* **176**, 191 (2001).

[24] D. Domínguez-Villar, S. Lojen, I.J. Fairchild, A. Baker, and S. Moreton, Is Current Global Warming Being Recorded in Postojna Cave and Their Stalagmites? in *Abstracts of the 18th International Karstological School 'Classical Karst: Dinaric Karst'*, edited by A. Mihevc, M. Prelovšek and N. Zupan (Karst Research Institute ZRC SAZU, Postojna, 2010), pp. 30–31.

[25] W.G. Mook, J.C. Bommerson, and W.H. Staverman, Carbon Isotope Fractionation between Dissolved Bicarbonate and Gaseous Carbon Dioxide, *Earth Planet. Sci. Lett.* **22**, 169 (1974).

[26] J.R. O'Neil and J. Barnes, ^{13}C and ^{18}O Compositions in Some Freshwater Carbonates Associated with Ultramafic Rocks and Serpentinites: Western United States, *Geochim. Cosmochim. Acta* **35**, 687 (1971).

[27] R. Letolle, P. Gegout, and M. Moranville-Regourd, Isotope Fractionation of Carbon during Precipitation of Carbonates at Very High pH, *CR Acad. Sci. Paris* **311**, 95 (1990).

[28] D. Genty, B. Vokal, B. Obelić, and M. Massault, Bomb ^{14}C Time History Recorded in Two Modern Stalagmites – Importance for Soil Organic Matter Dynamics and Bomb ^{14}C Distribution over Continents, *Earth Planet. Sci. Lett.* **160**, 795 (1998).

[29] L.S. Land, The Carbon and Oxygen Isotopic Chemistry of Surficial Holocene Shallow Marine Carbonate Sediment and Quaternary Limestone and Dolomite, in *Handbook of Environmental Isotope Geochemistry*, Vol. 3: *The Marine Environment*, edited by P. Fritz and J.C. Fontes (Elsevier, Amsterdam, 1989), pp. 191–217.

[30] C.H. Hendy, The Isotopic Geochemistry of Speleothems – I. The Calculation of the Effects of Different Modes of Formation on the Isotopic Composition of Speleothems and Their Applicability as Palaeoclimatic Indicators, *Geochim. Cosmochim. Acta* **35**, 810 (1971).

[31] A. Goede, D.C. Green, and R.S. Harmon, Late Pleistocene Palaeotemperature Record from a Tasmanian Speleothem, *Aust. J. Earth Sci.* **33**, 333 (1986).

[32] M. Gascoyne, Palaeoclimate Determination from Cave Calcite Deposits, *Quarter. Sci. Rev.* **11**, 609 (1992).

[33] J.A. Dorale, R.L. Edwards, and B.P. Onac, Stable Isotopes as Environmental Indicators in Speleothems, in *Karst Processes and the Carbon Cycle,* Final Report IGCP379, edited by D. Yuan and C. Zhang (Geological Publishing House, Beijing, 2002), pp. 107–120.

[34] C.S. Romanek, E.L. Grossman, and J.W. Morse, Carbon Isotopic Fractionation in Synthetic Aragonite and Calcite: Effects of Temperature and Precipitation Rate, *Geochim. Cosmochim. Acta* **56**, 419 (1992).

[35] C. Jiménez-López, E. Caballero, F.J. Huertas, and C.S. Romanek, Chemical, Mineralogical and Isotope Behaviour, and Phase Transformation during the Precipitation of Calcium Carbonate Minerals from Intermediate Ionic Solution at 25 °C, *Geochim. Cosmochim. Acta* **65**, 3219 (2001).

[36] E. Usdowski and J. Hoefs, $^{13}C/^{12}C$ Partitioning and Kinetics of CO_2 Absorption by Hydroxide Buffer Solutions, *Earth Planet. Sci. Lett.* **80**, 130 (1986).

[37] M. Čater and N. Ogrinc, Soil Respiration Rates and $\delta^{13}C$ (CO_2) in natural beech forest (*Fagus sylvatica* L.) in relation to stand structure, Isot. Environ. Health Stud. **47**, 221 (2011).

[38] M. Zimnoch, T. Florkowski, J.M. Necki, and R.E.M. Neubert, Diurnal Variability of $\delta^{13}C$ and $\delta^{18}O$ of Atmospheric CO_2 in the Urban Atmosphere of Kraków, Poland, *Isot. Environ. Health Stud.* **40**, 129 (2004).

[39] M. Green and H. Taube, Isotopic Fractionation in the OH–H_2O Exchange Reaction, *J. Phys. Chem.* **67**, 1565 (1963).

[40] E.R. Thornton, Solvent Isotope Effects in H_2O^{16} and H_2O^{18}, *J. Am. Chem. Soc.* **84**, 2474 (1962).

[41] Y. Bottinga and H. Craig, Oxygen Isotope Fractionation between CO_2 and Water, and the Oxygen Composition of Marine Atmospheric CO_2, *Earth Planet. Sci. Lett.* **5**, 285 (1969).
[42] H.M. Thiemens, T. Jackson, K. Mauersberger, B. Schueler, and J. Morton, Oxygen Isotope Fractionation in Stratospheric CO_2, *Geophys. Res. Lett.* **18**, 669 (1991).
[43] G.D. Farquhar, J. Lloyd, J.A. Taylor, L.B. Flanagan, J.P. Syvertsen, K.T. Hubick, S.C. Wong, and J.R. Ehleringer, Vegetation Effects on the Isotope Composition of Oxygen in Atmospheric CO_2, *Nature* **363**, 439 (1993).
[44] H.P. Affek, X. Xu and J.M. Eiler, Seasonal, and Diurnal Variations of $^{13}C^{18}O^{16}O$ in Air: Initial Observations from Pasadena, CA, *Geochim. Cosmochim. Acta* **71**, 5033 (2007).
[45] P. Sturm, M. Leuenberger, F.L. Valentino, B. Lehmann, and B. Ihly, Measurements of CO_2, Its Stable Isotopes, O_2/N_2, and ^{222}Rn at Bern, Switzerland, *Atmos. Chem. Phys.* **6** (7), 1991 (2006).
[46] M. Dietzel, J. Tang, A. Leis, and J.S. Köhler, Oxygen Isotopic Fractionation during Inorganic Calcite Precipitation – Effects of Temperature, Precipitation and pH, *Chem. Geol.* 268, **107** (2009).
[47] D. Romanov, G. Kaufmann, and W. Dreybrodt, Modeling Stalagmite Growth by First Principles of Chemistry and Physics of Calcite Precipitation, *Geochim. Cosmochim. Acta* **72**, 423 (2008).
[48] D. Romanov, G. Kaufman, and W. Dreybrodt, $\delta^{13}C$ Profiles along Growth Layers of Stalagmites: Comparing Theoretical and Experimental Results, *Geochim. Cosmochim. Acta* **72**, 438 (2008).
[49] E.A. Burton and L.M. Walter, The Effects of P_{CO_2} and Temperature on Magnesium Incorporation in Calcite in Seawater and $MgCl_2$–$CaCl_2$ Solutions, *Geochim. Cosmochim. Acta* **55**, 777 (1991).
[50] Y. Huang and I.J. Fairchild, Partitioning of Sr^{2+} and Mg^{2+} into Calcite under Karst-Analogue Experimental Conditions, *Geochim. Cosmochim. Acta* **65**, 47 (2001).
[51] R.J. Reeder and J.C. Grams, Sector Zoning in Calcite Cement Crystals: Implications for Trace Element Distributions in Carbonates, *Geochim. Cosmochim. Acta* **51**, 187 (1987).
[52] S. Lojen, A. Trkov, J. Ščančar, J.A. Vazquez-Navarro, and N. Cukrov, Continuous 60-Year Stable Isotopic and Earth-Alkali Element Records in a Modern Laminated Tufa (Jaruga, River Krka, Croatia): Implications for Climate Reconstruction, *Chem. Geol.* **259**, 242 (2009).
[53] Y. Yoshida, H. Yoshikawa, and T. Nakanishi, Partition Coefficients of Ra and Ba in Calcite, *Geochem. J.* **42**, 295 (2008).

Appendix 9: Article: Paleoclimate proxies in sub-recent freshwater carbonate system in river Krka, Slovenia. In: *17th International Karstological Schoool "Classical Karst"* 2008. 4 (Karst Research Institute, Postojna, 2009).

PALAEOCLIMATE PROXIES IN SUB-RECENT FRESHWATER CARBONATE SYSTEM IN RIVER KRKA, SLOVENIA

Saša Zavadlav & Sonja Lojen

Jožef Stefan Institute, Jamova 39, Ljubljana, Slovenia, sasa.zavadlav@ijs.si

Abstract

Most convenient way for determining whether trace elements and stable isotopes of carbon and oxygen are suitable as past climate proxies is to evaluate their behaviour in recent systems, resembling the one we have chosen for our study. We present records of trace elements (Mg, Ca, Sr and Ba) and stable isotope ($\delta^{13}C$, $\delta^{18}O$) variations in freshwater stream carbonate (tufa). The relationships between parameters measured in water and in carbonate were found to be very complex and need further study. High correlations exist between C and O stable isotope compositions and Mg concentrations which implies that much of the variation observed in these variables is controlled by the same or several linked processes. The other variables show weaker correlations or no correlation at all, as in the case of Ca. Commonly used isotope palaeotemperature equations were applied to estimate the tufa precipitation temperature. The differences between measured and calculated water temperature reached up to 6 °C which shows specific demeanour of river Krka's hydrology and its tufa occurrence.

Keywords: recent tufa, palaeoclimate, stable isotopes, carbon, oxygen, trace elements.

INTRODUCTION

For some time now terrestrial carbonates such as speleothems, lake sediments and tufas are known as palaeoenvironmental and palaeoclimatic archives. Tufa calcite precipitation is controlled by a combination of physico-chemical conditions and biomediation, however, inorganic precipitation is predominant when dissolved CO_2 in karst groundwater outgases at spring, water-falls or other obstructions that cause water turbulence. Since morphological, geochemical and isotopic characteristics of tufas reflect the climatic conditions during the period of their growth (Andrews et al., 1993; Pedley et al.; 1996; Andrews et al., 1997; Ihlenfeld et al., 2003; Andrews, 2006; Liu et al., 2006; Lojen et al., 2009) the importance of tufas as palaeoenvironmental indicators is only increasing through the last decade.

Fig. 1: Location map of the investigated area.

For the purposes of determining whether tufa carbonates are suitable as palaeoclimate proxies we tend to study the sub-recent tufa system of the river Krka in Slovenia through a period of 4 years (Fig. 1). River Krka is typical karst river with predominantly limestone watershed and mainly groundwater recharge, especially in the upper part of the river flow where most intensive tufa production occurs. First tufa barriers are formed in a few kilometres downstream of the spring and they continuously appear throughout a more than 50 km long river section. In this paper are shown results of the first year of the investigation from November 2007 until December 2008. The aim of preliminary data processing is to determine whether ^{18}O and earth-alkali elements are suitable as palaeoclimate proxies in river Krka tufa system.

MATERIALS AND METHODS

Sampling of water for stable isotope and earth-alkali elements analysis was performed every two months on stationary sampling points from spring to the outfall of the river. Carbonates were collected in September 2008 on sixteen tufa barrages.

Water samples were taken for analysis of stable isotope composition of oxygen ($\delta^{18}O$) and dissolved inorganic carbon ($\delta^{13}C$-DIC) and for determining concentrations of earth-alkali elements (Mg^{2+}, Ca^{2+}, Sr^{2+}, Ba^{2+}). For the latter samples of water were filtered *in-situ* through 0.45 μm cellulose-nitrate membrane filters and acidified with suprapure nitric acid (0,5 mL per 100 mL of sample), while in the laboratory the concentrations were measured either by inductive coupled plasma mass spectrometry (ICP-MS) or atomic emission spectrometry (ICP-AES). The stable isotope composition of DIC was determined in 5 mL samples injected into evacuated septum tubes containing 100 % phosphoric acid. The CO_2 released was analysed with a Europa 20-20 continuous-flow isotope ratio mass spectrometer with ANCA TG trace gas separation module. $\delta^{18}O$ of water was determined by the CO_2 equilibration technique (12 h at 25 °C, Epstein and Mayeda, 1953; O'Neil, 1969). The analyses were performed using a dual inlet Varian MAT 250 isotope ratio mass spectrometer. Carbonates for $\delta^{13}C$ and $\delta^{18}O$ analysis were prepared by digestion in 100 % phosphoric acid at 25 °C for 24 h according to the method of McCrea (1950). CO_2 released during acid treatment was analysed using Varian MAT 250 mass spectrometer. The stable isotope compositions of oxygen in water are reported as deviations (δ-values in ‰) relative to VSMOW, and relative to VPDB for carbon dissolved in the water and in the carbonate.

RESULTS AND DISCUSSION

An important assumption in freshwater carbonate research is that precipitation of calcium carbonate occurs by physico-chemical mechanisms, and consequently is in thermodynamic equilibrium with ambient water and other environmental conditions (Pentecost and Riding, 1986; Zhang et al., 2001, Ihlenfeld et al., 2003). However, some studies (e.g. Janssen et al., 1999; Rogerson et al., 2008) showed that biological influence on tufa precipitation should not be neglected, nor when studying stable isotopes composition or trace elements in tufas, where the biological component has a greater influence on carbon rather then on oxygen isotopes (Janssen et al., 1999), neither for trace elements.

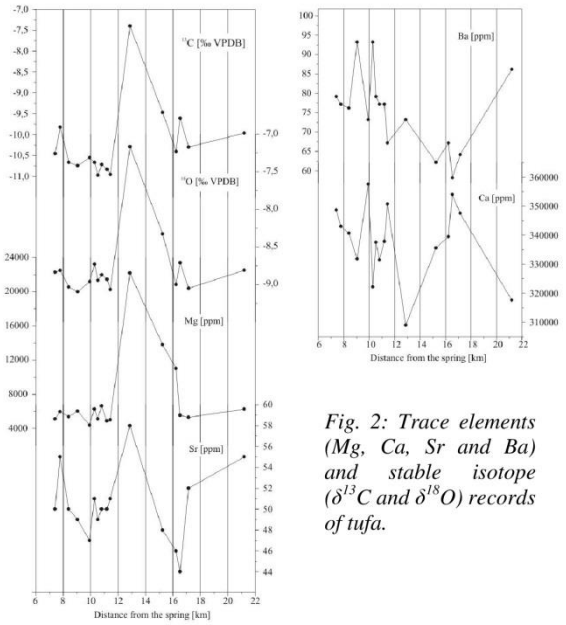

Fig. 2: Trace elements (Mg, Ca, Sr and Ba) and stable isotope ($\delta^{13}C$ and $\delta^{18}O$) records of tufa.

Figure 2 shows the concentrations of trace elements, as well as $\delta^{13}C$ and $\delta^{18}O$ values of tufa plotted against the distance from the spring of the river. The highly significant correlations existing between C and O (r = 0,93), Mg and O (r = 0,91) and between Mg and C (r = 0,86) imply that much of the variation observed in these variables is controlled by the same or at least by different but linked processes. Sr is showing a somewhat weaker relationship with some components, like O (r = 0.50), C (r = 0.48), Mg (r = 0.38) and Ba (r = 0.34). Surprisingly Ca shows a negative correlation with all the other trace

elements, as well as with $\delta^{13}C$ and $\delta^{18}O$ ($-0.47 < r < -0.63$), which is also evident in the antyclinal variation of these two variables.

Some previous papers (Huang and Fairchild, 2001; Ihlenfeld et al., 2003; Lojen et al., 2009) have shown that concentrations of Mg in tufa deposits can be used as palaeothermometers but in the case of river Krka's tufa system first results show quite the opposite. No correlation is observed between Mg/Ca ratio and temperature of water ($r = -0.03$), which could be due to the complicated hydrological conditions of the river Krka aquifer, despite the fact that Mg and Mg/Ca ratio of tufa carbonate are in good correlation with $\delta^{18}O$ of carbonate. Since Mg/Ca ratio in water is related to differential dissolution of dolomite and calcite, water residence time and water temperature these results require further research.

$\delta^{18}O$ values of the Krka river for water along with subsidiary streams vary between –10.33 and –7.73 ‰ and show seasonal variability up to 2.60 ‰. Since the $\delta^{18}O$ values seem to be highest in the winter and summer, the variability in ^{18}O enrichment cannot be ascribed only to seasonal evaporation effects. The $\delta^{18}O$ values of bulk tufa range between –9.16 to –7.17 ‰ with an average value of -8.77 ‰.The comparison with $\delta^{18}O$ values of sub-recent tufa calcites from different locations shows, that river Krka's tufa can be fitted in-between slightly less negative tufas from Japan (Hori et al., 2009) and more negative Australian tufas (Ihlenfeld et al., 2003). However, due to similar hydrological and geological background best agreement can be observed with Dinaric karst tufas from Plitvice Lakes (Srdoč et al., 1985) and Krka River (Croatia, Lojen et al., 2004).

Presuming that the ^{18}O oscillations in the tufa mainly reflects variations in water temperature the temperature of carbonate precipitation was estimated (Fig. 3) using known palaeotemperature equations derived by Anderson and Arthur (1983) and Hays and Grossman (1991). In both cases estimated temperatures depart from the measured mean annual water temperature. The difference between measured and calculated temperature reaches up to 6 °C.

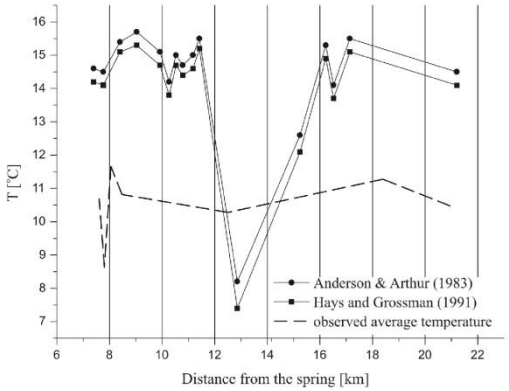

Fig. 3: Comparison of temperature records derived from $\delta^{18}O$ of carbonate and average measured $\delta^{18}O$ of water calculated using Anderson and Arthur (1983) and Hays and Grossman (1991) equations.

Shift between measured and calculated temperature could be ascribed to complicated hydrology of the river Krka's system. These deviations are a result of variable surface and sub-surface water recharge and changing aquifer processes, meaning changeable water retention time and differential calcite dissolution. However, preliminary results of tufa occurrence in river Krka show its specific environmental characteristics that need further research.

REFERENCES

Anderson, T.F. & Arthur, M.A., 1983: Stable isotopes of oxygen and carbon and their application to sedimentologic and palaeoenvironmental problems. In: Stable Isotopes in Sedimentary Geology. Society of Economic Palaeontologists and Mineralogists, Short Course Notes, 10.

Andrews, J.E., Riding, R. & Dennis, P.F., 1993: Stable isotopic compositions of recent cyanobacterial carbonates from the British Isles: local and regional environmental controls. Sedimentology, 40 (2), 303-314.

Andrews, J.E., Riding, R. & Dennis, P.F., 1997: The stable isotope record of environmental and climatic signals in modern terrestrial microbial carbonates from Europe. Palaeogeography, Palaeoclimatology, Palaeoecology, 129 (1-2), 171-189.

Andrews, J.E., 2006: Palaeoclimatic records from stable isotopes in riverine tufas: Synthesis and review. Earth-Science Reviews, 75, 85-104.

Hays, P.D. & Grossman, E.L., 1991: Oxygen isotopes in meteoric calcite cements as indicators of continental palaeoclimate. Geology, 19, 441-444.

Hori, M., Kawai, T., Matsuoka, J. & Kano, A., 2009: Intra-annual perturbations of stable isotopes in tufas: effects of hydrological processes. Geochimica et Cosmochimica Acta, 73, 1684-1695.

Ihlenfeld, C., Norman, M.D., Gagan, M.K., Drysdale, R.N., Maas, R. & Webb, J., 2003: Climatic significance of seasonal trace element and stable isotope variations in a modern freshwater tufa. Geochimica et Cosmochimica Acta, 67, 2341-2357.

Jensenn, A., Swennen, R., Podoor, N. & Keppens, E., 1999: Biological and diagenetic influence in Recent and fossil tufa deposits from Belgium. Sedimentary Geology, 126, 75-95.

Liu, Z., Zhang, M., Li, Q. & You, S., 2003: Hydrochemical and isotope characteristics of spring water and travertine in the Baishuitai area (SW China) and their meaning for palaeoenvironmental reconstruction. Environmental Geology, 44, 698-704.

Lojen, S., Trkov, A., Ščančar, J., Vázquez-Navarro, J.A. & Cukrov, N., 2009: Continuous 60-year stable isotopic and earth-alkali element records in a modern laminated tufa (Jaruga, river Krka, Croatia): Implications for climate reconstruction. Chemical Geology, 258, 242-250.

Pedley, M., Andrews, J., Ordonez, S., Garcia del Cura, M.A., Gonzales Martin, J.-A. & Taylor, D., 1996: Does climate control the morphological fabric of freshwater carbonates? A comparative study of Holocene barrage tufas from Spain and Britain. Palaeogeography, Palaeoclimatology, Palaeoecology, 121 (3-4), 239-257.

Pentecost, A. & Riding, R., 1986: Calcification in cyanobacteria. In Biomineralisation in Lower Plants and Animals, 73-90, Oxford.

Rogerson, M., Pedley, H.M., Wadhawan, J.D. & Middleton, R., 2008: New insights into biological influence on the geochemistry of freshwater carbonate deposits. Geochimica et Cosmochimica Acta, 20, 4976-4987.

Srdoč, D., Horvatinčić, N., Obelić, B., Krjacar, I. & Sliepčević, A., 1985: Procesi taloženja kalcita u krškim vodama s posebnim osvrtom na Plitvička jezera (Calcite deposition processes in karstwaters with special emphasis on the Plitvice Lakes, Yugoslavia). Krs. Jugosl., 11 (4-6), 1-104.

Zhang, D.D., Zhang, Y., Zu, A. & Cheng, X., 2001: Physical mechanisms of river waterfall tufa (travertine) formation. Journal of Sedimentary Research, 71, 205-216.